Douglas M. Ruthven
Shamsuzzaman Farooq
Kent S. Knaebel

Pressure Swing Adsorption

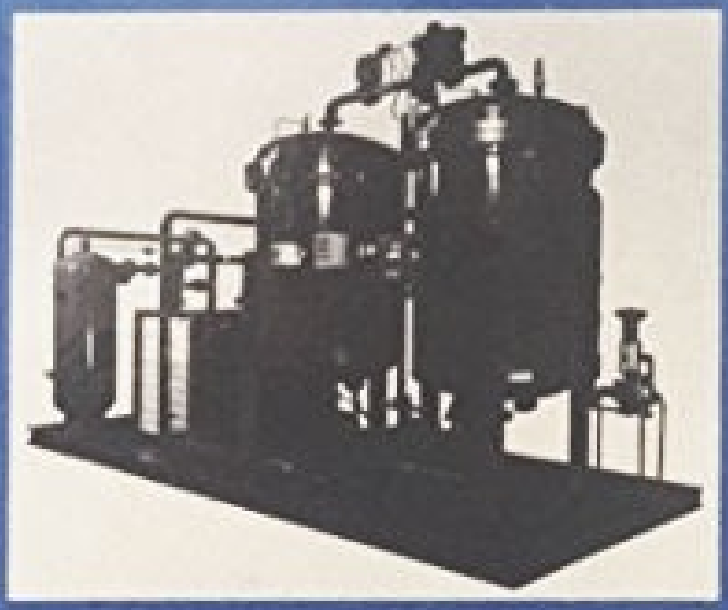

VCH

Pressure
Swing
Adsorption

Pressure Swing Adsorption

Douglas M. Ruthven
Shamsuzzaman Farooq
Kent S. Knaebel

WILEY-VCH
NEW YORK • CHICHESTER • WEINHEIM • BRISBANE • SINGAPORE • TORONTO

GCE - Exhibit 1068, Page 3
GCE Gas Control Equipment Inc. v. VBOX, Inc.
IPR2023-00326

A NOTE TO THE READER:
This book has been electronically reproduced from digital information stored at John Wiley & Sons, Inc. We are pleased that the use of this new technology will enable us to keep works of enduring scholarly value in print as long as there is a reasonable demand for them. The content of this book is identical to previous printings.

Copyright © 1994 by John Wiley & Sons, Inc.

No part of this publication may be reproduced, stored in a retrieval system or transmitted in any form or by any means, electronic, mechanical, photocopying, recording, scanning or otherwise, except as permitted under Sections 107 or 108 of the 1976 United States Copyright Act, without either the prior written permission of the Publisher, or authorization through payment of the appropriate per-copy fee to the Copyright Clearance Center, 222 Rosewood Drive, Danvers, MA 01923, (978) 750-8400, fax (978) 750-4470. Requests to the Publisher for permission should be addressed to the Permissions Department, John Wiley & Sons, Inc., Ill River Street, Hoboken, NJ 07030, (201) 748-6011, fax (201) 748-6008, E-Mail: PERMREQ@WILEY.COM.

To order books or for customer service please, call 1(800)-CALL-WILEY (225-5945).

Library of Congress Cataloging-in-Publication Data

Ruthven, Douglas M. (Douglas Morris), 1938—
Pressure swing adsorption/Douglas M. Ruthven, Shamsuzzaman Farooq. Kent S. Knaebel.
p. cm.
Includes bibliographical references and index.
ISBN 0-471-18818-2
1. Adsorption. I. Farooq. Shamsuzzaman. II. Knaebel. Kent S. 1951--. III. Title.
TP156.A35R78 1993
660'.28423—dc20 93-33965
CIP

Preface

Although pressure swing adsorption (PSA) is not a new process, it is really only during the past decade that such processes have achieved widespread commercial acceptance as the technology of choice for more than a few rather specific applications. Nowadays, however, PSA processes are widely used, on a very large scale, for hydrogen recovery and air separation, and further important applications such as recovery of methane from landfill gas and production of carbon dioxide appear to be imminent. The suggestion for a book on this subject came from Attilio Bisio, to whom we are also indebted for his continuing support and encouragement and for many helpful comments on the draft manuscript.

The authors also wish to acknowledge the seminal contributions of two pioneers of this field, the late Frank B. Hill and Robert L. Pigford. Several of their publications are cited in the present text, but their influence is far broader than the citations alone would suggest. Suffice it to say that much of the book would not have been written without their encouragement and the stimulus provided by their widsom and insight. Several graduate students and post-doctorals have made major contributions, most of which are recognized explicitly by citations. However, they, as well as others whose work may not have been directly referenced, also contributed in a very real way by helping the authors, through discussion and argument, to understand and appreciate some of the subtleties of PSA systems. It would be remiss not to mention by name M. M. Hassan, J. C. Kayser, N. S. Raghavan, and H. S. Shin.

This book is not intended as an exhaustive review of PSA technology, neither is it a design manual. Rather, we have attempted to present a coherent general account of both the technology and the underlying theory. Perhaps more than in other processes the rational design and optimization of a pressure swing adsorption process requires a reasonably detailed mathematical model. The two commonly used approaches to PSA modeling, equilibrium theory, and dynamic numerical simulation are discussed in some detail in Chapters 4 and 5. Inevitably these chapters are somewhat mathematical in approach. The details may be important only to those who are involved in process design and optimization but we hope that the more general reader will still be able to gain some insight concerning the underlying principles and the strengths and limitations of the various approaches.

A three-way collaboration between authors inevitably raises some difficulties since it becomes hard to maintain consistency in style and emphasis and to avoid repetition between different sections of the text. We hope, however, that the advantages of a more authoritative treatment of the subject will more than compensate for any such deficiencies. From our perspective the collaboration has proved interesting and instructive, and we have encountered no serious disagreements amongst ourselves.

UNB, Fredericton, Canada D. M. Ruthven

GCE - Exhibit 1068, Page 5
GCE Gas Control Equipment Inc. v. VBOX, Inc.
IPR2023-00326

National University of Singapore S. Farooq
Adsorption Research Inc., Dublin, Ohio K. S. Knaebel
June 1993

Contents

List of Symbols **xi**

Greek Symbols **xv**

Subscripts **xvii**

Figure Credits **xix**

1. Introduction 1
1.1 Historical Development of PSA Processes 4
1.2 General Features of a PSA Process 5
1.3 Major Applications of PSA 7
References 9

2. Fundamentals of Adsorption 11
2.1 Adsorbents 11
2.2 Adsorption Equilibrium 23
2.3 Adsorption Kinetics 34
2.4 Adsorption Column Dynamics 52
References 63

3. PSA Cycles: Basic Principles 67
3.1 Elementary Steps 67
3.2 Equilibrium-Controlled Separations for the Production of Pure Raffinate Product 71
3.3 Recovery of the More Strongly Adsorbed Species in Equilibrium-Controlled Separations 83
3.4 Cycles for the Recovery of Pure Raffinate Product in Kinetically Controlled Separations 85
3.5 Cycle for Recovery of the Rapidly Diffusing Species 93
References 94

4. Equilibrium Theory of Pressure Swing Adsorption 95
4.1 Background 95
4.2 Mathematical Model 97
4.3 Model Parameters 102
4.4 Cycle Analysis 105

4.5 Experimental Validation 133
4.6 Model Comparison 137
4.7 Design Example 143
4.8 Heat Effects 148
4.9 Pressurization and Blowdown Steps 151
4.10 Conclusions 161
References 163

5. Dynamic Modeling of a PSA System 165
5.1 Summary of the Dynamic Models 166
5.2 Details of Numerical Simulations 184
5.3 Continuous Countercurrent Models 201
5.4 Heat Effects in PSA Systems 207
References 217

6. PSA Processes 221
6.1 Air Drying 221
6.2 Production of Oxygen 226
6.3 Production of Nitrogen 230
6.4 PSA Process for Simultaneous Production of O_2 and N_2 232
6.5 Hydrogen Recovery 235
6.6 Recovery of CO_2 242
6.7 Recovery of Methane from Landfill Gases 244
6.8 Hydrocarbon Separations 246
6.9 Process for Simultaneous Production of H_2 and CO_2 from Reformer Off-Gas 246
6.10 PSA Process for Concentrating a Trace Component 251
6.11 Efficiency of PSA Processes 258
References 263

7. Extensions of the PSA Concept 265
7.1 The Pressure Swing Parametric Pump 265
7.2 Thermally Coupled PSA 270
7.3 Single-Column Rapid PSA System 278
7.4 Future Prospects 286
References 287

8. Membrane Processes: Comparison with PSA 289
8.1 Permeability and Separation Factor 289
8.2 Membrane Modules 295
8.3 Calculation of Recovery–Purity Profiles 299
8.4 Cascades for Membrane Processes 301
8.5 Comparison of PSA and Membrane Processes for Air Separation 303
8.6 Future Prospects 305
References 306

Appendix A. The Method of Characteristics 307

References 311

Appendix B. Collocation Form of the PSA Model Equations 313
B.1 Dimensionless Form of the LDF Model Equations 313
B.2 Collocation Form of the Dimensionless LDF Model Equations 315
B.3 Dimensionless Form of the Pore Diffusion Model Equations (Table 5.6) 318
B.4 Collocation Form of the Dimensionless Pore Diffusion Model Equations 320

Appendix C. Synopsis of PSA Patent Literature 327
C.1 Introduction 327
C.2 Inventors and Patents 328
C.3 Concluding Remarks 338

Index 345

List of Symbols

a	sorbate activity; external area per unit volume for adsorbent sample (Eq. 2.46)
A	adsorbent surface area per mole (Eq. 2.10); $A_{cs} + A'$ (Table 5.10); membrane area (Eq. 8.1)
A'	cross-sectional area of column wall (Table 5.10)
A_{cs}	internal cross-sectional area of column
A_s	Helmholtz free energy (Eq. 2.11)
$A(k, i)$	collocation coefficient for internal (intraparticle) concentration profile (Appendix B)
$AH(j, i)$	collocation coefficient for velocity profile during pressurization (Appendix B)
$Ax(j, i)$	collocation coefficient for the external (fluid-phase) concentration profile (Appendix B)
b	Langmuir constant
b_o	pre-exponential factor $\left(b = b_o e^{-\Delta U/RT}\right)$
B	mobility coefficient (Eq. 2.29); constant in Eq. 4.76
$B(k, i)$	collocation coefficient for the intraparticle (internal) phase Laplacian
$Bx(j,i)$	collocation coefficient for the external fluid-phase Laplacian
c	sorbate concentration in gas phase
c_o	sorbate concentration in feed
C	total gas-phase concentration
C_g	volumetric heat capacity of gas (ρC_p)
C_s	volumetric heat capacity of solid (ρC_p)
$C_{p\ \mathrm{steel}}$	heat capacity of steel wall (mass basis) (Table 5.10)
d	internal diameter of adsorbent column
D	diffusivity
D_c	micropore or intracrystalline diffusivity
D_e	effective diffusivity
D_K	Knudsen diffusivity
D_L	axial dispersion coefficient
D_m	molecular diffusivity
D_p	pore diffusivity
E	diffusional activation energy
E_A	enrichment of heavy component $\left(\bar{y}/y_{AF}\right)$
$f_{i,j}$	isotherm function for component i at composition j
f'_j	isotherm slope (dq^*/de) at composition j
F	total feed volume
F_s	free energy of adsorbed phase (Eq. 2.11)
F_A, F_B	fractions of components A, B desorbed from column during depressurization
G	purge-to-feed velocity ratio
G_s	Gibbs free energy of adsorbed phase (Eq. 2.8)
h	overall heat transfer coefficient
ΔH	enthalpy change on adsorption
J	flux of sorbate
k	overall mass transfer (LDF) rate coefficient based on adsorbed phase concentration
K	adsorption equilibrium constant or isotherm slope; constant in Eq. 7.5
K_c	adsorption equilibrium constant on crystal (microparticle) volume
K'	adsorption equilibrium constant or isotherm slope based on sorbate pressure
K_o, K'_o	pre-exponential factors (Eq. 2.2)
K_L	effective thermal conductivity of steel wall (Table 5.10)
L	adsorbent bed length
L_B, L_A	phenomenological coefficients

M	molecular weight; constant in quadratic isostherm expression
n	exponent in Freundlich isotherm expression
n_a	moles of adsorbable component (Eq. 2.8)
n_s	moles of solid adsorbent (Eq. 2.8)
N	flux relative to fixed frame of reference (Eq. 2.26); total moles (gaseous and adsorbed) in bed at time t
p	partial pressure of sorbate
p_s	saturation vapor pressure
P	absolute pressure (in column)
P'	rate of change of pressure during feed step (Eq. 4.35)
P_H	high pressure (at end of pressurization)
P_F	feed pressure
P_L	low pressure (during purge step)
P_{cH}	high pressure for compressor
P_{cL}	low pressure for compressor
Pe	Peclet number $(v_{oH}L/D_L)$
$\wp$	absolute pressure ratio P_H/P_L
$\wp_1$	pressure ratio P_H/P_F
$\wp_F$	pressure ratio P_F/P_L
$\wp_H$	pressure ratio P_H/P_L (end of pressurization versus end of blowdown)
$\wp_c$	absolute compression ratio P_{cH}/P_cL
q	adsorbed phase concentration
q^*	equilibrium value of q
q_o	value of q at equilibrium with feed (concentration c_o)
$\overline{q}$	value of q averaged over an adsorbent particle
q_s	saturation limit
Q	molar gas flow rate
r	radial coordinate in microparticle
r_c	microparticle radius
r_{in}, r_{out}	inner and outer radii of column
R	radial coordinate in a microparticle; gas constant (R_g); product recovery
R_p	macroparticle radius
S_E	equilibrium selectivity K_A/K_B
S_k	kinetic selectivity D_A/D_B
Sh	Sherwood number $2R_pk_f/D_m$
t	time
t^*	adsorption or desorption time
T	temperature
T_o	feed temperature
ΔU	internal energy change or adsorption
v	interstitial gas velocity
v_o	interstitial gas velocity at inlet
$\overline{v}$	dimensionless interstital gas velocity v/v_{oH}
V	volume
w_c	velocity of concentration front
w_t	velocity of temperature front
w'_c	velocity of shock front
x	mole fraction (of component A) in adsorbed phase; dimensionless adsorbed phase concentration averaged over a macroparticle $\overline{q}_i/\overline{q}_{is}$
x_c	dimensionless adsorbed phase concentration averaged over a microparticle (q/q_s)
X	fraction of complete purge
y	mole fraction of A in gas phase

$\overline{y}_{bd}$	average mole fraction (of raffinate product *B*) in blowdown gas
$\overline{y}_{pdt}$	average mole fraction (of raffinate product *B*) in high-pressure product stream
z	axial distance
Z	dimensionless axial distance z/L

Greek Symbols

α permeability ratio (intrinsic separation factor); $t_H/(t_H+t_L)$ (in Table 5.9)

α' separation factor $x(1-y)/y(1-x)$ or $y(1-x)/x(1-y)$

α_k kinetic selectivity (effective)—see Eq. 2.46

β parameter characterizing heat effect $\left[(\Delta H/C_s)(\partial q^*/\partial T)_p\right]$ in Eq. 2.46; adsorption selectivity parameter β_A/β_B; b_iC

β_i ratio of hold-up component i in void space as fraction of total hold-up $\left[1+((1-\varepsilon)/\varepsilon)K_i\right]^{-1}$

γ ratio of gas heat capacities at constant pressure and constant volume

γ_E ratio of Langmuir constants b_B/b_A

γ_k ratio of micropore diffusivities D_{cB}/D_{cA}

γ_s ratio of saturation capacities q_{Bs}/q_{As}

Γ dimensionless parameter $(r_c^2/D_{Ac})(3k_f/R_p)(C/q_{As})$

Γ' dimensionless parameter $(r_c/D_{Ac})(C/q_{As})k_f$

ε voidage of adsorbent bed

$\int_p$ porosity of adsorbent particle

ζ $\left[1+\xi P_H y_F \beta_{A_0}(1-\beta)\right]^{-1}$ (Chapter 4)

η mechanical efficiency of compression; dimensionless radial coordinate R/R_p

θ adsorption selectivity parameter θ_A/θ_B

θ_i dimensionless concentration q_i/q_{is} (Chapters 2 and 5); parameter $\theta_i(P,y_1,y_2)=\left[1+((1-\varepsilon)/\varepsilon)((f_{i2}-f_{i1})/(y_{i2}-y_{i1}))(RT/P_H)\right]^{-1}$, where 1 and 2 refer to arbitrary states (Chapter 4)

θ_c dimensionless adsorption or desorption time $(\grave{o}_p D_p/R_p^2)(c_0/q_0)t^*$ (for macropore control) or $D_c t^*/r_c^2$ for micropore control

λ ratio of dead volume to column volume; non-linearity parameter q_o/q_s

μ chemical potential; viscosity; mean residence time in column

Ξ parameter $((1-\varepsilon)/\varepsilon)(M_A/RT)$

ξ $(1-\varepsilon)M_A/\varepsilon R$

ρ density

σ^2 variance of pulse response

τ dimensionless time variable, tv_{OH}/L (LDF model); tD_c/r_c^2 (pore diffusion model)

ϕ parameter $\grave{o}A_{cs}LP_L/\beta_A RT$

Φ surface potential

Ω parameter defined by Eq. 5.16; integral function used in determining recovery for pressurization with feed

Subscripts

A, *B*	components *A* (more strongly adsorbed) and *B* (less strongly adsorbed)
B	blowdown step
c	micropore or intracrystalline
ci	component *i* in microparticle
C	column
DV	dead volume
e*i*	equivalent value (for component *i*) in countercurrent flow model
F	feed or feed end
G	purge-to-feed ratio
H, OH, *i*H	high-pressure step, at inlet during high-pressure step, and for component *i* during high-pressure step
i	refers to species *i* (*A* or *B*).
*i*p, *i*s	species *i* in microparticle, species *i* at saturation
I	intermediate
L, oL, *i*L	low-pressure (purge) step, at inlet during low-pressure step, and for component *i* during low-pressure step
o, o*i*	limiting or reference value, limiting or reference value for component *i*
O	outlet or effluent
p	macropore or macroparticle
P	product end or pressurization step
PU	purge step
R	rinse step
s	saturation value
S	condition following pressurization step
SH	shock wave
w	at wall
W	combined blowdown and purge step effluent; waste or byproduct
0, 1, 2	initial state, ahead of shock, and behind shock
Superscript	* is sometimes used to denote and emphasize “equilibrium value”

Figure Credits

Chapter 2

Figure 2.3 From H. Jüntgen, K. Knoblauch, and K. Harder, *Fuel* **60**, 817 (1981). Reprinted with permission of the publishers, Butterworth-Heinemann Ltd.
Figure 2.4 From K. Chihara and M. Suzuki, *Caubon* **17**, 339 (1979). Reprinted with permission of Pergamon Press PLC.
Figure 2.12 Adapted from G. A. Sorial, W. H. Granville, and W. O. Daley, *Chem. Eng. Sci.* **38**, 1517 (1983) with permission of Pergamon Press PLC.
Figure 2.16 From H. J. Schröter and H. Jüntgen in *Adsorption Science and Technology.* NATO ASI E158, p. 289, A. E. Rodrigues, M. D. Le Van, and D. Tondeur, eds. Kluwer, Dordrecht (1989). Reprinted with permission of K. Kluwer, Academic Publishers.
Figures 2.24 and 2.25 From *Principles of Adsorption and Adsorption Processes*, by D. M. Ruthven, John Wiley, New York (1984). Reprinted with permission of John Wiley and Sons Inc.
Figure 2.26 From A. I. Liapis and O. K. Grosser, *Chem. Eng. Sci.* **37**, 958 (1982). Reprinted with permission of Pergamon Press PLC.

Chapter 3

Figure 3.2 From G. F. Fernandez and C. N. Kenney, *Chem. Eng. Sci.* **38**, 834 (1983). Reprinted with permission of Pergamon Press PLC.
Figure 3.5 From C. W. Skarstrom in *Recent Developments in Separation Science* Vol 2, p. 95, N. N. Li, ed., CRC Press, Cleveland, OH (1975). Reprinted with permission of the copyright holder, CRC Press, Boca Raton, FL.
Figure 3.10 From J. C. Davis, *Chemical Engineering*, Oct 16th, 1972 p. 88. Excerpted from *Chemical Engineering* by special permission. Copyright (1972) McGraw Hill Inc, New York, NY 10020.
Figure 3.14 Reprinted with permission from R. T. Yang and S. J. Doong, *AIChE Jl* **31**, 1829 (1985). Copyright American Institute of Chemical Engineers.
Figures 3.15 and 3.16 From K. Knoblauch, *Chemical Engineering* **85** (25), 87 (1978). Excerpted from *Chemical Engineering* by special permission. Copyright (1972) McGraw Hill Inc, New York, NY 10020.
Figure 3.19 From A. Kapoor and R. T. Yang, *Chem. Eng. Sci.* **44** 1723 (1989). Reprinted with permission of Pergamon Press PLC.

Chapter 4

Figure 4.24 From A. E. Rodrigues, J. M. Loureiro, and M. D. Le Van, *Gas Separation and Purification* **5**, 115 (1991). Reprinted with permission of the publishers, Butterworth-Heinemann Inc.
Figure 4.25 From Z. P. Lu, J. M. Loureiro, A. E. Rodrigues, and M. D. Le Van, *Chem. Eng. Sci.* **48**, (1993). Reprinted with permission of Pergamon Press PLC.
Figure 4.26 From D. M. Scott, *Chem. Eng. Sci.* **46**, 2977 (1991). Reprinted with

permission of Pergamon Press PLC.
Figure 4.27 From J. Hart, M. J. Baltrum, and W. J. Thomas, *Gas Separation and Purification* **4**, 97 (1990). Reprinted with permission of the publishers, Butterworth-Heinemann Inc.

Chapter 5

Figure 5.1 (a) Reprinted from the PhD thesis of P. M. Espitalier-Noel, University of Surrey (1988); (b) Reprinted from the PhD thesis of H. S. Shin, University of Ohio (1988); with kind permission of the authors.
Figure 5.2 From A. Kapoor and R. T. Yang, *Chem. Eng. Sci.* **44**, 1723 (1989). Reprinted with permission of Pergamon Press PLC.
Figure 5.5 Reprinted with permission from P. L. Cen, W. N. Chen, and R. T. Yang, *Ind. Eng. Chem. Process Design Develop.* **24**, 1201 (1985). Copyright 1985, American Chemical Society.
Figures 5.6 and 5.7 From A. Kapoor and R. T. Yang, *Chem. Eng. Sci.* **44**, 1723 (1989). Reprinted with permission of Pergamon Press PLC.
Figure 5.11 Reprinted with permission from M. Suzuki, *AIChE Symp. Ser.* **81** (242), 67 (1985). Copyright American Institute of Chemical Engineers.
Figure 5.13 Reprinted with permission from S. J. Doong and R. T. Yang, *AIChE Jl* **32**, 397 (1986). Copyright American Institute of Chemical Engineers; and from P. Cen and R. T. Yang, *Ind. Eng. Chem. Fund* **25**, 758 (1986). Copyright 1986, American Chemical Society.
Figure 5.14 Reprinted from the PhD thesis of P. M. Espitalier-Noel, University of Surrey (1988), with kind permission of the author.

Chapter 6

Figures 6.2 and 63 Reprinted with permission from D. H. White and G. Barclay, *Chem. Eng. Prog.* **85** (1), 25 (1989). Copyright American Institute of Chemical Engineers.
Figure 6.4 From C. W. Skarstrom in *Recent Developments in Separation Science*, Vol. 2, N. N. Li, ed., p. 95, CRC Press, Cleveland (1975). Reprinted with permission of the copyright holder, CRC Press Inc., Boca Raton, FL.
Figure 6.7 From J. Smolarek and M. J. Campbell in *Gas Separation Technology*, p. 28, E. F. Vansant and R. Dewolfs, eds., Elsevier, Amsterdam (1990). Reprinted with permission of Elsevier Science Publishers BV.
Figures 6.10 (a) and (c) and 6.11 From S. Sircar in *Adsorption Science and Technology*, NATO ASI E158 p. 285, A. E. Rodrigues, M. D. Le Van, and D. Tondeur eds., Kluwer, Dordrecht (1989). Reprinted with permission of Kluwer, Academic Publishers.
Figure 6.13 From T. Tomita, T. Sakamoto, U. Ohkamo, and M. Suzuki in *Fundamentals of Adsorption II*, p. 569 (1986), A. I. Liapis, eds. Reprinted with permission of the Engineering Foundation.
Figure 6.16 From E. Pilarczyk and K. Knoblauch in *Separation Technology*, p. 522 (1987), N. Li and H. Strathmann, ed. Reprinted with permission of the Engineering Foundation.
Figure 6.17 From H. J. Schröter and H. Juntgen in *Adsorption Science and Technology* NATO ASI E158 p. 281 (1989). Reprinted with permission of Kluwer, Academic Publishers.

Figure 6.18 From E. Pilarczyk and H. J. Schröter in *Gas Separation Technology*, p. 271 (1990), E. F. Vansant and R. Dewolfs, eds. Reprinted with permission of Elsevier Science Publishers BV.
Figure 6.19 Reprinted with permission from R. T. Cassidy and E. S. Holmes, *AIChE Symp. Ser.* **80** (233), 74 (1984). Copyright American Institute of Chemical Engineers.
Figure 6.20 From S. Sircar in *Adsorption and Technology*, p. 285, NATO ASI 158, A. E. Rodrigues, M. D. Le Van, and D. Tondeur, eds., (1989). Reprinted with permission of Kluwer, Academic Publishers; and from R. Kumar et al., paper presented at AIChE National Meeting, Houston, April 1991, with permission of the authors.
Figure 6.24 From S. Sircar, Fourth International Conference on Adsorption, Kyoto, May 1992 (plenary lecture). Reprinted with permission of the author.
Figures 6.25 and 6.26 From R. Banerjee, K. G. Narayankhedkar, and S. P. Sukhatine, *Chem. Eng. Sci.* **45**, 467 (1990). Reprinted with permission of Pergamon Press PLC.
Figure 6.27 From R. Banerjee and K. G. Narayankhedkar, *Chem. Eng. Sci.* **47**, 1307 (1992). Reprinted with permission of Pergamon Press PLC.

Chapter 7

Figure 7.1 Reprinted with permission from N. H. Sweed, *AIChE Symp. Ser.* **80** (233), 44 (1984). Copyright American Institute of Chemical Engineers.
Figures 7.2 and 7.3 Reprinted with permission from U.S. Patent 4,354,854 (1982), with kind permission of George Keller II.
Figures 7.5, **7.6**, **7.7 and 7.8** Reprinted from reports of Highquest Engineering Inc., with kind permission of Bowie Keefer, Highquest Engineering Inc.
Figure 7.10 Reprinted with permission from C. W. Kenney, Proceedings of 5th Priestley Conference on Gas Separations, Birmingham (1989) p. 273–286. Copyright Royal Society of Chemistry.
Figure 7.11 Reprinted with permission from P. H. Turnock and R. A. Kadlec, *AIChE Jl* **17**, 335 (1971). Copyright American Institute of Chemical Engineers.
Figures 7.12 and 7.13 Reprinted with permission from D. E. Kowler and R. H. Kadlec, *AIChE Jl* **18**, 1207 (1972). Copyright American Institute of Chemical Engineers.
Figure 7.14 Reprinted with permission from S. J. Doong and R. T. Yang, *AIChE Symp. Ser.* **84** (264), 145 (1988). Copyright American Institute of Chemical Engineers.
Figure 7.15 Reprinted from a hitherto unpublished manuscript with kind permission of the authors D. M. Scott, E. Alpay, and C. N. Kenney.

Chapter 8

Figure 8.3 From K. Haraya, T. Hakuta, K. Obuta, Y. Shindo, N. Itoh, K. Wakabayshi, and H. Yoshitome, *Gas Separation and Purification* **1**, 4 (1987). Reprinted with permission of the publishers, Butterworth-Heinemann Ltd.
Figure 8.4 From W. J. Koros, G. K. Fleming, S. M. Jordan, T. H. Kim, and H. H. Hoehn, *Progress in Polymer Sci.* **13**, 339 (1988). Reprinted with permission of Pergamon Press PLC.
Figure Figure 8.6 (c) Reprinted with permission of Dow-Generon Inc.
Figure 8.10 From R. M. Thorogood, *Gas Separation and Purification* **5**, 83 (1991). Reprinted with permission of the publishers, Butterworth-Heinemann Ltd.
Figure 8.11 Reprinted with permission from R. W. Spillman, *Chemical Engineering*

Progress **85** (1), 41 (1989). Copyright American Institute of Chemical Engineers.

CHAPTER 1 Introduction

Pressure swing adsorption (PSA) is not a new process and, like most good inventions, with the advantage of hindsight the principle appears obvious. As in all adsorption separation processes, the essential requirement is an adsorbent that preferentially adsorbs one component (or one family of related components) from a mixed feed. This selectivity may depend on a difference in adsorption equilibrium or on a difference in sorption rates (kinetic selectivity). In certain cases the difference in rates may be so great that the slower-diffusing species is in effect totally excluded from the adsorbent (size-selective sieving), and in this situation a very efficient separation can obviously be achieved.

All adsorption separation processes involve two principal steps: (1) *adsorption*, during which the preferentially adsorbed species are picked up from the feed; (2) *regeneration* or *desorption*, during which these species are removed from the adsorbent, thus "regenerating" the adsorbent for use in the next cycle. The general concept is shown in Figure 1.1. It is possible to obtain useful products from either the adsorption or regeneration steps or from both steps. The effluent during the adsorption step is purified "raffinate" product from which the preferentially adsorbed species have been removed. The desorbate that is recovered during the regeneration step contains the more strongly adsorbed species in concentrated form (relative to the feed) and is sometimes called the "extract" product.

The essential feature of a PSA process is that, during the regeneration step, the preferentially adsorbed species are removed by reducing the total pressure, rather than by raising the temperature or purging with a displacing agent (although a low-pressure purge step is commonly included in the cycle). The process operates under approximately isothermal conditions so that the useful capacity is the difference in loading between two points, corresponding to the feed and regeneration pressures, on the same isotherm [Figure 1.1(a)]. Figure 1.1(b) shows schematically the movement of the concentration profiles during the high-pressure feed and low-pressure regeneration steps. The feed step is normally terminated before the more strongly adsorbed component breaks through the bed, while the regeneration step is generally terminated before the bed is fully desorbed. At cyclic steady state the profile therefore oscillates about a mean position in the bed.

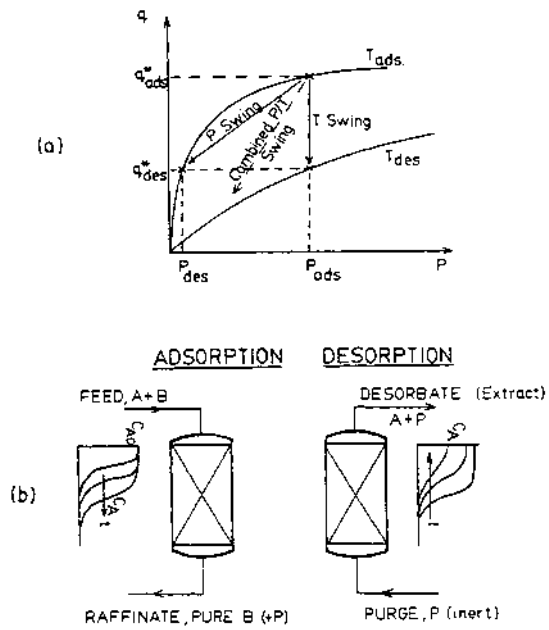

Figure 1.1 The concept of a PSA process, (a) Change in equilibrium loading with pressure, (b) Idealized sketch showing movement of the adsorbed phase concentration profile for the more strongly adsorbed species in a simple two-bed PSA process.

A major advantage of PSA, relative to other types of adsorption process such as thermal swing, is that the pressure can be changed much more rapidly than the temperature, thus making it possible to operate a PSA process on a much faster cycle, thereby increasing the throughout per unit of adsorbent bed volume. The major limitation is that PSA processes are restricted to components that are not too strongly adsorbed. If the preferentially adsorbed species is too strongly adsorbed, an uneconomically high vacuum is required to effect desorption during the regeneration step. Thus, for very strongly adsorbed components thermal swing is generally the preferred option since a modest change of temperature produces, in general, a relatively large change in the gas–solid adsorption equilibrium constant.

PSA processes are no more complex than most of the more conventional separation processes, but they are different in one essential feature: the process operates under transient conditions, whereas most processes such as absorption, extraction, and distillation operate under steady-state conditions. As a result, both the conceptual framework and the design procedures are quite different. This difference can best be explained in mathematical terms. A steady-state process can be described mathematically by an ordinary differential equation (or a set of ordinary differential equations), and to obtain the relationship between the operating variables and the process performance requires only the integration of this set of equations. By contrast, a transient process is described by a set of partial differential equations and this requires a more complex solution procedure. As a result the relationship between the process performance and the operational variables is generally less obvious. Procedures for the design and scaleup of PSA units are for the most part available in the open literature. However, they have not yet been generally accepted as part of the normal chemical engineering curriculum and, as a result, a certain air of mystery persists.

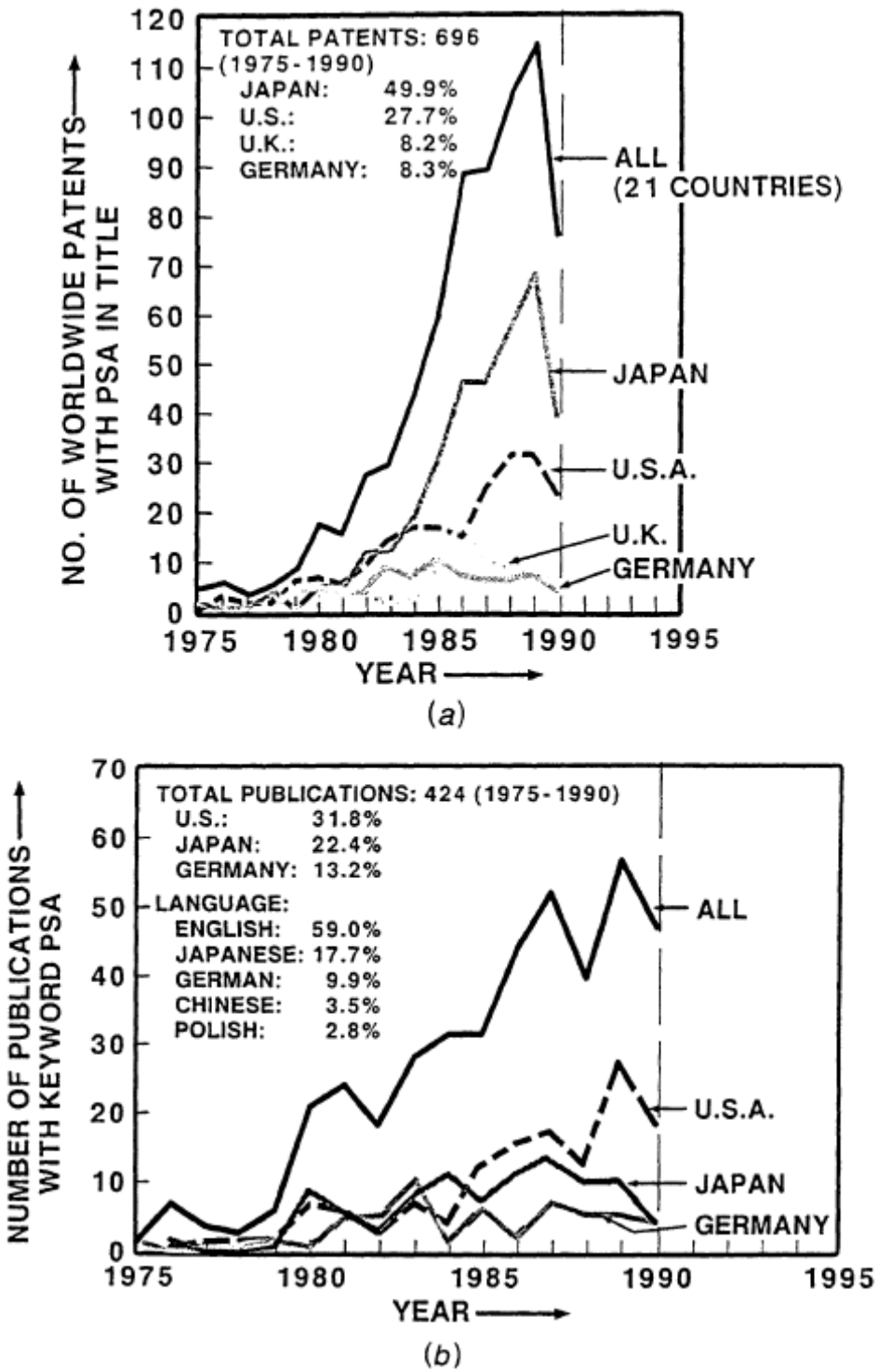

Figure 1.2 The growth of PSA technology from 1975 to 1990 as shown by (a) numbers of patents and (b) numbers of publications. (Courtesy of Dr. S. Sircar, Air Products and Chemicals, Inc.)

Despite their early inception, it was really only during the 1980s that PSA processes gained widespread commercial acceptance. This is illustrated in Figure 1.2, which shows a plot of the annual numbers of publications and U.S. patents relating to PSA processes

against the year. The reasons for this unusually long delay between the invention and commercialization of such processes are not entirely clear, but it seems likely that the opposition of entrenched interests in the cryogenic gas industry and the lack of familiarity with the underlying principles among practicing engineers were probably significant factors. During the 1970s interest in alternative separation processes was stimulated by the escalation of energy costs associated with the rising price of crude oil. Although energy costs fell during the 1980s, the impetus to examine alternative processes and to match the technology to the product specifications has continued.

1.1 Historical Development of PSA Processes

The introduction of PSA processes is commonly attributed to Skarstrom[1] and Guerin de Montgareuil and Domine[2] in 1957–1958. However, many of the essential features of this type of process were delineated much earlier in the papers of Kahle[3,4] and in the pioneering patents of Hasche and Dargan,[5] Perley,[6] and Finlayson and Sharp,[7]* which were filed between 1927 and 1930 but have been largely overlooked by more recent authors. The Air Liquide process, developed by Guerin de Montgareuil and Domine, utilized a vacuum swing, whereas the Esso process, pioneered by Skarstrom, used a low-pressure purge to clean the adsorbent bed following the blowdown step. Details of both cycles, which are still in common use, are given in Chapter 3. Some other key dates in the chronological development of PSA technology are summarized in Table 1.1. The patents mentioned are discussed in greater detail in Appendix C.

Table 1.1 Milestones in the Historical Development of PSA Processes[a]

Date	
1930–1933	First PSA patents issued to Finlayson and Sharp (U.K. 365,092), Hasche and Dargan (U.S. 1,794,377), and Perley (U.S. 1,896,916)
1953–1954	Papers by H. Kahle[3,4] outlining the principle of PSA (including heat storage) and giving details of a PSA process for removal of CO_2, hydrocarbons, and water vapor from air
1955–1956	Synthetic zeolites produced commercially
1957–1958	French patent 1,223,261, P. Guerin de Montgareuil and D. Domine (Air Liquide)[2]; the "vacuum swing" PSA cycle is described. U.S. Patent 2,944,627, C. W. Skarstrom (Esso Research and Engineering)[1]; the low–pressure purge step is introduced, and the importance containing the thermal wave is emphasized
1960–1965	Development and commercialization of the "Heatless Drier" for small-scale air drying and early versions of the "Isosiv" process for separation of linear hydrocarbons
1965–1970	Development and commercialization of PSA hydrogen purification
1970–1972	First large-scale O_2 PSA processes
1972–1973	O_2 selective carbon sieves produced commercially
1976	PSA nitrogen process using CMS adsorbent
1976–1980	Small–scale medical oxygen units
1982	Large–scale vacuum swing processes for air separation
1988	Second generation zeolite adsorbents for air separation by vacuum swing, making VSA competitive with cryogenic distillation up to 100 tons/day

[a] See also R. T. Cassidy and E. S. Holmes, *AIChE. Symp. Series* **80**(233) 68–75 (1984).

* The authors are grateful to Dr. Norman Kirkby of the University of Surrey for pointing out this reference.

1.2 General Features of a PSA Process

There are five general features of a PSA system that to a large extent explain both the advantages and limitations of the technology and hence determine the suitability for a given application:

1. Product purity. The raffinate product (the less strongly adsorbed or slower-diffusing species) can be recovered in very pure form, whereas the extract product (the more strongly adsorbed or faster-diffusing species) is generally discharged in impure form as a byproduct. Various modifications to the cycle are possible to allow recovery of the preferentially adsorbed species. However, these all add complexity to the cycle; so the process fits best where a pure raffinate product is required.
2. Yield or fractional recovery. In a PSA process, the fractional recovery (i.e., the fraction of the feed stream that is recovered as pure product) is generally relatively low compared with processes such as distillation, absorption, or extraction. The recovery can be increased by including additional steps in the cycle and by increasing the number of adsorbent beds, but both these modifications increase the capital cost. A PSA process therefore fits best when the feed is relatively cheap so that a high product yield is not a matter of primary concern.
3. Concentration of trace impurities. Where a highly selective adsorbent is available a PSA process can provide a valuable means of concentrating trace impurities, but this application has not yet been developed to any significant extent.
4. Energy requirements. Like most separation processes, the energy efficiency of a PSA process is relatively low. The First Law efficiency (separation work relative to energy consumed) is in fact comparable with that of processes such as distillation or extraction, but a PSA system uses mechanical energy, which is in general more expensive than heat. The power cost is the major component of the operating cost for a PSA system. However, if the feed is already available at high pressure, these costs may be greatly reduced, since not only are the capital costs and power requirement reduced, but the cost of product recompression will generally be much lower than the cost of compressing the feed to the higher operating pressure. A PSA system is therefore especially useful where the feed is available at elevated pressure.

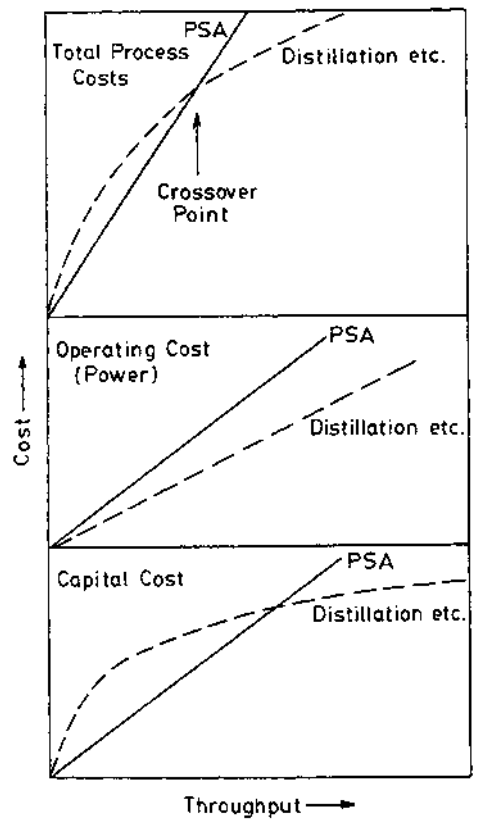

Figure 1.3 Variation of cost with throughput for PSA and cryogenic air separation processes.

5. Scaling characteristics. The operating costs of most separation processes increase approximately linearly with throughput. The capital cost of a PSA process is also approximately linear with throughput, but for most other processes the capital cost curve is highly nonlinear, with the incremental cost being smaller for the larger units (Figure 1.3). As a result, when the overall costs are considered, the economics tend to favor PSA at low to moderate throughputs and to favor other processes such as cryogenic distillation for very large-scale operations. Of course the actual costs and the crossover point vary considerably depending on the particular separation and the process configuration, but the form of the cost versus throughput curve is generally similar.
6. Pressure range. The term *vacuum swing adsorption* (VSA) is often used to denote a PSA cycle with desorption at subatmospheric pressure. This is a semantic choice. The performance of any PSA process is governed by the ratio of absolute (rather than gauge) pressures. That desorption at subatmospheric pressure often leads to improved performance is due to the form of the equilibrium isotherm rather than to any intrinsic effect of a vacuum.

1.3 Major Applications of PSA

Some of the major commercial PSA processes are listed in Table 1.2, and a summary of the chronology is given in Table 1.1. The first three applications (air separation, air drying, and hydrogen purification) were in fact foreseen and demonstrated by Skarstrom.[1,8] These

remain the most important practical applications for this technology, although newer processes such as carbon dioxide recovery and natural gas purification are gaining increased acceptance. In all three of the major processes the feed is relatively cheap, so that the relatively low recovery is not an overriding economic factor. In both air drying and hydrogen recovery a pure raffinate product is required, and in hydrogen recovery the impure hydrogen is often available at elevated pressure. Purity of the product is important in nitrogen production, but generally somewhat less so in oxygen production. In a typical hydrogen purification process the product purity is commonly 99.995% or even higher. For nitrogen production a purity of 99.9% is easily attainable, but it is generally more economic to produce 99.5% N_2 by PSA with final polishing by a "de oxo" unit. The commonly quoted oxygen product purity of 93–95% is somewhat misleading since the impurity is almost entirely argon—which is adsorbed with the same affinity as oxygen on most adsorbents.

Table 1.2. Some Major PSA Processes

Process	Product	Adsorbent	Type of System
H_2 recovery from fuel gas	Ultrapure H_2	Act. C or zeolite	Multiple-bed system
Heatless drier	Dry air (for instruments)	Act. $A1_2O_3$	Two-bed Skarstrom cycle (or vacuum–pressure swing cycle
Air separation	O_2 (+Ar)	5A Zeolite	Two-bed Skarstrom cycle
Air separation	N_2(+ Ar)	CMS	Two-bed self-purging cycle
Air separation	N_2 and O_2	5A Zeolite or CaX	Vacuum swing system
Isosiv	Linear/Branched hydrocarbons	5A Zeolite	Molecular sieve separation with vacuum swing
Landfill gas separation	CO_2 and CH_4	CMS	Vacuum swing

The largest-scale PSA processes are generally to be found in petroleum refinery operations—hydrogen purification and hydrocarbon separation processes such as Isosiv. In such processes product rates up to 10^6 SCFH (> 100 tons/day) are not uncommon. In the other main areas of application (drying and air separation) PSA units are generally economic only at rather smaller scales. For example, for large-scale oxygen or nitrogen production (> 100 tons/day) it is difficult to compete economically with cryogenic distillation. However, there are many small-scale uses for both oxygen and nitrogen (e.g., home oxygen units for asthmatic patients and nitrogen units for purging the fuel tanks of fighter aircraft or for purging the interiors of trucks and warehouses to prolong the shelf life of fruit and vegetables). For such applications the robustness and portability of a PSA system provide additional advantages that reinforce the economic considerations. In these applications the most direct competition comes from small-scale membrane systems, which offer many of the same advantages as a PSA system. A brief comparison of these two classes of process is included in Chapter 8.

To understand the process options and the factors involved in design and optimization of PSA systems, some background in the fundamentals of adsorption and the dynamic behavior of adsorption columns is required. These aspects are considered in Chapter 2. A wide variety of different cycles have been developed in order to increase energy efficiency,

improve product purity, and improve the flexibility of the operation. The basic cycles and a few of the more advanced cycles are reviewed in Chapter 3, while more detailed aspects of process modeling are discussed in Chapters 4 and 5. Chapter 6 is devoted to a detailed description of some current PSA processes, while some of the future trends in process development are discussed in Chapter 7.

References

1. C. W. Skarstrom, U.S. Patent 2,944,627 (Feb. 1958) to Esso Research and Engineering Company.
2. P. Guerin de Montgareuil and D. Domine, French Patent 1,223,261 (Dec. 1957) to Air Liquide. See also U.S. Patent 3,155,468 (1964) to Air Liquide.
3. H. Kahle, *Chemie Ing. Technik* **23**, 144 (1953).
4. H. Kahle, *Chemie Ing. Technik* **26**, 75 (1954).
5. R. L. Hasche and W. N. Dargan, U.S. Patent 1,794,377 (1931).
6. G. A. Perley, U.S. Patent 1,896,916 (1933).
7. D. Finlayson and A. J. Sharp, U.K. Patent 365,092 (Oct. 15, 1930) to British Celanese Corp.
8. C. W. Skarstrom, "Heatless Fractionation of Gases over Solid Adsorbents," In *Recent Developments in Separation Science*, Vol. II, pp. 95–106, N. Li ed., CRC Press, Cleveland (1972).

CHAPTER 3
PSA Cycles: Basic Principles

The mode of operation of a PSA separation process was explained in general terms in Chapter 1 without any discussion of the details of the operating cycle. The choice of a suitable operating cycle is in fact critical, and a wide range of different cycles have been proposed to optimize different aspects of the overall process. The underlying principles governing the choice of operating cycle are reviewed in this chapter.

PSA processes may be categorized according to the nature of the adsorption selectivity (equilibrium or kinetic) and whether the less strongly (or less rapidly) adsorbed species (the raffinate product) or the more strongly (or more rapidly) adsorbed species (the extract product) is recovered at high purity. The various possible combinations of these criteria yield four different classes of process. Since the factors that dominate the choice of operating cycle and the mode of operation are somewhat different, these four categories are discussed sequentially.

3.1 Elementary Steps

Any PSA cycle can be considered as a sequence of elementary steps, the most common of which are:

1. Pressurization (with feed or raffinate product);
2. High-pressure feed with raffinate withdrawal;
3. Depressurization or "blowdown" (cocurrent or countercurrent to the feed);
4. Desorption at the lower operating pressure; this may be accomplished by evacuation, purging the bed with the raffinate product or, in a kinetically controlled process, by slow equilibration with consequent evolution of the slower-diffusing sorbate;
5. Pressure equalization (which is used in many cycles, prior to the blowdown step, to conserve energy and separative work);
6. Rinse (purging with the preferentially adsorbed species at high pressure, following the adsorption step).

Table 3.1. Summary of the Elementary Steps Used in PSA Cycles

Elementary step	Mode of operation	Principal features
Pressurization	1. Pressurization with feed from the feed end	Enrichment of the less selectively adsorbed species in the gas phase at the product end
	2. Pressurization with raffinate product from the product end prior to feed pressurization	Sharpens the concentration front, which improves the purity and recovery of raffinate product

High-pressure adsorption	1. Product (raffinate) withdrawal at constant column pressure	Raffinate product is delivered at high pressure
	2. The column pressure is allowed to decrease while the raffinate product is drawn from the product end	Very high recovery of the less selectivity adsorbed species may be achieved, but the product is delivered at low pressure
Blowdown	1. Countercurrent blowdown to a low pressure	Used when only raffinate product is required at high purity; prevents contamination of the product end with more strongly adsorbed species
	2. Cocurrent blowdown to an intermediate pressure prior to countercurrent blowdown	Used when extract product is also required in high purity; improves extract product purity and may also increase raffinate recovery
Desorption at low pressure	1. Countercurrent desorption with product purge	Improves raffinate product at the expense of decrease in recovery; purge at subatmospheric pressure reduces raffinate product loss but increases energy cost
	2. Countercurrent desorption without external purge	Recovery enhancement while maintaining high product purity is possible only in certain kinetic separation
	3. Evacuation	High purity of both extract and raffinate products; advantageous over product purge when the adsorbed phase is very strongly held
Pressure equalization	The high- and low-pressure beds are either connected through their product ends or the feed and product ends of the high-pressure bed are connected to the respective ends of the low-pressure bed	Conserves energy and separative work
Rinse	The bed is purged with the preferentially adsorbed species after high-pressure adsorption at feed pressure in the direction of the feed	Improves extract product purity when the lighter species are coadsorbed in large amount with heavier components

The processes differ from one another in the sequence of the elementary steps and in the way in which these steps are carried out. Some of the more important variants and the benefits derived from them are summarized in Table 3.1.

To understand a PSA cycle properly it is necessary to know the way in which the

concentration profile moves and changes shape during each of the elementary steps. Gas-phase concentration profiles in an adsorption column that undergoes in sequence pressurization, high-pressure adsorption, blowdown, and low-pressure desorption are shown in Figure 3.1 for both equilibrium and kinetic separations. The profiles were calculated for pressurization with feed gas (from the feed end with the product end closed), reverse flow blowdown, and desorption with product purge, also in the reverse flow direction. It is clear that the movements of the concentration wave are similar in both cases. During pressurization the initial gas in the bed is pushed toward the closed product end, where it forms a plateau that is significantly enriched in the less strongly adsorbed species. The region before the plateau shows the penetration of the feed gas. This behavior is in agreement with the profiles measured by Fernandez and Kenney[1] for air pressurization in a bed of 5A zeolite (Figure 3.2). In the high-pressure feed step the concentration wave front travels down the column, and a raffinate product, enriched in the less strongly adsorbed species, is withdrawn at the product end. In the blowdown and purge steps the concentration wavefront is pushed back and a relatively clean initial bed condition is established for the next cycle. The more important features of these steps and their variants will be discussed in relation to various different cycles.

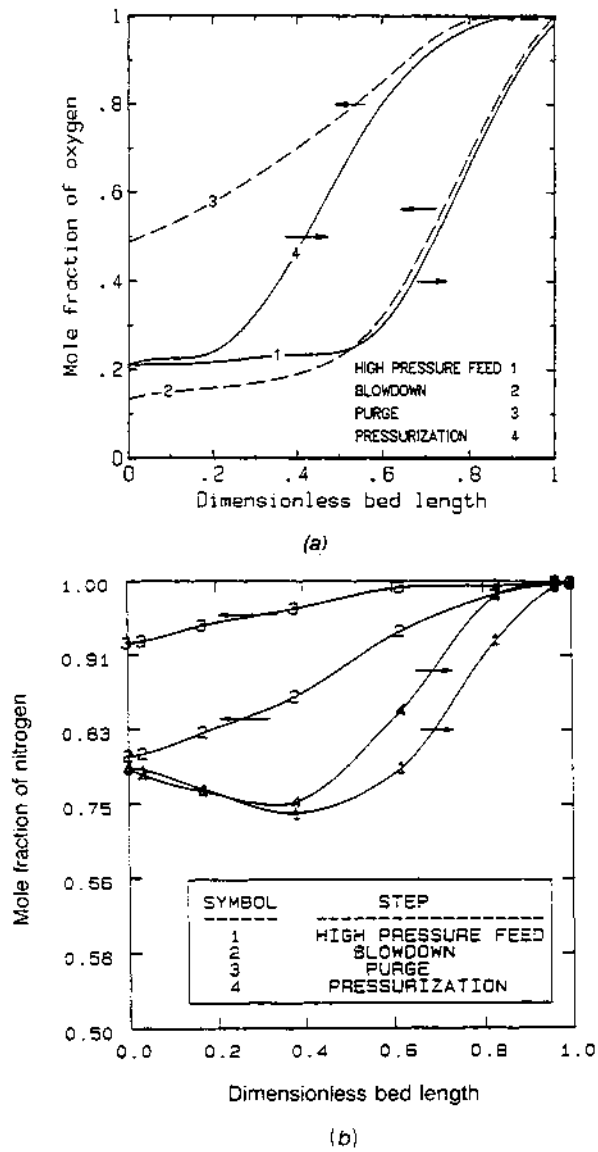

Figure 3.1 Computed steady-state gas-phase concentration profiles at the end of four elementary steps in (a) equilibrium-controlled PSA separation of air on 5A zeolite and (b) kinetically controlled separation of air on a modified 4A zeolite. The arrows indicate the direction of flow, the sequence of operation is 4,1,2,3; the simulation models are described in Section 5.2.

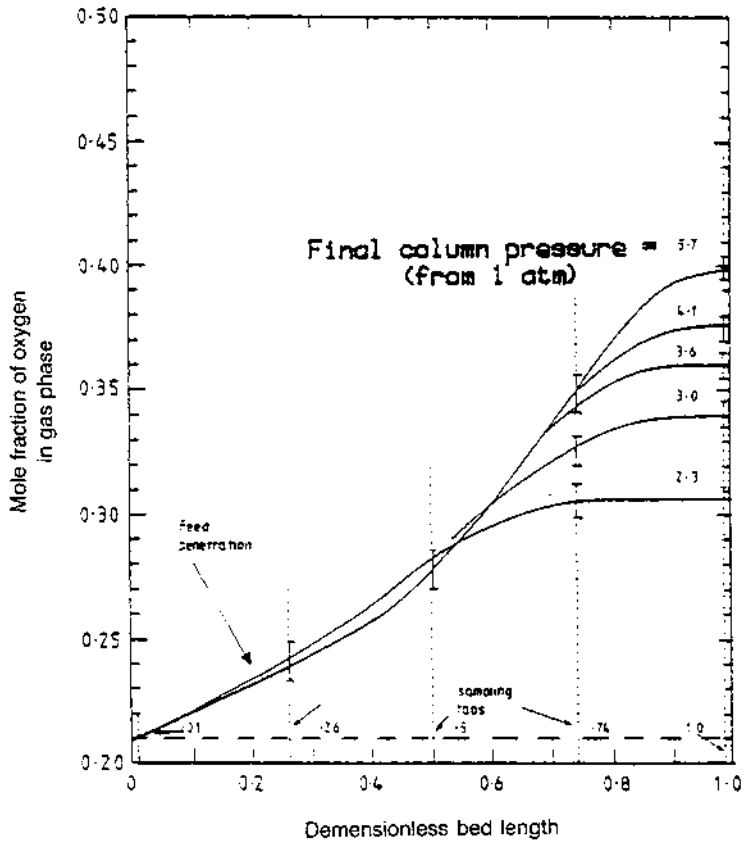

Figure 3.2 Experimental concentration profiles for air pressurization in a bed of 5A zeolite. The lines represent the best curves through the experimental data. (From Ref. 1; reprinted with permission.)

3.2 Equilibrium-Controlled Separations for the Production of Pure Raffinate Product

The early PSA cycles were developed for equilibrium separations, primarily for the recovery of the less strongly adsorbed raffinate product at high purity. In such a process the purity of the raffinate product and the extent of adsorbent regeneration depend on the partial pressure of the strongly adsorbed species in the void volume of the column at the end of the desorption step. In that step the desorbing gas, which is rich in strongly adsorbed species, occupies the void volume of the column, and, unless adequately removed from the bed, this gas will contaminate the raffinate product. The early PSA cycles were based on two different techniques for regenerating the adsorbent and cleaning the void volume. The cycle developed by Skarstrom[2] (see the following) employed atmospheric desorption with product purge, while the Air Liquide cycle[3] utilized vacuum desorption. Evacuation to a very low absolute pressure may be necessary to achieve reasonable regeneration by vacuum desorption, especially when the isotherm for the more strongly adsorbed component is of favorable (type I) form. However, vacuum desorption has other advantages (such as reduction in the power requirement) and is still widely used, particularly for kinetic separations.

3.2.1 The Skarstrom Cycle

The Skarstrom cycle[2,4] in its basic form utilizes two packed adsorbent beds, as shown schematically in Figure 3.3. The following four steps comprise the cycle:

1. Pressurization;
2. Adsorption;
3. Countercurrent blowdown; and
4. Countercurrent purge.

Both beds undergo these four operations and the sequence, shown in Figure 3.4, is phased in such a way that a continuous flow of product is maintained. In step 1, bed 2 is pressurized to the higher operating pressure, with feed from the feed end, while bed 1 is blown down to the atmospheric pressure in the opposite direction. In step 2, high-pressure feed flows through bed 2. The more strongly adsorbed component is retained in the bed and a gas stream enriched in the less strongly adsorbed component leaves as effluent at a pressure only slightly below that of the feed. A fraction of the effluent stream is withdrawn as product and the rest is used to purge bed 1 at the low operating pressure. The direction of the purge flow is also opposite to that of the feed flow. Steps 3 and 4 follow the same sequence but with the beds interchanged.

During the high-pressure adsorption step the gas phase behind the front has essentially the feed composition, while the composition beyond the front is enriched in the weak sorbate. Feeding continues until the product impurity level rises to the acceptable limit. In other words, the concentration front of the strong sorbate is allowed to break through to a preassigned limit. The idea behind the purge step is to flush the void spaces within the bed and to ensure that at least the end of the bed from which product will be withdrawn in the next half-cycle is completely free of the strong sorbate. At steady state the concentration front is pushed back in the blowdown and desorption steps by a distance that is exactly equal to the distance it has advanced in the pressurization and high-pressure adsorption steps. Reverse-flow regeneration prevents retention of the more strongly adsorbed species at the product end, thereby reducing the purge requirement. For highly favorable systems, forward-flow regeneration would require an unpractically large volume of purge to ensure complete cleaning of the bed through to the product end.

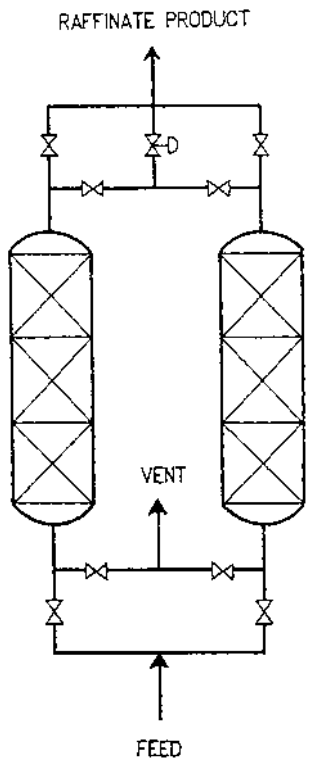

Figure 3.3 The basic two-bed pressure swing adsorption system.

From the preceding discussion it is clear that increasing purge improves product purity but at the expense of a decrease in product recovery, and after a certain point the gain in product quality becomes marginal, relative to the loss of product quantity. The effects of incomplete purge have been studied in detail by Matz and Knaebel.[5]

The original Skarstrom cycle was used for air drying.[2] This process, with a silica gel desiccant, was shown to reduce water content from 3800 ppm to less than 1 ppm, with the recovery of dry air being about 73%.[4] The process details along with the product profile are shown in Figure 3.5. The Skarstrom cycle is still widely used for small-scale air drying, and this cycle has also proved successful for other similar separations where the impurities are present at low concentration and the selectivity of the adsorbent is high. Under these conditions the raffinate product behaves as a nonadsorbing inert.

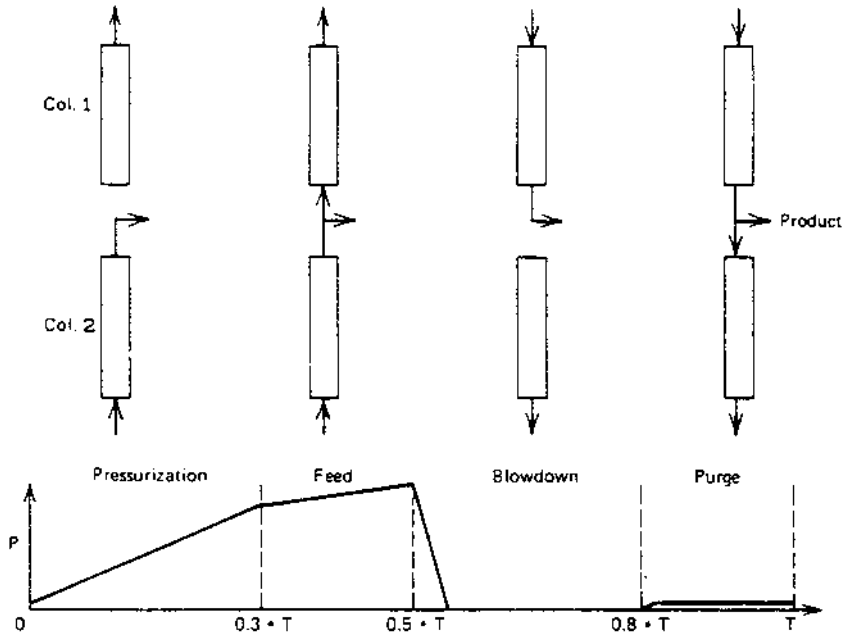

Figure 3.4 The sequence of steps in the basic Skarstrom PSA cycle.

Oxygen production from air using 5A or 13X zeolite as the adsorbent is an example of a bulk separation. The preferentially adsorbed species (nitrogen) is present at a relatively high concentration level, and there is significant coadsorption of the less strongly adsorbed species (oxygen). Such a separation can be achieved using the Skarstrom cycle, but a reasonably pure raffinate product can be achieved only at low fractional recovery, making the economics unattractive. In Skarstrom's original experiments using a 13X zeolite adsorbent, a 90% pure oxygen product was achieved only at a recovery of 10%.[6] The separation factor for this particular adsorbent appears to have been rather low (2.0), and a somewhat better performance can be expected with the higher separation factors (3–3.5) typically obtained with a well-dehydrated zeolite.[7] However, to improve the economics, further enhancement of the recovery–purity profile is obviously desirable.

In a Skarstrom cycle the column effluent during the blowdown and purge steps is normally waste gas (rich in the more strongly adsorbed species but containing a significant fraction of the less strongly held species). Skarstrom suggested that the purge backwash volume (measured at the purge pressure) should exceed the feed volume (measured at the high operating pressure) at all points in the beds during each cycle in order to obtain a pure product.[4] In practice the purge-to-feed volume should generally be between one and two. The relative contributions from blowdown and purge streams to the total loss of raffinate product depend on the level of the higher operating pressure. Since the product emerges at the high pressure while purging takes place at atmospheric pressure, the actual fraction of the product stream lost as purge is quite small and becomes negligible when the pressure ratio is large. On the other hand, the contribution from the blowdown loss increases with increasing pressure, and becomes completely dominant at high operating pressure, as may be seen from Figure 3.6. The improved performance of most of the more complex cycles comes from reduction of the blowdown losses.

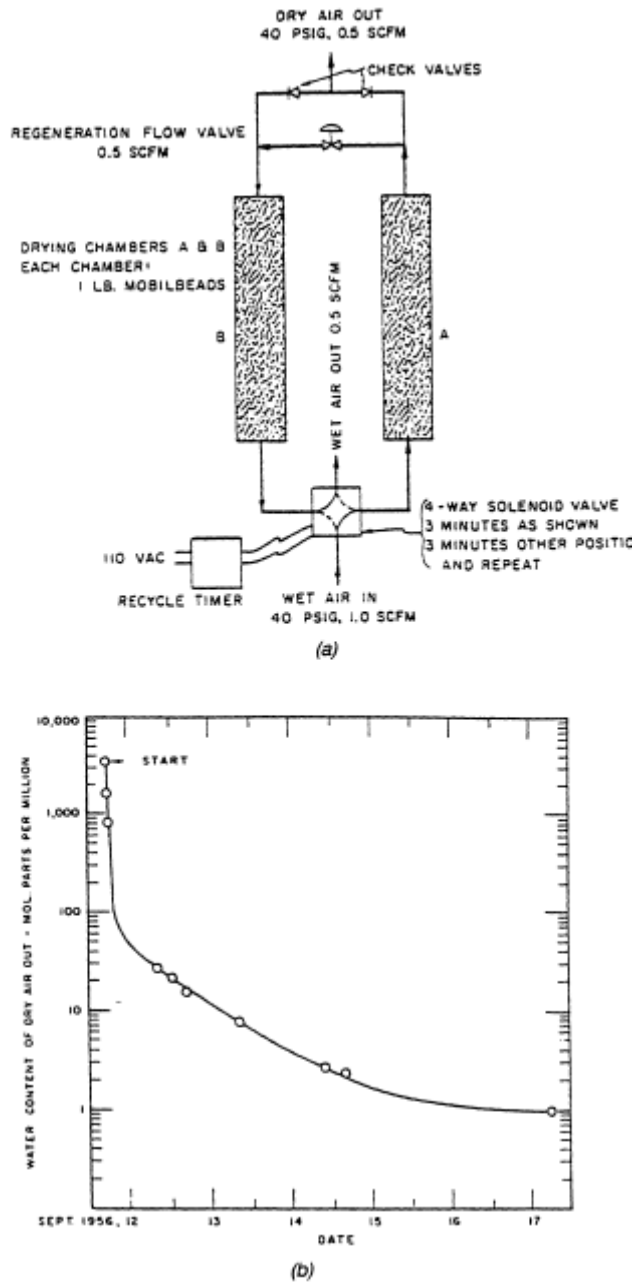

Figure 3.5 (a) Process details and (b) product profile for the PSA air drying system developed by Skarstrom. (From Ref. 4; reprinted with permission.)

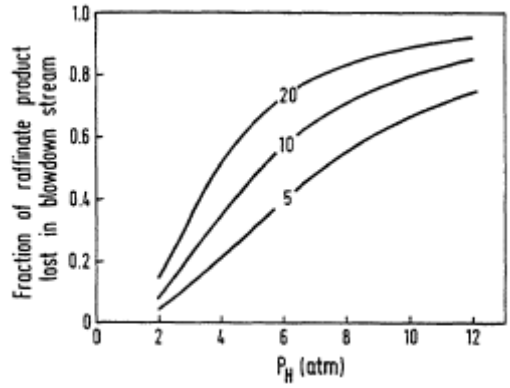

Figure 3.6 Variation of the blowdown stream contribution to the loss of raffinate product with feed pressure. A simple mass balance (assuming negligible adsorption of the raffinate product) yields for the fraction of the raffinate product lost in the blowdown stream

$$\left[1+v_{\mathrm{oH}}P_{\mathrm{L}}G\bar{X}_{\mathrm{pdt}}t_{\mathrm{pu}}\big/LP_{\mathrm{H}}\left(P_{\mathrm{H}}-_{\mathrm{L}}\right)\bar{X}_{\mathrm{bd}}\right]^{-1}$$

The profiles are shown for $G = 2.0$, $P_{\mathrm{L}} = 1.0$ atm, $t_{\mathrm{pu}} = 60$ s, $\bar{X}_{\mathrm{pdt}} = 0.95$, and $\bar{X}_{\mathrm{bd}} = 0.5$. The numbers on the curves indicate L/v_{OH} ratios.

3.2.2 Pressure Equalization

The first improvement over Skarstrom's original cycle was the introduction of a pressure equalization step proposed by Berlin.[8] A schematic diagram of the improved process and the modified sequence of operations are shown in Figure 3.7. After the first bed has been purged and the second bed has completed the high-pressure adsorption step, instead of blowing down the second bed directly, the two beds are connected through their product ends to equalize the pressure. The first bed is thus partially pressurized with gas from the outlet region of the second bed. Following pressure equalization the beds are disconnected and the first bed is pressurized with feed gas while the second bed is vented to complete the blowdown. The pressure equalization step conserves energy since the compressed gas from the high-pressure bed is used to partially pressurize the low-pressure bed and, since this gas is partially depleted of the strongly adsorbed species, separative work is also conserved. Blowdown losses are reduced to about half, with consequent improvement in the recovery of the raffinate product, as may be seen from Figure 3.8.

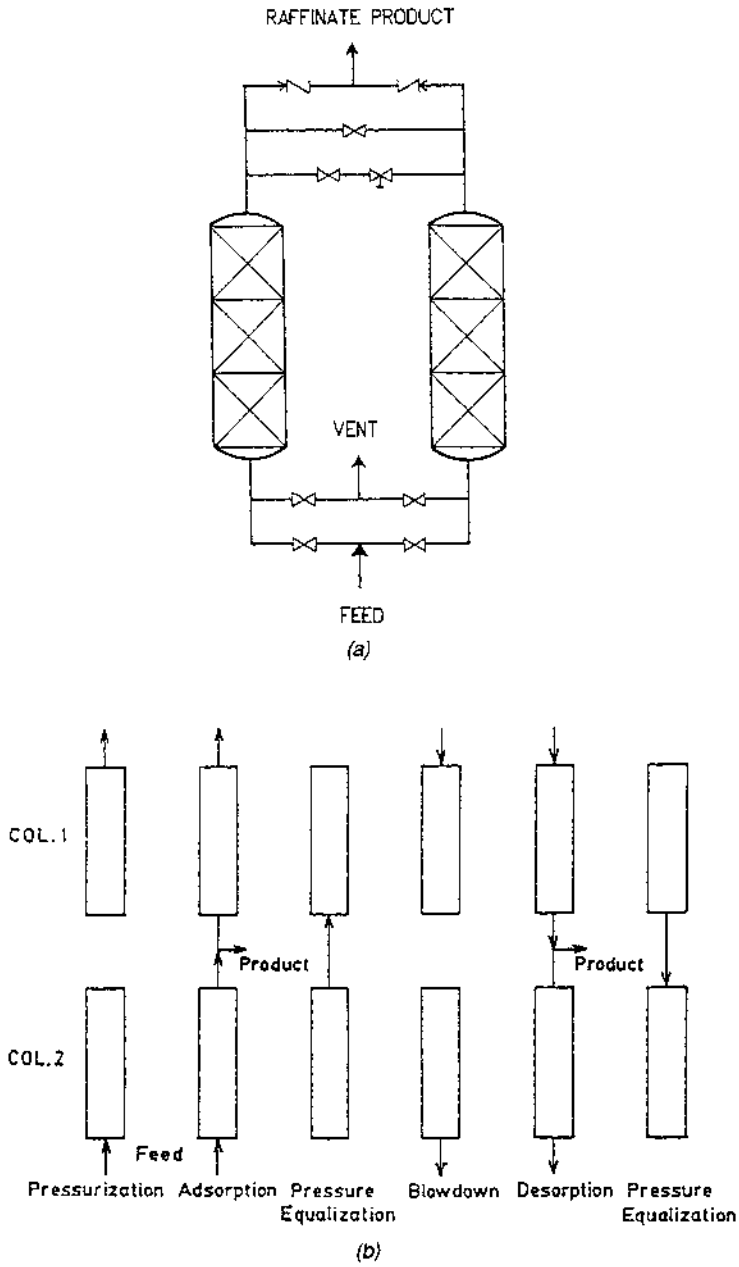

Figure 3.7 (a) Schematic diagram and (b) the sequence of operations in the modified Skarstrom cycle including pressure equalization.

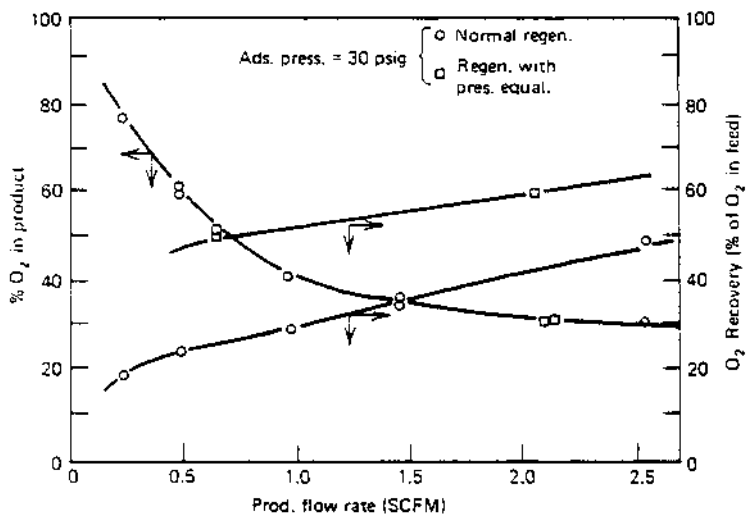

Figure 3.8 Purity and fractional recovery of O_2 in a two-bed PSA air separation unit showing improvement in recovery obtained by inclusion of pressure equalization step. (From Ref. 4; reprinted with permission.)

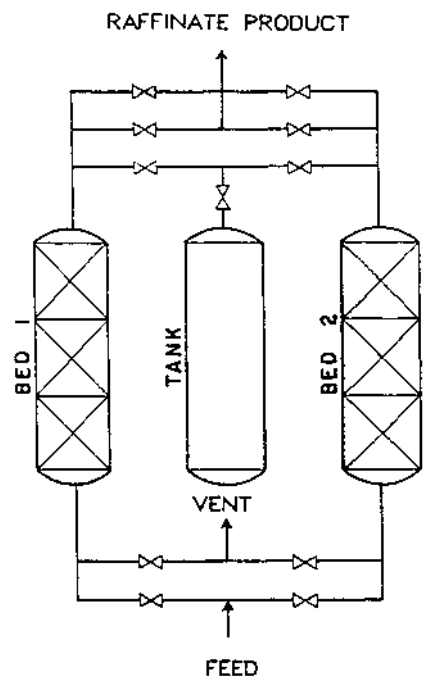

Figure 3.9 Schematic diagram of a PSA cycle showing the use of a third empty tank for reducing blowdown loss.

Prior to Berlin's modification of the Skarstrom cycle, another patent based on a different idea for reducing blowdown loss was assigned to Marsh et al.[10] The process scheme, shown in Figure 3.9, requires an empty tank in addition to the two adsorbent beds. At the end of the high-pressure adsorption step but well before breakthrough, the feed flow is stopped and the product end of the high-pressure bed is connected to the empty tank where a portion of the compressed gas, rich in the raffinate product, is stored. The blowdown of the high-pressure bed is completed by venting to the atmosphere in the

reverse-flow direction. The stored gas is then used to purge the bed after which the bed is finally purged with product gas. The product purge requirement is reduced, thereby increasing the recovery, but the savings in the specific energy of separation is less with this arrangement than with a direct pressure equalization step.

3.2.3 Multiple-Bed Systems

Further improvements in efficiency are generally achieved by using multiple adsorbent beds with a sequence of pressure equalization steps incorporated into the cycle.[11,12] In fact, multiple-bed systems also use the blowdown gas for purging other beds. Since this is done at a pressure level where further pressure equalization is not worthwhile, the resulting gain in recovery yields an additional benefit. One such example is shown schematically in Figure 3.10, which shows a typical large-scale air separation process for oxygen production. In this system, which utilizes three or four columns, one column is in the adsorption step and the other two (or three) columns are in various stages of pressurization, depressurization, or purging. The process operates at two intermediate pressures between the feed pressure and the exhaust pressure (usually atmospheric). At the end of the adsorption step, column 1, which is at high pressure, is connected at the discharge end to column 2, and the pressures are equalized. Prior to pressure equalization column 2 has just completed the purge step and is essentially at atmospheric pressure. A fraction of the remaining gas from bed 1 is used for reverse-flow purging of bed 3. When the pressure in bed 1 has fallen to the required level, beds 1 and 3 are disconnected and the residual gas from bed 1 is vented to atmosphere from the bed inlet. Bed 1 is then purged in reverse flow with gas from the fourth bed and repressurized to the first intermediate pressure from the second bed, which has just completed the adsorption step. Final repressurization is accomplished using a part of the product gas and the feed is then connected to the inlet of bed 1. The cycle configuration is summarized in Figure 3.11.

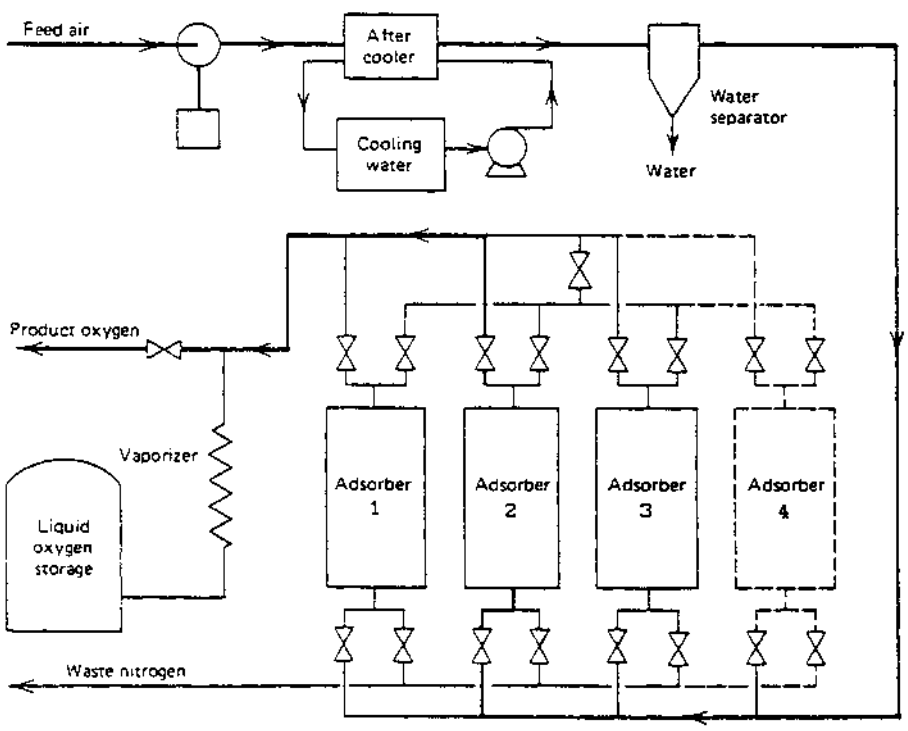

Figure 3.10 Schematic diagram of a three- or four-bed PSA system for air separation. (From Ref. 11; reprinted with permission.)

Vessel Number												
1	Adsorption			EQ1 ↑	CD ↑	EQ2 ↑	CD ↓	Purge ↓	EQ2 ↓	EQ1 ↓	R ↓	
2	CD ↓	Purge ↓	EQ2 ↓	EQ1 ↓	R ↓		Adsorption			EQ1 ↑	CD ↑	EQ2 ↑
3	EQ1 ↑	CD ↑	EQ2 ↑	CD ↓	Purge ↓	EQ2 ↓	EQ1 ↓	R ↓		Adsorption		
4	EQ1 ↓	R ↓		Adsorption			EQ1 ↑	CD ↑	EQ2 ↑	CD ↓	Purge ↓	EQ2 ↓

EQ—Equalization
CD —Cocurrent depressurization
CD —Countercurrent depressurization
R—Repressurization

↑—Cocurrent flow
↓—Countercurrent flow

Figure 3.11 Summary of the cycle for a four-bed PSA unit. (From Ref. 13; reprinted with permission.)

The idea of product repressurization was put forward for the first time in a very similar patent for hydrogen purification by Wagner.[14] Pressurization with product pushes the residual adsorbed components toward the feed end of the adsorber, thereby enhancing the product purity. The four-bed configuration allows continuous product withdrawal and eliminates the use of an empty tank for storing purge gas.

In multiple-bed systems greater conservation of energy and separative work are achieved at the cost of a more complex process scheme. In some large-scale hydrogen purification PSA systems up to twelve adsorbent beds are used.

3.2.4 Vacuum Swing Cycle

The simplest way to understand a vacuum swing cycle (VSC) is to consider it as a Skarstrom cycle in which the low-pressure countercurrent product purge step is replaced by a vacuum desorption. The product end of the column is kept closed and the vacuum is pulled through the feed end as shown in Figure 3.12. In a vacuum swing cycle, using the same high operating pressure as a Skarstrom cycle, for the same product purity, the loss of the less favorably adsorbed species in the evacuation step is normally less than the corresponding loss in the purge. The gain in raffinate recovery is achieved here at the expense of the additional mechanical energy required for the evacuation step. A significant energy saving is possible if the cycle is operated with the higher pressure slightly above atmospheric pressure and a very low desorption pressure. In the low-pressure (linear) range of the adsorption isotherm it is the pressure ratio and not the actual high-and low-pressure levels that determines the achievable purity and recovery. A vacuum swing cycle will therefore be advantageous over a Skarstrom cycle if a low-pressure product is acceptable. However, this advantage in operating cost is to some extent offset by the increased capital cost arising from the increased size of the equipment.

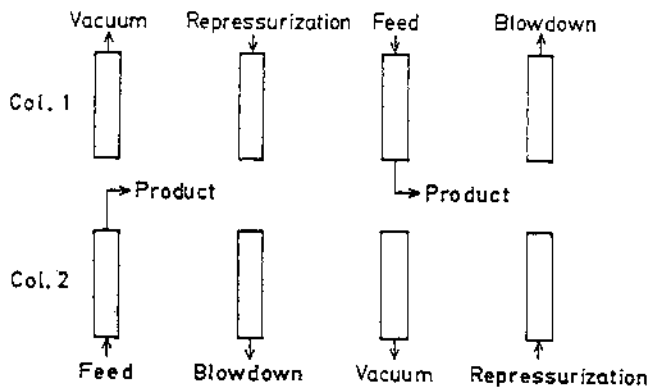

Figure 3.12 The sequence of steps in a vacuum swing cycle.

The idea of vacuum regeneration was originally proposed by Guerin de Montgareuil and Domine in a patent assigned to Air Liquide.[3] There are, however, several differences between the pressure swing cycle proposed by Montgareuil and Domine and the simplified vacuum swing cycle shown in Figure 3.12. Depending on the nature of the gas mixture to be separated, the Air Liquide process can vary in the number of adsorbent beds, the type of bed association, and the scheme of cyclic operation, as well as in other operating conditions. The number of beds can vary from one to six or more. A two-bed illustration of this process is given in Figure 3.13. Bed 1 is pressurized to the high operating pressure by introducing a compressed feed gas from the inlet end. The inlet end is then closed and the gas is expanded cocurrently through bed 2 and the effluent from this bed is recovered as raffinate product. When the pressure in bed 1 reaches a predetermined intermediate pressure, the discharge end of bed 1 is closed and the vacuum line (located at the middle of the bed) is opened for regeneration. At the same time the inlet end of bed 2 is opened to high-pressure feed stream, with the discharge end closed, for repressurization. The major disadvantage of the Air Liquide cycle is that the product is delivered at a low (subatmospheric) pressure. (Air separation using this cycle produced 98% oxygen at 51% recovery. This result was markedly superior to the performance of the competing Skarstrom cycle for the same separation. Additionally, the Air Liquide cycle also produces a nitrogen-rich stream (96.3% nitrogen at 58% recovery) from the evacuation step.

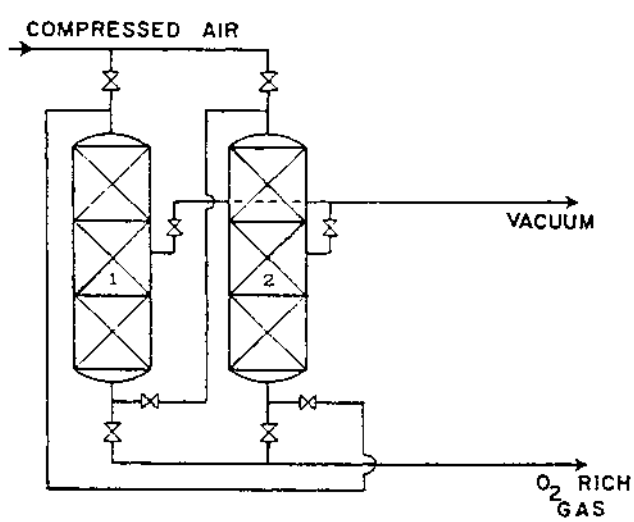

Figure 3.13 Schematic diagram of the two-bed Air Liquide PSA system. (After Montgareuil and Domine[3])

The gain in raffinate product recovery obtained here results from two improvements over the Skarstrom cycle. The recovery advantage of vacuum regeneration over purge has already been discussed. In addition, the cocurrent depressurization through an evacuated chamber actually conserves part of the raffinate product that would have otherwise been lost during evacuation. It is important to note that the gain in the raffinate recovery from cocurrent depressurization may not be achieved if this step is used in combination with (product) purge regeneration. Cocurrent depressurization contaminates the product end with the more strongly adsorbed species. Suh and Wankat[15] have shown that depending on the amount of the more strongly adsorbed species in the feed and the relative affinity of the components, the gain in the raffinate recovery from cocurrent depressurization may be outweighed by the increased purge requirement. Cocurrent depressurization is also beneficial in enhancing the purity of the strong adsorptive product (see Section 3.3).

3.3 Recovery of the More Strongly Adsorbed Species in Equilibrium-Controlled Separations

The vacuum swing cycle developed by Montgareuil and Domine and discussed in Section 3.2 was the first pressure swing process incorporating the provision for recovering the more strongly adsorbed species at high purity. The operations responsible for providing this additional benefit to the cycle are cocurrent depressurization and vacuum regeneration. The vacuum regeneration step produces the extract product. The region of the bed through which the feed penetrates during the high-pressure adsorption step is essentially at equilibrium with the feed gas. Since dispersive effects such as mass transfer resistance, axial dispersion, heat effects, and so on, are usually associated with equilibrium-controlled separation processes, there is always some spreading of the mass transfer zone. The region ahead of the mass transfer zone at the end of the high-pressure adsorption step is therefore available for further adsorption of the more strongly adsorbed species in the feed. By cocurrent depressurization the raffinate product remaining in the void space ahead of the mass transfer zone is pushed out of the bed and the more strongly adsorbed species is retained at the product end. Thus the mole fraction of the more strongly adsorbed species increases in both phases. The subsequent evacuation step therefore produces the extract product at high purity and recovery. If the situation is such that the length of unused bed prior to breakthrough is not sufficient to hold the strong adsorptive, then the high-pressure adsorption step is cut short well before breakthrough in order to provide with the additional capacity. Such an arrangement will reduce the adsorbent productivity and the optimum choice therefore depends primarily on the value of the extract product.

When the separation factor is low, the adsorbed phase concentrations of the light and heavy components are comparable. The reduction in the concentration of the lighter species in the bed as a result of cocurrent depressurization may not then be sufficient to meet the purity requirement for the extract product. A more effective method for improving extract purity is to purge (or rinse) the void spaces, after high-pressure adsorption, with the strongly adsorbed species in the direction of the feed.[16] The effluent gas during this step is produced at the feed pressure and has a feedlike composition so that the stream may easily be recycled.

The purity of the strongly adsorbed component depends critically on the use of

cocurrent depressurization or purging by the more strongly adsorbed species. The use of vacuum desorption is not particularly crucial unless one is dealing with strongly adsorbed species with a type I isotherm. For bulk separations involving components with moderate isotherm curvature, it is possible to achieve high quality of both raffinate and extract products by cycling in a pressure range above atmospheric. Yang and Doong[17] separated a 50:50 hydrogen–methane mixture over activated carbon into 97.8% hydrogen (raffinate product) with 90% recovery and 90% methane (extract product) with 89.9% recovery. Cocurrent depressurization was employed and the pressure was cycled between 120 and 35 psig. The two-bed, five-step, cycle used by Yang and Doong is shown in Figure 3.14. Cen and Yang[18] in another study repeated the same separation and demonstrated that the purity of the extract product is improved further by replacing the cocurrent depressurization step with a cocurrent methane purge step conducted at the feed pressure.

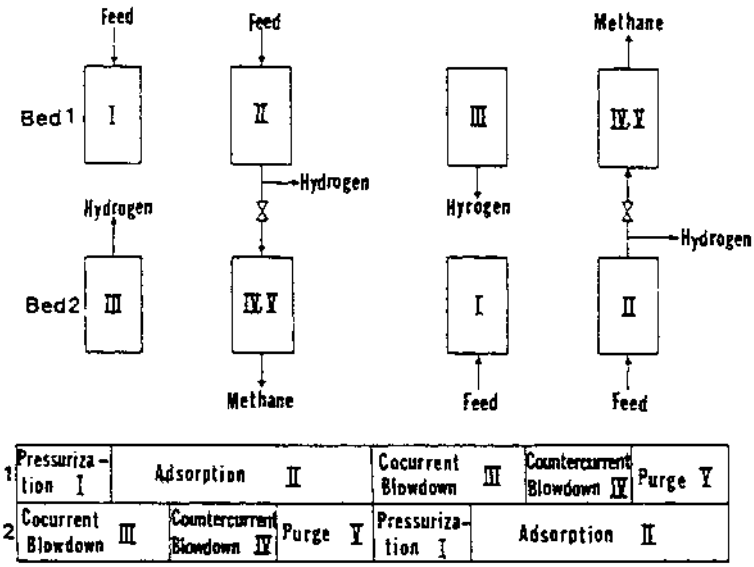

Figure 3.14 Schematic diagram of the two-bed, five-step PSA cycle used by Yang and Doong for recovery of both extract and raffinate products at high purity. (From Ref. 17; reprinted with permission.)

3.4 Cycles for the Recovery of Pure Raffinate Product in Kinetically Controlled Separations

The PSA cycles discussed so far, for both purification and bulk separation, were developed for separations based on equilibrium selectivity. The cycles used for kinetic separations are somewhat different. In such systems the choice of contact time is critical. Since the idea is to exploit the difference in the diffusion rates of the adsorbing molecules, the contact time must be short enough to prevent the system from approaching equilibrium but not so short as to preclude significant uptake. The crucial element in any kinetic separation is therefore the duration of the adsorption and desorption steps.

The only widely used commercial PSA process based on kinetic selectivity is air separation for nitrogen production using a carbon molecular sieve or 4A zeolite adsorbent. Kinetic separation of air for nitrogen production using Union Carbide RS-10 molecular sieve (modified 4A zeolite) has been investigated by Shin and Knaebel.[19] In a recent study Kapoor and Yang[20] have shown that methane–carbon dioxide separation (from landfill gas

or effluent gas from tertiary oil recovery) using carbon molecular sieve is another prospective candidate for kinetic separation.

Although with properly selected step times the Skarstrom cycle can be applied to a kinetic PSA separation, such a cycle is far from ideal. A major disadvantage is that the slowly diffusing raffinate product would be continuously adsorbed during the purge step. This difficulty can be avoided by use of vacuum desorption or by using a modified form of "self-purging" cycle.

3.4.1 Self-Purging Cycle

Equilibrium and kinetic data for the sorption of oxygen and nitrogen on the Bergbau–Forschung carbon molecular sieve[21] are shown in Figure 3.15 and summarized in Table 3.2. It is apparent that there is little difference in equilibrium but a large difference in diffusivity, with oxygen being the more rapidly adsorbed species. The high-pressure raffinate product in the carbon molecular sieve process is therefore nitrogen. In such a system purging with nitrogen to remove the faster diffusing oxygen from the bed (as in the Skarstrom cycle) is undesirable since, as well as wasting product, a certain fraction of the slowly diffusing nitrogen will be adsorbed, thus reducing the capacity for oxygen during the next adsorption step. The earlier kinetic nitrogen processes avoided this difficulty by using a vacuum to clean the bed rather than a purge, as illustrated in Figure 3.12. The general scheme for a vacuum swing carbon sieve process to produce nitrogen is shown in Figure 3.16. A better option is, however, available. At the end of the blowdown step the adsorbent contains both oxygen (fast diffusing) and nitrogen (slow diffusing). Thus, if the bed is simply closed at the product end and left for a period of time, the oxygen will diffuse out first, followed by nitrogen, so the system is, in effect, self-purging. The product purity is directly controlled by increasing feed pressure, and pressure equalization is incorporated to reduce the blowdown loss. A dual-ended pressure equalization is used in which the feed and product ends of the high-pressure bed are connected to the respective ends of the low-pressure bed. Most modern nitrogen PSA units therefore operate on the cycle shown in Figure 3.17, which incorporates both pressure equalization and a self-purging desorption step. Connecting both ends of the beds allows rapid pressure equalization and improves product purity since the oxygen-rich gas remains at the feed end of the pressurized bed. The higher recovery advantage of dual-ended pressure equalization, however, decreases with increasing product purity.

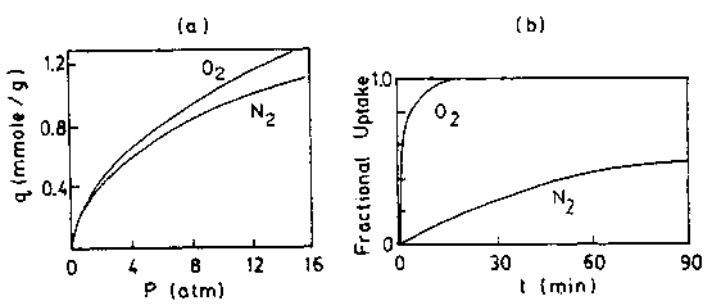

Figure 3.15 (a) Equilibrium isotherms and (b) experimental uptake curves for sorption of O_2 and N_2 on Bergbau–Forschung carbon molecular sieve. (From Ref. 21; reprinted with permission.)

Table 3.2. Equilibrium and Kinetic Data of Oxygen, Nitrogen, Methane, and Carbon Dioxide on Bergbau –Forschung Carbon Molecular Sieve and 4A Zeolite at 25°C

	Diffusional time constant (s^{-1})	Henry's constant[a]	Saturation constant (g moles/cm^3)
O_2–CMS[b]	2.70×10^{-3}	9.25	2.64×10^{-3}
N_2–CMS[b]	5.90×10^{-5}	8.90	2.64×10^{-3}
O_2–4A[c]	8.51×10^{-3}	2.10	1.72×10^{-2}
N_2–4A[c]	8.99×10^{-5}	4.26	1.20×10^{-2}
CO_2–CMS[d]	9.00×10^{-4}	135.83	2.85×10^{-3}
CH_4–CMS[d]	5.00×10^{-6}	25.83	1.74×10^{-3}

[a] Dimensionless basis.
[b] *Source*: Kinetic data from Ref. 24 and equilibrium data from Ref. 22.
[c] *Source*: Ref. 23.
[d] *Source*: Ref. 20.

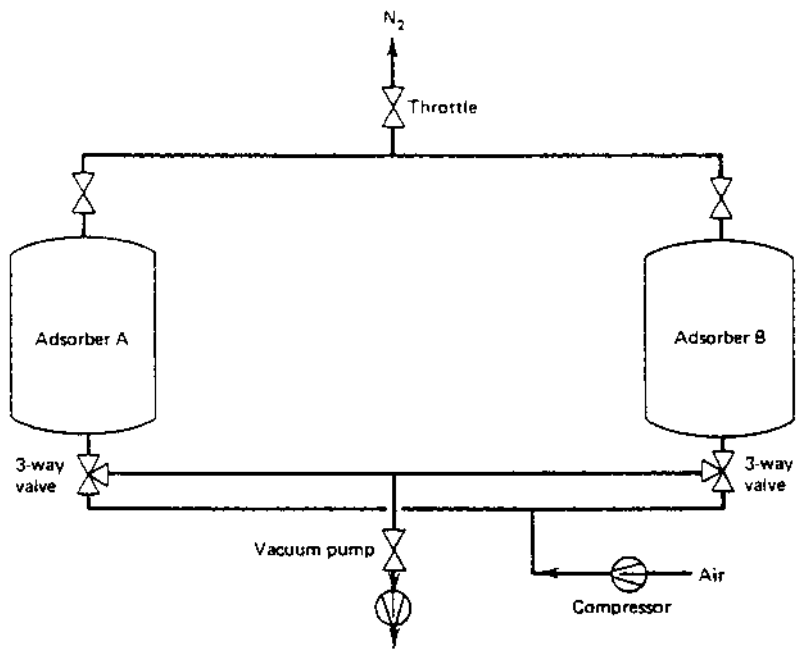

Figure 3.16 Schematic diagram of the Bergbau–Forschung PSA air separation process. (From Ref. 21; reprinted with permission.)

Kinetic selectivity may be increased by increasing the diffusivity of the faster component, oxygen, or further decreasing the diffusivity of the slower component, nitrogen. An increase in oxygen diffusivity will increase the nitrogen product purity without seriously affecting the recovery (see Figure 5.9). Intuitively it may appear that nitrogen recovery will increase with decreasing nitrogen diffusivity, and the best situation would be reached when there is practically no penetration of nitrogen. What is overlooked in this intuitive argument is the role of the desorbing nitrogen in a self-purging cycle. The desorbing nitrogen cleans the void volume of the adsorption column, and, unless there is significant uptake of nitrogen during the high-pressure adsorption step, inadequate self-purging will result in increased oxygen contamination in the nitrogen product. There is therefore a lower limit of nitrogen diffusivity below which the self-purging cycle becomes ineffective.

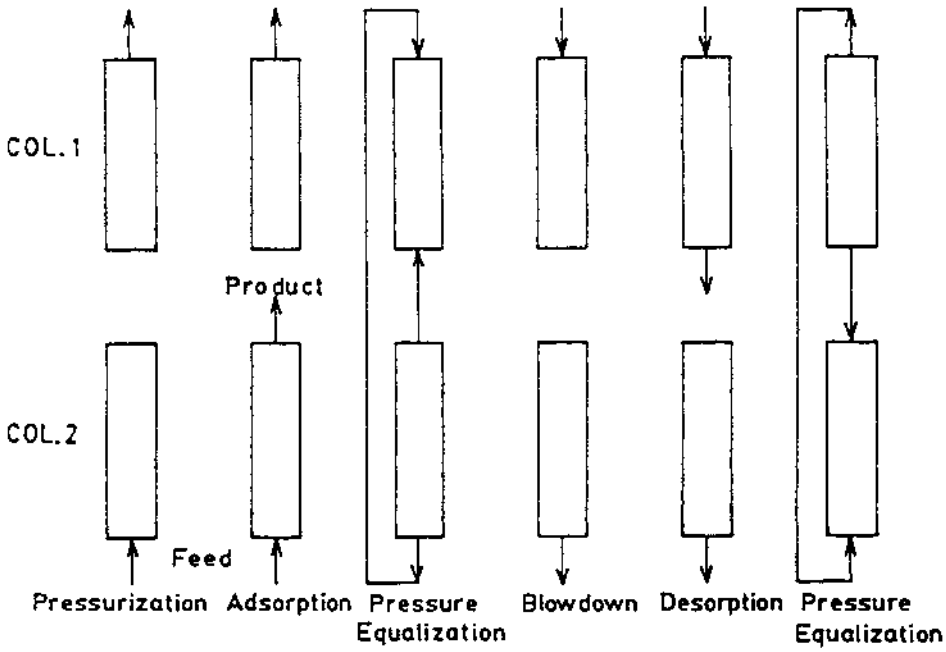

Figure 3.17 The sequence of operations in a two-bed PSA cycle including dual-ended pressure equalization and no purge.

3.4.2 Kinetic and Equilibrium Effects in Opposition

When equilibrium selectivity favors the slower-diffusing component, as in air separation for nitrogen production on modified 4A zeolite (see Table 3.2 for quantitative values), the system cannot be made self-purging since the amount of desorbing nitrogen is not sufficient to eliminate the residual oxygen concentration in the bed. For such a system conventional purge or vacuum regeneration is necessary. Shin and Knaebel[19] have reported an extensive experimental study of this system. They adopted the Skarstrom cycle in a single-bed apparatus and therefore enjoyed the additional freedom to optimize the cycle by varying independently the duration of the individual steps. Their experimental system is shown in Figure 3.18. In such an arrangement an additional tank was used for product storage (in order to supply the purge) and pressure equalization cannot be performed. However, the contents of the auxiliary tank may be used to partially repressurize the bed in a manner essentially equivalent to a pressure equalization step.

Blowdown and purge under vacuum were also investigated in this study for comparison. Some of the more important findings are summarized in Tables 3.3 and 3.4. As the pressure ratio increases, the purity increases, but the recovery is decreased. For the same purity both recovery and productivity increase with increasing feed pressure. The recovery gain is relatively less in the higher-pressure region, but the increase in productivity is consistent. Moreover, subatmospheric blowdown and purge are advantageous (in terms of recovery) at low feed pressures, but the advantage disappears as the feed pressure is increased. The latter finding further confirms that in a Skarstrom cycle blowdown loss becomes dominant at high feed pressure. Product purity may therefore be controlled by either the feed pressure or the purge rate or by a combination of both of these.

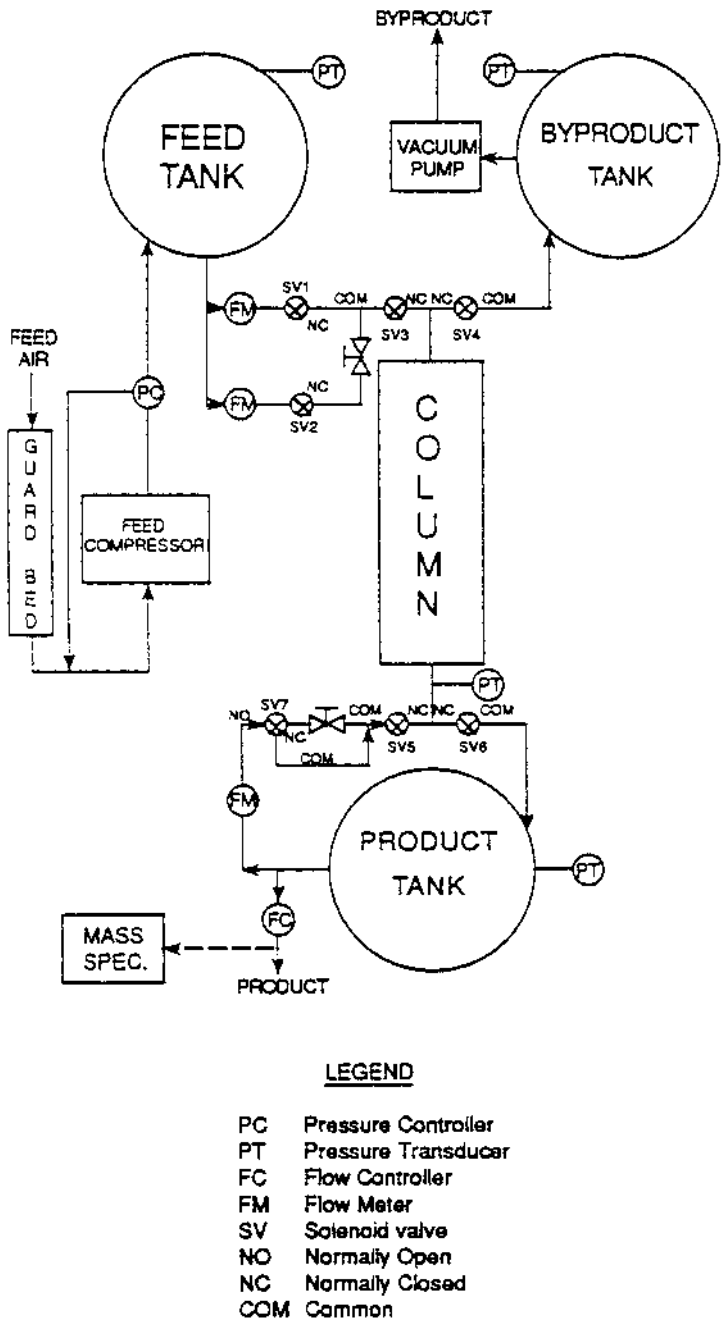

Figure 3.18 The single-bed experimental PSA system used by Shin and Knaebel to study air separation on a modified 4A zeolite. (From Ref. 19)

Table 3.3. Effect of Pressure Ratio on Separation of Air on Union Carbide RS-10 Molecular Sieve[a]

High pressure (kPa)	Low pressure (kPa)	Pressure ratio	Nitrogen recovery (%)	Product purity (mol % N_2)	Productivity
200	113	1.77	41.56	82.3	4.78
358	123	2.91	22.46	93.7	3.9
620	154	4.03	12.54	98.2	2.61
200	113	1.77	13.83	93.8	1.00

358	123	2.91	22.46	93.7	3.9
620	152	4.08	23.05	93.7	5.46

[a] High-pressure adsorption = 35 s, blowdown = 2 s, purge = 3 s, pressurization = 15 s. Purge volume = 0.0166 × 10^{-3} m^3 at STP.
Source: Ref. 19.

Table 3.4. Effect of Purge Pressure on Separation of Air on Union Carbide RS-10 Molecular Sieve[a]

High pressure (kPa)	200		358		620	
Low pressure (kPa)	113	60	123	78	152	119
Nitrogen recovery (%)	13.83	16.87	22.46	21.83	23.05	23.12
Product purity (mole % N_2)	93.8	93.8	93.7	93.7	93.7	93.7

[a] High-pressure adsorption = 35 s, blowdown = 2 s, purge = 3 s, pressurization = 15 s. Purge volume = 0.0166 × 10^{-3} m^3 STP.
Source: Ref. 19.

3.4.3 Equilibrium and Kinetic Effects Reinforce

Separation of methane from methane–carbon dioxide mixture on a carbon molecular sieve is an example where equilibrium is in favor of the faster-diffusing component, carbon dioxide. Relevant equilibrium and kinetic data are presented in Figure 3.19 and Table 3.2. A purity-versus-recovery plot for this separation (feed is 50:50 methane–to–carbon dioxide ratio) constructed from the data of Kapoor and Yang[20] in the region of their optimal operating point is shown in Figure 3.20. The effects of varying the high and low pressures and the product rates about their optimal values are also indicated. A cycle similar to that shown in Figure 3.14 was used, except that the countercurrent purge step was replaced by vacuum desorption through the feed end. It is clear from Figure 3.20 that there is an upper limit of the high operating pressure beyond which both purity and recovery decline. With atmospheric blowdown the maximum methane product purity that can be achieved by raising the adsorption pressure is therefore limited to about 70%. Further improvement in product purity is essentially controlled by the (subatmospheric) desorption pressure.

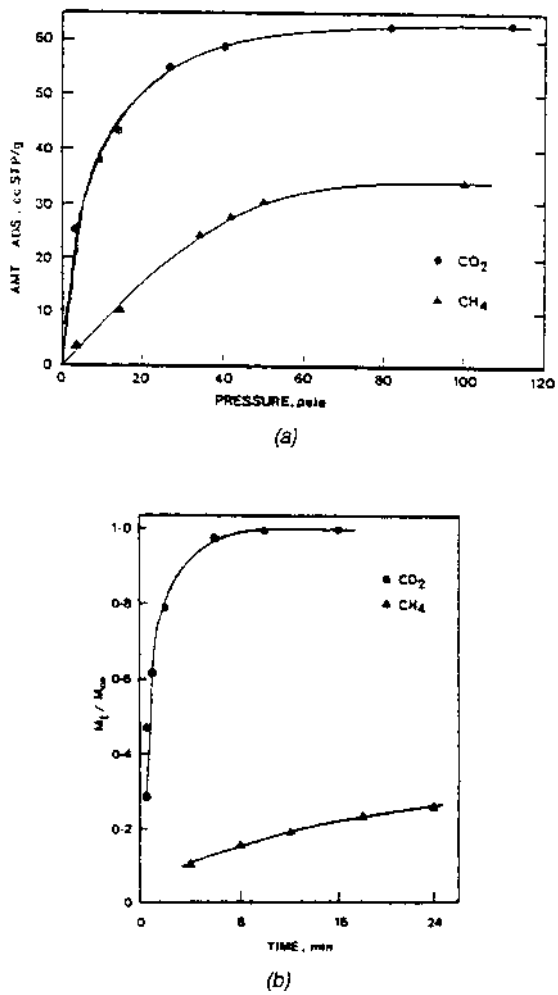

Figure 3.19 (a) Equilibrium isotherms and (b) experimental uptake curves for sorption of CO_2 and CH_4 on Bergbau–Forschung carbon molecular sieve. (From Ref. 20; reprinted with permission.)

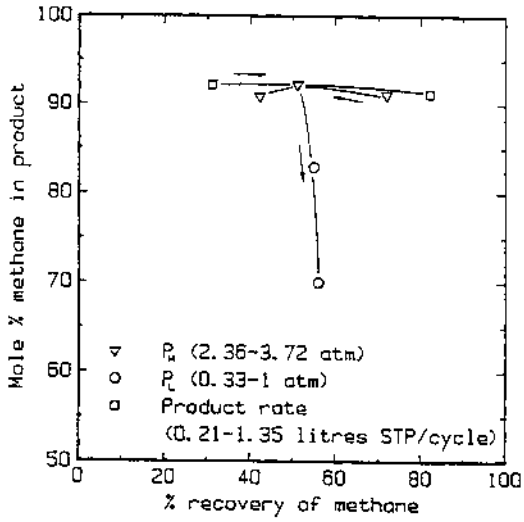

Figure 3.20 Effects of feed pressure, desorption pressure, and product rate on the experimental purity and

recovery of CH_4 from CH_4/CO_2 separation by pressure swing adsorption on a carbon molecular sieve. The arrows indicate the direction of increasing parameter values. (Data taken from Ref. 20.)

These observations provide an interesting contrast with similar performance profiles for the kinetic air separation process (Figure 3.21). In Figure 3.21 all profiles are monotonic with no evidence of an upper limit. While there must always be a theoretical limit for the high operating pressure, beyond which both recovery and purity decline, it is clear that this limit lies well beyond the normal range of operating pressures for air separation on a carbon molecular sieve and therefore does not limit the system performance. In contrast to the methane–carbon dioxide system, a high-purity nitrogen raffinate product can therefore be achieved simply by raising the adsorption pressure, without recourse to subatmospheric desorption.

The key difference between air separation and methane–carbon dioxide systems appears to lie in the shape of the equilibrium isotherm for the more strongly adsorbed species. For nitrogen–oxygen on CMS the isotherms are of linear or slightly favorable (type I) form, whereas, in the relevant pressure range, the isotherm for carbon dioxide on CMS is highly favorable, approaching the rectangular limit. If the isotherm for the faster-diffusing species is highly favorable, a very high feed pressure is not desirable, and the product purity is primarily controlled by the (subatmospheric) desorption pressure. The enhancement of performance to be expected in a kinetic PSA separation when equilibrium and kinetic effects reinforce will be observed only when the equilibrium relationship does not deviate too much from the linear form.

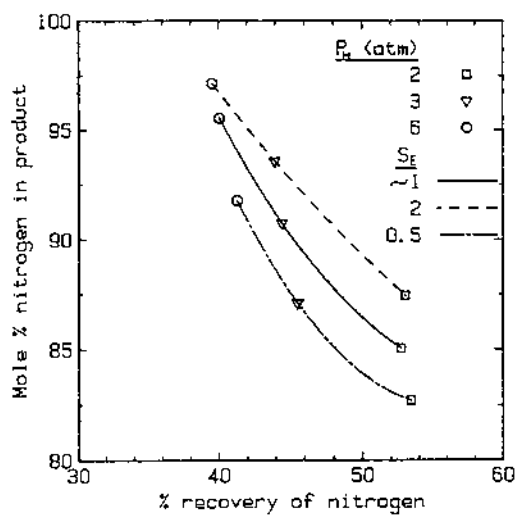

Figure 3.21 Performance of an air–carbon molecular sieve system operated on a modified Skarstrom cycle (no external purge) showing the effect of high operating pressure and equilibrium selectivity. Kinetic data and equilibrium data for $S_E \approx 1$ are given in Table 3.2. S_E has been varied by changing the oxygen equilibrium. (From Ref. 25)

3.5 Cycle for Recovery of the Rapidly Diffusing Species

In the kinetic separation of methane and carbon dioxide mixture on a carbon molecular sieve, discussed in Section 3.4, the rapidly diffusing component, carbon dioxide, was also recovered at high purity (over 90% purity and recovery). Cocurrent depressurization and

vacuum desorption, which are commonly employed in equilibrium-controlled separations to produce a high purity extract product, were, in this study, adapted to a kinetically controlled process by proper control of the contact time.

Some of the elementary steps discussed here are addressed in more detail in Chapter 4. The application of the basic principles in representative industrial PSA processes is discussed in Chapter 6.

References

1. G. F. Fernandez and C. N. Kenney, *Chem. Eng. Sci.* **38**, 834 (1983).
2. C. W. Skarstrom, U.S. Patent No. 2,944,627 (July 12, 1960), to Exxon Research and Engineering.
3. P. G. de Montgareuil and D. Domine, U.S. Patent No. 3,155,468 (1964), to Air Liquide.
4. C. W. Skarstrom, *Recent Developments in Separation Science*, Vol. 2, p. 95, N. N. Li, ed., CRC Press, Cleveland, Ohio, 1975.
5. M. J. Matz and K. S. Knaebel, *AIChE J.* **34**(9), 1486 (1988).
6. C. W. Skarstrom, U.S. Patent No. 3,237,377 (1966), to Exxon Research and Engineering.
7. S. Farooq, D. M. Ruthven, and H. A. Boniface, *Chem. Eng. Sci.* **44**(12), 2809 (1989).
8. N. H. Berlin, U.S. Patent No. 3,280,536 (Oct. 25, 1966), to Exxon Research and Engineering.
9. H. Lee and D. E. Stahl, *AIChE Symp. Ser.* **64**(134), 1 (1973).
10. W. D. Marsh, R. C. Hoke, F. S. Pramuk, and C. W. Skarstrom, U.S. Patent No. 3,142,547 (1964), to Exxon Research and Engineering.
11. J. C. Davis, *Chem. Eng.* Oct. 16 (1972), p. 88.
12. L. B. Batta, U.S. Patent No. 3,564,816 (1971), to Union Carbide Corporation.
13. R. T. Cassidy, in *A.C.S. Symp. Ser.* **135**, Adsorption and Ion Exchange with Synthetic Zeolites, W. H. Flank, ed., American Chemical Society, Washington, D.C., 1980, p. 275.
14. J. L. Wagner, U.S. Patent No. 3,430,418 (1969), to Union Carbide Corporation.
15. S.-S. Suh and P. C. Wankat, *AIChE J.* **35**(3), 523 (1989).
16. T. Tamura, U.S. Patent No. 3,797,201 (1974), to T. Tamura, Tokyo, Japan.
17. R. T. Yang and S. J. Doong, *AIChE J.* **31**(11), 1829 (1985).
18. P. L. Cen and R. T. Yang, *Separation Sci. Tech.* **21**(9), 845 (1986).
19. H.-S. Shin and K. S. Knaebel, *AIChE J.* **34**(9), 1409 (1988).
20. A. Kapoor and R. T. Yang, *Chem. Eng. Sci.* **44**(8), 1723 (1989).
21. K. Knoblauch, *Chem. Eng.* **85**(25), 87 (1978).
22. D. M. Ruthven, N. S. Raghavan, and M. M. Hassan, *Chem. Eng. Sci.* **41**, 1325 (1986).
23. O. W. Haas, A. Kapoor, and R. T. Yang, *AIChE J.* **34**(11), 1913 (1988).
24. S. Farooq and D. M. Ruthven, *Chem. Eng. Sci.* **46**(9), 2213 (1991).
25. S. Farooq and D. M. Ruthven, *Chem. Eng. Sci.* **47**(8), 2093 (1992).

CHAPTER 4

Equilibrium Theory of Pressure Swing Adsorption

4.1 Background

Since the introduction of PSA, a wide variety of mathematical models have been suggested, based on theories that extend from simple to complex. One of the first was a detailed model, presented by Turnock and Kadlec,[1] which accounts for nonlinear adsorption equilibrium, pressure drop, and temperature effects. That type of model is covered in the next chapter. Shortly thereafter, Shendalman and Mitchell[2] suggested a simpler type of PSA model, based on the assumption of local equilibrium. This type of model accounts mainly for mass conservation, and ignores transport phenomena. That might make the model seem trivial, but the basic equations of mass conservation account for time and axial position variations of flow, pressure, and composition, which are essential in pressure swing adsorbers.

The model of Shendalman and Mitchell was based on a four-step PSA cycle in which a trace contaminant was adsorbed from a nonadsorbing carrier. Thus, it applies only in very restrictive cases, such as cleanup of hydrogen or helium containing less than 1% of methane or nitrogen using activated carbon as the adsorbent. Over the past decade, there have been several extensions of the basic ideas proposed by Shendalman and Mitchell; many of these developments are explained in this chapter. For example, the model has now been extended to binary mixtures having arbitrary compositions, with both components adsorbing, and in cycles composed of diverse steps. The models are not perfect, but realistic PSA applications can be studied relatively easily.

Most PSA applications exploit equilibrium selectivity, and systems are usually designed to minimize the negative effects of mass transfer resistance. In such cases, the trends and, frequently, even precise measures of PSA performance can be predicted accurately from local equilibrium models. In particular, estimates of product recovery are often excellent, even when mass transfer resistances are large, because mass conservation predominates over diffusion and heat effects. That such models can be accurate, without requiring extensive experimental data, has made them valuable as a tool for PSA simulation and design. Other advantages of equilibrium theories are: they help to identify proper combinations of operating conditions; under certain conditions they reduce to very simple algebraic performance equations relating the operating and design parameters; they clarify the underlying links between steps, conditions, adsorbent properties, and performance; and as a result they may facilitate conception and optimization of novel cycles.

Another major advantage is that the model parameters may be obtained directly from

equilibrium measurements; so it is not necessary to fit experimental PSA data. In the simplest case, that is, when isotherms are practically linear, the adsorbent–adsorbate interactions can be lumped together as a single parameter, roughly analogous to the inverse of selectivity. It is even possible to incorporate dispersion by accounting for dead zones at the entrance or exit of the adsorbent bed.

As explained in Chapter 3, the conventional four-step PSA cycle for separation of a binary mixture comprises feed, blowdown, purge, and pressurization, as illustrated in Figure 3.11. Each of these steps serves a vital function that contributes to successful operation of the PSA system. By accounting for the relations governing flow and transfer between the gas and adsorbent, equilibrium models are able to predict the phenomena occurring in each step. It is then easy to combine these relations to predict overall performance. Extending the basic equations, and modifying the conditions of the conventional steps allows complex properties, conditions, and cycles to be simulated.

Before proceeding with mathematical details, the reader may wish to scan Section 4.4 on Cycle Analysis. For example, Eqs. 4.27, 4.37, 4.44, and 4.45 are final equations that predict product recoveries for a variety of cycles. Those equations should convey the idea that, even though the PSA cycles and governing equations may seem complicated, they can be solved in closed forms that are simple and yet have broad applicability. A separate Section, 4.5, covers Experimental Validation, in which predictions of some of the models are compared with experimental data.

The restrictions of the equilibrium theory are evident in the following two groups of inherent assumptions. The first group is generally valid for equilibrium-based PSA separations, and they make the resulting equations amenable to solution by simple mathematical methods.

1. Local equilibrium is achieved instantaneously between the adsorbent and adsorbates at each axial location.
2. The feed is a binary mixture of ideal gases.
3. Axial dispersion within the adsorbent bed is negligible.
4. Axial pressure gradients are negligible.
5. There are no radial velocity or composition gradients.
6. Temperature is constant.

The second group links the equations and conditions to a particular cycle and geometry. The assumptions of a simple four-step cycle and adsorption system are listed, though they may be modified to reflect other cycles or conditions without affecting the applicability of the equilibrium theory.

7. All of the adsorbent is utilized during the feed and purge steps.
8. Pressure is constant during the feed and purge steps.
9. The isotherms may be linear or nonlinear, but they are uncoupled.
10. Dead volume at the adsorber entrance and exit is negligible.

Actually, in the first group of assumptions, all but the first could be relaxed within the confines of an equilibrium model. To drop those assumptions, however, would complicate the mathematics and diminish the simplicity of the equilibrium approach. After all, if one resorts to orthogonal collocation or other potent mathematical methods to account for dispersion, pressure drop, etc., there is no point in restricting such a model to instantaneous mass transfer. Nevertheless, some aspects of detailed models are mentioned in this chapter,

along with the effects of axial pressure drop (see Section 4.9). In addition, the assumption that PSA operation be isothermal is not necessarily rigid. In fact, heat effects appear in a variety of ways, some of which are covered in Section 4.8. The effects of relaxing many of the second set of assumptions are also discussed in this chapter (see Sections 4.4.3–4.4.6).

4.2 Mathematical Model

The simplest PSA cycle studied in this chapter is shown in Figure 4.1, which shows the basic steps and conventions of position and direction. The bottom of that figure will be discussed later, but it shows how compositions move through the adsorbent bed during each step, with the shaded region depicting the penetration of some of the more strongly adsorbed (or "heavy") component, while the plain region contains only the pure, less strongly adsorbed (or "light") component. In this chapter the heavy and light components are referred to as *A* and *B*, respectively.

The following individual component balance applies to binary mixtures in which both components adsorb, so they are coupled in the gas phase, but are assumed independent in the adsorbed phase:

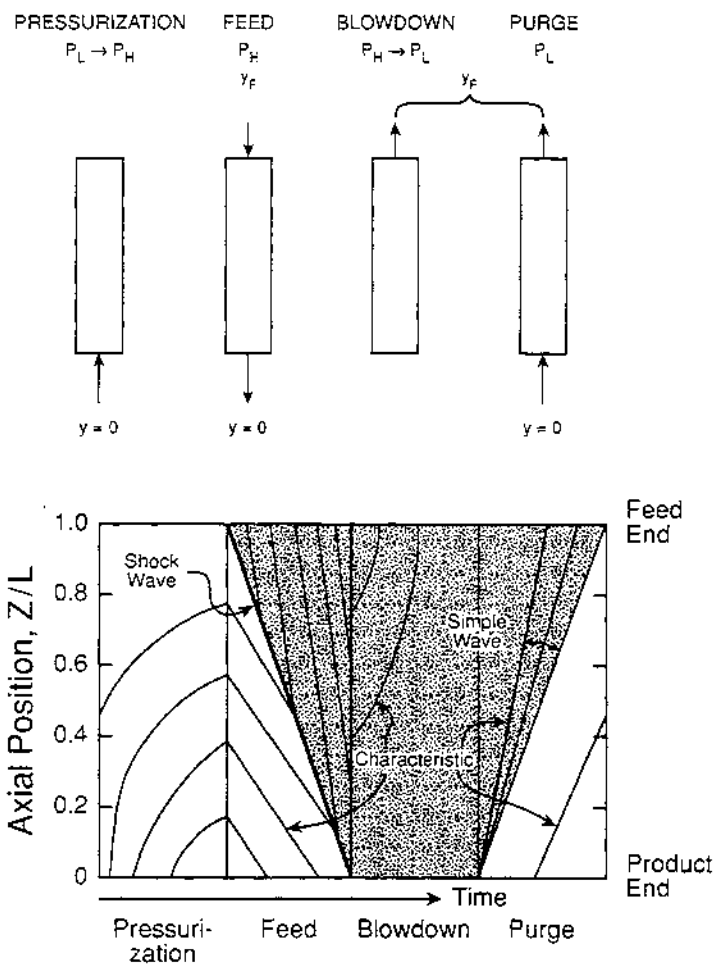

Figure 4.1 Steps in a conventional PSA cycle; orientation of column and streams. (Top) Flows and compositions associated with each step. (Bottom) Positions-versus-time representation of each step. Shaded regions depict penetration of heavy component.

$$\varepsilon\left(\frac{\partial Py_i}{\partial t}+\frac{\partial vPy_i}{\partial z}\right)+RT\left(1-\varepsilon\right)\frac{\partial q_i}{\partial t}=0 \tag{4.1}$$

The subscript i refers to component A or B. Shendalman and Mitchell[2] and Chan et al.[3] considered the case of a trace amount of component A being adsorbed from a carrier, B. Shendalman and Mitchell took the carrier to be nonadsorbing, while Chan et al. accounted for adsorption of the carrier. In both cases, the interstitial velocity, v, was taken to be independent of composition (and of both time and axial position at constant pressure). As it is written, however, Eq. 4.1 applies to bulk separations as well as removal of a dilute contaminant.

An important detail is the definition of the void fraction ε. If the adsorbed phase concentrations are expressed on a particle volume basis (i.e., including intraparticle porosity), then ε is simply the extra-particle or interstitial bed voidage. Such a definition is logical where mass transfer rates are finite and when the mass transfer resistance is associated with external film diffusion, macropore diffusion, or solid-side mass transfer resistance at the particle surface. With this definition, the bed density $\left(\rho_{\mathrm{B}}\right)$, particle density $\left(\rho_{\mathrm{p}}\right)$, and the solid or microparticle density $\left(\rho_{\mathrm{c}}\right)$, and the corresponding void fractions are related by:

$$\rho_B=\left(1-\varepsilon_B\right)\rho_{\mathrm{p}}=\left(1-\varepsilon_B\right)\left(1-\varepsilon_{\mathrm{p}}\right)\rho_{\mathrm{c}},\qquad \varepsilon\cong\varepsilon_B$$

When micropore resistance is dominant, or indeed under the assumption of local equilibrium on which this chapter is based, it is more logical to regard the external void fraction as the sum of the particle macroporosity and the bed voidage (i.e., all gas space outside the micropores). The densities and void fraction are then related by:

$$\rho_B=\left(1-\varepsilon\right)\rho_{\mathrm{c}},\qquad \varepsilon\cong\varepsilon_B+\left(1-\varepsilon_B\right)\varepsilon_{\mathrm{p}}$$

ρ_{c} corresponds to the density determined with a fluid that penetrates the external voidage and the macropores but not the micropores. Since these definitions affect the magnitude of the isotherm parameters, it is essential to maintain consistency when equilibrium data are incorporated into a PSA model.

The balance equations are modified by substituting adsorption isotherm expressions for each component in the form,

$$q_i=f_i\left(\frac{Py_i}{RT}\right)=f_i\left(c_i\right) \tag{4.2}$$

Examples are given in Chapter 2. Following assumption 6 above, the temperature is fixed, so the second term of Eq. 4.1 can be determined from Eq. 4.2. as:

$$\frac{\partial q_i}{\partial t}=\frac{1}{RT}f'\left(Py_i\right) \tag{4.3}$$

Inserting this into Eq. 4.1 yields:

$$\frac{\partial P y_i}{\partial t} + \beta_i \frac{\partial v P y_i}{\partial z} = 0 \tag{4.4}$$

where $\beta_i = \left\{1 + \left[(1-\varepsilon)/\varepsilon\right] f_i'\right\}^{-1}$, which is a function of the component partial pressure. Note that when the isotherms of both components are linear, this parameter is constant, although here it is treated as if it depends on partial pressure. Simply adding the appropriate forms of Eq. 4.4 for the respective components yields the overall material balance, which governs the interstitial flow in the packed bed. Hence, this expression may be employed to determine the local velocity in terms of composition, pressure, and adsorbent–adsorbate interactions. The result is

$$\frac{v_2}{v_1} = \exp\left(\int_{y_{A_1}}^{y_{A_2}} \frac{1-\beta}{1+(\beta-1)y_A} dy_A\right) \cong \frac{1+(\beta-1)y_1}{1+(\beta-1)y_2} \tag{4.5}$$

where the approximation is only exact for linear isotherms, and $\beta = \beta_A/\beta_B$, which for nonlinear isotherms may depend on pressure and composition, but for linear isotherms it is constant. During pressurization and blowdown, the composition, pressure, and interstitial velocity vary with time at each axial position. The details are beyond the current scope (see Section 4.9), but the result for linear isotherms is

$$v = \frac{-z}{\beta_B\left[1+(\beta-1)y_A\right]} \frac{1}{P} \frac{dP}{dt} \tag{4.6}$$

The simplicity of equilibrium-based theories arises because the coupled first-order partial differential equations governing the material balances can be recast as two ordinary differential equations that must be simultaneously satisfied. The mathematical technique employed is called the *method of characteristics*. A brief explanation is given in Appendix A. The resulting equations are:

$$\frac{dz}{dt} = \frac{\beta_A v}{1+(\beta-1)y_A} \tag{4.7}$$

and

$$\frac{dy_A}{dP} = \frac{(\beta-1)(1-y_A)y_A}{\left[1+(\beta-1)y_A\right]P} \tag{4.8}$$

Equation 4.7 defines characteristic trajectories in the *z*, *t* plane. First of all, Eq. 4.8 shows that when pressure is constant, composition is also constant, and the characteristics given by Eq. 4.7 are straight lines. Conversely, when pressure varies with time, the composition varies according to Eq. 4.8, and the characteristics are curved. Examples of characteristics are shown in the bottom portion of Figure 4.1, for example, as lines during feed and purge and as curves during pressurization and blowdown. It is important to note that characteristics do not end at the end of a step; rather, they continue in an altered form. Since composition can be determined along any characteristic, knowing the initial composition, they provide an excellent means for performing stepwise material balances

for PSA cycles.

The blowdown step is governed by Eqs. 4.7 and 4.8, while the subsequent purge step can be analyzed with Eq. 4.7 alone. These steps essentially regenerate the adsorbent. In many conventional adsorption systems, regeneration creates a wave that gradually moves through the bed, which is commonly referred to as a *proportionate pattern* or *dispersive front* (see Section 2.4). In the remainder of this chapter, it is referred to as a *simple wave*, partly because it contrasts with the term *shock wave* which is discussed below (see also Section 2.4.1), and to suggest an association with equilibrium behavior (as opposed to kinetic or dispersive effects).

To complete the analysis of even the simplest PSA cycle, it is necessary to account for the uptake step(s). In particular, the feed step involves uptake of the more strongly adsorbed component. As in conventional adsorption systems, a sharp concentration front is created by this uptake that is sometimes called a *constant pattern* or *self-sharpening* profile. At the extreme of local equilibrium behavior, the front is a step change, and is called a *shock wave*. Since equilibrium effects are emphasized in this chapter, the term *shock wave* will be used, even though in real systems dissipative effects may diminish the sharpness. A shock wave is shown in the bottom portion of Figure 4.1 in the feed step. It appears as a thick line at which characteristics intersect, and it separates the shaded region (depicting presence of the heavy component) from the plain region (depicting the pure light component). Examples of breakthrough data (from experiments in which methane was admitted to a bed of activated carbon previously pressurized with nitrogen) are shown in Figure 4.2, illustrating the sharpness attainable in many PSA applications.

It is the velocity of a shock wave through the packed bed that governs the duration of the feed and rinse steps. Similarly, that velocity is controlled by the rate of flow into and out of the system; hence, the material balance, is also affected. The velocity of the shock wave depends on the interstitial fluid velocities at the leading and trailing edges of the wave. These are related by equating the shock wave velocities based on the conditions for both components A and B to get

$$v_{\mathrm{SH}} = \theta_A \frac{v_2 y_{A_2} - v_1 y_{A_1}}{y_{A_2} - y_{A_1}} \tag{4.9}$$

where, in general,

$$\theta_i = \theta_i\left(P_{\mathrm{H}}, y_1, y_2\right) = \left(1 + \frac{1-\varepsilon}{\varepsilon}\frac{f_{i_2} - f_{i_1}}{y_{i_2} - y_{i_1}}\frac{RT}{P_{\mathrm{H}}}\right)^{-1}$$

1 and 2 refer to the leading and trailing edges of the wave, respectively, and f_{i_j} is given by Eq. 4.2 for component i at composition j.

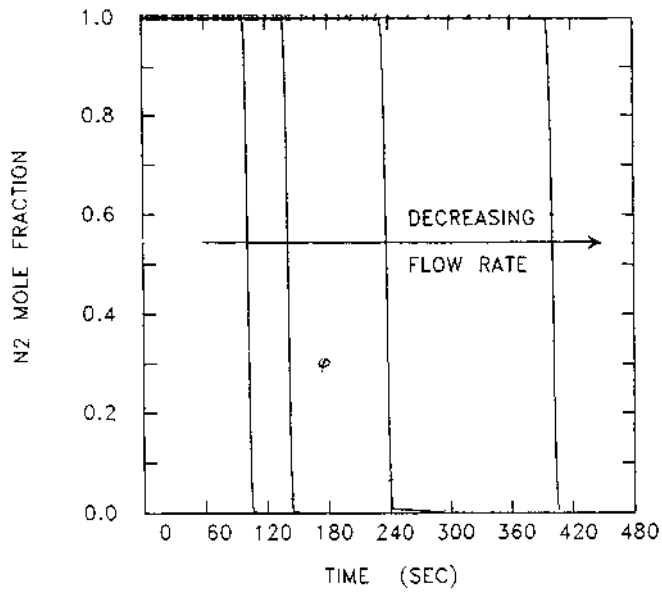

Figure 4.2 Breakthrough data of N_2 and CH_4 on activated carbon at 2.7 atm and 25°C.

A balance for component A around the shock front yields an expression for the velocities ahead of and behind it,

$$\frac{v_2}{v_1} = \frac{1+(\theta-1)\,y_{A_1}}{1+(\theta-1)\,y_{A_2}} \tag{4.10}$$

where $\theta = \theta_A/\theta_B$. Again, Appendix A treats this subject somewhat more generally and thoroughly.

4.3 Model Parameters

Two parameters provide the simplest means by which to express the impact of adsorbent–adsorbate interactions on PSA performance. The parameter β is evaluated at a specific composition using tangents of the respective isotherms. The parameter θ, however, is evaluated at a jump discontinuity using chords of the respective isotherms. For systems having linear isotherms, β and θ are identical.

The amount of adsorbate held in a unit volume of adsorbent is sometimes referred to as the *column isotherm*. In terms of the definitions given, the column isotherm is

$$\frac{c_i}{\theta_i} = \frac{y_i P}{RT}\left(1+\frac{1-\varepsilon}{\varepsilon}\frac{f_i}{y_i}\frac{RT}{P}\right).$$

In terms of wave movements, this is the cumulative amount of adsorbate i admitted at P and y_i to an initially clean adsorbent (i.e., totally evacuated or prepressurized with a less strongly adsorbed component), stopping at breakthrough. The column isotherm is discussed later in other contexts.

The parameters β and θ are related to velocities via Eqs. 4.5, 4.9, and 4.10. Therefore, it is possible to measure their effective values in breakthrough experiments. In one type of

experiment, a fixed bed of adsorbent is initially purged and pressurized with the light component. The feed is then admitted to the bed at the same pressure. By simply monitoring the influent and effluent flow rates, the value of θ (or β when both isotherms are practically linear) may be found from:

$$\theta = \theta\left(P, 0, y_F\right) = 1 - \frac{1 - Q_{\text{out}}/Q_{\text{in}}\,|_F}{y_{A_F}}$$
$$\left(= \beta \text{ for linear isotherms}\right) \tag{4.11}$$

where the product is pure (i.e., $y_{A_P} = 0$), the bed pressure is kept constant, $\Delta P = 0$, and the volumetric flow rates, Qs, are constant. In an alternative type of experiment the adsorbent bed is initially equilibrated with feed. Then the pure heavy component is admitted to the bed at the same pressure. By simply monitoring the influent and effluent flow rates, the value of θ (or β) may be found from:

$$\theta = \theta\left(P, y_{\text{F}}, y = 1\right) = \frac{1 - y_{\text{F}}}{Q_{\text{in}}/Q_{\text{out}} - y_{\text{F}}}$$
$$\left(= \beta \text{ for linear isotherms}\right) \tag{4.12}$$

Note that when both isotherms are linear, the values obtained in the two types of experiments should be consistent, but if isotherm curvature is significant, the values of θ determined in the two types of experiments may be different. In that case, the first type of measurement would be more useful when the light component is desired, and the second type would be more useful when the heavy component is desired.

This approach has several advantages: a range of different operating conditions (feed composition, pressures, and cycle times) can be examined, the effects of minor variations in packing and/or adsorbent properties can be assessed directly, and even effects of dispersion and diffusion can be identified and easily resolved.

As mentioned earlier, examples of experimental breakthrough curves, for methane (A)–nitrogen (B) on activated carbon, are shown in Figure 4.2. The results are plotted as θ versus Reynolds number ($\text{Re} = \rho\varepsilon v d_{\text{P}}/\mu$, where ρ and μ are the gas density and viscosity, εv is the gas superficial velocity, and d_{P} is the particle diameter) in Figure 4.3. In that figure, absolute pressure is shown as a parameter, and results for air (A)–oxygen (B) on zeolite 5A, and nitrogen (A)–helium (B) on activated carbon are also included. Some of the pressures were sufficiently low for the isotherms to be nearly linear, while others were at pressures high enough for isotherm curvature to be significant. Furthermore, the dependence of θ (or β) on Re is similar among the different cases, reflecting the impact of dissipative effects. For each data set, the minimum value of θ corresponds to conditions in which the combined effects of diffusion and dispersion are minimal. At that point, θ is typically found to be larger (worse) than the value predicted from isotherm data alone by about 0.02 to 0.05. The optimal Reynolds number (Re) for all the cases, except nitrogen–helium, is in the range of 9 to 18. The elapsed time per breakthrough experiment is on the order of a few minutes, while batchwise isotherm measurements are much more time consuming.

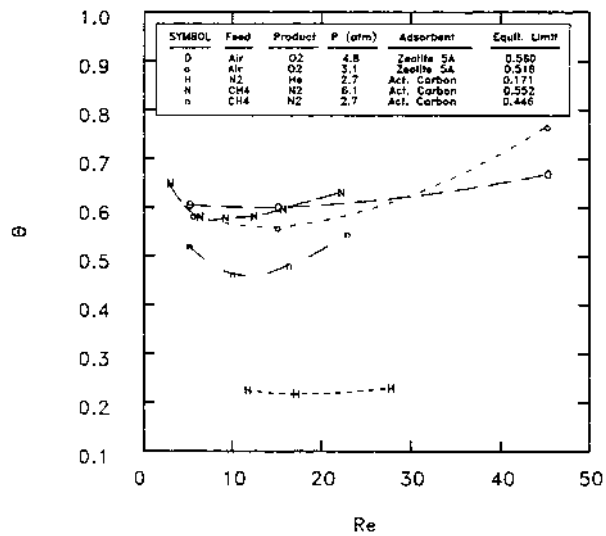

Figure 4.3 Effect of Re on adsorption selectivity parameter, θ, for air–O_2 on zeolite 5A (Ball[5]), and N_2 and He on activated carbon, and N_2 and CH_4 on activated carbon.

For certain compositions, when the isotherms are quite nonlinear, there may be a selectivity reversal, indicated by $\theta > 1$. This can occur when the partial pressure of the heavy component is so large that θ_A becomes greater than θ_B. In that case, if a shock front existed, it would begin to disintegrate and a simple wave would form. The resulting breakthrough pattern would have a tail (at high partial pressures) that might be falsely diagnosed as an effect of mass transfer resistance (see Figure 2.23). Generally, other complications are possible due to multiple conceivable values of the velocities and the parameters θ_i and θ. The compositions bounding the shock front are constrained by the influent and effluent compositions, but due to entropic effects they may tend to lie somewhere between those. For multicomponent systems, the phenomenon of "rollup" can cause local maxima of the lighter components, resulting in a shock velocity slower or faster than expected. Subtleties arise because the choice is subject to a uniqueness condition. Applications to PSA have been discussed by Kayser and Knaebel.[4] When the curvature of the isotherms is not too severe (i.e., at low partial pressures), the uniqueness condition will be automatically satisfied, and the shock velocity predicted by Eq. 4.9 will be valid for $y_{A_2} = y_{A_F}$ (i.e., the feed composition).

4.4 Cycle Analysis

Certain preliminaries are essential for predicting PSA performance. First, one must determine basic properties, and among these, for the local equilibrium theory to be accurate, mass transfer resistances must be small. One must then decide on the steps comprising the PSA cycle, and choose operating conditions, such as feed composition, pressures, and step times. At that point, material balances and thermodynamic relationships can predict overall performance in terms of: flow rates, product recovery, byproduct composition, and power requirements.

The key concept involved in applying equilibrium models is that each step is intended to accomplish a specific change. For steps such as pressurization and countercurrent

blowdown, the specific change is obvious. Other steps are more subtle because they may proceed until breakthrough is imminent, complete, or some fraction thereof. Such operating policies link the flow rates, step times, bed size, etc. of those steps, and depending on initial and final states, may impact other steps in the cycle. In that sense the goals of the steps are not at all open ended.

As an example of stepwise material balances, the number of moles contained in an influent or effluent stream during any step can be determined from appropriate velocities, as given by Eqs. 4.5, 4.7, 4.9, and 4.10. The choice depends on the nature of the step. The moles added to or removed from the column in each step can be expressed as the integral over time of the instantaneous molar flow rate(s), or as the difference between the final and initial contents of the column. General expressions are:

$$\Delta N_A = \left(\overline{Q_{A_{\text{in}}}} - \overline{Q_{A_{\text{out}}}}\right) t_{\text{step}} = N_A\big|_{\text{final}} - N_A\big|_{\text{initial}} \tag{4.13}$$

$$\Delta N_{\text{TOTAL}} = \left(\overline{Q_{\text{in}}} - \overline{Q_{\text{out}}}\right) t_{\text{step}} = N_{\text{TOTAL}}\big|_{\text{final}} - N_{\text{TOTAL}}\big|_{\text{initial}} \tag{4.14}$$

where the products of the average molar flow rates and time are:

$$\overline{Q_A} t_{\text{step}} = \int_0^{t_{\text{step}}} \frac{\varepsilon A_{\text{CS}} P v y_A}{RT} dt \tag{4.15}$$

$$\overline{Q} t_{\text{step}} = \int_0^{t_{\text{step}}} \frac{\varepsilon A_{\text{CS}} P v}{RT} dt \tag{4.16}$$

For steps in which pressure is constant, the influent flow rate or effluent flow rate can be set to complete the step within the allocated step time. No matter which is specified, the other can be easily determined if both compositions are known, via Eq. 4.5 or 4.10, depending on whether a shock front exists in the column.

For steps in which pressure varies, it is easier to specify the rate of pressure change, because the volumetric flow rate varies as pressure changes. Employing Eq. 4.5, Eq. 4.16 can be written as:

$$\overline{Q} t_{\text{step}} = \int_0^{t_{\text{step}}} Q \frac{dt}{dP} dP \tag{4.17}$$

For some steps, it is convenient to determine the flows from the molar contents of the column, when the composition profiles are known. For either A or B, the contents are:

$$N_i = \int_0^L \left[\varepsilon c_i + (1-\varepsilon) f_i(c_i)\right] A_{\text{CS}} dz \tag{4.18}$$

where f_i is the isotherm function, given by Eq. 4.2. This relation is equivalent to the *column isotherm* mentioned in Section 4.3. In the same vein, the total column contents are obtained by summing the amounts of both components.

$$N_{\text{TOTAL}} = \int_0^L \left(\varepsilon c + (1-\varepsilon)\left[f_A(c_A) + f_B(c_B)\right]\right) A_{\text{CS}} dz \tag{4.19}$$

Now these balance equations can be combined to predict the overall performance of some PSA cycles. As discussed in Chapter 3, the simplest PSA cycles employ four steps,

so they will be considered first. The steps comprise: pressurization either by feed or product, feed at constant pressure until breakthrough is imminent, countercurrent blowdown, and complete purge (so that all of the heavy component is exhausted). The version employing feed for pressurization is usually called the *Skarstrom cycle*,[6] and is discussed in Section 3.2. Several variations of the Skarstrom cycle have been analyzed via the local equilibrium theory, including steps with incomplete purge,[7–9] simultaneous pressurization and feed and simultaneous feed and cocurrent blowdown,[10] cocurrent blowdown,[11] rinse,[12] etc. As shown in Sections 4.4.1–6, the final results of those models are surprisingly simple. Futhermore, experiments conducted over a wide range of conditions have confirmed their validity, as shown in Section 4.5.

4.4.1 Four-Step PSA Cycle: Pressurization with Product

The cycle covered in this section is shown in Figure 4.1, and it is probably the simplest PSA cycle, at least from a mathematical viewpoint. One result of that simplicity is that it has been possible to extend the equilibrium theory, in closed form, to systems exhibiting nonlinear isotherms.[3] For the sake of clarity, although generality is sacrificed, the discussion is given here in terms of a specific type of mixture, viz., in which the light component has a linear isotherm while the isotherm for the heavy component is nonlinear (e.g., a Langmuir or quadratic isotherm). When both isotherms are practically linear, the equations presented here can be easily simplified, and when both are nonlinear, the preceding equations can be adapted, although the resulting expressions become somewhat more complicated.

As mentioned previously, step times, velocities, and molar flow rates are interrelated through material balances. Therefore, since the influent and effluent moles required for a certain step are fixed by Eqs. 4.13 through 4.19, the choice of step time really only affects the interstitial velocity. For some steps that choice is critical. For example, during the feed step the flow rate affects the apparent selectivity, as suggested in Figure 4.3, as well as pressure drop. In contrast, the time allotted for the purge step is usually chosen in order to synchronize steps occurring in parallel beds. Pressure drop and mass transfer rates are normally of little importance while purging. From a mathematical viewpoint, the velocities in the feed and purge steps are governed by the rates at which the shock and simple waves propagate through the bed, as given by Eqs. 4.5, 4.7, 4.9, and 4.10. These equations relate the interstitial velocity, the length of the bed, the step time, and the column isotherm, as follows:

$$v_{\text{in}} t\big|_{\text{F}} = L/\theta_A \tag{4.20}$$

$$v_{\text{in}} t\big|_{\text{PU}} = L/\beta_A \tag{4.21}$$

Note that the feed step is assumed to produce the pure light component at high pressure, so in Eq. 4.20 $\theta_A = \theta_A\,(P_{\text{H}}, y = 0, y_{\text{F}})$. Furthermore, since in Eq. 4.21 the purge gas is also presumed to be pure, $\beta_A = \beta_{A_0}$. In this section, the light component is assumed to have a linear isotherm, so in the following treatment $\beta_B = \beta_{B_0} = \theta_B$.

Accordingly, the moles required for the feed and purge steps may be determined from Eqs. 4.13 through 4.21 as

$$\overline{Q_{\text{in}}t}\big|_{\text{F}} = \phi \mathscr{A} \tilde{A}\, \beta_{A_0} / \theta_A \tag{4.22}$$

$$\overline{Q_{\text{in}}t}\big|_{\text{PU}} = \phi \beta_{A_0} / \beta_A = \phi, \qquad \text{if } y_{A_{\text{in}}} = 0 \tag{4.23}$$

where $\phi = \varepsilon A_{\text{CS}} L P_{\text{L}} / \beta_{A_0} RT$, $\qquad \tilde{A} = P_{\text{H}} / P_{\text{L}}$,

$$\beta_0 = \frac{\beta_{A_0}}{\beta_{B_0}} = \left(1 + \frac{1-\varepsilon}{\varepsilon} K_B\right) \Big/ \left(1 + \frac{1-\varepsilon}{\varepsilon} K_A\right)$$

and K_i is the Henry's law coefficient of component i.

The moles of the pure, light product withdrawn during the feed step may be determined from Eqs. 4.10 and 4.22, as follows

$$\overline{Q_{\text{out}}t}\big|_{\text{F}} = \phi \tilde{A} \left[1 + (\theta - 1)\, y_{A_{\text{F}}}\right] \beta_{A_0} / \theta_A \tag{4.24}$$

where θ_A has the same value as in Eqs. 4.20 and 4.22.

The pressurization with product step in this cycle follows the purge step; so the bed is presumed to contain only the pure, light component. Thus, Eq. 4.17 yields

$$\overline{Q_{\text{in}}t}\big|_{\text{PR}} = \phi \beta_0 \left[\tilde{A} - 1\right] \tag{4.25}$$

Consequently, the *rate* of pressurization is immaterial; only the initial and final pressures matter.

The definition of *recovery* of the light component for this four-step cycle, with pressurization by product is:

$$R_B = \frac{\overline{Q_{\text{out}}t}\big|_{\text{F}} - \overline{Q_{\text{in}}t}\big|_{\text{PR}} - \overline{Q_{\text{in}}t}\big|_{\text{PU}}}{\overline{Q_{\text{in}}t}\big|_{\text{F}}\, y_{B_{\text{F}}}} \tag{4.26}$$

Thus, by combining Eqs. 4.22 through 4.26 and rearranging, one obtains:

$$R_B = (1 - \theta)\left(1 - \frac{\zeta}{\tilde{A}\, y_{B_{\text{F}}}}\right) \tag{4.27}$$

where $\zeta = 1 \Big/ \left[1 + \left(\xi P_{\text{H}} y_{\text{F}} \beta_{A_0}\right) \Big/ \left(1 - \beta_0\right)\right]$ is a factor that deviates from unity only for nonlinear isotherms. For example, when component A follows a quadratic isotherm, $q_A = K_A c_A + M_A c_A^2$ and component B follows a linear isotherm, $q_B = K_B c_B$, one gets

$$\xi = \frac{1-\varepsilon}{\varepsilon} \frac{M_A}{R}$$

Some specific results of Eq. 4.27 are shown in Figure 4.4 for the case of linear isotherms ($M_A = 0$ and $\zeta = 1$). This figure illustrates the effects of feed composition and pressure ratio on product recovery, for two adsorbent selectivities, $\beta = 0.1$ and 0.9. These selectivities span the range of very easy (e.g., hydrogen purification) to quite difficult (e.g., separation of argon from oxygen), respectively. The results are shown as

three-dimensional surfaces that have quite similar shapes, despite the large difference in selectivities. Both surfaces approach an asymptote at high pressure ratios and, to a lesser extent, as the percentage of the heavy component in the feed approaches zero. Conversely, recovery of the light component always decreases as the amount of the heavy component in the feed increases. Later, in Section 4.6, additional comparisons are made that focus on the effect of isotherm curvature.

Another measure of overall PSA performance is the *enrichment* of the byproduct, $E_A = \overline{y}_{A_W} / y_{A_F}$. This may be of interest when the more strongly adsorbed component is valuable. If that component is very valuable, the

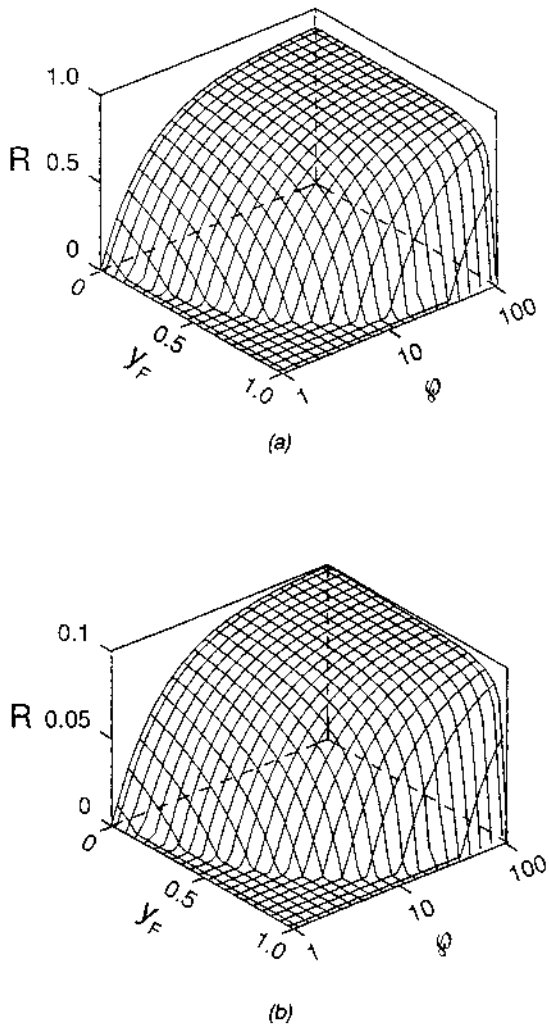

Figure 4.4 The effect on recovery of feed composition and pressure ratio, for β (a) = 0.1 and (b) 0.9, for pressurization with product.[13]

present four-step cycle (with complete purge) may not be the best choice. More will be said about alternatives later in this chapter. Nevertheless, a simple material balance can be used to determine this parameter, regardless of the operating conditions. The following relation applies for any cycle that splits a binary mixture in which the light component is obtained as a pure product, and the only other effluent stream is the byproduct:

$$E_A = \frac{1}{1 - y_{B_F} R_B} \tag{4.28}$$

4.4.2 Four-Step PSA Cycle: Pressurization with Feed

What may seem to be the simplest modification of the four-step cycle outlined previously is to pressurize with feed rather than the light product. This arrangement was actually the cycle proposed by Skarstrom.[6] It seems intuitively possible, if not probable, that pressurizing with feed rather than product could produce more net product (i.e., have a higher recovery). That is, on physical grounds it is easy (but deceptive) to regard pressurization as a "parasitic" step, since no product evolves. At first glance, the basic mathematics would seem to confirm these expectations. For example, in the case of pressurization with feed, N_{PR}, the moles consumed for pressurization, appears in the denominator of the definition of recovery, as shown in Eq. 4.29. For the counterpart cycle (pressurization with product), N_{PR} appears as a negative term in the definition of recovery, Eq. 4.26. Thus, in both cases it would appear that pressurization is deterimental to performance. Following that notion, it might be deduced that the relatively less valuable feed should be employed for this purpose, as opposed to the pure product.

Following this reasoning, it is useful to examine pressurization with feed as an alternative to pressurization with product, primarily in order to better understand the PSA cycle, and secondarily to gain insight into the development of equilibrium models. As mentioned earlier, both Shendalman and Mitchell[2] and Chan et al.[3] ignored the effect of the heavy component on the molar flows and velocities. As a result, their models do not distinguish between the amount of gas required for pressurization with feed versus product. Their predicted recovery of the light component, restricted to the case of complete purge, is:

$$R_S \equiv \frac{N_{HP} - N_L}{y_{B_F}\left(N_H + N_{PR}\right)} = \frac{\tilde{A}^{1-\beta} - 1}{y_{B_F}\left[\tilde{A}^{1-\beta} + \beta\left(\tilde{A} - 1\right)\right]} \tag{4.29}$$

Note that $y_{B_F} \to 1$ was assumed by both Shendalman and Mitchell and Chan et al., so it would be superfluous in the denominator on the right-hand side in their versions. It is included here only for completeness. In addition, Shendalman and Mitchell assumed that $\beta = \beta_{A_0}$ and $\beta_B = 1$, while Chan et al. assumed $\beta = \beta_{A_0} / \beta_{B_0}$.

Removing the restrictions on feed composition and including the impact of sorption on the interstitial gas velocity leads to a more widely applicable and accurate model for most PSA systems. That approach was followed by Knaebel and Hill[13] for a system having linear isotherms. Their relation to predict recovery of the light component, also restricted to the case of complete purge is:

$$R_B = \frac{\tilde{A}\Omega - 1}{y_{B_F}\left[\tilde{A}\Omega + \beta\left(A\tilde{A} - 1\right)\right]} \tag{4.30}$$

In this equation the parameter, Ω (= Θ in the original paper), is determined by integration via Runge–Kutta or a similar approach, and is somewhat involved. In general, $\Omega \alpha \tilde{A}^{-\beta} y_{B_F}$

when $\beta \to 0$ (e.g., 0.1), while for larger values of β, Ω is somewhat larger than that product. Since Ω is not a simple function of feed composition, adsorbent selectivity, or operating pressures, one might expect that the dependence of recovery would be equally complex. The discrepancies between the models, due to differences in their inherent assumptions, are discussed in Section 4.6. In addition, some of the subtleties of the pressurization step are discussed in Section 4.9.

As in the previous section, specific results calculated from Eq. 4.30 are shown in Figure 4.5, for the case of linear isotherms. That figure illustrates the effects of feed composition and pressure ratio on product recovery for two adsorbent selectivities, $\beta = 0.1$ and 0.9, which span the range of very easy to quite difficult PSA applications. The results, again are shown as three-dimensional surfaces that in this case have quite different shapes, due to the difference in selectivities. As for pressurization with product, recovery of the light component always decreases as the amount of the heavy component in the feed increases. In addition, both surfaces approach an asymptote at high pressure ratios, but, for the low-selectivity case ($\beta = 0.9$), there is a ridge representing maximum recovery at low pressure ratios.

Another relevant issue is the inherent differences between the pressurization methods discussed. Though there may be differences in mechanical complexity and other details, the most significant difference is, more than likely, between the recoveries of the light product. To expand on that point, Figure 4.6 shows the incremental improvement in recovery for pressurization by product versus pressurization by feed as affected by feed composition and pressure ratio, again for $\beta = 0.1$ and 0.9. The comparison is again limited to systems having linear isotherms. As can be seen, regardless of the conditions and parameters, the recovery of the light component that is attainable by pressurization with product is generally superior to that obtainable by pressurization with feed. The percentage difference is small for systems with high selectivities, but grows larger as selectivity drops. Perhaps surprisingly, the difference increases as the pressure ratio ($\wp$) increases.

This result underscores the fallacies of the previous intuitive arguments in favor of pressurization by feed, and shows that it is a misconception to view pressurization as a "parasitic" step. The primary underlying principle is that, when the adsorbent is pressurized with feed, the adsorbent near the feed end contacts the feed at essentially the lowest pressure in the cycle. This allows the more strongly adsorbed component to penetrate farther into the bed, because less is adsorbed by that adsorbent than if the gas were fully pressurized. As a result, that adsorbent is less than fully utilized. Thus, despite the fact that pressurization does not contribute directly towards production, it can diminish the useful capacity of the adsorbent.

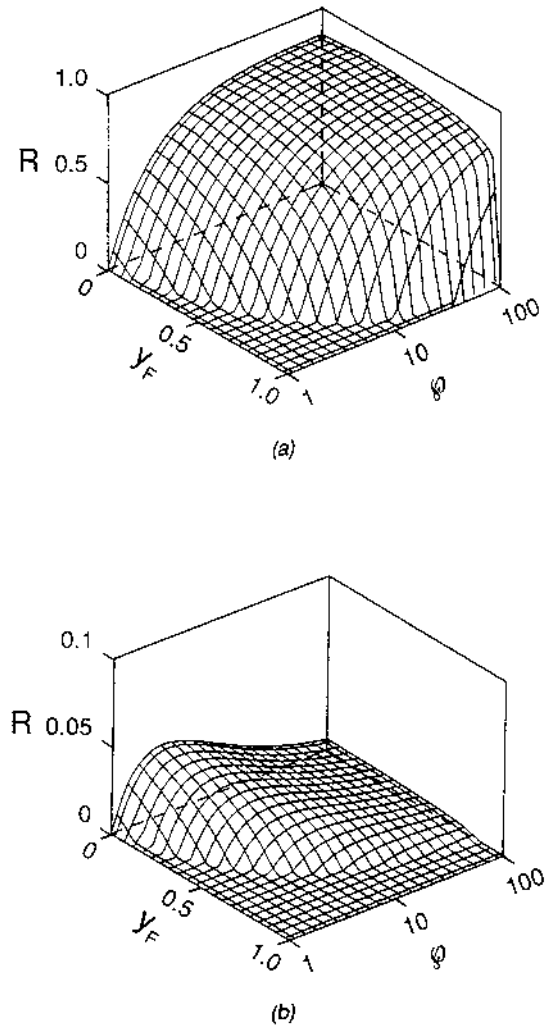

Figure 4.5 The effect on recovery of feed composition and pressure ratio, for β(a) = 0.1 and (b) 0.9, and for pressurization with feed.[13]

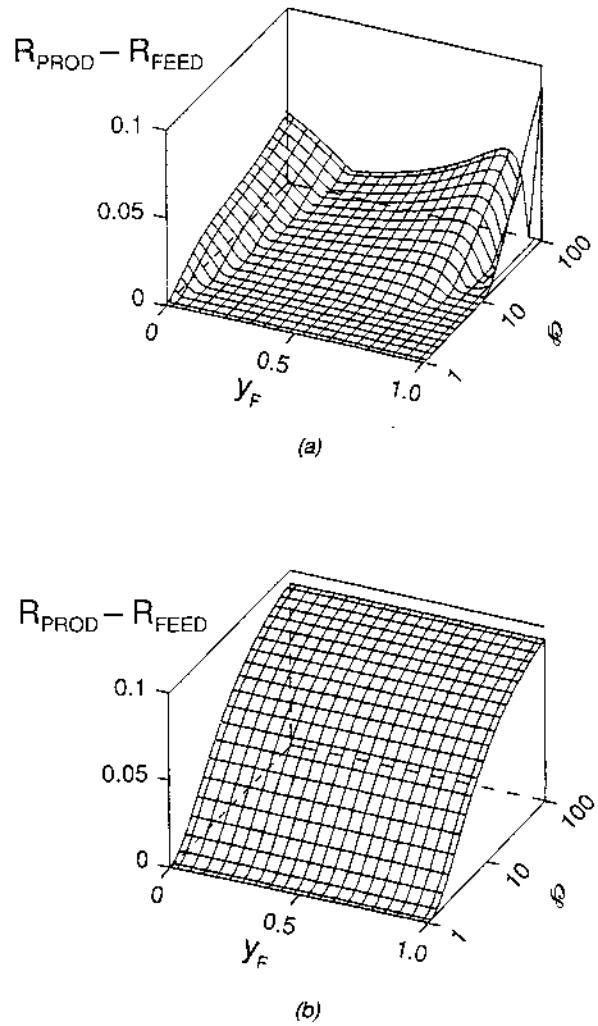

Figure 4.6 Difference in recoveries for pressurization with product versus pressurization with feed as a function of feed composition and pressure ratio, for β (a) =0.1 and (b) 0.9.[13]

4.4.3 Four-Step PSA Cycle: Incomplete Purging

The two cycles considered so far in this section are simple, and relatively easy to analyze. Unfortunately, however, they are not particularly efficient in terms of their performance relative to power requirements. That is, they generally require high pressure ratios to attain high recoveries. For this section, we consider a simple modification of the four-step PSA cycle described in Section 4.4.1. It will be seen that this modification, which simply involves varying the extent of purging, can lead to remarkably higher recovery at relatively low pressure ratios.

Incomplete purging has been common in industrial practice, as mentioned by Wagner[14] and Wankat.[15] Quantitative studies of the extent of purge have focused mainly on flow rate ratios, especially the purge-to-feed ratio. For example, the effects of the purge-to-feed ratio on light-product purity were studied by Yang and Doong,[16] Doong and Yang,[17] and Yang.[18] Their results implied that it was not feasible to increase recovery by decreasing the purge-to-feed ratio and still maintain high product purity. Kirkby and Kenney[19] showed

theoretically and experimentally that there is an optimum extent of purging, for which product purity and recovery are maximized. Their cell model suggested that the optimum corresponded to complete purge, but their experiments revealed that a lesser amount was optimal. An equilibrium-based model was developed by Matz and Knaebel[7] to assess the effect of purge on PSA performance, based on systems having linear isotherms, and that work is the basis of the following discussion. Recently, Rousar and Ditl[9] solved the same basic equilibrium-based equations analytically to determine the optimum purge amount, and they examined operation in a regime that yields impure light product.

By its nature, incomplete purging leaves a composition *tail*, or *heel*, at the feed end of the column, containing some of the more strongly adsorbed component. Subsequent pressurization with product (also countercurrent to the feed) pushes that residual material toward the feed end. More subtly, it also reduces the gas-phase mole fraction of the more strongly adsorbed component in that region, since the heavy component is preferentially taken up as pressurization proceeds. The presence of the compressed tail reduces the quantities of both the feed admitted and the gross product obtained during the feed step. The relative amounts consumed and/or produced during each step depend on the extent of purge, as well as on the conditions and parameter values. Generally, reducing the amount of purge always results in increased recovery, but beyond some limit (described below) there is no assurance that pure product can be obtained.

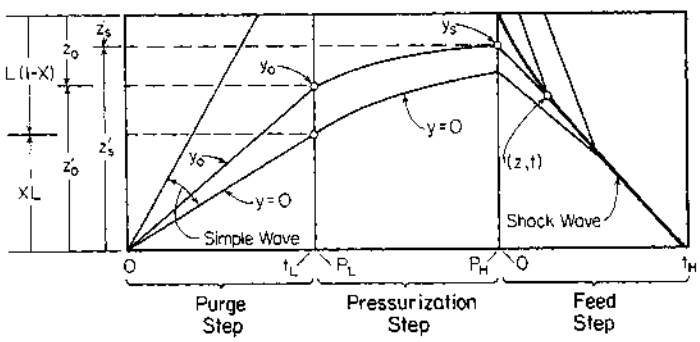

Figure 4.7 Paths of characteristics in the purge, pressurization, and feed steps, for a fractional extent of purge of X. Note: z' is measured from the bottom toward the top, and z is measured in the reverse direction.[7]

It may help to visualize the action of the steps in terms of wave movements, as in the discussion of Figure 4.1. A schematic diagram of the wave movements in the relevant steps is given in Figure 4.7, although in this figure the shading that represents the influx of the heavy component has been omitted. The purge step is still characterized by a simple wave. This wave spreads as it propagates over the length of the column, as shown on the left-hand side of the diagram.

The key feature of the extent of purging is the fraction of the column X that is completely purged. That is, X is the fraction of L over which $y = 0$ at the end of the purge step, t_L. Because they are linearly related, this is identical to the fraction of the amount of gas required to purge the bed completely, via Eqs. 4.21 and 4.23, as

$$X = \frac{\beta_A v_{in} t|_{\mathrm{PU}}}{L} = \frac{\overline{Qt}|_{\mathrm{PU}}}{\overline{Qt}|^*_{\mathrm{PU}}} \tag{4.31}$$

where $\beta_A v_{\text{in}} t|_{\text{PU}}$ is the distance into the bed that is fully purged and $\overline{Qt}|^*_{\text{PU}}$ is the number of moles required for complete purge.

An arbitrary characteristic in the simple wave is denoted by its composition, y_0. The one that just reaches the effluent end of the column as the purge step ends is special. Its mole fraction is called $y_0|_{z=L}$. An operational constraint is that this should be less than the "expanded" feed mole fraction, or, if it is not, when it is repressurized it will simply revert to the feed composition. In other words, if this constraint is not met, regeneration will be incomplete, and the effective length of the column will be reduced, leading to premature breakthrough. Mathematically, this amounts to the following inequality $y_{\text{S}}|_{z=L} < y_{\text{F}}$. Generally, the value of y_{S} can be determined from its initial composition and the imposed pressure ratio,

$$y_{\text{S}}|_z = \left[y_0 \left(\frac{1-y_{\text{S}}}{1-y_0} \right)^{\beta} \right]_z \tilde{A}^{\beta-1} \tag{4.32}$$

The ultimate axial position, denoted z_{S}, is coupled to the original position z_0 by

$$z_{\text{S}} = z_0 \left(\frac{y_{\text{S}}}{y_0} \right)^{\beta/(1-\beta)} \left(\frac{1-y_0}{1-y_{\text{S}}} \right)^{1/(1-\beta)} \left(\frac{1+(\beta-1)y_{\text{S}}}{1+(\beta-1)y_0} \right) \tag{4.33}$$

Any greater extent of purge than the amount indicated by this inequality will drive off a sufficient portion of the more strongly adsorbed component so that net product is possible. At any rate, the composition at the end of the purge step can be determined from the fractional extent of purge as follows,

$$y_0|_{z=L} = \frac{1-X^{1/2}}{1-\beta} \tag{4.34}$$

Thus, beginning with values of X and y and inserting them into Eqs. 4.7 and 4.34, one can determine the composition profile in the column at the end of the purge step. One can subsequently employ Eqs. 4.32 and 4.33 to predict, by tracing characteristics, the profile after pressurization.

The feed step is affected by the profile in the column at the end of pressurization because characteristics having composition y_{S} encounter characteristics at the feed composition, forming a shock wave. Since the composition at the leading edge varies nonlinearly along the shock path, it may be necessary to determine the path by integration using a Runge–Kutta routine.

Since the composition profile at the beginning of the feed step is complicated, it is conceivable that variations of composition and velocity, along with the differing adsorption selectivities of the components, could lead to unusual waveforms (e.g., the formation of double shock fronts), which are possible for a single adsorbate that has a Type IV isotherm. If that were the case, column behavior would be difficult to understand and analyze. Applying the *entropy condition* and the method of characteristics, however, leads to the conclusion that multiple shock waves cannot occur at conditions typically encountered in PSA cycles.[7]

Having summarized the necessary modifications to the basic model, and discussed some of the subtleties, it is appropriate to look at some results. The recovery of pure product can be predicted for this cycle by combining the foregoing analysis with Eq. 4.26. From an engineering standpoint, the most interesting cases to consider are those were dramatic improvements are possible, for example, in relation to the simpler cycles discussed earlier. Perhaps the most interesting type of application at the present state of PSA technology is the situation in which both the feed composition and adsorbent selectivity are moderate. Separation of oxygen from air using zeolite 5A is a realistic example of such a system. Air is composed mainly of nitrogen (78.03%), oxygen (20.99%), and argon (0.94%) (for simplicity the minor constituents are omitted here), and the temperature is taken to be 45°C, which assures that the isotherms are nearly linear (up to about 6 atm). Furthermore, the adsorption isotherms of argon and oxygen on 5A zeolite practically coincide, so argon and oxygen are not separated. The adsorbent–adsorbate interactions are characterized by $\beta = \theta = 0.593$ (Kayser and Knaebel[20]).

Two types of comparisons are possible: fixing the extent of purge and varying the pressure ratio, or vice versa. The results are shown in Figures 4.8 and 4.9, respectively. The former shows extents of purge of 100% and 50%, and pressure ratios from 1.45 to 100. The recovery based on complete purge passes the break-even point at a pressure ratio of 4.6, reaches 22% at a pressure ratio of 10, and approaches about 39% as the pressure becomes very large. Conversely, at 50% purge the recovery at a pressure ratio of 1.45 is 23%, rises to nearly 39% at a pressure ratio of 10, and attains the maximum value of about 40% at a high pressure ratio. Figure 4.9 shows pressure ratios of 2.0 and 4.0, with extents of purge from 45% to 100%. Both cases show nil recovery for high extents of purge, and over 30% recovery as the extent of purge reaches the minimum value for which pure product is attainable.

To summarize these results: reducing the extent of purge to about 50% of completion allows recovery to pure oxygen at low pressure ratios. As the pressure ratio increases, the improvement is still significant, though the returns diminish. The only potential advantage foreseen for purging more than the minimum amount is to compensate for any transport resistances or dispersive effects that could cause contamination of the product. Such effects would be greater for faster cycling, so there is bound to be an optimum at which product purity and recovery are balanced against adsorbent productivity and the power requirement.

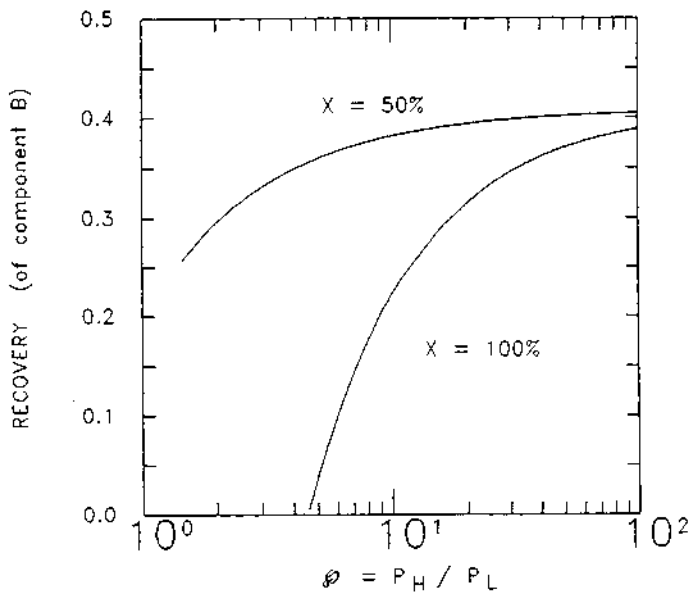

Figure 4.8 Effect on light product recovery of pressure ratio, for extents of purge of 50% and 100%, for β = 0.593 and y_F = 0.78.

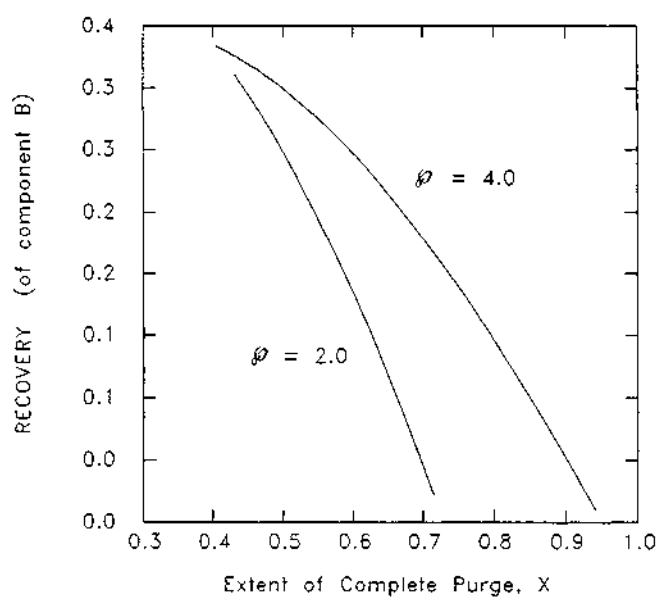

Figure 4.9 Effect of extent of purge on light product recovery for pressure ratios of 2.0 and 4.0, for β = 0.593 and y_F = 0.78.

4.4.4 Four-Step PSA Cycle: Pressure Variation During Feed

Modifications of certain PSA steps could lead to simplified equipment or superior performance. For example, the simplest PSA cycle is a two-step cycle that combines the pressurization and feed steps, and the blowdown and purge steps. This cycle requires the minimum number of valves and very simple control logic. Conversely, a number of studies have shown that cocurrent blowdown can significantly increase the recovery of the light

product. Therefore, it seems promising to combine the feed and blowdown (cocurrent) steps, even though doing so would involve some mechanical complications. The local equilibrium theory is a natural choice to study such cycles because it can focus on the impact of major parameters and operating conditions, without the intrusion of extraneous effects which would involve adjustable parameters.

The interstitial flow rate can be found from the total material balance (i.e., the sum of Eq. 4.1 or 4.4 for both components). These equations can be integrated with boundary conditions (y_F, v_F, specified at the feed end of the bed) in order to evaluate the velocity and composition at other points in the adsorbent bed. The individual component balance for component A, can then be solved, yielding results that are slightly more complicated characteristics than those described by Eqs. 4.7 and 4.8:

$$\frac{dz}{dt} = \frac{\beta\left(\psi_O - P'z\right)}{P\left[1+\left(\beta-1\right)y_A\right]^2} \tag{4.35}$$

$$\frac{dy_A}{dz} = \frac{\left(\beta-1\right)\left[1+\left(\beta-1\right)y_A\right]\left(1-y_A\right)y_A}{\beta\left[\left(\psi_O/P'\right)-z\right]} \tag{4.36}$$

where $P' = dP/dt = \left(\psi_O - \psi_F\right)/L$ and $\psi_O = \beta_B v_O P\left[1+\left(\beta-1\right)y_{AO}\right]$ in which the subscript O refers to the outlet, and the subscript F refers to the feed end of the packed bed. When pressure varies linearly with time, P' is constant, as are the molar flow rates. A hypothetical problem could arise if imposing a pressure shift caused the shock wave to degrade into a diffuse front. The step time would then have to be shortened to maintain high product purity, which would reduce recovery. On that point, Kayser and Knaebel[10] concluded via the *entropy condition* that unless the pressure shift causes a dramatic increase in pressure drop or mass transfer resistance, the equilibrium tendency should preserve the shock front.

When the pure, less strongly adsorbed component, B, is used to pressurize the column from P_L to P_F, and when the feed step involves a pressure shift (e.g., partial pressurization by feed or partial cocurrent blowdown) to P_H, the recovery of the pure, less strongly adsorbed component can be expressed as:

$$R = \frac{1+\left(\beta\tilde{A}_I^{\beta-1}-1\right)y_{A_F}}{\tilde{A}_I^{\beta}\left(1-y_{A_F}\right)} \times\left[1-\frac{1/\beta+\left(\tilde{A}_F-1\right)}{\tilde{A}_H-\tilde{A}_F}\left(\frac{\tilde{A}_I^{\beta}\left[1+\left(\beta-1\right)y_{A_F}\right]}{1+\left(\beta\tilde{A}_I^{\beta-1}-1\right)y_{A_F}}-1\right)\right] \tag{4.37}$$

where $\tilde{A}_I = P_H/P_F$, $\tilde{A}_F = P_F/P_L$ and $\tilde{A}_H = P_H/P_L$. Only two pressure ratios of the three mentioned are independent; the latter quantities are preferred because they are constrained to be greater than unity. Suh and Wankat[21] studied separate feed and cocurrent blowdown steps, and found that the distinct steps can yield better recovery than when combined.

Figure 4.10 shows predictions of product recovery as affected by the latter pressure ratios. Three cases are shown involving separations that are "difficult," either because the feed is predominately the heavy component, or because the adsorption selectivity is poor,

or both. These are represented by: (a) $\beta = 0.1$ and $y_F = 0.9$; (b) $\beta = 0.9$ and $y_F = 0.1$; and (c) $\beta = 0.9$ and $y_F = 0.9$, respectively. It can be seen that recovery always increases by combining feed and partial cocurrent blowdown: the increase can be dramatic for a large value of $\wp_F$ and a low or moderate value of $\wp_H$. Conversely, recovery always declines when pressurization and feed are combined (i.e., $\wp_F < \wp_H$). The first plot shows the case of excellent selectivity, but the feed is very contaminated with the heavy component; the results suggest that, for this system, combined feed and cocurrent blowdown will yield only a small improvement over conventional PSA. The second plot, in which the selectivity is poor and the feed is predominately the light component, shows that very large improvements in recovery are possible for combined feed and cocurrent blowdown. For example, the maximum recovery via conventional PSA is 10% (at a very high pressure ratio). Combining feed and cocurrent blowdown can match that recovery at a pressure ratio of only 6, or vastly exceed it (e.g., reaching 25% recovery at a pressure ratio of 50). The third example shows a system having poor adsorbent selectivity and heavily contaminated feed. Recovery is improved for this case, too, by, for example, initially pressurizing to a pressure ratio of 50 then feeding while blowing down cocurrently to a pressure ratio of 15. The result exceeds the maximum recovery of the conventional cycle (at very high pressure ratios). Increasing the initial pressure ratio to 100 yields a 50% increase in recovery. The advantages of increased recovery must, of course, be weighed against the inherent costs of increased complexity and additional power for recompressing the product, if that is necessary.

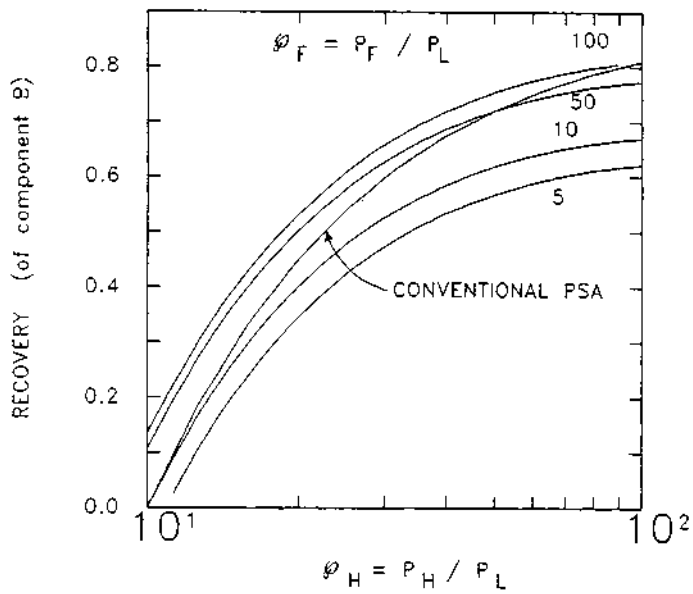
$\varphi_F = P_F / P_L$
100
50
10
5
CONVENTIONAL PSA
RECOVERY (of component B)
0.8
0.6
0.4
0.2
0.0
10^1
10^2
$\varphi_H = P_H / P_L$

(a)

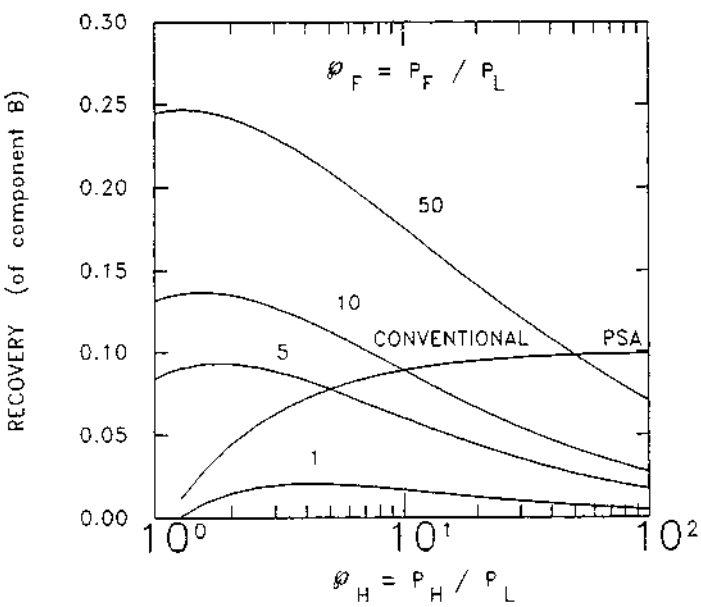
$\varphi_F = P_F / P_L$
50
10
5
1
CONVENTIONAL PSA
RECOVERY (of component B)
0.30
0.25
0.20
0.15
0.10
0.05
0.00
10^0
10^1
10^2
$\varphi_H = P_H / P_L$

(b)

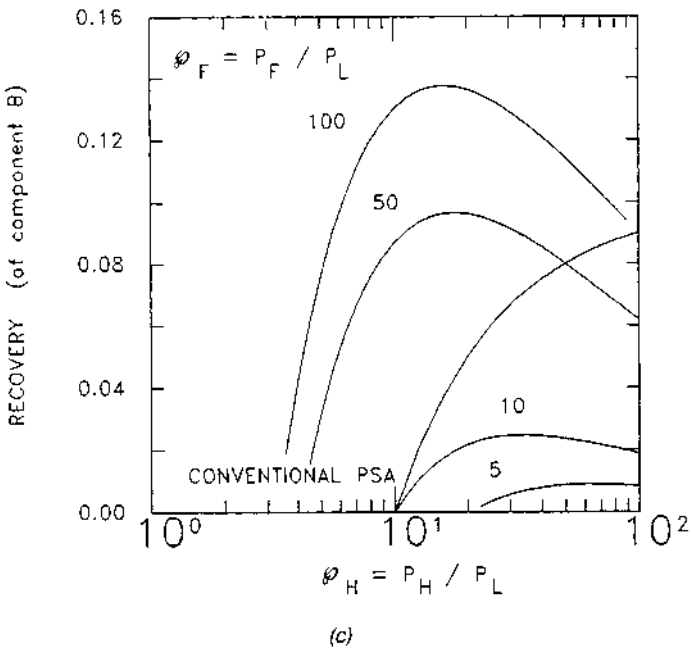

Figure 4.10 Recovery as affected by pressure ratios, for a four-step cycle in which the feed step pressure rises or falls, (a) $\beta = 0.1$, $y_F = 0.9$; (b) $\beta = 0.9$, $y_F = 0.1$; (c) $\beta = 0.9$, $y_F = 0.9$.

4.4.5 Five-Step PSA Cycle: Incorporating Rinse and Incomplete Purge

In this section a rinse step is added to the four-step PSA cycle discussed in Section 4.4.3. The added rinse step follows the feed step, and it begins by admitting the pure heavy component to the bed. This displaces the residual feed, which is recycled. In so doing, the adsorbent bed becomes saturated with the heavy component. Therefore, during the blowdown step, the heavy component is recovered as the pressure drops from P_H to P_L. At least part of the heavy component must be recompressed (to P_H) for use in the subsequent rinse step. The cycle is shown schematically in Figure 4.11.

Though called rinse, the action of this step could also be thought of as a high-pressure purge. A major formal distinction between rinse and purge is that rinsing involves a composition shock wave, while purging involves a simple wave. Arguments can be made for directing the flow during the rinse step either cocurrent or countercurrent to the feed. Factors such as mechanical complexity and product purity affect the choice. For now, since the mathematical model to be discussed assumes local equilibrium, implying that ideal shock fronts exist during the feed and rinse steps, the direction does not affect performance. To be definite (and to favor the mechanically simpler version), the rinse flow is taken to be counter to that of the feed.

The present PSA cycle also includes incomplete purging. The equations that govern the purge, pressurization, and feed steps in this cycle are identical to those that apply in the four-step cycle covered in Sections 4.4.1 and 4.4.3. Similarly, the equations that govern the rinse step in this cycle are analogous to those for the feed step. That is, the relation between the interstitial velocity, the length of the bed, the step time, and the column isotherm is obtained from Eqs. 4.5, 4.7, 4.9, 4.10, and follows along the same lines as Eq. 4.20:

$$v_{\text{out}} t|_{\text{R}} = L/\theta_B \tag{4.38}$$

Similarly, the corresponding expression involving the rinse step molar effluent rate, step time, pressure ratio, and coefficients that represent geometry and adsorbent–adsorbate interactions is similar to Eq. 4.22. As a result, the molar quantities in the effluent and influent are:

$$\overline{Q_{\text{out}}t}|_{\text{R}} = \phi\tilde{A}\,\beta_{A_0}/\theta_B \tag{4.39}$$

$$\overline{Q_{\text{in}}t}|_{\text{R}} = \phi\tilde{A}\left[1+(\theta-1)\,y_{A_{\text{F}}}\right]\beta_{A_0}/\theta_A \tag{4.40}$$

where $\theta = \theta(P_{\text{H}}, y_{\text{F}}, y=1)$. Note that the form of Eq. 4.40 is identical to that of Eq. 4.24. For nonlinear isotherms, since the parameters are evaluated under different conditions, the results may be different.

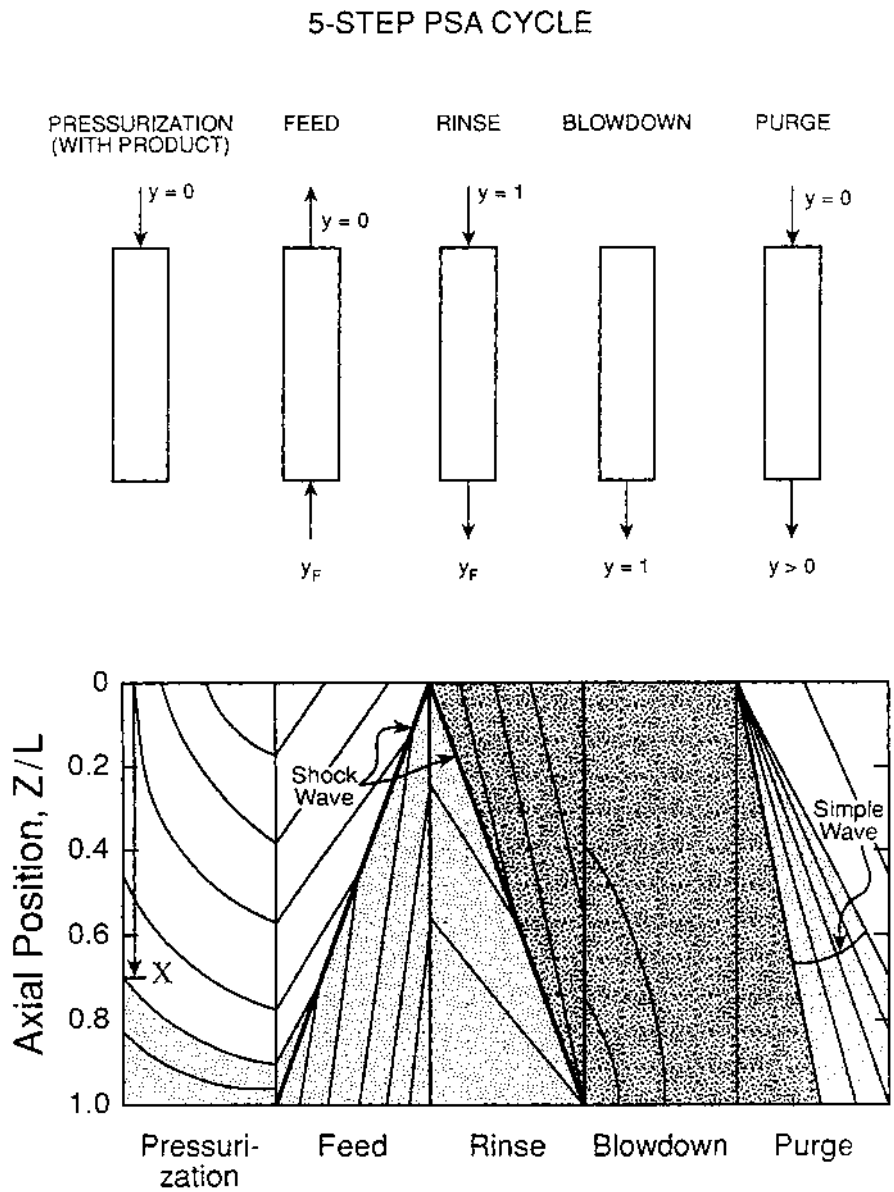

Figure 4.11 Five step cycle-including a rinse step. (Top) Flows and composition associated with each step. (Bottom) Position-verus-time representation of each step. Shaded region depicts penetration heavy component. *X* denotes fraction of completion of purge step.

The blowdown step is critical to this cycle since it is the source of the heavy component product. It follows the rinse step, so the bed is presumed to contain only the pure, heavy component. The most direct approach to determine the net effluent is simply to determine the difference the initial and final states, according to Eq. 4.18 (since the contents are assumed to be pure *A*). The result is:

$$\overline{Q_{\text{out}}}t|_{\text{BD}} = \phi\beta A_0 \left(\frac{\tilde{A}}{\theta_A\left(P_{\text{H}}, y=0, y=1\right)} - \frac{1}{\theta_A\left(P_{\text{L}}, y=0, y=1\right)} \right) \tag{4.41}$$

Thus, as for pressurization, the *rate* of blowdown is immaterial; only the initial and final pressures matter.

The light and heavy product recoveries from the current five-step cycle, based on complete purge and nonlinear isotherms are:

$$R_B = 1 - \frac{\theta_A / \beta_{A_0} - \theta}{\tilde{A}\, y_{B_{\text{F}}}\left(1-\theta\right)} \tag{4.42 A}$$

where $\theta = \theta\left(P_{\text{H}}, y_{\text{F}}, y=0\right)$ and $\theta_A = \theta_A\left(P_{\text{H}}, y_{\text{F}}, y=0\right)$.

$$R_A = \frac{\tilde{A}\left[\varphi_1 + \left(1-\theta\right) y_{\text{F}} - 1\right] - \varphi_2}{\tilde{A}\, y_{\text{F}}\left(\varphi_3 - \theta\right)} \tag{4.43}$$

where $\theta = \theta\left(P_{\text{H}}, y=1, y_{\text{F}}\right)$, $\varphi_1 = \theta_A\left(P_{\text{H}}, y=1, y_{\text{F}}\right) / \theta_A\left(P_{\text{H}}, y=1, y=0\right)$, $\varphi_2 = \theta_A\left(P_{\text{H}}, y=1, y_{\text{F}}\right) / \theta_A\left(P_{\text{L}}, y=1, y=0\right)$, and $\varphi_3 = \theta_A\left(P_{\text{H}}, y=1, y_{\text{F}}\right) / \theta_A\left(P_{\text{H}}, y_{\text{F}}, y=0\right)$.

For linear isotherms, these equations simplify to:

$$R_B = 1 - \frac{1}{\tilde{A}\, y_{B_{\text{F}}}} \tag{4.44}$$

$$R_A = 1 - \frac{1}{\left(1-\beta\right)\tilde{A}\, y_{A_{\text{F}}}} \tag{4.45}$$

In this cycle, just as for the four-step cycle mentioned in Section 4.4.3, the recovery of the light component can be improved by reducing the amount of pure light product consumed in the purge step. The analysis of incomplete purge here is identical to that presented earlier, since the steps are basically the same. A minor detail is that, at the outset of the purge step, more of the heavy component remains in the column than in the four-step cycle, when the blowdown step follows the feed step.

The present cycle differs somewhat from the cycle suggested by Sircar,[22] which also includes a rinse step and is described in Section 6.4. Differences between the cycles are mainly in the details, such as the flow direction in certain steps. Both cycles were reduced to practice for the purpose of splitting air, and the ranges of pressure ratios are nearly

identical, implying that the power required would be equivalent. Experimentally, however, these cycles performed differently, and the resulting recoveries and product purities are compared in Section 4.5. That section also compares the experimental results with the theoretical predictions presented here [see Figures 4.14(a) and 4.14(b)].

4.4.6 Four-Step PSA Cycle: Columns with Dead Volume

This section covers a method for estimating the magnitude of effects caused by dead volume, via an equilibrium model. The effects of dead volume are diverse—they vary depending on which end of the adsorbent bed is affected, and they depend on which step of the cycle is being considered. As shown here, the effects are also typically more severe when adsorbent selectivity is poor.

Notwithstanding the last assumption stated in Section 4.1, an inescapable feature of adsorption columns is dead volume at both the feed end and product end of the fixed bed. The primary reason is that, if plug flow is to be established in the adsorbent bed, the gas must be allowed uniform access in the direction of flow. For an ordinary cylindrical column, with axial feed and discharge nozzles and bad retention plates, this could amount to a dead volume (at each end) of 5 to 10% or more of the volume of the adsorbent bed.

Breakthrough curves obtained from most commercial columns exhibit "rounding" arising from axial dispersion, mass transfer resistance, or back mixing before or after the adsorbent bed. If dead volume is largely responsible for the rounding, it should be easy to diagnose. At a given pressure, temperature, velocity, etc., one can simply compare the breakthrough curve of a conventional column with one in which dead volume has been minimized. Examples of the latter, shown in Figure 4.2, were obtained with commercial adsorbents at velocities and pressures typical of commercial systems, but in a column in which dead volume was minimized. Of course, if rounding exists, it could also be an artifact of the slow response of the sampling instrument.

Dead volume at the product end of a PSA column affects the steps differently, as follows:

Blowdown. If, during the previous feed step, breakthrough had not begun, retained pure product partially purges the bed during blowdown; if breakthrough had begun, the gas that expands from this volume is merely additional (unnecessary) waste.

Purge. If breakthrough had not begun during the feed step, less gas is consumed during purge because of the contribution during blowdown; if breakthrough had begun, excess gas is necessary to cleanse this volume before the adsorbent can begin to be purged.

Pressurization. Extra pure light product is required to pressurize this space, though it is recovered during the feed step.

Feed. No effect except to retain part of the product gas, if breakthrough was prevented; if breakthrough had begun, mixing in this region dampens the contamination of the product stream leaving the column.

In comparison, dead volume at the feed end of a PSA column has the following effects:

Blowdown. No effect except to retain part of the waste gas.

Purge. Same as blowdown.

Pressurization. Excess pure light component is necessary to pressurize this space.

Feed. Feed gas mixes with the pure light component, resulting in a "diffuse" front entering the adsorbent bed.

Thus, there are several disadvantages to dead volume, and few advantages. In fact, the only positive aspect is the possibility that the dead volume at the product end of the column may hold sufficient pure product to partially purge the bed during blowdown. That benefit is balanced by the fact that the gas will be less effective at purging the column than gas admitted during the purge step (at low pressure), because it needlessly expels gas while desorption is in progress.

The following development is based on linear isotherms and the four-step cycle described in Section 4.4.1. The cycle is composed of pressurization with product, constant pressure feed, countercurrent blowdown, and complete purge. To the extent possible, both feed-end and product-end dead volumes are considered. Again in this section, compositions are expressed in terms of the heavy component, *A*. Some of the concepts to be presented have been examined by Kolliopoulos.[23]

For simplicity, the analysis begins with the blowdown step. This is because the gas retained in the product-end dead volume and exhausted in that step contributes to purging. It is presumed that the feed step stops at the point of imminent breakthrough, so that the gas retained in that dead volume, having $\text{volume} = V_{\text{DV}_\text{P}}$, is not contaminated (i.e., $y_{\text{DV}_\text{P}} = 0$). The approach taken is to determine the extent of purging that occurs during blowdown, and then to determine the additional amount needed during the purge step. The amount of pure light component required for pressurization is increased by that needed to fill the dead volumes. Under these assumptions, the feed step is not directly affected by product-end dead volume, but only by the feed-end dead volume.

To predict the composition profile at the conclusion of blowdown, one must follow characteristics representing different initial compositions and axial positions. The characteristics velocity is given by Eq. 4.35. Perhaps the most important characteristic is the one that identifies the extent of purging due to expansion of gas from the dead space:

$$\left.\frac{dz}{dt}\right|_{y=0} = \frac{\beta}{P}\left(\psi_0 - P'z\right) \tag{4.46}$$

where $\psi_0 = \beta_B v_0 P$, which is nil if $V_{\text{DV}_\text{P}} = 0$, $P' = \left(P_\text{L} - P_\text{H}\right)/t_\text{BD}$, and t_BD is the time allotted for blowdown. This can be rearranged to get the distance into the bed (measured from the product end) that is completely purged,

$$z_0 = z|_{y=0} = \frac{\psi_0}{P'}\left(1 - P^{-\beta}\right) \tag{4.47}$$

A material balance for the dead volume demands that

$$\psi_0 = \beta_B V_{\text{DV}_\text{P}} P' / A_\text{CS}\varepsilon = \beta_B \lambda_\text{P} L P' / \varepsilon \tag{4.48}$$

where $\lambda_\text{P} = V_{\text{DV}_\text{P}} / V_\text{C}$ and $V_\text{C} = \pi d_\text{C}^2 L/4$ is the volume of the adsorbent bed. When this is combined with the preceding relations, the fraction of complete purge that is attained during blowdown is found.

$$X = \frac{z_0}{L} = \frac{\lambda_P \beta_B}{\varepsilon}\left(1 - \tilde{A}^{-\beta}\right) \tag{4.49}$$

The bed is assumed to have been saturated with feed at high pressure during the preceding feed step. If the feed-end dead volume is very large, however, the actual concentration of A may be less. That possible discrepancy is neglected here. Thus, as blowdown proceeds, the residual gas becomes enriched in component A and is pushed towards the outlet end. The composition shifts to y_{BD}, as in Eq. 4.32, which yields:

$$y_{BD} = 1 - \left(1 - y_F\right)\left(\frac{y_{BD}}{y_F}\tilde{A}^{\beta-1}\right)^{1/\beta} \tag{4.50}$$

The characteristic having this composition propagates according to Eq. 4.33, which may be combined with a material balance to obtain:

$$\begin{aligned} X^* &= \left.\frac{z}{L}\right|_{y_{BD}} \\ &= \frac{\lambda_p \beta_B}{\varepsilon}\left[1 - \frac{1+(\beta-1)y_{BD}}{1+(\beta-1)y_F}\left(\frac{1-y_F}{1-y_{BD}}\right)^{1/(1-\beta)}\left(\frac{y_{BD}}{y_F}\right)^{\beta/(1-\beta)}\right] \end{aligned} \tag{4.51}$$

The dimensionless distance, X^*, reached by the expanding feed gas is measured from the product end. Thus, Eqs. 4.49 and 4.51 define the partially purged region between completely purged and expanded feed.

Before proceeding, it may be enlightening to consider the potential impact of dead volume at both ends of the column, and the variety of possibilities that arise. For example, the adsorbent selectivity, feed composition, pressure ratio, and size of the product-end dead volume all affect the ultimate position of the partially purged region. So, assuming that there is dead volume at the feed end, the contents of this space may be: unaffected, partly affected, or completely purged as a result of expansion of the pure light component from the product-end dead volume. Similar additional possibilities arise in other steps of the cycle, leading to many permutations and contingencies. Hence, the overall problem is difficult to generalize.

To determine the effluent composition during the countercurrent blow-down step, the material balance for the feed-end dead volume is combined with the foregoing balances of the adsorbent bed and product-end dead volume. The former yields y_{BD} (P(t)) at z = L via Eq. 4.50. The overall balance equation is:

$$\frac{V_{DV_F}}{RT}\frac{d\left(Py_{out}\right)}{dt} = \frac{P}{RT}\left[\dot{V}_L y_{BD}\left(P(t)\right) - \dot{V}_{out} y_{out}\right] \tag{4.52}$$

By applying the chain rule for differentiation and simplifying, this reduces to:

$$\frac{dy_{out}}{dt} = \frac{\varepsilon/\beta_B - \lambda_P}{\lambda_F}\left(\frac{y_{BD} - y_{out}}{(1-\beta)(1-y_{BD})y_{BD}}\right) \tag{4.53}$$

where $\lambda_F = V_{DV_F}/V_C$. This expression may be integrated either analytically or via a

Runge–Kutta routine. The result of the former approach is given by Eq. 4.54, although in terms of time and effort, the numerical approach may well be easier.

$$y_{\mathrm{BD}_{\mathrm{out}}} = y_{\mathrm{F}}\left(\frac{1-y_{\mathrm{BD}}}{1-y_{\mathrm{F}}}\frac{y_{\mathrm{F}}}{y_{\mathrm{BD}}}\right)^{\eta}\left(1-\eta\sum_{i=0}^{\infty}\frac{y_{\mathrm{F}}-1}{\prod_{j=0}^{i}(\eta-j)}\right) + \eta\, y_{\mathrm{BD}}\sum_{i=0}^{\infty}\frac{y_{\mathrm{BD}}-1}{\prod_{j=0}^{i}(\eta-j)} \tag{4.54}$$

where. $\eta = \left(\varepsilon/\beta_B - \lambda_{\mathrm{P}}\right)/\lambda_{\mathrm{F}}$.

The dead volume at the feed end is assumed to be well mixed, and thus cannot be *completely* purged. For practical purposes, it is sufficient to purge the adsorbent completely. In fact, in view of the earlier discussion of incomplete purge, even this is often unnecessary. The quantity of light component essential for complete purging of the adsorbent bed is:

$$\overline{Q_{\mathrm{in}}t}|_{\mathrm{PU}} = \phi\left(1-\frac{\beta_B\lambda_{\mathrm{P}}}{\varepsilon}\left(1-\tilde{A}^{-\beta}\right)\right) \tag{4.55}$$

This is less than the amount required for a column having $V_{\mathrm{DV_P}} = 0$, by the fraction of the bed that had been purged by residual product during the blowdown step.

To continue the analysis, it is necessary to find the final composition in the feed-end dead volume during the purge step. Two phases are relevant: during the first, the heavy component concentration increases (reflecting residual material in the feed-end dead volume), and during the second there is diminishing concentration of the heavy component (which continues until the adsorbent is purged). The column outlet concentration during the first phase is given by:

$$y_{\mathrm{PU}_{\mathrm{out_I}}} = y_{\mathrm{BD}} - \left(y_{\mathrm{BD}} - y_{\mathrm{BD}_{\mathrm{out}}}\right) \times \exp\left(-\frac{\varepsilon}{\beta_A\lambda_{\mathrm{F}}}\left[1+(\beta-1)\,y_{\mathrm{BD}}\right]\left(1-X^*\right)\right) \tag{4.56}$$

The second phase is characterized by gradual cleansing of the feed-end dead volume, which depends on the relative volume at the product end, as follows:

$$y_{\mathrm{PU}_{\mathrm{out_{II}}}} = y_{\mathrm{PU}_{\mathrm{out_I}}}e^{\alpha(\theta_0-1)} + \frac{1}{1-\beta}\left[\alpha e^{-\alpha\theta_0} - \left(1-\frac{1}{\alpha}\right)\left(1-e^{\alpha(\theta_0-1)}\right)\right] \tag{4.57}$$

where $\alpha = 2\varepsilon/\lambda_{\mathrm{F}}\beta_A$, $\theta_0 = \left(t^*/t_L\right)^{1/2} = \left[1+(\beta-1)\,y^*\right]\left(1-X^*\right)^{1/2}$ and X^* is given by Eq. 4.51. When the product-end dead volume is small, the ultimate composition leaving the column during purge is:

$$y_{\mathrm{PU}_{\mathrm{out_{II}}}} = \left(y_{\mathrm{PU}_{\mathrm{out_I}}} - y^* - \frac{\beta_A \lambda_{\mathrm{F}}}{2\varepsilon(1-\beta)} \right) \exp\left(-\frac{2\varepsilon}{\beta_A \lambda_{\mathrm{F}}} (1-\beta) y^* \right) + \frac{\beta_A \lambda_{\mathrm{F}}}{2\varepsilon(1-\beta)} \tag{4.58}$$

The pressurization step demands excess material to pressurize the dead volume. The precise amount, according to the ideal gas law, is independent of composition. Nevertheless, at the feed end, since material flows into the dead volume as pressure increases, the composition changes. The moles required for pressurization become:

$$\overline{Q}t\,|_{\mathrm{PR}} = \phi(\tilde{A} - 1)\left(\beta + \frac{\beta_A(\lambda_{\mathrm{F}} + \lambda_{\mathrm{P}})}{\varepsilon} \right) \tag{4.59}$$

The composition in the feed-end dead volume at the end of pressurization becomes:

$$y_{\mathrm{PR}_{\mathrm{final}}} = \frac{y_{\mathrm{PU}_{\mathrm{out_{II}}}}}{\tilde{A}} \tag{4.60}$$

Finally, the feed step is potentially somewhat involved due to the presence of the heavy component in the feed-end dead volume. The feed immediately begins to shift that composition, but it displaces material into the bed simultaneously. The composition in the feed-end dead volume varies with time according to:

$$y_{\mathrm{in}} = y(z=0,\, t') = y_{\mathrm{b}}(t) = y_{\mathrm{F}} + \left(y_{\mathrm{PR}_{\mathrm{final}}} - y_{\mathrm{F}} \right) e^{-\left(\varepsilon v_{\mathrm{F}} A_{\mathrm{CS}} / V_{\mathrm{DV_F}}\right) t'} \tag{4.61}$$

Material at this composition enters the bed at t', and it reaches the shock wave at t. The shock wave velocity varies as the composition at its trailing edge varies, that is,

$$\left.\frac{dz}{dt}\right|_{\mathrm{SH}} = \beta_A v_{\mathrm{F}} \frac{1 + (\beta - 1) y_{\mathrm{F}}}{1 + (\beta - 1) y_{\mathrm{b}}} \tag{4.62}$$

Likewise, the velocity of the characteristic that intersects the shock wave at the trailing edge varies depending on its composition, as follows:

$$\left.\frac{dz}{dt}\right|_{y_{\mathrm{b}}} = \beta_A v_{\mathrm{F}} \frac{1 + (\beta - 1) y_{\mathrm{F}}}{\left[1 + (\beta - 1) y\right]^2} = \frac{z}{t - t'} \tag{4.63}$$

Solving Eqs. 4.61 and 4.63 simultaneously for y_{b} yields an expression for t' in terms of z and t. The path of the shock wave can be determined by integrating Eq. 4.62, for example

$$\left.\frac{dz}{dt}\right|_{\mathrm{SH}} = K\left[1 + (\beta - 1) y_{\mathrm{b}}\right] = f\left(y_b\left(z, t, t'(z,t)\right)\right) \tag{4.64}$$

To simulate a complete PSA cycle when both dead volumes are significant calls for only two more parameters to be specified than for a system without dead volumes. Despite that, the pressure ratio, feed composition, and adsorbent selectivity all affect the impact of both dead volumes. Hence, to present a general perspective would require more space than is available here. As an alternative, it is possible to keep details to a minimum, yet get a sense of the important factors, by restricting attention to a single dead volume. Since it is

conceivable that the product-end dead volume may improve PSA performance by its passive purging action, it is more interesting than feed-end dead volume alone, for which all the foreseen effects are negative. For that reason, the discussion that follows is focused mainly on product-end dead volume.

Figures 4.12(a)–(d) show the combined effects of product-end dead volume and pressure ratio on recovery of the light component in a four-step PSA cycle. The cycle is the same as that shown in Figure 4.1, except for dead volume in the column. Each figure applies to a different feed composition and adsorbent selectivity. While examining the details, it may be revealing to keep in mind some historical facts. Early PSA systems for hydrogen purification used modest pressure ratios (e.g., $\wp \leq 10$), had high adsorbent selectivity (e.g., $\beta \leq 0.1$), and the feed was predominately the light component ($y_F \leq 0.1$). Figure 4.12(a) is based on those conditions, and it shows that the effect of dead volume on recovery is small. Thus, hindsight affirms these theoretical results; that is, hydrogen purification systems could contain significant dead volume, as in conventional adsorbers, without suffering much loss in recovery. At the present time, increasingly more difficult PSA applications are being considered, and an appropriate question is whether column designs need to be modified to accommodate them. For example, the predicted recovery for a system having low adsorbent selectivity is shown in Figure 4.12(b). To be specific, the conditions are the same as for Figure 4.12(a), except that $\beta = 0.9$ in that figure instead of $\beta = 0.1$. The effect of dead volume is severe, except at low pressure ratios (e.g., $\wp \leq 3$). Conversely, at moderate to large pressure ratios (e.g., $\wp \geq 10$), there is a 50% drop in recovery for only 10% dead volume, and nil recovery for dead volumes of 20% or greater.

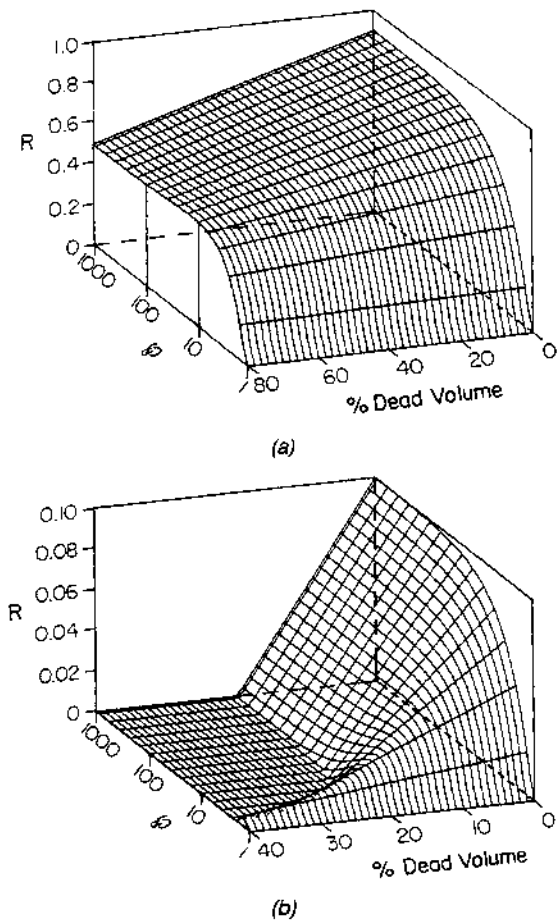

Figure 4.12 Predicted recovery versus pressure ratio and percent dead volume: (a) $\beta = 0.1$, $y_F = 0.1$, (b) $\beta = 0.9$, $y_F = 0.1$.[23]

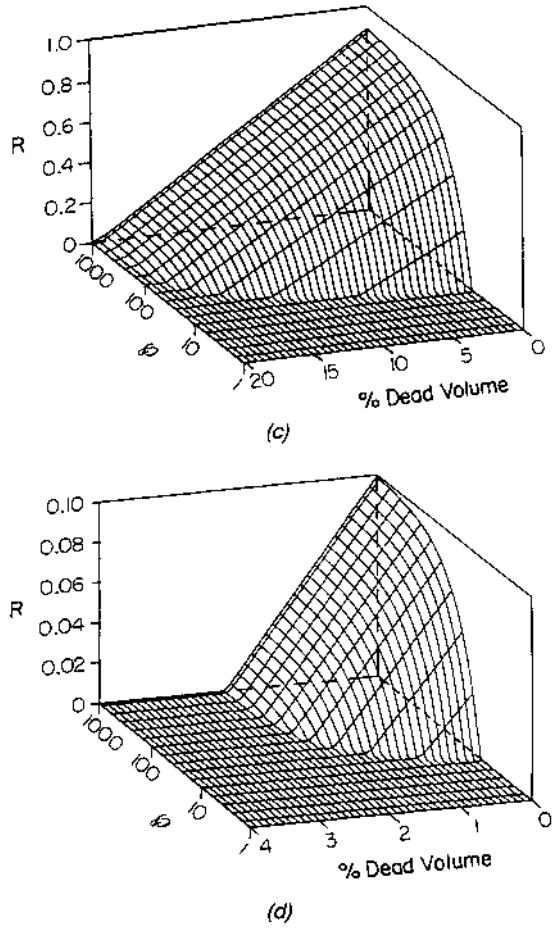

Figure 4.12 Predicted recovery versus pressure ratio and percent dead volume: (c) $\beta = 0.1$, $y_F = 0.9$, (d) $\beta = 0.9$, $y_F = 0.9$.[23]

In the same vein, another type of difficult PSA separation exists when the feed is mostly the more strongly adsorbed component (e.g., $y_F = 0.9$). In that case, the loss of recovery as shown in Figure 4.12(c), on a fractional basis, follows the same trends as in Figure 4.12(b), even though in this case the adsorbent selectivity is large. Applications that are difficult in both regards, that is, they have both low adsorbent selectivity and a high level of the more strongly adsorbed component in the feed, are extremely sensitive to dead volume, as shown in Figure 4.12(d). In that case, merely 2% dead volume is sufficient to destroy the potential recovery. From these results a rule-of-thumb is apparent: the fractional dead volume that will lead to nil recovery is: $\Lambda_p |_{R=0} \cong 0.02/y_F\beta$.

4.5 Experimental Validation

The beauty of local equilibrium theories lies in their simplicity and their ability to draw attention to the most important operating conditions, geometric parameters, and physical properties. Unless these predictions agree with reality, however, that beauty is superfluous. This section reviews some of the experimental work that has been deliberately aimed at verifying local equilibrium theories.

The early experimental studies appear to have been conducted as "black-box" studies,

in which cycling frequency, feed-to-purge flow rate ratios, pressures, etc. were varied systematically. As these parameters were manipulated, the performance (flow rates, product and byproduct purities) and other variables were monitored. Comparisons with theory were made retrospectively. Perhaps the first comparison of this sort was that of Mitchell and Shendalman.[24] Their application was the removal of 1% CO_2 from a helium carrier using silica gel. They did not find close correspondence with their equilibrium theory; so they introduced a mass transfer resistance to account for the discrepancy. This modification allowed them to bracket the observed behavior, but neither model was accurate over the entire range of conditions. Flores-Fernandez and Kenney[25] developed a more broadly applicable equilibrium theory, and solved it via finite differences and a commercial package known as CSMP. They tested their model by experimentally separating oxygen from air using 5A zeolite, and obtained fair agreement: within 15% for the prediction of feed flows, and within 12% for the prediction of recovery.

More recently a different approach has been taken, which is to build an experimental system in such a way that the inherent assumptions of the equilibrium theory are closely approached, then to operate it in such a way that the best possible performance is expected. This approach has the advantage of examining conditions that are of most practical interest, as well as using the theory as a tool to guide the experiments. Several different cycles have been evaluated this way, but to conserve space only three are discussed here. They are: the four-step cycle employing pressurization with product, a four-step cycle with combined feed and cocurrent blowdown, and a five-step cycle incorporating a rinse step in order to obtain two pure products. The underlying theory of all these cycles was discussed earlier in this chapter.

The first test determined the validity of the theory that was described in Section 4.4.1, which applies for the four-step pressurization-with-product cycle, shown in Figure 4.1. The experimental system was a two-bed apparatus containing zeolite 5A, designed to separate oxygen from dry air (Kayser and Knaebel[20]). The temperature and pressures were such that nearly linear isotherms were expected, and the equipment was designed so that the assumptions cited in Section 4.1 were valid (including minimal dead volume). Six sets of experimental conditions were tested, and for each, the system was operated until cyclic steady state was achieved. The pressure ratio range was from 6.5 to 840, and the average temperatures were 45 and 60° C. It should be noted that argon, which appears as about 1% in dry air, adsorbs nearly identically to oxygen, so the targeted "pure" light product is actually about 95% oxygen and 5% argon. Product recovery was of primary interest, since it is predicted quantitatively by the theory. Results of the experiments and the predictions of Eq. 4.27 are shown in Figure 4.13. Recall that there are no adjustable parameters in the model, so the extent of agreement is not due to empirical fitting. The average absolute deviation between the experimental and predicted recoveries was 1.5%, and the product purity averaged 99.6% (nitrogen-free oxygen and argon). These experiments provide strong evidence that, for this system, the equilibrium theory is essentially correct.

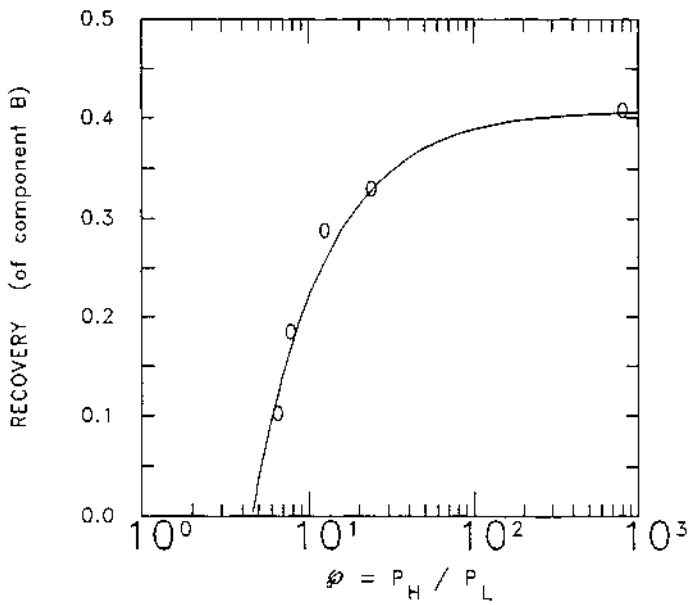

Figure 4.13 Experimental recovery versus predicted recovery (according to Eq. 4.27) for oxygen (and argon) separation from air using 5A zeolite at 45° C.[20]

Although the results described are reassuring, they focus on the high-pressure feed step; the pressurization, purge, and especially blowdown are ancillary steps. So a major question still remains as to the validity of equilibrium theories when *pressure changes* are vital to the cycle, rather than practically immaterial. This issue was examined in two separate types of experiments. The first type of experiment looked at the acceleration or deceleration of the shock wave during the feed step, in conjunction with decreasing or increasing pressure, respectively.[26] Comparing experimental results with predictions of the theory showed nearly perfect agreement for both increasing and decreasing pressure. Second, PSA experiments involving simultaneous feed and cocurrent blowdown have been conducted in a two-bed apparatus.[27] The theory for this type of cycle was discussed in Section 4.4.4. The application was to split oxygen from air with zeolite 13X. Six experiments were conducted in which two pressure ratios were varied independently. A summary of the conditions and results is given in Table 4.1.

Table 4.1. Conditions and Results of PSA Experiments with Combined Feed and Cocunent Blowdown[27]

Run	$\wp_F$	$\wp_H$	R_{expt}	R_{theory}	Δ (%)
1	12.77	10.43	25.4	26.5	–1.1
2	13.18	10.95	28.4	27.1	1.3
3	17.41	14.35	29.6	31.4	–1.8
4	22.91	19.03	34.1	34.6	–0.5
5	33.73	25.12	35.9	38.5	–2.6
6	33.29	21.06	37.4	39.1	–1.7

The average absolute deviation of the light product recovery between theory and these experiments was only 1.5%, just as it was for the experiments having constant pressure during the feed step. This close agreement provides additional evidence that the local

equilibrium theory is indeed valid, and is relatively insensitive to the cycle and operating conditions.

Finally, a set of experiments has been conducted in which a rinse step was introduced, in order to extract the heavy component as a pure product. In addition, the purge step was left incomplete, in order to achieve high recovery of the light component. The relevant theory is described in Section 4.4.5. The specific application was to split dry air to get oxygen (with residual argon) and nitrogen using zeolite 5A as the adsorbent. In those experiments, a single bed was used, and pressure ratios were varied between 6 and 20. Generally, it was possible to reduce the level of impurities in the products to about 1% (i.e., O_2 in N_2, and N_2 in O_2) and to achieve corresponding product recoveries between 27% and 90%. The predicted and experimental recoveries of both products agreed well, even though they varied with the applied pressure ratio, as shown in Figures 4.14(a) and (b).

In addition, Figure 4.15 shows a cross-plot of the experimental results from those experiments, along with results obtained by Sircar[22] for a very similar cycle. The axes depicted are product purity and recovery. Sircar's results show a commonly observed trend: as recovery increases, product purity decreases. The data from the experiments described, however, show that purity can be maintained at high levels as recovery increases, without a significant increase in power consumption.

To conclude this section, it appears that the equilibrium theory is accurate and reliable for different PSA cycles, even for relatively difficult separations. Parenthetically, it should be mentioned that other experimental evidence, shown in Figure 4.3, indicates that the equilibrium theory should be valid for a wide range of applications, although the degree of agreement depends on the Reynolds number in the bed. Finally, across the spectrum of potential PSA applications the intrusion of heat effects can be expected to vary widely. Such effects may be either beneficial or detrimental, as discussed in Section 4.8.

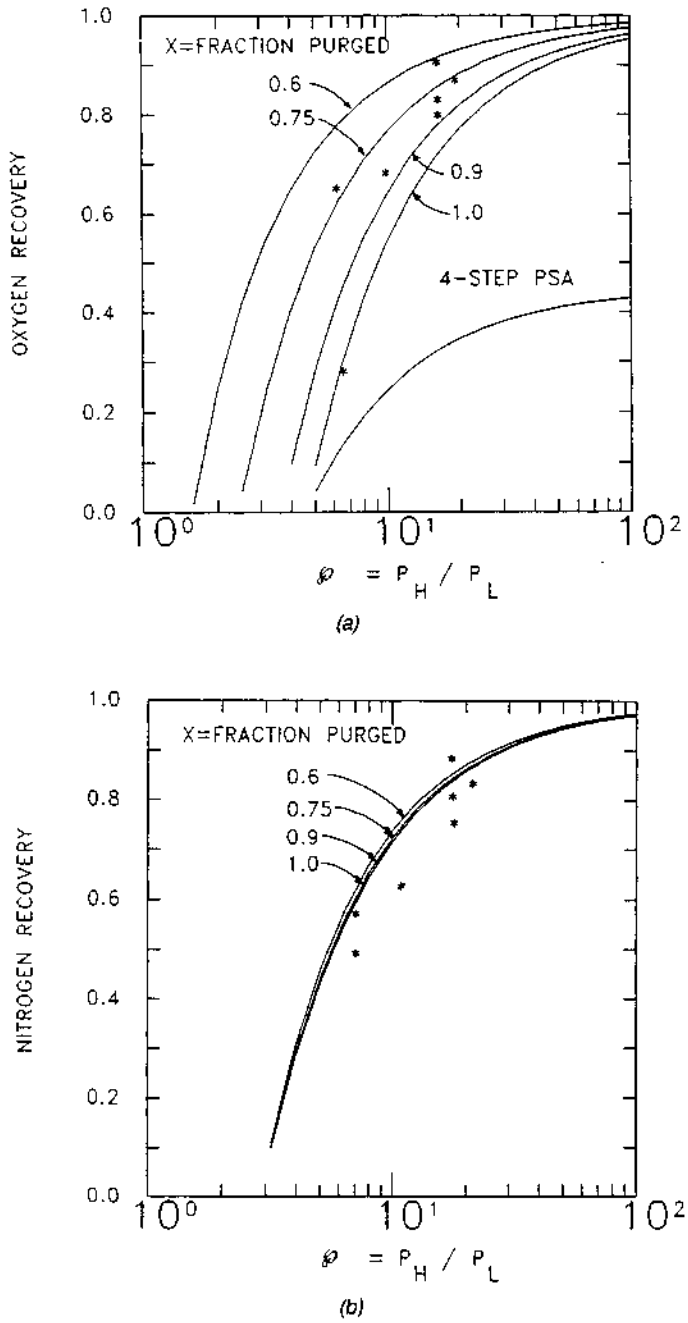

Figure 4.14 Recoveries of (a) oxygen and (b) nitrogen from air, for a five-step cycle, with an incomplete purge step.[12]

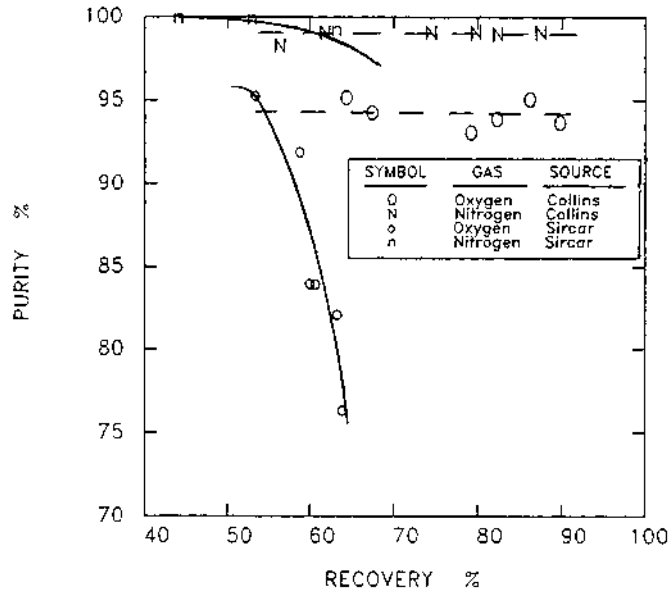

Figure 4.15 Recoveries and purities of oxygen and nitrogen from air, comparing the present five-step cycle[12] with a similar cycle proposed by Sircar.[22]

4.6 Model Comparison

This section examines the salient features of four distinct local equilibrium-based models that have been developed over the past several years. In general, it is fair to say that the obvious differences between these models are, remarkably, not in the final equations. Rather the differences lie in the *allowable* values of certain variables, which affect the parameters of the models. The original derivations contained subtle assumptions that imposed tight restrictions on the parameters. Thus, it was not merely an oversight that larger ranges of the parameters were not examined.

4.6.1 Four-Step PSA Cycle: Pressurization with Product

The first and simplest model, that of Shendalman and Mitchell,[2] can be applied to the PSA cycle shown in Figure 4.1, and the resulting equation for recovery can be expressed in the same form as Eq. 4.27. This model assumes that the more strongly adsorbed component is a trace contaminant and that it follows Henry's law, while the carrier is not adsorbed. In terms of the parameters used above, these are: $y_{B_F} \cong 1 (\text{i.e.}, y_{AF} \to 0)$, $\zeta = 1$, $\beta = \theta = \beta_{A_0} = \beta_A$, and $\beta_B = \theta_B = 1$. The next equilibrium model, developed by Chan, Hill, and Wong,[3] is less restrictive, though it also assumes that the more strongly adsorbed component is very dilute. It allows for adsorption of the carrier gas (following a linear isotherm). These restrictions amount to the following: $y_{B_F} \cong 1$, $\zeta = 1$, and $\beta = \theta = \beta_{A_0} / \beta_{B_0}$. Both of these theories ignore the effects of uptake (and release) on the interstitial gas velocity. That assumption allows the cycle to be analyzed easily, but it leads to potentially serious errors, because it implies that the molar flows of feed and product are identical, and similarly that the amount of gas required for pressurization is equal to the amount exhausted during blowdown.

A similar model, suggested by Knaebel and Hill,[13] incorporated adsorption of both components of an arbitrary binary mixture [i.e., $y_{B_F} \in (0,1)$]. Thus, the variation of velocity arising from composition variations was taken into account. Adsorption equilibrium, however, was still restricted to linear isotherms. Hence, the parameters of that model are: $\zeta = 1$, $\beta = \theta = \beta_{A_0} / \beta_{B_0}$ and $\beta_{i_0} = \theta_i$. Finally, the model of Kayser and Knaebel,[4] which is the basis of Eqs. 4.1–4.27, allows for nonlinear isotherms, as well as arbitrary composition. Thus, in that model the parameters are distinct, and the following combinations are allowed: $\zeta \neq 1, \beta \neq \theta \neq \beta_{A_0} \neq \beta_A$, and $\beta_B \neq \theta_B$ (although the last inequality is dropped in the examples to follow).

If we use the result of the most complete derivation to predict recovery, viz., Eq. 4.27, the differences between the models are reflected in the allowable values of the parameters. To emphasize the impact of the different parameters on the four models, two different adsorbent–adsorbate systems, which are both simulated at two different sets of conditions, will be discussed in the following paragraphs.

In the first PSA system, a very light gas, helium, is to be removed from nitrogen (cf. Figures 4.2 and 4.3). Nitrogen is much more adsorbable than helium, but not to the point that the isotherm is very nonlinear (at or below 2 atm). The first set of conditions represents what might be thought of as an *ideal* PSA application, since the light gas is taken as the major component. It is perhaps not surprising that there is excellent agreement (i.e., within about 3%) among the Shendalman–Mitchell, Chan et al., Knaebel–Hill, and Kayser–Knaebel models for that situation, and that the predicted recovery is high. The second set of conditions involves a significant shift: now the heavy component is the major component of the feed, and the pressure is high enough so that curvature of its isotherm is important. As a result, the two simplest models agree, but they must be incorrect since the heavy component is *not* merely a trace contaminant. The Knaebel–Hill model accounts correctly for composition, yielding a 15% reduction of recovery. Correcting for curvature of the nitrogen isotherm, via the Kayser–Knaebel model, reduces the recovery again by 23%.

Table 4.2. Comparisons of Four Local Equilibrium Models for a Four-Step PSA Cycle Employing Pressurization with Product[a]

System and model	Low $\wp$ and low concentration				High $\wp$ and high concentration			
	θ_A	θ_B	θ	R	θ_A	θ_B	θ	R
N_2–He	$y_{A_F} = 0.10, \tilde{A} = 5$				$y_{A_F} = 0.90, \tilde{A} = 50$			
1	0.171	1	0.171	0.663	0.171	1	0.171	0.812
2	0.171	0.956	0.179	0.657	0.171	0.956	0.179	0.805
3	0.171	0.956	0.179	0.638	0.171	0.956	0.179	0.657
4	0.172	0.956	0.180	0.636	0.286	0.956	0.299	0.426
N_2–O_2	$y_{A_F} = 0.10, \tilde{A} = 5$				$y_{A_F} = 0.79, \tilde{A} = 20$			
1	0.0579	1	0.0579	0.754	0.0579	1	0.0579	0.895
2	0.0579	0.163	0.356	0.515	0.0579	0.163	0.356	0.612
3	0.0579	0.163	0.356	0.501	0.0579	0.163	0.356	0.490
4	0.0583	0.163	0.359	0.497	0.0795	0.163	0.489	0.301

[a] Model 1 is the Shendalman–Mitchell model, $y_{A_F} \to 0$. Model 2 is the Chan–Hill–Wong model, $y_{A_F} \to 0$. Model 3 is the Knaebel–Hill model. Model 4 is the Kayser–Knaebel model. For N_2–He and N_2–O_2, the value of P_L used for the "low-$\wp$" comparison was 1 atm. For N_2–He, the value of P_L used for the "high-$\wp$" comparison was 0.5 atm. For N_2–O_2, the value of P_L used for the "high-$\wp$" comparison was 0.25 atm. These values, and the pressure ratios, allowed P_H to stay within the range of equilibrium data. He–N_2: Adsorbent = activated carbon, temperature = 20°C, $q_A = 10.63c_A - 12{,}826c_A^2$, $q_B = 0.1c_B$, $\varepsilon = 0.6874$. O_2–N_2: Adsorbent = Zeolite 13X, temperature = 0°C, $q_A = 15.013c_A - 24{,}547c_A^2$, $q_B = 4.7542c_B$, $\varepsilon = 0.480$.

The second PSA system is intended to separate oxygen (the light gas) from nitrogen using zeolite 13X. The first set of conditions in Table 4.2, are *less ideal* than for helium and nitrogen, because oxygen is much more adsorbable than helium. This shows the inadequacy of the Shendalman–Mitchell model. The heavy component is dilute, however, so there is little difference between the Chan–Hill–Wong and Knaebel–Hill models. Since the total pressure is relatively low, the curvature of the nitrogen isotherm is not significant, so the Kayser–Knaebel model is in good agreement with the previous two models. The second set of conditions, again, differs significantly from the first set: the feed is taken to be air, so the heavy component, nitrogen, is the majority of the feed. In addition, the pressure is high enough so that the curvature of the nitrogen isotherm is important. This leads to serious discrepancies among all the models. The Kayser–Knaebel model accounts for all the effects, and yields a significantly lower, but more realistic prediction of the recovery.

Figures 4.16 and 4.17 expand the scope of the oxygen–nitrogen example cited by showing a larger range of operating pressures. The basis is the same as described in Table 4.2. For the hypothetical feed composition of 10% nitrogen and 90% oxygen, shown in Figure 4.16, all the model predictions, except those of Shendalman and Mitchell (which does not account for sorption of oxygen), are in good agreement at low to moderate pressure ratios. Even when curvature of the nitrogen isotherm is taken into account, the differences are minor, as long as P_L is small. When it is raised to just 0.25 atm, to correspond to the comparison in Table 4.2, the effect of curvature becomes pronounced at high pressure ratios.

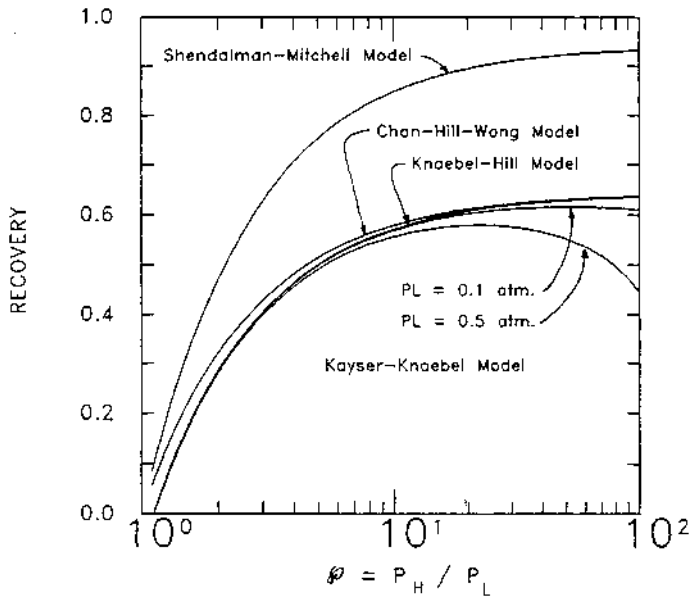

Figure 4.16 Predicted recoveries versus pressure ratio for separation of 10% nitrogen from oxygen with zeolite 13X.

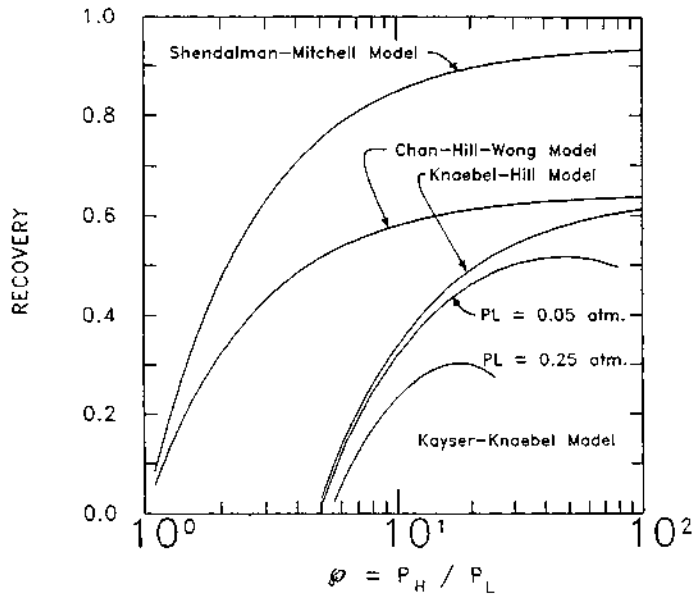

Figure 4.17 Predicted recoveries versus pressure ratio for separation of 79% nitrogen from oxygen with zeolite 13X.

For the more typical feed composition of 79% nitrogen and 21% oxygen, shown in Figure 4.17, there is practically no agreement among the models. That figure clearly shows the magnitude of deviations caused by ignoring: (1) sorption of the light component (the difference between the Shendalman–Mitchell model and that of Chan et al.), (2) composition dependence of interstitial velocity (the difference between the model of Chan et al. and the Knaebel–Hill model), (3) the effect of isotherm curvature (the difference between the model of Knaebel–Hill and the Kayser–Knaebel model), and finally (4) the

impact of absolute pressure when the isotherms are not linear (the difference between the values of P_L within the Kayser–Knaebel model). In all of these comparisons, recovery (at a given pressure ratio) is always diminished by taking into account more of the effects mentioned.

4.6.2 Four-Step PSA Cycle: Pressurization with Feed

The differences between the assumptions of the models of Chan et al.[3] and Knaebel and Hill[13] are also evident in PSA cycles that employ pressurization with feed. This section briefly discusses the qualitative and quantitative differences between Eqs. 4.29 and 4.30.

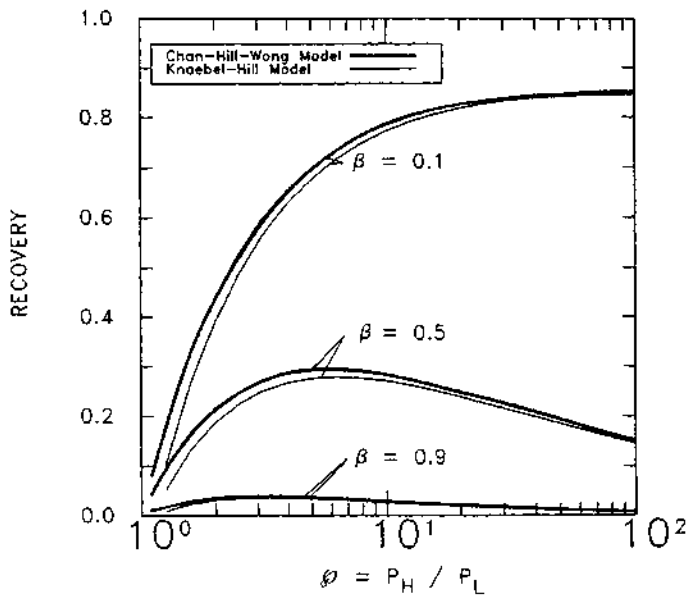

Figure 4.18 Recovery versus $\wp$ for various adsorbent selectivities, $y_{B_F} = 0.9$, comparing the models of Chan et al. and Knaebel and Hill.

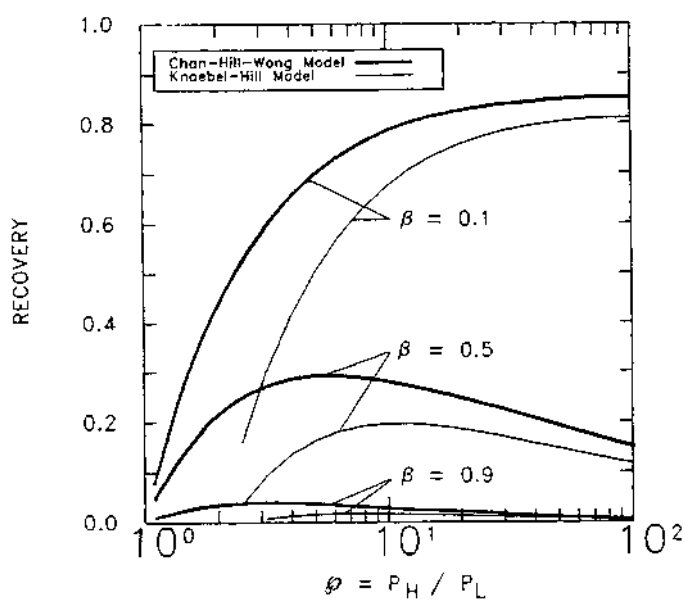

Figure 4.19 Recovery versus $\wp$ for various adsorbent selectivities, $y_{B_F} = 0.1$ according to the model of Knaebel and Hill.

The approach follows that of the previous section in which conditions are chosen first to be reasonably valid for both models; the conditions are then altered to violate the simpler model. In both cases the model predictions are compared to show the magnitudes of the potential errors due to oversimplification. Generally, Figures 4.18 and 4.19 compare the models of Chan et al. and Knaebel and Hill by showing the dependence of recovery on $\wp$ for various adsorbent selectivities. Specifically, Figure 4.18 shows relatively close predictions for $y_{A_F} = 0.1\left(y_{B_F} = 0.9\right)$. Conversely, Figure 4.19 shows larger discrepancies between the predicted recoveries, especially at lower pressure ratios, for $y_{A_F} = 0.5\left(= y_{B_F}\right)$. It should be emphasized that the lower values are considered to be more accurate, because the assumptions are less restrictive. In both figures, the differences diminish as the pressure ratio increases, implying that the impact of composition dependence on gas velocity becomes relatively smaller. Both of those figures also show that maximum recovery occurs at an intermediate pressure ratio for systems with moderate to low selectivities (i.e., $\beta >$ 0.4). Such behavior is not observed for the case of pressurization with product, except for nonlinear isotherms at relatively high values of P_L.

4.7 Design Example

Ordinarily, *open-ended* design of a PSA system might mean an involved optimization of the production rate, pressures (and other operating conditions), adsorbent, steps within the cycle, and equipment. Conversely, to design a PSA system for a *specific* application is more straightforward, because one would be given specifications for the feed and purified product streams and perhaps the adsorbent. Important steps for that case, which is really a subset of an open-ended design, include: obtaining relevant isotherms and other properties, selecting a PSA cycle, estimating recovery of the desired product at various operating pressures (assuming that sufficient product purity could be attained), determining power requirements and adsorbent bed sizes associated with each operating pressure range, and finally estimating the costs of the adsorbent, power, vessels, valves, etc. to arrive at the total cost. Detailed design considerations would address the product purity question, and ancillary details that affect the optimum conditions, and therefore the cost. Such details, though, are beyond the scope of this example. The purpose here is to illustrate rough sizing of a specific PSA system, generally following the steps listed, and employing the equilibrium theory.

The application considered here is production of 100 N m^3 per hour of oxygen (at 4.0 bar) from air, which is at ambient pressure and temperature. To avoid possible confusion in dealing with too many degrees of freedom, a number of arbitrary choices are made so that the focus can be kept on PSA rather than auxiliary issues. For example, one would ordinarily consider pretreatment of the feed to remove contaminants that could reduce adsorption capacity (e.g., in this case integrating desiccant with this system). For simplicity, however, the air fed to this system is assumed to be dry and free of contaminants. Thus, only the main constituents [nitrogen (78.03%), oxygen (20.99%), and argon (0.94%), i.e., 99.96% of "standard" air] are considered. In addition, the adsorbent is

chosen to be zeolite 5A. Coincidentally, the adsorption isotherms of argon and oxygen on 5A zeolite are practically identical, so argon is treated as oxygen in the PSA analysis. Selecting the operating temperature to be 45° C ensures that the isotherms are essentially linear up to about 6 atm (so there is no effect of absolute pressure on PSA performance). In addition, at that temperature the adsorbent–adsorbate interactions are characterized by β_A = 0.10003, ε = 0.478, ρ_B = 810 kg/m^3, and $\beta = \theta = 0.593$.[20]

Even within these constraints, there remain many options: for operating conditions, one could optimize the pressure ratio, extent of purge, and possibly the pressure manipulation scheme (cf. Sections 4.4.1–4.4.4). One could also consider producing purified nitrogen as a byproduct via a five-step cycle, since it offers very high potential oxygen recovery (cf. Section 4.4.5). To be concise, however, only two four-step PSA cycles are evaluated here, both operating at pressures sufficient to meet the product pressure specification. Both cycles employ pressurization with product, the first with complete purge, and the second with minimal purge.

In reviewing the steps mentioned pertaining to design of a specific PSA system, one might get the impression that, as far as PSA calculations are concerned, simply estimating PSA recovery is sufficient. It is not. An overall balance is required to determine the amount of adsorbent needed, then to size the bed and to predict the necessary power requires stream flow rates and pressures for individual steps. To refine the performance estimates further (e.g., to see the relationship between bed dimensions, flow rates, recovery, and pressure drop), one can use the Reynolds number in the fixed bed. Considering briefly Figure 4.3, one can see that there is a broad optimum of apparent adsorbent selectivity versus Reynolds number. In this example, the Reynolds number is stipulated to be 15, to be close to the equilibrium limit. One can see from Figure 4.3, however, that *doubling* it would increase the apparent value of $\theta = \beta$ only from about 0.59 to about 0.64, which means a loss of recovery of only about 15%. Hence, considering that less adsorbent can be used if velocities are raised, there is an economically optimum Reynolds number that is higher than at the apparent equilibrium limit.

Once the cycle and adsorbent are set, the variables that affect the optimum pressure ratio are the recovery and the power requirement. For the sake of simplicity, we will restrict consideration to adiabatic compression of an ideal gas,

$$\tilde{A} = \frac{\gamma}{\gamma - 1}\frac{\mathrm{QRT}}{\eta}\left(\tilde{A}_{\mathrm{C}}^{(\gamma-1)/\gamma} - 1\right) \tag{4.65}$$

where γ is the ratio of specific heats at constant pressure and constant volume, Q is the molar flow rate, η is the mechanical efficiency, and $\wp_{\mathrm{C}}$ is the compression ratio, $P_{\mathrm{C_H}}/P_{\mathrm{C_L}}$. For a four-step cycle, it is common to operate above atmospheric pressure so that only a feed compressor is needed, so $P_{\mathrm{L}} = P_{\mathrm{C_L}} \cong 1\,\mathrm{atm}$, and $\tilde{A}_{\mathrm{C}} \cong \tilde{A}$. It is possible, however, to extend to subatmospheric pressure for blowdown and purge. This operating range is often referred to as *vacuum swing adsorption* (VSA), as if to imply that there is something inherently different about it from PSA. In that case, $P_{\mathrm{L}} < 1$ atm, and there are $\tilde{A}_{\mathrm{C}}$s for both a gas compressor and vacuum pump to be considered, along with equipment costs and power requirements, though $\wp$ (and R_B) for the PSA system would be unaffected by the absolute pressure. While on the subject of costs, those of the major components are taken to

be: \$5 per kg of 5A zeolite, \$0.05 per kWh, and \$0.20 per N m^3 of 95% oxygen at 4 bar.

For the case of complete purge, recovery can be estimated via Eq. 4.27. It is easy to see that if P_L = 1 atm and P_H = 4 atm so that $\wp$ = 4, the predicted recovery is negative. Therefore, rather than considering the gamut of possibilities, we can set P_L = 0.25 atm, and $\wp$ = 16, which implies a recovery of 29.1%. The required net product, 100 Nm^3/h is equivalent to 1.24 mol/s. According to the definition of recovery, given by Eq. 4.26, the molar feed rate, Q_{in_F}, for the case of complete purge, is 19.36 mol/s. This is continuously fed, we will use two parallel columns to allow one to go through blowdown, purge, and pressurization while the other column receives feed air.

From Eq. 4.22 we find that for a given bed of adsorbent: $\phi/t_F = 1.21\,\text{mol/s}$, where $\phi = \varepsilon A_{CS} L P_L / \beta_A RT = 4.58\times10^{-5} V_{ads}$ and V_{ads} is the volume of the adsorbent in cm^3. Accordingly, $V_{ads}/t_F = 26,442.0\,\text{cm}^3/\text{s}$. The Reynolds number is defined as $\text{Re} = \varepsilon\rho v_{in_F} d_P / \mu$. where $\varepsilon\rho v_{in_F} = Q_{in_F} M_F / A_{CS}$; thus $\text{Re} = 148\,000./A_{CS}$. Setting Re = 15, we find that A_{CS} = 9850 cm^2; hence the column diameter is 112 cm. Returning to the ratio V_{ads}/t_F we can determine $L/t_F = 2.685\,\text{cm/s}$. Now, we are free to choose the length of the bed, say, L = 161 cm. The result is that the feed-step duration, t_F = 60 s, and the volume of adsorbent (for a two-bed system) is V_{ads} = 3.17 m^3, which, based on its bulk density of 810 kg/m^3, is equivalent to 2.57 metric tons of adsorbent.

Based on these values and a mechanical efficiency of 80%, the required power can be estimated. First of all the power for compression of the feed from 1 to 4 atm is 109 kW, and that to compress the subatmospheric blowdown and purge effluent from 0.25 atm to atmospheric pressure is 28.8 kW. Note that the amount of gas evolved during blowdown at any intermediate pressure can be determined from Eqs. 4.19 and 4.50, assuming that the bed is saturated with feed prior to blowdown. Hence the costs associated with the complete purge case would be: \$55,079 per year for power and \$12,851 for the adsorbent. Additional costs (for vessels, compressor, vacuum pump, valves, piping, instrumentation, site development, maintenance, and fees) should be proportional to these. These are balanced against a projected value of \$160,000 per year for the product.

For the case of incomplete purge, the calculations are somewhat more involved. The minimum extent of purge for the adsorbent properties and conditions cited and for P_L = 1 atm so that $\wp$ = 4, is X = 41%. This corresponds to a recovery of 36.55% (cf. Figure 4.9), and a required feed flow rate of $Q_{in_F} = 15.41\,\text{mol/s}$. Again, setting the Reynolds number at 15 leads to a column diameter of 100 cm. Using the same feed duration as before, t_F = 60 s leads to a column length of L = 176 cm. Thus, the volume of adsorbent needed to fill two columns is V_{ads} = 2.76 m^3. Based on the bulk density of 810 kg/m^3, this is equivalent to 2.24 metric tons of adsorbent. The necessary power, in this case, is only for compression of the feed from 1 to 4 atm. The result is 88.7 kW (about two-thirds of that required in the first case).

Therefore, the costs associated with the incomplete purge case would be: \$34,668 per year for power and \$11,197 for the adsorbent. As before, additional costs (for vessels, etc.) should be proportional to these. These are also balanced against a projected value of \$160,000 per year for the product. In this case the power cost has been reduced by 37%,

and the adsorbent cost has been reduced by 13%. In addition, this system does not require a vacuum pump or as many valves (e.g., for blowdown in successive stages), so the entire system is simpler and less expensive. A final, subtle point that has not been taken into account is that the cycle time could possibly be reduced for this case (since less uptake and release occur), which would lead to less required adsorbent, and a further reduction in cost.

4.8 Heat Effects

The term *heat effect* is frequently applied to a conspicuous change in performance that coincides with a temperature fluctuation. Although the term is introduced here, it is covered more quantitatively in Section 5.4. Viewing a packed bed pressure swing adsorption system, there are two main heat effects: heat is released as a heavy component displaces a light component due to the preferential uptake, and compression raises the gas temperature. Of course, heating due to adsorption and compression is at least partially reversible, since desorption and depressurization both cause the temperature to drop. The relative magnitudes of such temperature swings are affected by heats of adsorption, heat capacities, and rates of heat and mass transfer. Hence, the potential effects on performance are many, and they depend on operating conditions, properties, and geometry, sometimes in complicated ways. For example, at a constant pressure, a cycle of adiabatic adsorption followed by adiabatic desorption involves less uptake and release than the isothermal counterpart. As a result, one might expect poorer performance from an adiabatic system as opposed to an isothermal system, but that is not necessarily true for PSA, as shown later.

The term *heat effects* has acquired a connotation of mystery and confusion. This is especially true in the field of PSA since many different effects occur simultaneously. Thus, determining cause-and-effect relationships is not trivial. In fact, some unusual thermal behavior was revealed in a patent disclosure by Collins[28] that continues to perplex some industrial practitioners. Collins stated that, "Contrary to the prior art teachings of uniform adsorbent bed temperature during pressure swing air separation, it has been unexpectedly discovered that these thermally isolated beds experience a sharply depressed temperature zone in the adsorption bed inlet end. … The temperature depression hereinbefore described does not occur in adsorbent beds of less than 12 inches effective diameter." Without attempting to unravel those observations, it may be instructive to consider what happens in a small column, to see detailed effects directly and to infer their causes, and to become aware of the range of potential effects.

For most systems, the principal heat effect arises from simultaneous axial bulk flow, adsorption, and heat release due to adsorption. These phenomena lead to composition and thermal waves that propagate toward the product end of the column. For many PSA applications, these fronts coincide, and the induced temperature shifts just due to adsorption are often greater than 10° C and may exceed 50° C (Garg and Yon[29]). It is shown later that temperature shifts during a typical PSA cycle need not significantly affect the adsorption selectivity, even though relatively large changes in absolute capacity may occur. For systems with small amounts of a strongly adsorbed contaminant or a very weakly adsorbed carrier, however, the thermal wave may lead the composition wave (see Section 2.4) and in such cases the adsorption selectivity can be dramatically affected.

Temperature profiles for a typical bulk separation application are shown in Figure 4.20. That figure shows the internal column temperatures during a PSA cycle in which oxygen is being separated from air using zeolite 5A with a pressure swing of 1 to 5 atm. Five

thermocouples were placed at the centerline of the column at equal spacings. They were small and had exposed junctions for fast response. The pressurization step (up to 39 s) appears as a linear increase of temperature measured at all the thermocouples. During the feed step (continuing to 149 s), the temperature is stable until the composition front passes, and then a sharp rise occurs and a new plateau is reached. Simultaneous measurements indicate that for this system the temperature front coincides with the composition front. Blowdown causes a nearly instantaneous temperature drop due to simultaneous depressurization and desorption (until 161 s). Finally the purge step exhibits a small drop in temperature as desorption of the heavy component is completed, followed by a gradual rise back towards the ambient (influent) temperature (completed at 205 s).

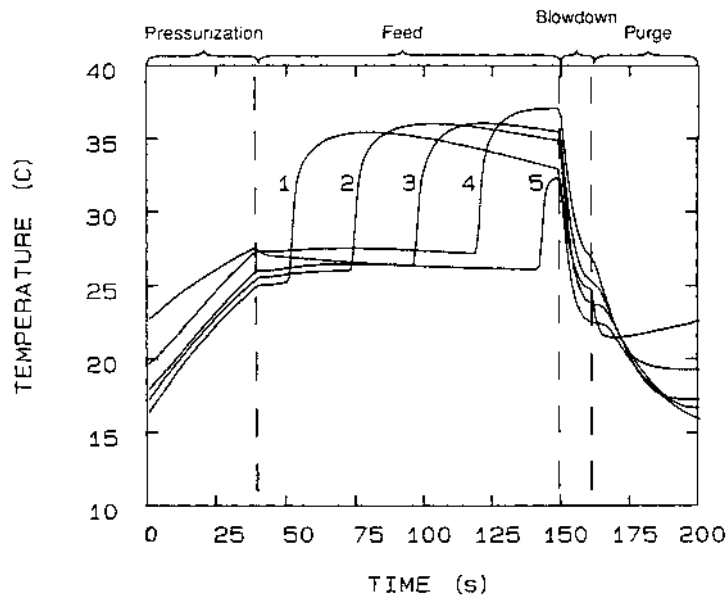

Figure 4.20 Bed temperature histories for a four-step PSA cycle, from pressurization through purge. The numbers 1 through 5 indicate thermocouple locations in the bed, from near the feed end to near the product end. The application is production of oxygen from air with zeolite 5A. The pressure range is from 1.0 to 5.0 atm.

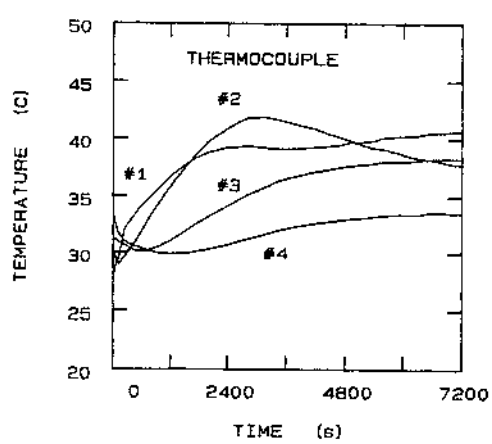

Figure 4.21 Bed temperature histories during a four-step PSA cycle in which water vapor is removed from air with silica gel at 25°C and a pressure ratio of 4.

For comparison, temperature profiles for the feed step in a PSA air dryer, which is a typical contaminant removal application, are shown in Figure 4.21. That figure shows internal column temperatures for air drying by silica gel with a pressure range of 1 to 4 atm. The four thermocouples were identical to those in the previous case. In this figure the front that propagates through the bed is barely discernible, and is certainly not sharp.

Knowing some of the details of temperature fluctuations during PSA cycles, it is appropriate to explore the effect of temperature on overall PSA performance for a bulk separation. The clearest and simplest indication of temperature dependence comes from the limiting case of linear isotherms in the four-step cycle discussed in Section 4.4.1. Each stream depends differently on individual component β values which are themselves dependent on temperature. The overall recovery, however, depends only on β_0 (which is written simply as β here). First of all, consider the overall dependence of recovery on temperature from Eq. 4.27,

$$\frac{\partial R_B}{\partial T} = \left(\frac{1}{\tilde{A}\, y_{B_F}} - 1 \right) \frac{\partial \beta}{\partial T} \tag{4.66}$$

where

$$\beta = \frac{\beta_A}{\beta_B} = \left(\frac{\varepsilon}{1-\varepsilon} + K_B \right) \Big/ \left(\frac{\varepsilon}{1-\varepsilon} + K_A \right)$$

and

$$K_i = K_{i_0} \exp\left[\frac{\Delta H}{R} \left(\frac{1}{T_0} - \frac{1}{T} \right) \right]$$

is the temperature-dependent Henry's law coefficient of component i. Combining these yields

$$\frac{\partial \beta}{\partial T} = \frac{K_A \Delta H_A}{RT^2 \left[\varepsilon/(1-\varepsilon) + K_A \right]^2} \left[\frac{\varepsilon}{1-\varepsilon} \left(\frac{K_B \Delta H_B}{K_A \Delta H_A} - 1 \right) + K_B \left(\frac{\Delta H_B}{\Delta H_A} - 1 \right) \right] \tag{4.67}$$

To cite a specific example, the parameters for separating oxygen from air using zeolite 5A at 45° C are: $K_A = 8.24$, $K_B = 4.51$, $\Delta H_A \approx -6.0$ kcal/mol, $\Delta H_B \approx -3.0$ kcal/mol, and $\int = 0.478$, so $\partial \beta_A / \partial T = 0.00269\,\mathrm{K}^{-1}$, $\partial \beta_B / \partial T = 0.00209\,\mathrm{K}^{-1}$, and $\partial \beta / \partial T = 0.00856\,\mathrm{K}^{-1}$.[20,30] At very high pressure ratios, only the second term in Eq. 4.66 is important, and the limit is: $\partial \beta_B / \partial T = -0.00856\,\mathrm{K}^{-1}$; that is, recovery would decrease by slightly less than 1% if the average temperature increased 1° C. At a more reasonable pressure ratio of 5, however, the first term in Eq. 4.66 is about –0.05, which would require an average temperature increase of 20° C for recovery to decrease 1%. At lower pressure ratios, Eq. 4.66 predicts that the recovery would increase, rather than decrease, if the average temperature increased.

Next, the flows involved in each step can be examined to see how temperature fluctuations from step to step may affect the overall recovery. That is, the temperature dependence of each stream can be found from the isotherm parameters. For the sake of discussion, quantities are identified only by orders of magnitude, and the temperature of

the high-pressure product is taken as the base temperature. Relative to that, the temperature reached at the end of pressurization is practically the same. The fact that pressurization begins at a lower temperature is less important, since equilibration at the final temperature and pressure determines the quantity of gas admitted. The temperature encountered by the feed is higher (due to the heat released by uptake). Finally, the temperature during blowdown (which does not affect recovery) and purge is lower due to depressurization and desorption. Hence, looking at each term in Eq. 4.26 reveals the effects of temperature shifts for individual steps:

$$\Delta R_B\left(\Delta T_{\mathrm{STEP}}\right) \approx \frac{0-0-\left[\Delta\left(1/\beta_A\right)/\Delta T\right]\left[\Delta T|_{\mathrm{PU}}\right]}{\left[\Delta\left(1/\beta_A\right)/\Delta T\right]\left[\Delta T|_{\mathrm{F}}\right]} = -\frac{[-][-]}{[-][+]} \tag{4.68}$$

Thus, the net effect of temperature shifts during this four-step cycle is positive. That is, the recovery of the light component should be somewhat greater when the natural temperature shifts occur than if the system were forced to remain isothermal. The net effect is expected to be minor since, according to the basis chosen, only the purge and feed streams are affected, and the increase of the purge stream should be small relative to the decrease of the feed stream.

Before leaving this subject, it is worthwhile to point out that the conclusion just reached is not general: different cycles will respond to temperature shifts differently. For example, for cycles in which the heavy component is produced during blowdown (cf. Section 4.4.5), the most important stream in determining recovery is the blowdown step. This step involves a large temperature drop (relative to the pressurization, high-pressure product, and rinse steps) due to desorption and depressurization. As can be seen from Eq. 4.41, the net effect is that the adsorbent retains more of the heavy component than it would under isothermal conditions (i.e., the magnitude of the second term on the right-hand side is larger), so recovery is diminished.

Aside from gaining a better understanding of PSA systems via their inherent thermal response, there is an even greater incentive to understand this behavior. To elaborate, in many PSA systems it is important to prevent complete breakthrough, (e.g., during feed and cocurrent blowdown steps), which would reduce the purity of the product. Conversely, if breakthrough is not imminent at the end of these steps, the product recovery cannot be as high as possible, since any purified gas left in the column is exhausted with the byproduct. Similarly, a rinse step should be allowed to proceed until breakthrough is just complete. To go further would reduce recovery, and to stop prematurely would reduce purity. Accordingly, both high product purity and high-recovery PSA performance can be achieved by terminating such steps very precisely. A minor problem is that many composition sensing instruments have long response times or large sample volumes, so that on-line measurements are often impractical. That is where the thermal response comes in.

The fact that the shock wave of temperature usually coincides with the composition front can be exploited to control the timing. Evidence for that is shown both in Figure 4.20, which was described previously, and in Figure 4.22, in which, again, oxygen is being separated from air. In the latter figure, the pressure increases from 2.0 to 5.2 atm. as feed is being admitted to and product is being slowly released from the column. As can be seen, the average temperature in the bed rises, but the sharpness and magnitude of the temperature front are essentially the same as when pressure was constant. Equivalent, but

reverse effects occur when the bed pressure decreases.[26] The possibility of controlling the step times in this manner can prevent reduced recovery [e.g., due to diminished adsorbent capacity or when operating conditions (or ambient conditions) vary significantly]. In fact, this concept was used to control feed and rinse step times for the five-step cycle experiments described in Section 4.5 [cf. Figures 14(a) and (b)].

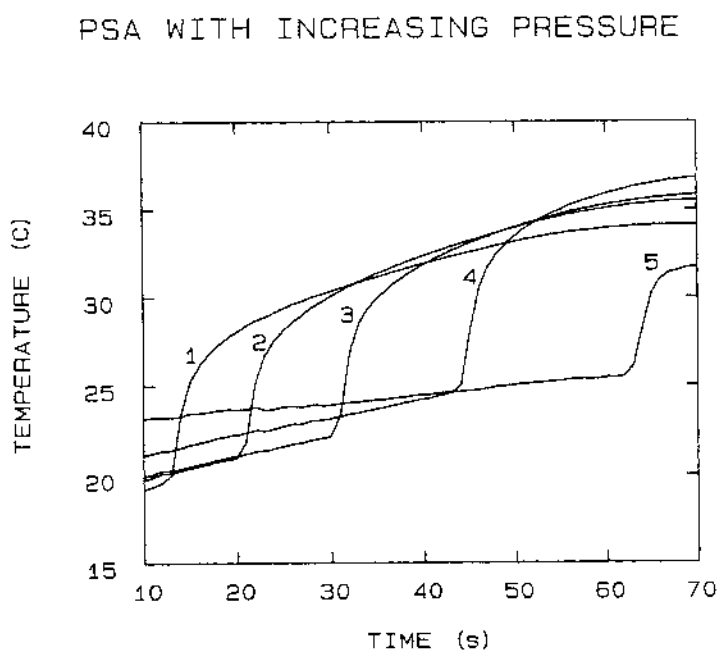

Figure 4.22 Bed temperature histories for a combined pressurization and feed step. The numbers 1 through 5 indicate thermocouple locations in the bed, from near the feed end to near the product end. The application is production of oxygen from air with zeolite 5A. The pressure increases linearly with time from 2.0 to 5.2 atm.[26]

4.9 Pressurization and Blowdown Steps

Until now, attention has been focused on complete PSA cycles and overall effects. There are, however, cases in which the individual steps are important. For example, when the heavy component of a mixture is valuable, it may be desired as the sole product or as a co-product. In that case, the blowdown step, in particular, is vital to the performance of the PSA system, and it is important to know the composition of the effluent as a function of pressure, or to predict the composition profile in the bed at the end of blowdown. In other situations (e.g., involving pressurization by feed or by an intermediate product from a parallel bed) it may be of interest to predict the composition profile in the bed during pressurization.

In that vein, perhaps the first treatment of composition profiles at various extents of pressurization was given by Flores Fernandez and Kenney.[25] They assumed local equilibrium and neglected pressure drop, and they solved the equations by finite differences. A subsequent model that examined pressurization and included effects of axial dispersion, but not of mass transfer resistance or pressure drop, was developed by Rousar and Ditl.[31] Another local equilibrium model was proposed by Kumar,[32] and it was one of very few to incorporate an energy balance. That model was used to analyze adiabatic

blowdown behavior. More detailed models are discussed later in this section.

This section first examines the simplest cases of pressurization and blowdown, and suggests that the key features predicted by more sophisticated models can be obtained analytically. In such cases, much less effort is required, and reasonably accurate estimates of the expected behavior can be obtained. That approach neglects axial pressure drop and mass transfer resistance, as is the case throughout this chapter. Later in this section, however, the impact of pressure drop on pressurization and blowdown is considered.

It turns out that the coupling of velocity, composition, and pressure is graspable for systems governed by linear isotherms, but when nonlinear isotherms are involved the additional complexity makes the set of equations unwieldy and to get detailed simulations via the method of characteristics is not practical. In addition, as noted in the previous section, the pressurization and blowdown steps also may give rise to significant temperature shifts that affect the validity of predictions based on isothermal models.

For pressurization a number of possibilities exist, and the two simplest extremes have already been covered, viz., pressurization with product (see Section 4.4.1), and with feed (see Section 4.4.2). These were assumed to begin with an initial condition in which the bed was purged with the pure light component. When the bed has not been completely purged, simulating pressurization is slightly more complicated (see Section 4.4.3). All three cases represent cyclic steady-state outcomes of operating a PSA cycle at local equilibrium, without dispersive effects. A slightly more complex situation occurs during startup, when the gas used for purging (and possibly pressurization) is not pure. Other possible complications arise from minor variations in operating procedures. For example, a pressure equalization step employs the gas evolved from one column (as it depressurizes) for pressurizing a parallel column. Such gas may have a slowly or suddenly varying composition, due to uneven rates of desorption, poor synchronization of the valves, or contamination by residual material in the connecting fittings.

Pressurization at startup or with gas having variable composition can be regarded as fitting the following possible scenarios: (1) Pressurizing with gas that gradually becomes leaner in the heavy component, during which a shock wave cannot form, or (2) pressurizing with gas that gradually becomes richer in the heavy component, during which a shock wave *may* form if the composition change is sufficiently large, or (3) pressurizing with gas that is significantly richer in the heavy component than the initial interstitial gas, for which formation of a shock wave is unavoidable. For simplicity, let us restrict consideration to a cycle having complete purge. To determine whether a shock wave may form, one must simply examine whether the characteristics intersect (in the space–time domain being considered). The paths of the characteristics are given by Eq. 4.33, and the composition as a function of pressure can be determined from Eq. 4.32. When the characteristics do not intersect, regardless of the initial and boundary conditions, that pair of equations is sufficient to predict the composition profile during pressurization. On the other hand, situations that result in the formation of shock waves require a few additional steps to predict the ultimate composition profile. When pressure varies, the shock wave trajectory can be determined by employing Eq. A.7 from Appendix A, as follows

$$v_{\mathrm{SH}} = \theta_A \frac{\Delta v P y_A}{\Delta P y_A} \tag{4.69}$$

The interstitial velocity is obtained by summing Eq. 4.4 for components A and B.

$$\frac{\partial P}{\partial t}+\beta_B\frac{\partial vP}{\partial z}+\left(\beta_A-\beta_B\right)\frac{\partial vPy_i}{\partial z}=0 \tag{4.70}$$

In this equation, the axial dependence of pressure can be neglected, which, given the dependence of pressure on time, leaves a separable ordinary differential equation,

$$\frac{d\ln P}{dt}+\beta_B\frac{dv}{dz}+\left(\beta_A-\beta_B\right)\frac{dvy_i}{dz}=0 \tag{4.71}$$

Integration requires boundary conditions, and a convenient set is: $v = v_F$ at $z = L$, and $v = 0$ at $z = 0$. The result is the expression that was simply stated earlier in this chapter:

$$v\left(P,y,z,t\right)=\frac{-z}{\beta_B\left[1+\left(\beta-1\right)y\right]}\frac{d\ln P}{dt} \tag{4.6}$$

When Eqs. 4.6 and 4.69 are combined, the shock wave velocity may be found from

$$v_{\mathrm{SH}}=\frac{-\beta z}{\left[1+\left(\beta-1\right)y_1\right]\left[1+\left(\beta-1\right)y_2\right]}\frac{d\ln P}{dt} \tag{4.72}$$

The dependence of y_1 on P, and that of y_2 on z, can be expressed via Eqs. 4.7 and 4.8, respectively. By combining those with Eq. 4.72, the coupled material balances can be solved to get:

$$y_2=\frac{\alpha y_1}{1+\left(\alpha-1\right)y_1} \tag{4.73}$$

where $\alpha=y_{20}\left(1-y_{10}\right)/\left[y_{10}\left(1-y_{20}\right)\right]$ and y_{10} and y_{20} are the initial compositions at the leading and trailing edges of the shock wave, respectively. Thus, α is a sort of selectivity, analogous to relative volatility for vapor–liquid equilibrium.

Thus, to find the ultimate axial position of the shock front at any pressure requires a sequence of steps: the initial conditions give α; then the composition ahead the shock front can be found from

$$y=1-\left(1-y_0\right)\left(\frac{y}{y_0}\tilde{A}^{\beta-1}\right)^{1/\beta} \tag{4.74}$$

(which is essentially the same as Eqs. 4.32 and 4.50); next the composition behind the shock can be determined from Eq. 4.73; and finally the axial position can be computed from

$$z=z_0\left(\frac{y}{y_0}\right)^{\beta/(1-\beta)}\left(\frac{1-y_0}{1-y}\right)^{1/(1-\beta)}\left(\frac{1+\left(\beta-1\right)y}{1+\left(\beta-1\right)y_0}\right) \tag{4.75}$$

(which is essentially the same as Eq. 4.33) using the composition shift at the trailing edge of the shock front.

To illustrate the point, it is appropriate to compare such results with those obtained by

finite difference techniques. Figure 4.23 shows predictions of the previous equations and those presented by Rousar and Ditl[31] for oxygen enrichment. It can be seen that the endpoints coincide, as does much of all three profiles. The principal distinction is due to rounding, which is inherently due to dispersion being included in the numerically derived results. All the results shown for the equilibrium theory were obtained with a calculator in several minutes time. Similar results have been obtained by Flores Fernandez and Kenney,[25] and are shown in Figure 3.2.

If we turn our attention now to blowdown, and still restrict conditions to local equilibrium, it is clear that blowdown is simpler than pressurization. That is because there is no interaction between the initial and boundary conditions. Furthermore, in previous sections of this chapter, the initial condition prior to blowdown was usually taken to be uniform, which led to relatively simple material balance calculations. Some subtleties arise for the case of pressurization with feed (cf. Section 4.4.2), when dead volume at the product end was considered (cf. Section 4.4.6), and when the heat effects accompanying blowdown were found to be deleterious (cf. Section 4.8). The most important feature of blowdown is the effluent composition, which in most instances continuously changes as pressure falls, except when a rinse step precedes blowdown, yielding the pure heavy component throughout blowdown. Another topic of practical interest is the ultimate composition profile in the bed following blowdown.

If the initial composition profile is known, applying the local equilibrium model for systems with linear isotherms is fairly simple. For example, in order to predict the effluent composition during blowdown or the residual interstitial gas composition following blowdown, one need only apply characteristic equations such as Eqs. 4.74 and 4.75, where y_0 and z_0 represent the initial composition and position of a particular characteristic. For a given set of initial conditions, it is easiest to choose a final composition y, then to determine the necessary pressure ratio $\wp$, and finally the ultimate axial position z. Otherwise (i.e., given the pressure ratio), a root-finding procedure is needed to determine the final composition. When the initial composition profile is uniform, Eq. 4.75 indicates that there will be no axial composition gradient as the pressure falls. Regardless, Eqs. 4.18 and 4.19 can be used with the composition–position–pressure information to determine the average composition and quantity of the effluent during blowdown. To relate these to flow rates, it would be necessary to select a depressurization rate: simplistically dP/dt = constant, or somewhat more realistically, d In P/dt = constant, although any operating policy can be accommodated.

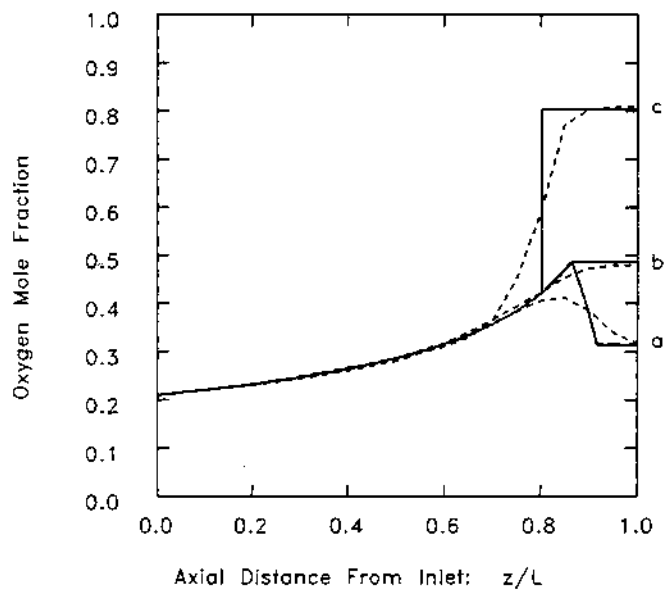

Figure 4.23 Composition profiles during pressurization of a bed of zeolite 5A, to which various mixtures of oxygen and nitrogen are admitted. P = 6 atm. Initial conditions: (a) $y_{O_2} = 0.1$, (b) $y_{O_2} = 0.21$, (c) $y_{O_2} = 0.60$. $\beta = 0.517$. Numerical results from Rousar and Ditl.[31]

In the models presented earlier in this chapter, the pressure gradient through the column is assumed to be negligible. In that situation the basic equations governing pressurization and blowdown steps are not much more complicated than those for steps at constant pressure. Neglecting pressure drop is reasonable for most conventional PSA units, but it is clearly inappropriate for single column, rapid pressure swing processes, which are discussed in Section 7.3. The detailed modeling of pressurization and blowdown steps, taking into account pressure gradients through the column, has attracted much attention recently. For example, a detailed model was suggested by Lu et al.,[33–35] who studied both pressurization and blowdown. Their model included mass transfer resistances, axial dispersion, intraparticle convection, and axial pressure drop, but not heat effects, and was solved by finite differences. Other similar models have been suggested,[36–41] and a brief summary of the major conclusions from that work is given here.

To a first approximation, the pressure drop through a packed adsorbent bed can be represented by Darcy's Law:

$$v = -\frac{B}{\mu}\frac{\partial P}{\partial z} \tag{4.76}$$

Coupling this with the differential fluid phase mass balance for a plug flow system (cf. Eq. 5.2) with rapid equilibration yields

$$\left.\frac{\partial P}{\partial t}\right|_z = \frac{B}{\mu\left[\varepsilon + (1-\varepsilon)\left(dq^*/dc\right)\right]}\frac{\partial}{\partial z}\left[P\left(\frac{\partial P}{\partial z}\right)_t\right]_t \tag{4.77}$$

where, for an isothermal system, dq^*/dc represents simply the local slope of the

equilibrium isotherm. The appropriate initial and boundary conditions are, for pressurization:

$$P = P_i, \quad t = 0, \quad \text{for all } z$$
$$P = P_{\mathrm{H}}, \quad t > 0, \quad \text{for } z = 0$$
$$\left.\frac{\partial P}{\partial z}\right|_{z=L} = 0 \tag{4.78}$$

with P_{H} and P_{L} interchanged for blowdown.

When pressure drop through the column is negligible, Eq. 4.77 is equivalent to Eq. 4.6, which was discussed previously. For a pure gas, A, it reduces to:

$$\frac{dP}{dt} = \pm \beta_A P v / z \tag{4.79}$$

where the sign reflects the orientation of the column and the direction of flow. This may be integrated directly to obtain the dimensionless time required to pressurize or depressurize the bed:

$$\tau = \frac{\text{volume of gas fed to the column}}{\text{holdup in the column}} = \ln \tilde{A} \tag{4.80}$$

which was obtained originally by Cheng and Hill.[37] In this situation, pressurization and blowdown are symmetric processes. This symmetry is lost, however, when the pressure gradients are significant since the pressure response is then governed by Eq. 4.77, which is nonlinear. This is illustrated in Figure 4.24, which shows pressure profiles for pressurization [Figure 4.24(a)]

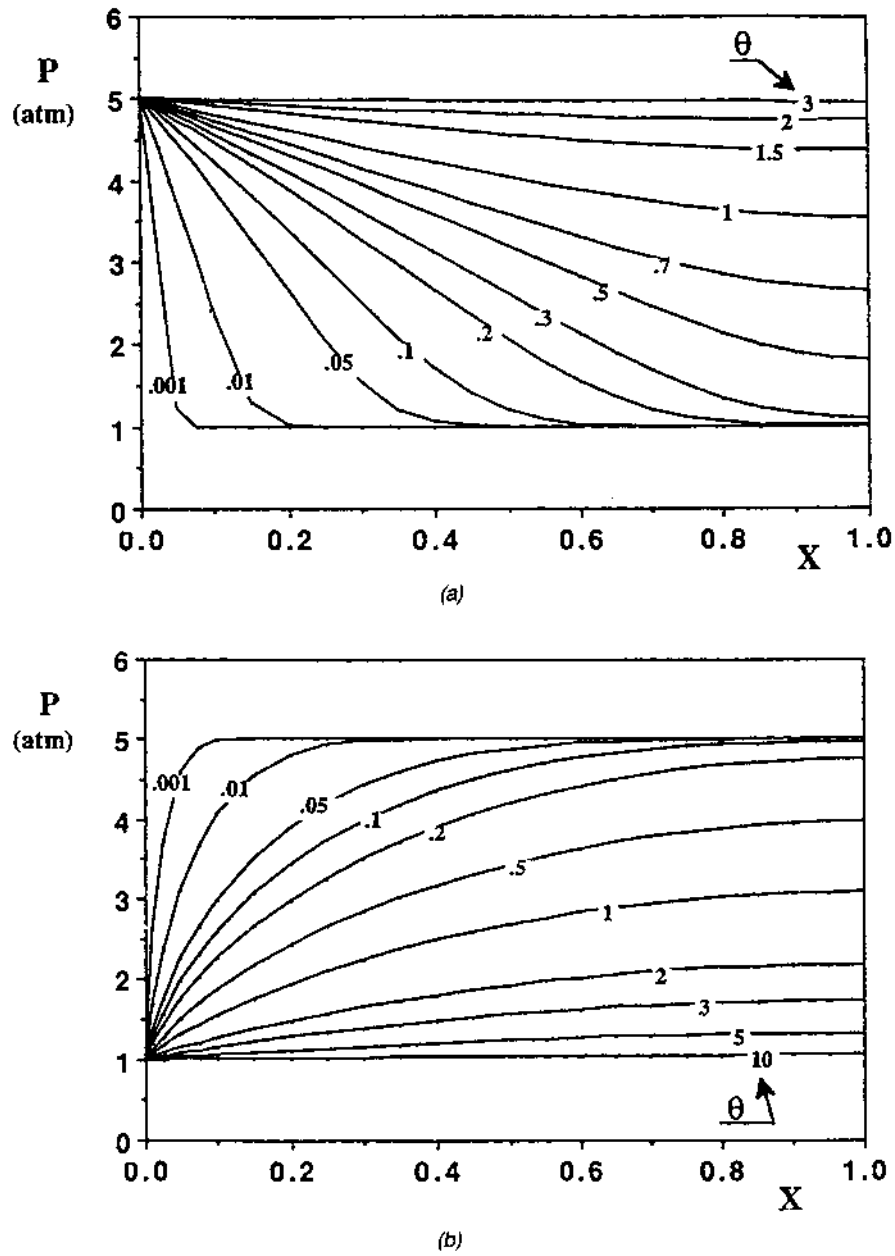

Figure 4.24 Axial pressure profiles during (a) pressurization and (b) blowdown of an adsorbent bed with a nonadsorbing gas. P_H = 5 atm, P_L = 1 atm, L = 1 m, reference velocity –0.2 ms^{-1}, θ = dimensionless time. (From Rodrigues et al.,[36] with permission.)

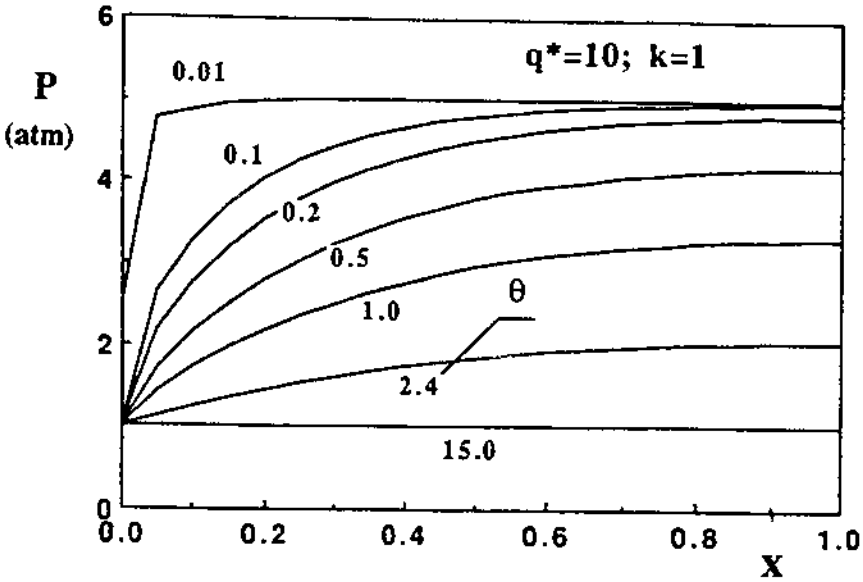

(a)

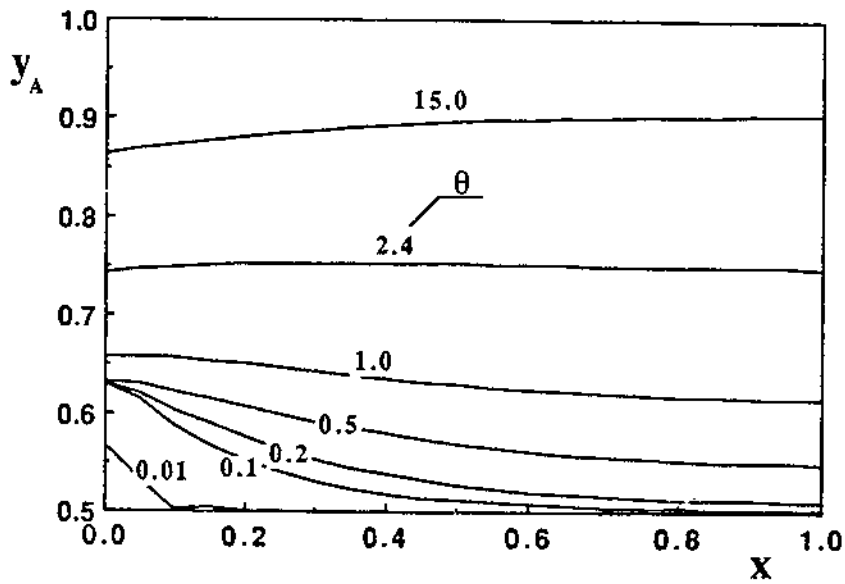

(b)

Figure 4.25 Theoretical profiles of (a) reduced total pressure and (b) mole fraction of the more strongly adsorbed component (y_A) during blowdown of an adsorbent bed. P_H = 5 atm, P_L = 1 atm, y_0 = 0.5, K = 10 (linear isotherm), θ = dimensionless time. (From Lu et al.,[35] with permission.)

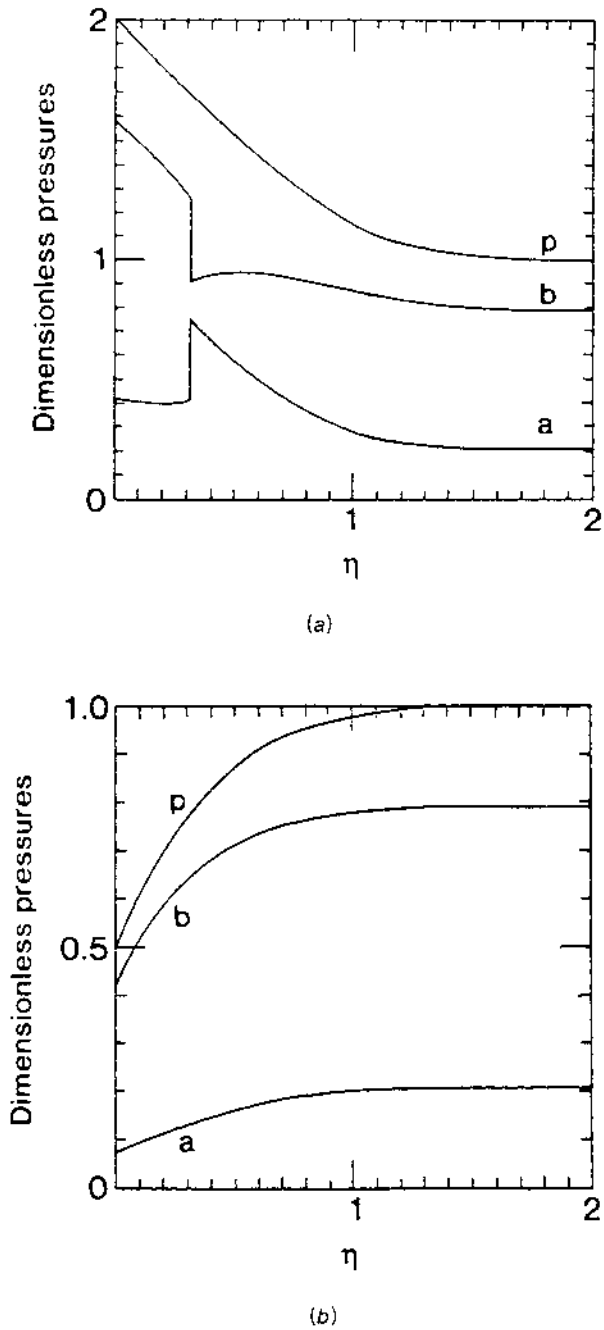

Figure 4.26 Theoretical profiles of total pressure (p), mole fraction of O_2 (a) and mole fraction of N_2 (b) during pressurization and blowdown of a 5A zeolite bed equilibrated with air, calculated from the analytic solution. (From Scott,[38] with permission.)

and blowdown [Figure 4.24(b)], over identical pressure ratios, calculated by numerical integration of Eq. 4.77.[36] Blowdown is clearly slower than pressurization. The dimensionless times for pressurization and blowdown are, respectively, about three and ten times the characteristic time defined by:

$$t_c = \frac{\mu \varepsilon L^2}{B\left(P_H - P_L\right)} \tag{4.81}$$

In this example, the pressure profiles during pressurization and blowdown both assume the form of simple propagating waves. With mixtures of differently adsorbed components (or with mixtures of inert and adsorbing species) the profiles assume more complex forms. Many such ramifications, including the effect of a nonlinear isotherm and the effect of using the Ergun equation for pressure drop (in place of Darcy's Law) have been investigated by Rodrigues et al.[33–36]

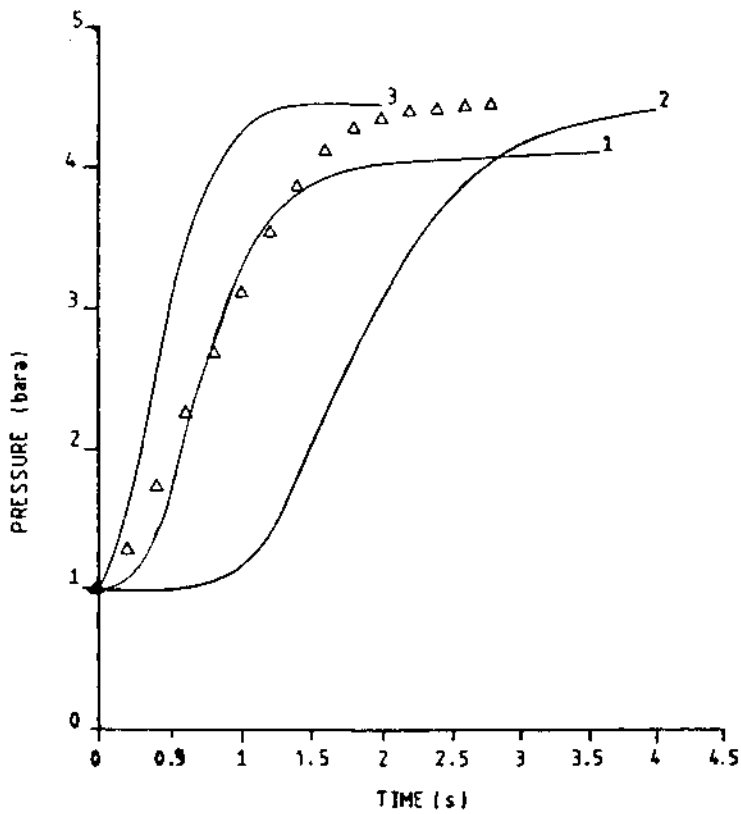

Figure 4.27 Comparison of experimental pressure profile for pressurization of an activated carbon bed with CO_2 and theoretical profiles predicted from (1) finite mass transfer model (LDF), (2) equilibrium adsorption model, and (3) model for no adsorption. (From Hart et al.,[39] with permission.)

One situation of special interest is to use a PSA process to concentrate strongly adsorbed component(s) from a feed of low concentration. An example of this was studied by Rodrigues et al.[36] The bed is initially at equilibrium with a linearly adsorbed light component, at mole fraction 0.5 and a total pressure of 5.0 atm. As the bed is depressurized to atmospheric pressure, the pressure along the axis of the bed responds as shown in Figure 4.25(a). Simultaneously, as shown in Figure 4.25(b), the mole fraction of the more strongly adsorbed component rises rapidly at the open end of the bed, to about 0.65, and the profile then pivots about this point until it reaches a more or less uniform profile through the bed. Thereafter, the profile remains almost uniform through the bed, rising asymptotically

towards $y_A \approx 0.90$. At this point, essentially all the less strongly adsorbed species have been removed from the bed, and it would be possible, in principle, to recover the strongly adsorbed species in highly concentrated form by deep evacuation of the bed (see Section 6.10).

An alternative approach has been followed by Scott,[38] who has shown that, if the column can be regarded as infinitely long, a relatively simple analytical solution may be obtained. Profiles of pressure and composition for pressurization and blowdown, calculated with parameters representative of air–zeolite 5A, are shown in Figure 4.26. The composition profiles for pressurization [Figure 4.26(a)] show a complex wave form that includes a partial shock, which appears as an inflection at small values of θ. The profiles for blowdown [Figure 4.26(b)] contain only simple waves; that is, they are everywhere concave downwards.

The effect of finite mass transfer rate has been investigated by Hart et al.[39] Their experimental data for pressurization of an activated carbon bed with CO_2 are shown in Figure 4.27 together with theoretical curves calculated according to three different assumptions: negligible adsorption, instantaneous adsorption, and adsorption at a finite rate according to the linear driving force (LDF) model ($k = 0.2\ s^{-1}$). The experimental data lie closest to the finite rate model, although there is a significant deviation in the long-time region. It seems likely that this deviation may be attributed to heat effects, which will reduce adsorption in the long-time region.

4.10 Conclusions

The local equilibrium theory approach is the simplest available for simulating or designing PSA systems. Furthermore, when data are sparse (e.g., no PSA pilot plant data), it is the most reliable method because it does not depend on semiempirical parameters that can only be determined from data. Such methods can lead to excellent designs when kinetics are fast. Even when kinetics are slow (though not controlling), such methods can predict overall performance (e.g., in terms of recovery and byproduct enrichment) very well. The main and perhaps only drawback is that, when kinetic constraints are important, it becomes impossible to estimate product purity reliably.

Nevertheless, a variety of aspects of PSA operation can be taken into account by equilibrium-based theories. Some that are illustrated in this chapter are: a variety of cycle and step options, wide ranges of operating conditions, isotherm nonlinearity, heat effects, and deadzones in PSA columns. In several instances, the simple theories have been verified experimentally, so there is little doubt as to their reliability when the assumptions are reasonably valid.

Chilton once said, "The simpler things become in a piece of research or development, the closer one has come to the truth." Pigford added to that, "The simpler an explanation is, the more widely it will be understood, appreciated, and used."[42] In pressure swing adsorption systems, it is impossible to achieve greater simplicity than local equilibrium models provide and still retain fundamental understanding of the process. Whether the model predictions are close to the truth or not depends on the extent to which the assumptions are valid. For all that, it is seldom possible to improve performance beyond the capability predicted by an equilibrium model because dissipative effects nearly always diminish performance. Hence, striving to conform to those assumptions can be worthwhile, not only because it will be possible to predict performance accurately and

simply, but, more important, because performance will be superior. Whether modeling via the local equilibrium approach can be "understood, appreciated, and used" depends mainly on whether the implied superior PSA performance can be achieved in real applications.

Future efforts should be directed towards a unified treatment of equilibrium based separations accounting for the several diverse factors that until now have been accounted for separately. An example would be to account for the effects of nonlinear isotherms on sequential pressurization by feed and feed steps. Another facet to examine is the coupling of isotherms, since it is widely observed that the light component adsorbs proportionately less in a mixture than the amount due to uptake of the heavy component. This effect would tend to improve PSA performance, and might partially compensate for the effects of being nearly adiabatic (which is physically realistic), as opposed to the assumed isothermal condition of the adsorbent bed. Furthermore, experimental work could be done to validate the combined effects, to analyze cycles of more complex steps, and to account for a wider variety of properties and conditions. One example would be to generalize the dependence of the observed "effective" separation capacity of an adsorbent, especially with respect to flow conditions, as alluded to in Figure 4.3.

References

1. P. H. Turnock and R. H. Kadlec, "Separation of Nitrogen and Methane via Periodic Adsorption," *AIChE J*. **17**, 335 (1971).
2. L. H. Shendalman and J. E. Mitchell, "A Study of Heatless Adsorption in the Model System CO He, I.," *Chem. Eng. Sci*. **27**, 1449–58 (1972).
3. Y. N. I. Chan, F. B. Hill, and Y. W. Wong, "Equilibrium Theory of a Pressure Swing Adsorption Process," *Chem. Eng. Sci*. **36**, 243–51 (1981).
4. J. C. Kayser and K. S. Knaebel, "Pressure Swing Adsorption: Development of an Equilibrium Theory for Binary Gas Mixtures with Nonlinear Isotherms," *Chem. Eng. Sci*. **44**, 1–8 (1989).
5. D. J. Ball, M.S.Ch.E. Thesis, Ohio State University, Columbus, OH, 1986.
6. C. W. Skarstrom, "Use of Phenomena in Automatic Plant Type Gas Analyzers," *Ann. N.Y. Acad. Sci*. **72**, 751–63 (1959).
7. M. J. Matz and K. S. Knaebel, "Pressure Swing Adsorption: Effects of Incomplete Purge," *AIChE J*. **34**(9), 1486–92 (1988).
8. P. C. Wankat, "Feed–Purge Cycles in Pressure Swing Adsorption," *Separ. Sci. and Tech*. (submitted 1992).
9. I. Rousar and P. Ditl, "Pressure Swing Adsorption: Analytical Solution for Optimum Purge," *Chem. Eng. Sci*. (submitted 1992).
10. J. C. Kayser and K. S. Knaebel, "Integrated Steps in Pressure Swing Adsorption Cycles," *Chem. Eng. Sci*. **44**, 3015–22 (1988).
11. S.-S. Suh and P. C. Wankat, "Combined Cocurrent-Countercurrent Blowdown Cycle in Pressure Swing Adsorption," *AIChE J*. **35**, 523–26 (1989).
12. J. E. Collins and K. S. Knaebel, Paper presented at the AIChE Annual Meeting, San Francisco, CA (1989).
13. K. S. Knaebel and F. B. Hill, "Pressure Swing Adsorption: Development of an Equilibrium Theory for Gas Separations," *Chem. Eng. Sci*. **40**, 2351–60 (1985).
14. J. L. Wagner, "Selective Adsorption Process," U.S. Patent No. 3,430,418 (1969).
15. P. C. Wankat, *Large Scale Adsorption and Chromatography*, *I*, CRC Press, Boca Raton, FL., 95 (1986).

16. R. T. Yang and S. J. Doong, "Gas Separation by Pressure Swing Adsorption: A Pore Diffusion Model for Bulk Separation," *AIChE J*. **31**, 1829–42 (1985).

17. S. J. Doong and R. T. Yang, "Bulk Separation of Multicomponent Gas Mixtures by Pressure Swing Adsorption: Pore/Surface Diffusion and Equilibrium Models," *AIChE J*. **32**, 397–410 (1986).

18. R. T. Yang, *Gas Separation by Adsorption Processes*, Butterworths, Boston, MA, 328 (1987).

19. N. F. Kirkby and C. N. Kenney, "The Role of Process Steps in Pressure Swing Adsorption," *Fundam. of Adsorption*, Engng. Foundation, New York, 325 (1987).

20. J. C. Kayser and K. S. Knaebel, "Pressure Swing Adsorption: Experimental Study of an Equilibrium Theory," *Chem. Eng. Sci*. **41**, 2931–38 (1986).

21. S.-S. Suh and P. C. Wankat, "A New Pressure Swing Adsorption Process for High Enrichment and Recovery," *Chem. Eng. Sci*. **44**, 567–74 (1989).

22. S. Sircar, "Air Fractionation by Adsorption," *Separ. Sci. and Tech*. **24**(14 & 15), 2379–96 (1988).

23. K. P. Kolliopoulos, M.S.Ch.E. Thesis, Ohio State University, Columbus, OH, 1987.

24. J. E. Mitchell and L. H. Shendalman, "A Study of Heatless Adsorption in the Model System CO in H. II," *AIChE Symp. Ser*. **69**, 25 (1973).

25. G. Flores Fernandez and C. N. Kenney, "Modelling the Pressure Swing Air Separation Process," *Chem. Eng. Sci*. **38**, 827–34 (1983).

26. M. J. Matz and K. S. Knaebel, "Temperature Front Sensing for Feed Step Control in Pressure Swing Adsorption," *Ind. Eng. Chem. Res*. **26**(8), 1638 (1987).

27. R. R. Hill and K. S. Knaebel, "Effects of Combined Steps in Pressure Swing Adsorption Cycles: An Experimental and Theoretical Study," *Adsorption: Fundam. and Applic*., Proc. China–Jap.–USA Symp. on Adv. Ads. Separ. Sci. and Tech., Zhejiang Univ. Press (1988).

28. J. J. Collins, "Air Separation by Adsorption," U.S. Patent No. 4,026,680 (1977).

29. D. R. Garg and C. M. Yon, *Chem. Eng. Prog*. **82**(2), 54–60 (1986).

30. G. W. Miller, K. S. Knaebel, and K. G. Ikels, "Equilibria of Nitrogen, Oxygen, Argon, and Air in Molecular Sieve 5A," *AIChE J*. **33**, 194–201 (1987).

31. I. Rousar and P. Ditl, "Optimization of Pressure Swing Adsorption Equipment: Part I.," *Chem. Eng. Commun*. **70**, 67–91 (1988).

32. R. Kumar, "Adsorption Column Blowdown: Adiabatic Equilibrium Model for Bulk Binary Gas Mixtures," *Ind. Eng. Chem. Research* **28**, 1677–83 (1989).

33. Z. P. Lu, J. M. Loureiro, M. D. LeVan, and A. E. Rodrigues, "Intraparticle Convection Effect on Pressurization and Blowdown of Adsorbers," *AIChE J*. **38**, 857–67 (1992).

34. Z. P. Lu, J. M. Loureiro, M. D. LeVan, and A. E. Rodrigues, "Intraparticle Diffusion/Convection Models for Pressurization and Blowdown of Adsorption Beds with Langmuir Isotherm," *Separ. Sci. Tech*. 27, 1857–74 (1992).

35. Z. P. Lu, J. M. Loureiro, A. E. Rodrigues, and M. D. LeVan, "Pressurization and Blowdown of Adsorption Beds," *Chem. Eng. Sci*. **48**, 1699 (1993).

36. A. E. Rodrigues, J. M. Loureiro, and M. D. LeVan, *Gas Sep. and Purification*, **5**, 115 (1991).

37. H. Cheng and F. B. Hill, *AIChE J*. **31**, 95 (1985).

38. D. M. Scott, *Chem. Eng. Sci*. **46**, 2977 (1991).

39. J. Hart, M. J. Baltrum, and W. J. Thomas, *Gas Sep. and Purification*, **4**, 97 (1990).

40. N. Sundaram and P. C. Wankat. *Chem. Eng. Sci*. **43**, 123 (1988).

41. S. J. Doong and R. T. Yang, *AIChE Symp. Ser*. **84**(284), 145 (1989).

42. R. L. Pigford, Private communication. July 23, 1986.

CHAPTER 6 PSA Processes

In previous chapters we have described the principles underlying the operation of a PSA process and shown how the process may be represented in terms of simplified mathematical models. However, apart from the discussion in Chapter 3 concerning the factors governing the choice of cycle, the more practical aspects of PSA process design have been ignored and few details of comparative performance have been given. An account of several representative PSA processes that have been developed to the industrial scale is presented in this chapter together with comments on some of the more practical design aspects and the thermodynamic efficiency. Detailed information on practical design and system performance is not widely available in the open literature and the comments presented here therefore represent only a partial account. Further information can be obtained from the extensive patent literature, although the details are often confusing.

6.1 Air Drying

The "heatless drier" was the earliest practical PSA process, and the factors governing the design and performance were studied in detail by Skarstrom.[1] The process, which is widely used for small-scale applications such as the drying of instrument air operates on the simple two-bed Skarstrom cycle (see Section 3.2). Essentially bone-dry product air (1 ppm H_2O) can be readily achieved with either alumina or zeolite (4A or 5A) as the desiccant, but beaded alumina is the usual choice.

The equilibrium isotherm for water vapor on alumina is less strongly curved than the corresponding isotherm for zeolite adsorbents (see Figure 2.5) and as a result, the working capacity in a PSA system is higher. However, a more important consideration is that alumina beads are physically more robust than most other desiccants and do not fracture or suffer attrition under the rather harsh operating conditions of a PSA process. Indeed, provided that the feed air is clean, the life of a PSA drier packed with alumina beads is very long; continuous operation without changing the adsorbent over a period of 20 years has been reported.

6.1.1 Design Considerations

Product purity is normally the primary requirement and, since the water vapor concentration in the feed is generally quite low, a pressure equalization step is not normally included in the cycle. Minimization of the purge, subject to the requirement of a pure product, is therefore the major objective in optimization of the operating cycle. The process operates under essentially adiabatic conditions, and conservation of the heat of adsorption is therefore a major consideration determining the selection of operating conditions. In essence the desiccant bed must be sufficiently long that, during the adsorption step, the

thermal wave (which travels faster than the mass transfer zone) does not escape from the bed. The heat retained in the bed heats the purge gas during the desorption step, thus reducing the volume of purge required to desorb the water. If the bed is too short so that the thermal front is not contained, some of the heat will be lost (as sensible heat in the product stream). Under these conditions a greater volume of purge will be needed to clean the bed with consequent loss of process efficiency.

Skarstrom enunciated three general principles for the design of a "heatless drier":

1. Conservation of the heat of adsorption (as discussed). This requires relatively short cycles with low throughput per cycle.
2. Regeneration at low pressure using a fraction of the product stream as a reverse-flow purge. In order to produce a pure product the actual purge volume should exceed the actual feed volume at all points in the bed.
3. For a pure product the absolute pressure ratio (P_H/P_L) should be greater than the reciprocal of the mole ratio of the product to the feed.

It is clear that, under cyclic steady-state conditions, all water vapor entering with the feed must be removed in the purge (apart from the small loss in the blowdown). The maximum water vapor content of the purge gas will be the same as that of the high-pressure feed. Cyclic steady-state operation is therefore only possible with a volumetric purge-to-feed ratio greater than unity. The third principle also follows directly from the overall mass balance. A useful summary of the procedure that is normally followed in the design of a PSA drier has been given by White.[2]

6.1.2 Bed Diameter

The bed diameter is chosen in the normal way based on the design throughput requirement. The maximum velocity in upflow is normally limited to 75% of the minimum fluidization velocity to avoid the increased attrition resulting from particle vibration, which becomes serious, even in a well packed bed, as the fluidization velocity is approached. A somewhat higher velocity, perhaps double the fluidization velocity, can be tolerated in downflow.[3]

6.1.3 Bed Length

The bed length is determined primarily by the requirement to contain the temperature front, which, in an air drier, travels at a higher velocity than the concentration front (the mass transfer zone). The situation is as sketched in Figure 6.1. The concentration front is confined to the entry region of the bed and oscillates during the cycle over only a relatively small distance. The precise form of the profiles and the degree of penetration into the bed depend of course on the humidity level and cycle time as well as on the nature of the desiccant. Experimental concentration profiles from an operating unit are shown in Figure 6.2; the corresponding effluent concentrations are shown in Figure 6.3. The temperature front extends towards the product end of the bed, and the amplitude of its movement during the cycle is much greater than that of the concentration front. The area between the two limiting temperature fronts is proportional to the latent heat of the water adsorbed (and desorbed) during each cycle, while the area between the two concentration fronts is proportional to the mass of water adsorbed and desorbed in each cycle.

More than half the bed generally operates simply as a gas–solid heat exchanger, and it would indeed be possible to replace the adsorbent in this region by an inert solid with a

high heat capacity. Since the heat capacity of the inert solid can be higher than that of the adsorbent, a reduction in overall bed volume can be achieved. The required bed length (typically 1–2 m) is normally determined from a classical heat transfer calculation, following the method of Anzelius,[4] although a full dynamic simulation of the nonisothermal PSA cycle, as described in Section 5.4, is preferable, since such an approach provides more detailed and reliable information concerning the effects of the process variables.

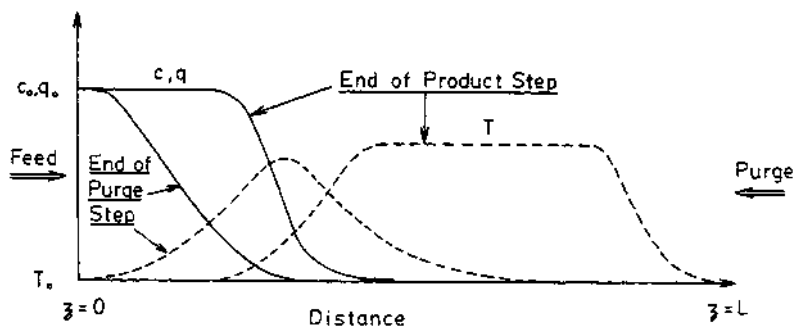

Figure 6.1 Sketch showing qualitative form of concentration and temperature profiles in a "heatless drier" at cyclic steady state. The precise form of the profiles depends on many factors, including the properties of the adsorbent and the duration of the cycle.

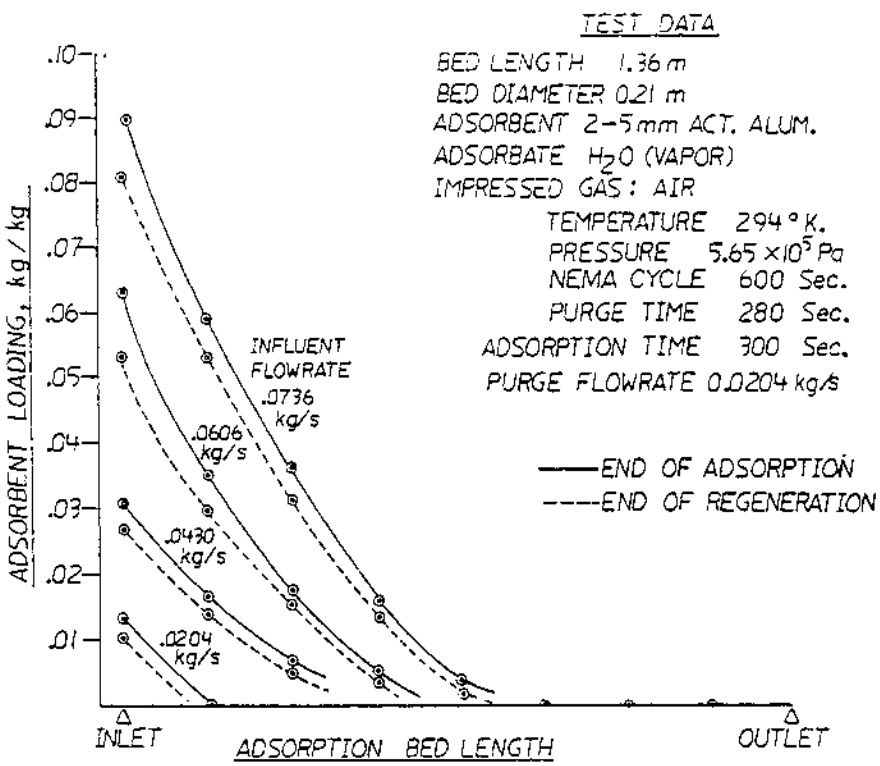

Figure 6.2 Experimental concentration profiles for a heatless air drier packed with an activated alumina adsorbent. (From D. H. White,[2] with permission.)

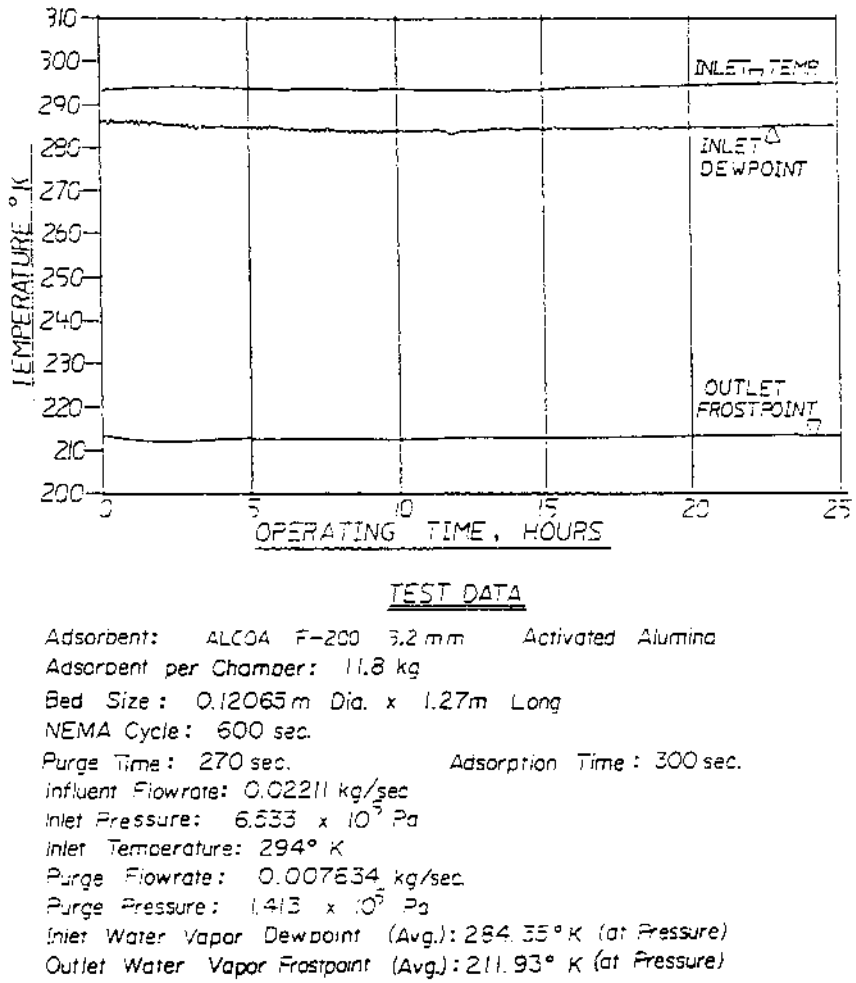

Figure 6.3 Performance test data showing constancy of effluent dew point over a 25 hour period for a "heatless drier" packed with an activated alumina adsorbent. (From D. H. White,[2] with permission.)

6.1.4 Purge Flow Rate

Under ideal equilibrium conditions the partial pressure of moisture in the purge stream leaving the bed will be the same as that of the entering feed. Consequently, the stoichiometric minimum purge volume (measured at purge pressure) is equal to the actual feed volume (measured at feed pressure). If the purge flow is reduced below this level, the steady-state mass balance will not be satisfied and the moisture front will slowly advance through the bed. To allow for the obvious deviation from the ideal equilibrium situation, a margin of at least 15% over the theoretical minimum purge is normally desirable:

$$\frac{\text{purge rate}}{\text{feed rate}} = 1.15\left(\frac{t_f}{t_p}\right)\left(\frac{P_L}{P_H}\right) \tag{6.1}$$

where the flow rates are expressed on a molar basis and t_f, t_p refer to the feed and purge times.

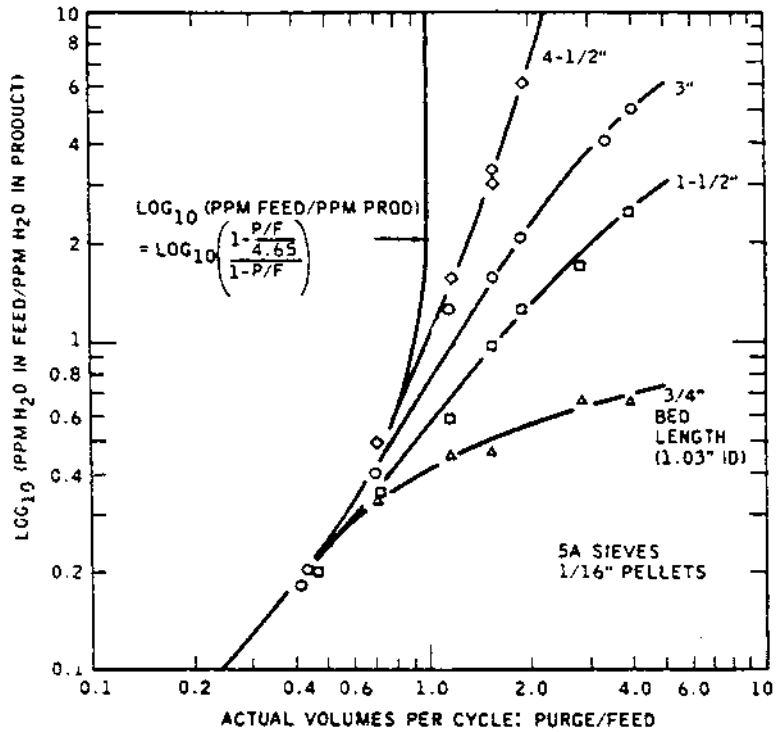

Figure 6.4 Effect of purge-to-feed ratio on product purity for a "heatless drier" packed with 5A zeolite. Feed 26 SCFH at 80° F, 4.7 atm, 6000 ppm H_2O. (From Skarstrom,[5] with permission.)

6.1.5 Product Purity

The product purity is determined by the bed length (or the dimensionless ratio L/vt_c) and the purge-to-feed ratio. Experimental results obtained with a column of 5A sieve of different lengths at various purge-to-feed ratios are summarized in Figure 6.4. The asymptotic line is simply calculated from the mass balance:

$$\frac{c_F}{c_p} = \frac{F - (P_L/P_H)P}{F - P} \tag{6.2}$$

With adequate purge and adequate bed length the product air is essentially bone dry. If the purge is insufficient or if the bed length is not long enough to contain the temperature wave, the performance deteriorates.

6.2 Production of Oxygen

Air separation to produce oxygen was one of the processes described in the early PSA patents of Skarstrom.[5] It has been commercialized at scales ranging from a few liters per minute, for medical oxygen, to tens of tons per day for industrial systems. A zeolite adsorbent, generally 5A or 13X, is normally used. When thoroughly dehydrated, such adsorbents show a selectivity towards nitrogen with a separation factor of about 3.0–3.5.[6] Oxygen and argon are adsorbed with almost the same affinity; so the separation is in effect between oxygen plus argon and nitrogen. The maximum attainable oxygen purity is therefore about 95–96%. The presence of argon as an impurity is of little consequence for

medical purposes, but it is a significant disadvantage for welding and cutting, since the flame temperature, and therefore the cutting speed, are significantly reduced. Substantially higher separation factors (α_{N_2/O_2} ~ 8–10, with correspondingly higher nitrogencapacity) have been reported for thoroughly dehydrated CaX and, various ionic forms of chabazite.[7,8] The Henry constant for nitrogen on these "second generation" adsorbents is too high to permit effective desorption at atmospheric pressure, making them unsuitable for use in a conventional PSA cycle operating at pressures above atmospheric. These adsorbents are, however, used in many of the more modern large-scale vacuum swing or pressure/vacuum swing processes. The development of these processes provides an excellent example of the need to tailor the process cycle to the properties of the adsorbent.

6.2.1 Small-Scale Medical Oxygen Units

At the scale of domestic medical oxygen units the cost of power is a less significant consideration than process simplicity and reliability. Most small-scale units use a two-bed system, operated on a Skarstrom cycle, sometimes with the addition of a pressure equalization step (see Figure 3.6). Typical performance data are shown in Figure 6.5 (see also Figure 3.7). Although a fairly high product purity is attainable, the recovery is relatively low so that the power consumption is high. A significant improvement in recovery can be achieved by the inclusion of a pressure equalization step (see Figure 3.8), but in small-scale units the additional complexity may not be justified.

6.2.2 Industrial-Scale Units

At larger scales of operation proper optimization of a PSA system is essential in order to compete with alternative processes such as cryogenic distillation. Recent trends have been reviewed by Smolarek and Campbell.[9] Capital and operating costs contribute almost equally to the overall cost of a PSA process, and the cost of power is by far the most important component of the operating cost. These considerations lead to competing requirements in optimization. Process efficiency and therefore power cost can be reduced by introducing additional pressure equalization steps, but the increased process complexity, requiring an increased number of beds and with the associated valves and piping, increases the capital cost.

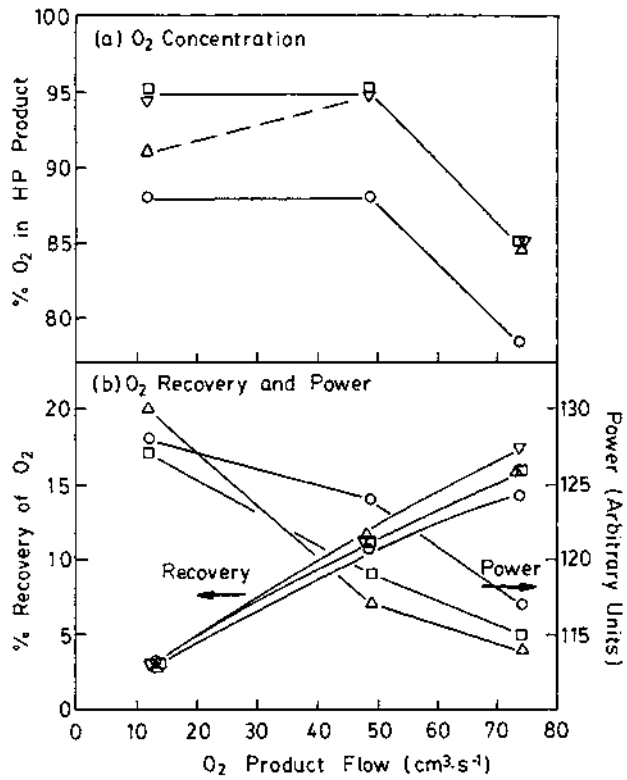

Figure 6.5 Experimental performance data for a simple two-bed PSA oxygen generator operated on a Skarstrom cycle. Note that for high product purity the recovery is less than 10%. (Previously unpublished experimental data.)

The "Lindox" process,[10] shown schematically in Figures 3.10 and 3.11, is typical of the first generation of large-scale PSA oxygen systems. The process operates on a modified Skarstrom cycle with two or three pressure equalization steps (depending on the number of beds). Both three-and four-bed versions were developed at scales of up to 40 tons/day of oxygen product. The process is normally operated between three and one atmosphere pressure and produces a 90% oxygen product gas (dry and free of CO_2) with an oxygen recovery of about 38% and a power requirement of about 1.7 kWh per 100 SCF oxygen product (equivalent to 48,000 J/mole product gas). Productivity is about 0.018 moles of oxygen product gas per kg of zeolite per cycle. The overall mass balance is shown in Figure 6.6, and a more detailed description of the cycle is given in Section 3.2.

Since the original commercialization of the Lindox process in the early 1970s a good deal of further development has occurred, leading to major improvements in process economics. To take full advantage of the higher selectivity and capacity of the "second generation" adsorbents requires desorption at subatmospheric pressure, necessitating the use of a vacuum swing or pressure/vacuum swing cycle. This leads to a substantial reduction in the adsorbent inventory relative to the traditional pressure swing process but at the cost of a somewhat more complex cycle with both a feed compressor and a vacuum pump. Since the valves and piping must be larger for vacuum operation, there is some penalty in capital cost, but this is more than offset by the reduction in adsorbent inventory and power cost.

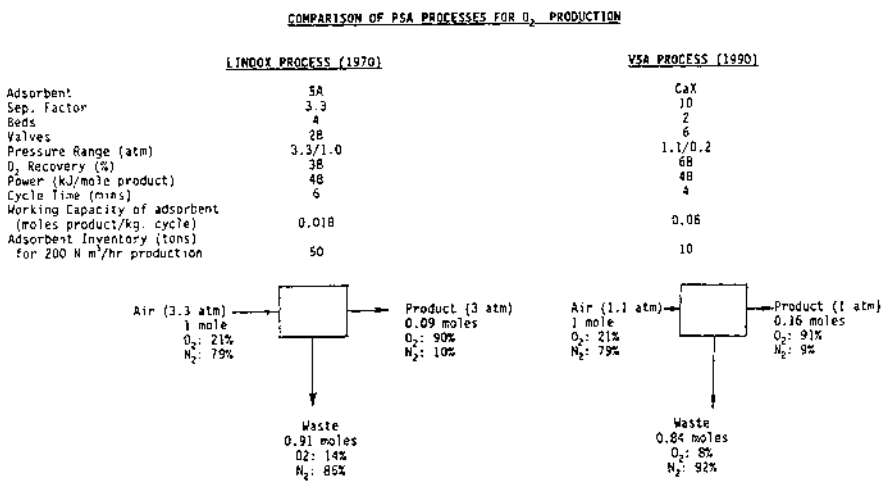

Figure 6.6 Comparison of LINDOX PSA oxygen process with a modern two-bed VSA process. Figures are approximate estimates based on information from a variety of sources.

Modern VSA oxygen systems generally operate between about 1.5–2.5 atmospheres on the high-pressure side with desorption at 0.25–0.35 atmospheres so the pressure ratio is substantially greater than for the earlier supra-atmospheric pressure processes. The cycle is basically similar to the original Air Liquide cycle (Figure 3.12) but with the addition of a pressure equalization step. The adsorbent (Ca*X*) is poisoned by traces of water or carbon dioxide so pre-beds are often included to remove these components. The use of vacuum desorption eliminates the requirement for multiple-bed systems to recover the energy of compression. As a result the more modern VPSA oxygen processes generally use only two beds rather than the three or four beds of the earlier large-scale pressure swing processes, with consequent reduction of capital costs. An approximate performance comparison between a modern VSA oxygen process and the original LINDOX process is given in Figure 6.6. Power requirements are similar, but the adsorbent inventory has been reduced to about 20% of that required in the first generation processes as a result of improved adsorbent capacity, reduced cycle time, and the elimination of the need for multiple beds. Such processes can also produce the nitrogen product in relatively pure form, which is of course an advantage where both oxygen and nitrogen are required. The VSA process is claimed to be competitive with cryogenic distillation for product rates of up to 3000 Nm^3/m or about 100 tons/day (see Figure 6.7).

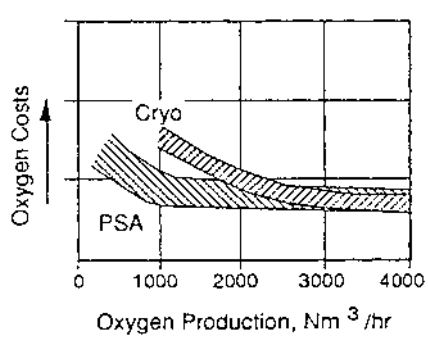

Figure 6.7 Comparative costs of oxygen produced by VS A and cryogenic processes as function of product rate. (From Smolarek and Campbell,[9] with permission.)

6.3 Production of Nitrogen

The most common PSA nitrogen process depends on the use of a kinetically selective carbon molecular sieve adsorbent in which oxygen diffuses faster than nitrogen. This difference in diffusion rates makes oxygen the preferentially adsorbed component, even though there is very little equilibrium selectivity (see Figure 2.11). The choice of contact time is critical since if the contact time is too short there will be no significant adsorption, while, if the time is too long, equilibrium will be approached and there will be no selectivity. In this type of process the argon goes with the nitrogen product since the diffusivities are similar.

Most modern nitrogen PSA processes use a two-bed configuration operated on the cycle shown in Figure 3.16.[11] Descriptions of the process have been given by Schroter and Jiintgen,[12] Pilarczyk and Knoblauch,[13] and by Nitrotec.[14] This system can produce 98-99% pure nitrogen (+ Ar) which is adequate for most purging and inerting operations. Although a higher-purity nitrogen product can be obtained directly from this process, it is generally more economic to use a final ("DEOXO") polishing step. The stoichiometric quantity of hydrogen required to oxidize the residual oxygen is introduced, and the gas stream is then passed over a catalyst bed in which essentially all the oxygen is oxidized to water, which is then removed by adsorption on a zeolite desiccant.

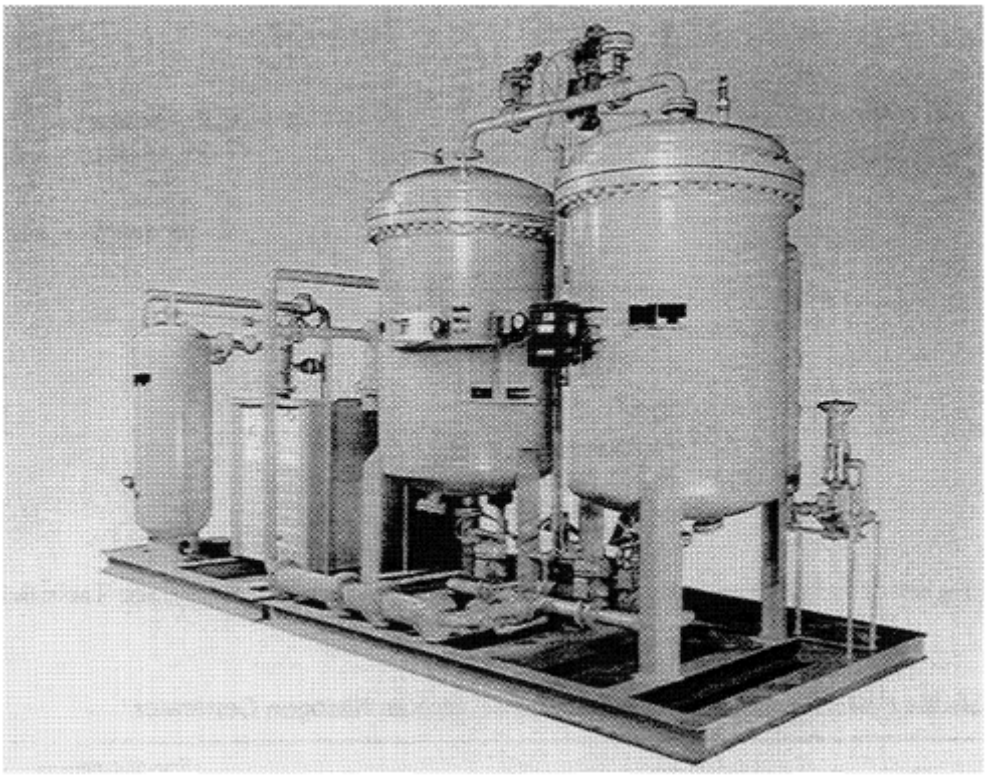

Figure 6.8 Small-scale skid-mounted PSA nitrogen generator. (Courtesy of Nitrotcc, Inc.[14])

A schematic diagram of the Bergbau Forschung process is shown in Figure 3.15, and a typical small-scale unit, produced and marketed by Nitrotec, is shown in Figure 6.8. The process operates between 6–8 and 1 atmospheres pressure. Standard units are produced in varying sizes with nitrogen product rates from 60 to 60,000 SCFH. A typical overall mass

balance is shown in Figure 6.9, and representative performance data are summarized in Table 6.1. The reduction in throughput and the corresponding reduction in recovery and the increase in the specific energy requirement with increasing purity of the nitrogen product are clearly apparent. The economics of this type of process are at their best in the 98–99% purity range at product rates of 200–800 Nm^3/h, although much larger units (up to 4800 Nm^3/hr or about 150 tons/day) have been built.[15] Typical operating costs (assuming electric power at $0.05 per kwh) are about $0.30–0.40 per 1000 SCF (28 Nm^3) for 98% and 99.5% purity respectively (1992 figures)*. At this level costs are comparable with a cryogenic unit over a fairly wide range and only at the highest purity levels (> 99.5%) and production rates (> 200 tons/day) does the cryogenic system gain a clear economic advantage (see figure 8.10).

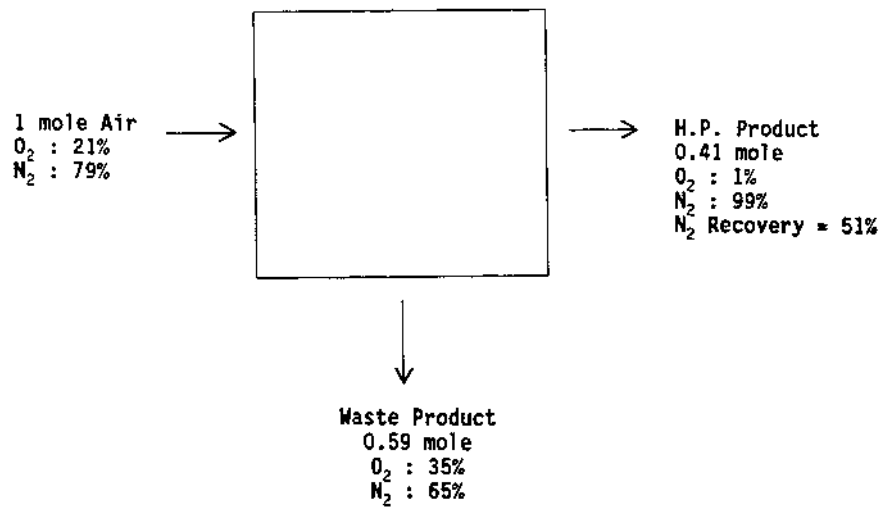

Figure 6.9 Overall mass balance for PSA nitrogen production process. See Table 6.1.

Table 6.1. Performance Characteristics of Nitrotec Nitrogen Generator[a]

Product rate ($N\ m^3/h$)	O_2 impurity (%)	N_2 recovery (%)	Power (kW)	Specific energy (kWh/Nm^3 product)
96	3	84	26	0.27
57	1.0	51	23	0.40
39	0.5	35	20	0.51
21	0.1	15	16	0.76

[a] Feed rate: 140 Nm^3/h, half-cycle time 2 mins; adsorbent beds (2): 76 cm diam × 150 cm height (approx); working pressure: 8 atm/1 atm. Data are from Nitrotec brochure,[14] courtesy Nitrotec Corporation, Glen Burnie, MD, and other sources.

6.4 PSA Process for Simultaneous Production of O_2 and N_2

Most PSA processes produce one pure product and an impure byproduct, but by proper design of the operating cycle it is in fact possible to produce two reasonably pure products,

* These cost estimates were kindly provided by Mr. Herbert Reinhold of Nitrotec.

subject of course to the limitations imposed by the overall mass balance. An example of such a process is the Air Products vacuum swing adsorption process (VSA),[16,17] which is described here. Another similar cycle is discussed in Sections 4.4.5 and 4.5. The process operates with what is basically a two-bed system, but each "bed" actually consists of a prebed for impurity removal in series with the main adsorption bed. The sequence of operations, which involves five distinct steps, is shown schematically in Figure 6.10(b). The following description is taken from Sircar.[17]

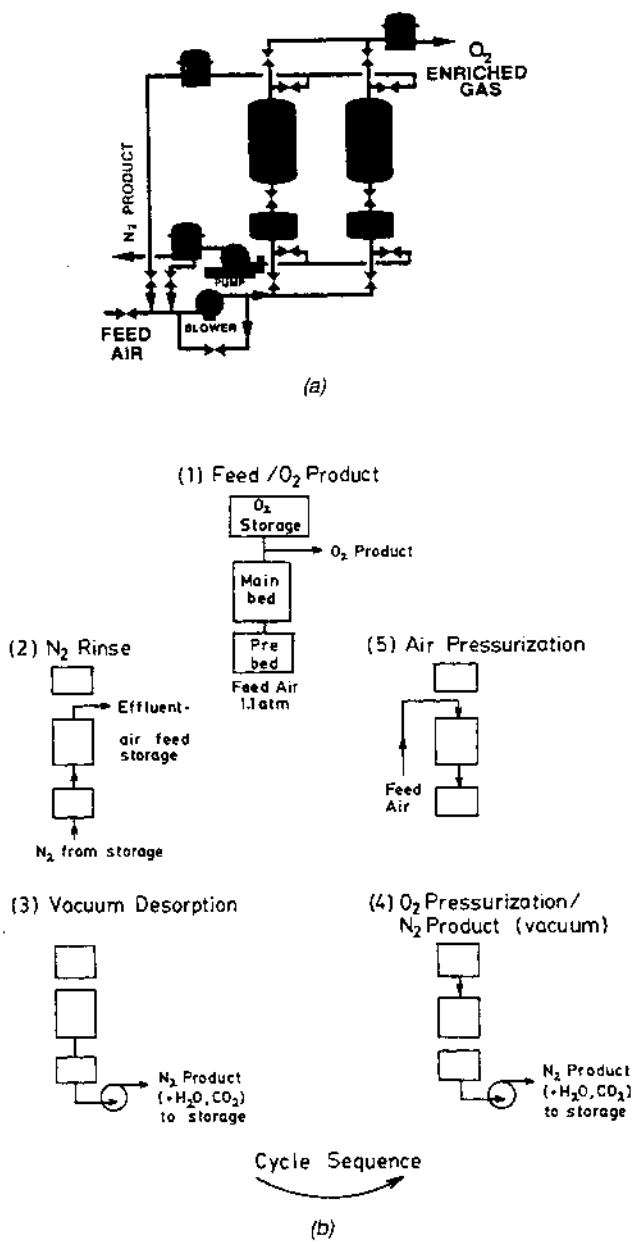

Figure 6.10 Schematic diagrams showing (a) the flowsheet for the Air Products vacuum swing process for simultaneous production of O_2 and N_2 and (b) the sequence of the operating cycle.[17]

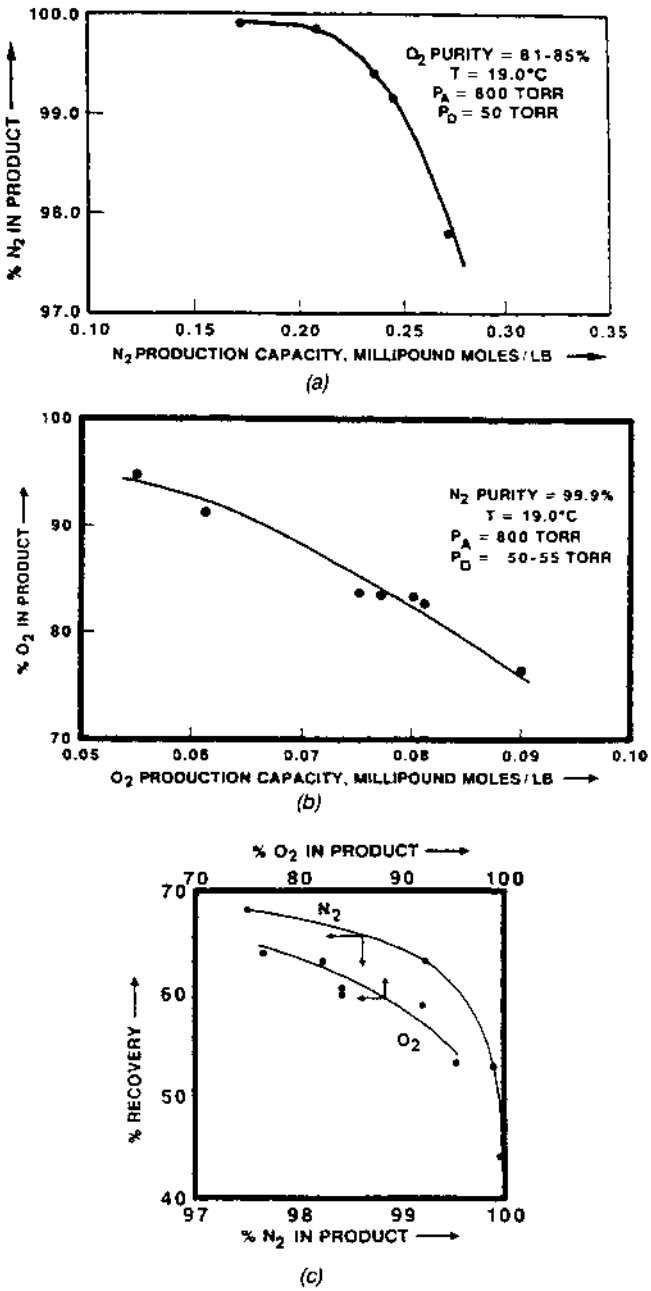

Figure 6.11 Performance of Air Products Vacuum swing air separation process. Adsorbent, Na mordenite; feed pressure, 1.05 atm; desorption pressure (main bed), 50–55 Torr; prebed, 25–30 Torr, (a) Nitrogen product purity; (b) oxygen product purity as a function of product rate; and (c) recovery–purity profile for both products. (From Sircar[17] with permission.)

Feed/O_2 Product. Air at near-ambient pressure is passed through the prebed and main bed, which have been previously raised to ambient pressure in steps (d) and (e) of the cycle. H_2O and CO_2 are removed in the prebed, and the dry CO_2 free air then passes to the main bed, where N_2 is selectively desorbed to yield the oxygen-rich product stream, some of which is stored in a gas tank for use as the pressurization gas in step (c). This step is terminated at or before the breakthrough of N_2.

N_2 Rinse. A stream of the N_2-rich product is passed through both the prebed and the main bed in the cocurrent direction. The effluent is a dry CO_2 free gas with a composition close to that of air. A part of this gas is therefore recycled as feed air to reduce the load on the prebed. This step is continued until both the prebed and main bed are essentially saturated with nitrogen.

Vacuum Desorption. Both adsorbers are now evacuated from the O_2 product end (countercurrent direction), producing the nitrogen-enriched product stream. This stream, however, contains essentially all the CO_2 and H_2O desorbed from the prebed. A fraction of this gas is stored for use as the nitrogen rinse (step b) in the other pair of beds, while the remainder is withdrawn as the N_2-rich product. Evacuation is continued in this manner until the pressure reaches a preset value at which the valve between the prebed and the main bed is closed.

Evacuation/O_2 Pressurization. Evacuation of the prebed is continued with the desorbate being added to the nitrogen-rich product. Meanwhile the main bed is pressurized with part of the oxygen-rich product from the storage tank.

Air Pressurization. Finally the interconnecting valve between the pre and main beds is opened, and the prebed is brought up to feed pressure with oxygen from the storage tank through the main bed, thus completing the cycle. The performance is shown in Figure 6.11. (See also Figures 4.14 and 4.15.)

6.5 Hydrogen Recovery

The increasing demand for hydrogen, particularly in petroleum refining and petrochemical processing, has provided a strong economic motivation to develop processes to recover hydrogen from refinery fuel gases, coke oven gases, and other similar sources as well as from more traditional sources such as reformer off gas. For most applications a high-purity hydrogen product is required (at least 99.99% and often 99.999%). Since hydrogen is adsorbed much less strongly than almost any other species, a well-designed pressure swing system can meet this challenge. Indeed this is one application for which PSA has a clear advantage over almost all other possible approaches, for many of which these purity levels are unattainable.

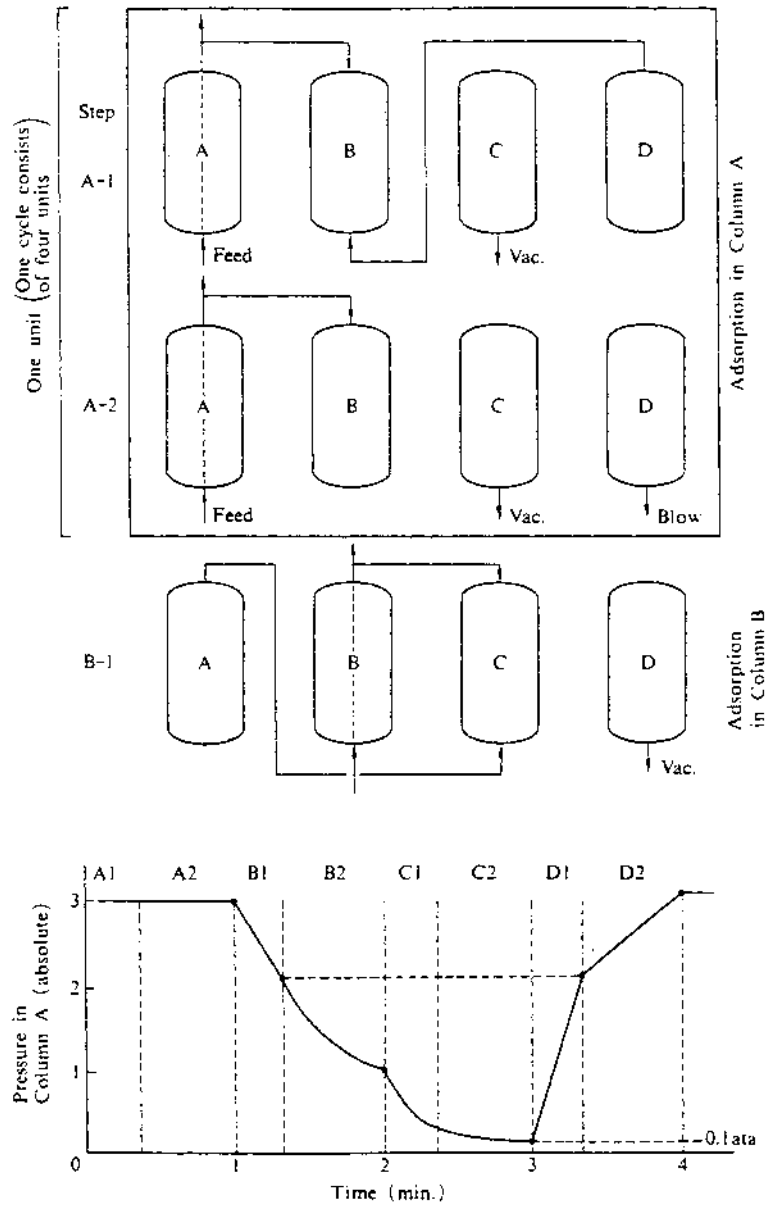

Figure 6.12 Sequence of bed switching and pressure variation in a four-bed hydrogen PSA process. (From Suzuki,[29] with permission.)

Commercial implementation of PSA processes for hydrogen recovery dates from the late 1960s, but the earlier processes were small-scale three-or four-bed units with relatively modest performance (~ 70% recovery) de signed to provide local sources of high-purity hydrogen.[18–23] Large-scale multiple-bed processes were developed in the late 1970s, the first being the 41 MMSCFD plant at the Wintershall AG Lingen refinery in Germany.[24] These processes, which employ up to twelve beds with several pressure equalization steps, can achieve hydrogen recoveries in the 85–90% range at 99.99% purity from a typical feed containing 75% H_2.[25–28]

Table 6.2. Details of Test Conditions and Performance Data for a Four-Bed Hydrogen PSA Purification System

Adsorbent	5A zeolite
Size	1–4 mm (4–18 mesh)
Form	spherical beads
Bulk density	0.74 kg/l
Feed cone.	
H_2	69.2 vol %
N_2	26.8
CO	2.2
CH_4	1.8
Pressure	
Adsorption P_a	8.6 kg/cm^2
Purge P_p	1.5 kg/cm^2
First equilibration P_1	5.2 kg/cm^2
Second equilibration P_3	1.9 kg/cm^2

Run no.	1	2	3	4	5	6	7	8	9	10	11
Feed rate (Nl/min)[a]	14.9	14.6	14.6	21.0	20.9	20.9	8.3	8.3	14.6	14.6	14.5
Cycle Time (min)	12.0	24.0	48.0	8.4	16.8	33.6	21.0	42.0	4.7	6.0	8.0
Column size	4.3 cm i.d. × 200 cm L.								4.3 cm i.d. × 100 cm L.		
Adsorbent (kg)	2.06 × 4 bed								1.0 × 4 bed		
Product cone.											
H_2 (vol %)	99.73	85.61	76.19	99.38	84.22	76.55	99.93	83.48	99.87	97.93	88.41
N_2	0.27	13.41	21.15	0.62	14.52	20.86	0.07	15.19	0.13	2.06	10.9
CO	0.0	0.52	1.48	0.0	0.68	1.45	0.0	0.68	0.0	0.0	0.39
CH_4	0.0	0.47	1.18	0.0	0.58	1.14	0.0	0.65	0.0	0.01	0.30
H_2 Recovery (%)	77.7	88.4	94.9	77.2	90.3	94.6	77.7	90.5	70.0	78.6	83.9
Adsorbent productivity Q (Nl/kg ads., cycle)	21.7	42.7	84.9	21.4	42.6	85.2	21.3	42.5	17.0	21.8	29.0
Space velocity (l/min)	0.66	0.63	0.62	0.90	0.87	0.84	0.37	0.37	1.30	1.29	1.26

[a] Nl = liters at 273 K 1 atm.
From Tomita et al.,[23] with permission.

6.5.1 The Four-Bed Process

The system for the four-bed process is essentially similar to the four-bed oxygen process (Lindox) shown in Figures 3.9 and 3.10. A mixed adsorbent of activated carbon and 5A zeolite is commonly used, although, since the selectivity for most impurities relative to hydrogen is high, almost any adsorbent can be employed. Production of a hydrogen product with 99.99% purity at 75% recovery from a feed containing 70–80% hydrogen is claimed for the four-bed process with two pressure equalization steps. The process operates between 20-30 atmospheres and 1–2 atmospheres. The cycle is shown in Figure 6.12. Details concerning the optimization have been given by Doshi et al.[22] Results of an experimental pilot scale study of the four-bed hydrogen PSA process have been reported by Tomita et al.[23] Some of their results are presented in Table 6.2 and Figure 6.13.

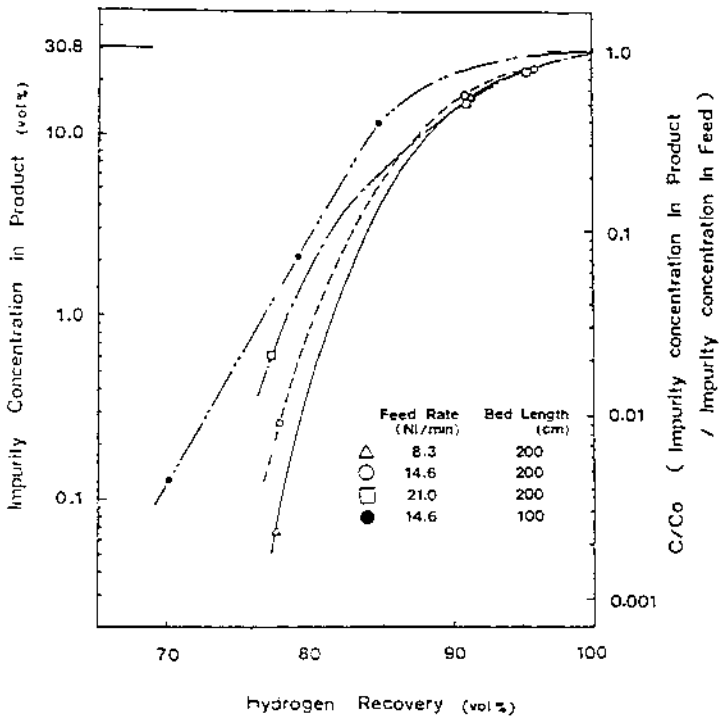

Figure 6.13 Experimental recovery-purity profile for four-bed H_2 PSA system. (From Tomita et al.,[23] with permission.)

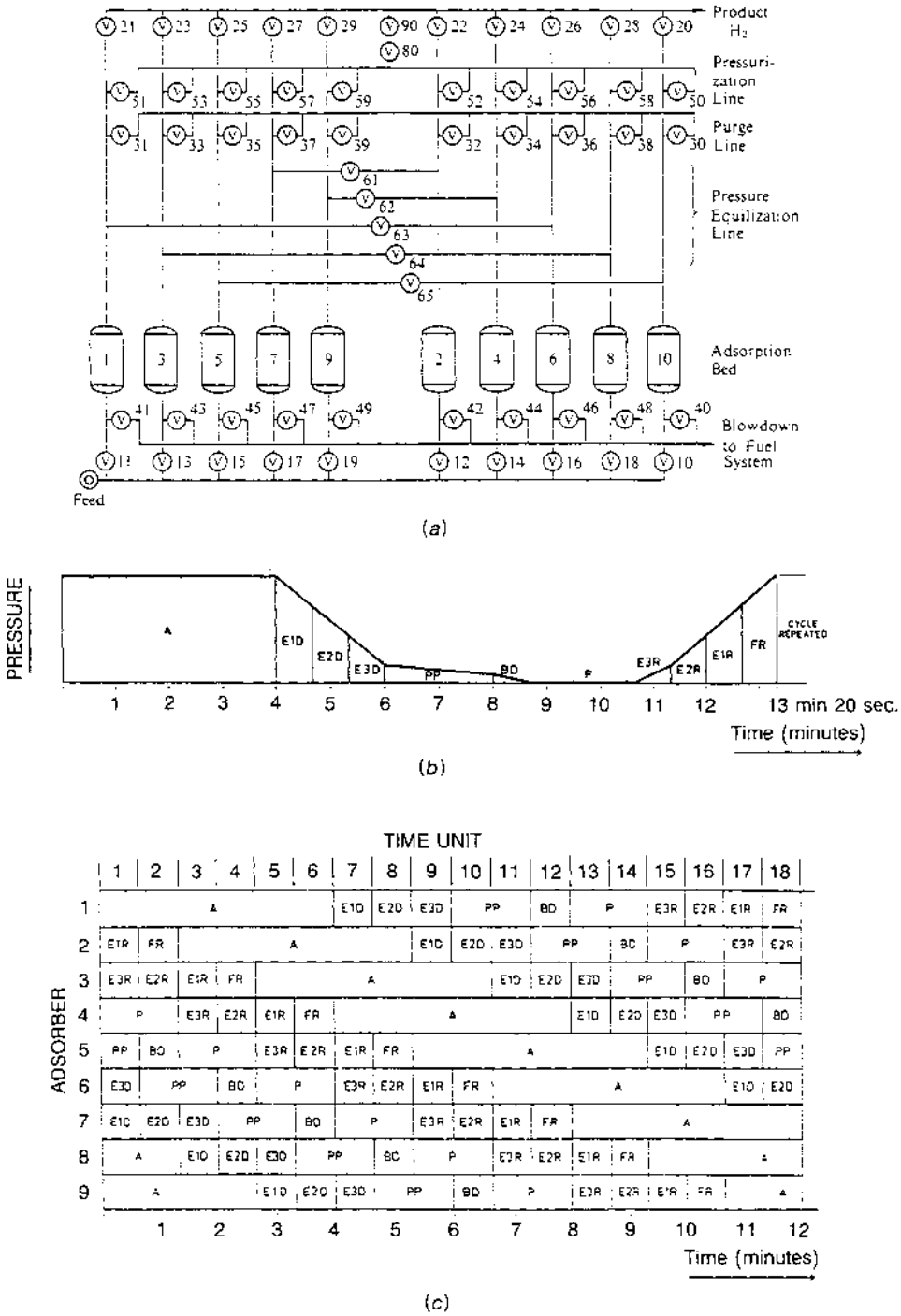

Figure 6.14 (a) Flowsheet, (b) pressure history, and (c) switching sequence for polybed (ten-bed) PSA hydrogen purification process. (Courtesy of Union Carbide.)

A detailed theoretical optimization of the design of a zeolite-based hydrogen PSA unit, for feed and product specifications typical of industrial practice, has been carried out by Smith and Westerberg.[30] Their results illustrate clearly the economy obtained from an optimal choice of operating pressures and the number of equalization steps. For

smaller-scale plants a single equalization step is preferable, but as the throughput increases the optimum shifts towards two or three equalization steps as a result of the proportionately greater importance of operating versus capital costs (see Figure 1.3). The optimal operating pressure, for a system with two equalizations, is about 18 atm. These conclusions are in line with current industrial practice.

6.5.2 Polybed Process

The polybed process operates on a similar principle but with seven to ten beds and at least three pressure equalization steps. This increases the hydrogen recovery to the 85–90% range, but the improvement in performance must be weighed against the increase in capital cost. The process flowsheet is shown in Figure 6.14. Both four-bed and polybed processes operate typically with a pressure ratio 20–30 atm/1 atm. The overall mass balance is shown in Figure 6.15. Purities as high as 99.9999% are achievable with the polybed system, although 99.999% is more common.

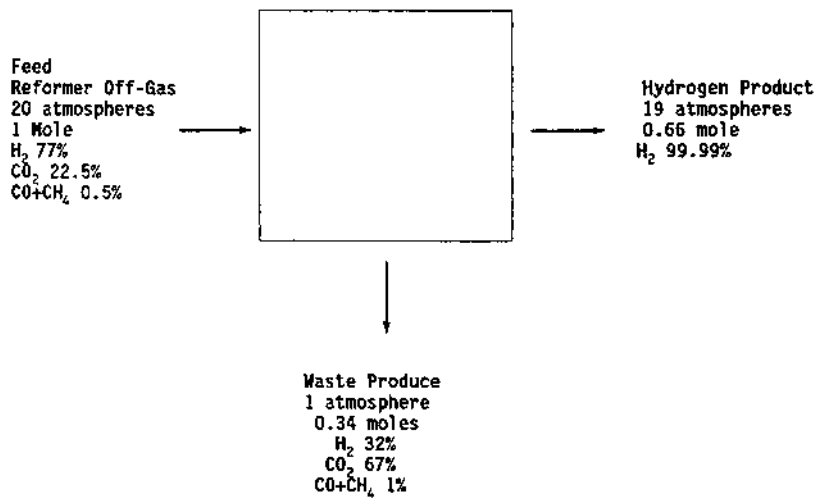

Figure 6.15 Mass balance for polybed PSA hydrogen purification process.

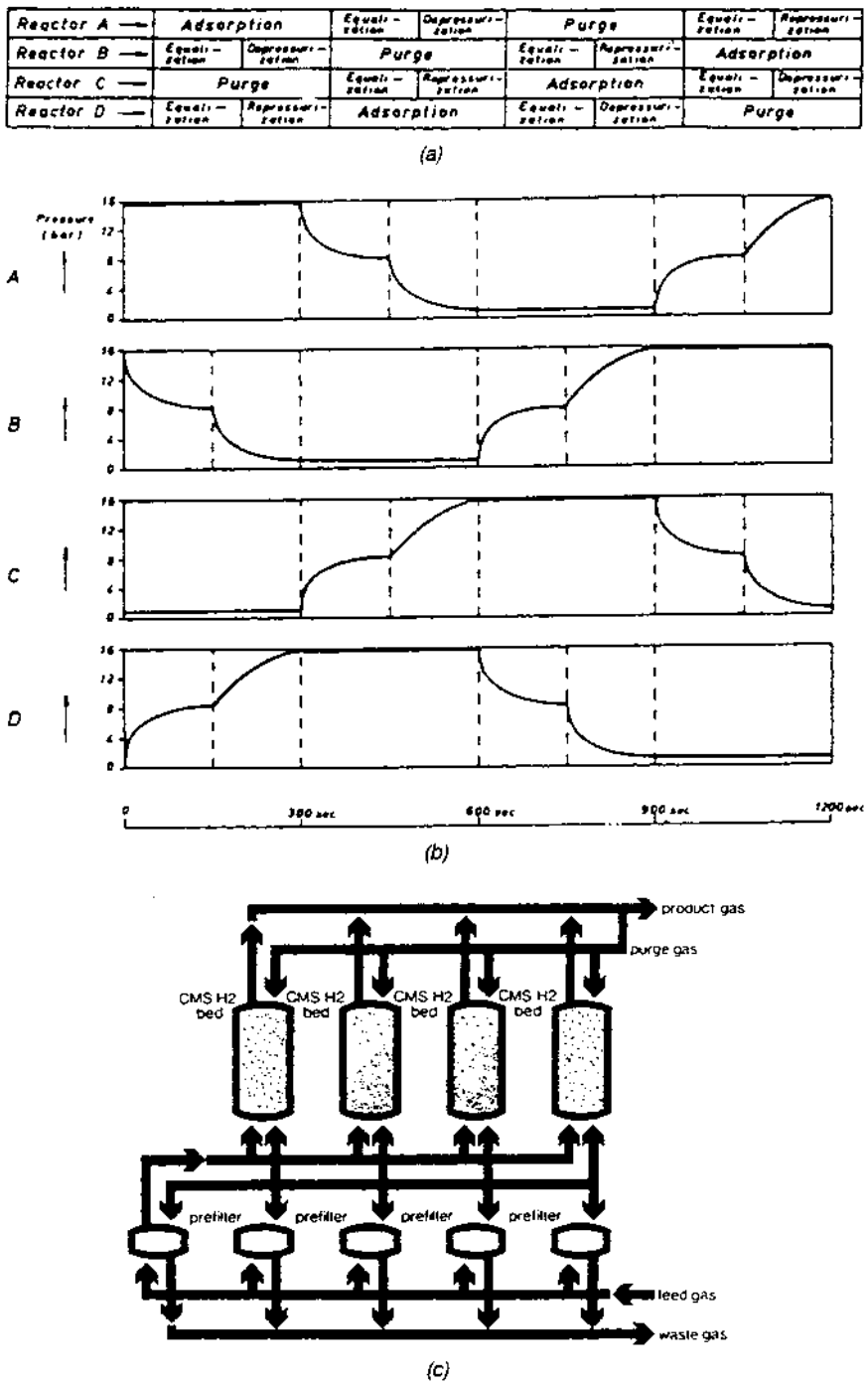

Figure 6.16 Switching sequence, pressure history, and schematic flowsheet for four-bed carbon molecular sieve hydrogen purification process. (From Pilarczyk and Knoblauch,[13] with permission.)

Table 6.3. Composition of Typical Coke Oven Gas

Components	Concentration (% by vol.)
H_2	59.99
CH_4	22.76

N_2	6.68
CO	5.45
C_2H_4	1.66
O_2	1.40
CD_2	1.26
C_2H_6	0.53
C_3H_6	0.11
C,H_2	0.09
C_3H_8	0.02
C_4H_6	0.02
C_6H_6	0.02
C_4H_6	0.01
C_4H_{10}	0.01
C_5H_{12}	0.01
C_6H_{14}	0.01
C_7H_{16}	0.01
C_7H_8	0.01

Source: Ref. 30.

6.5.3 Bergbau -Forschung Process

As an alternative to the zeolite-based hydrogen recovery processes developed by Union Carbide, Bergbau–Forschung has developed equivalent processes using a wide-pore carbon molecular sieve as the adsorbent. A four-bed system is used with five smaller preadsorption beds containing activated carbon and operating between atm and 1 atm. The process sequence, which is basically similar to that used in the four-bed Union Carbide system, is shown in Figure 6.16. This system has been used primarily to recover hydrogen from coke oven gas containing about 60% hydrogen (see Table 6.3). Hydrogen product purities as high as 99.999% at a recovery of 85% are claimed, and the largest units have a product rate of 10^4 Nm^3/h. The performance thus appears to be broadly similar to that of the Union Carbide polybed system, but since only four beds are used, there should be a capital cost advantage.

6.6 Recovery of CO_2

Carbon dioxide is present at relatively high concentrations (15–35%) in the flue gases from many industries such as steel and lime production. Since CO_2 is strongly adsorbed on many adsorbents, including both zeolites and carbon molecular sieves, a vacuum desorption system is necessary. A high selectivity for CO_2 is achieved by the use of a narrow-pore carbon molecular sieve adsorbent, similar to that used for nitrogen production. However, the process differs from the nitrogen process in that the product (CO_2) is the more strongly adsorbed component. A simple two-bed vacuum swing system operating between about 1.2 and 0.05 atm has been developed and built at a Japanese steel works.[31] The process schematic is shown in Figure 6.17. 99% product purity and a recovery of 80% at a product rate of 3000 N m^3/h are claimed. A more complex four-bed version of this process has also been developed to the pilot plant stage.[32] The schematic of the process is shown in Figure 6.18 and performance data are given in Table 6.4. As a result of environmental pressures the possibility of extracting CO_2 from the stack gases of coal-fired power stations is under active study at the pilot plant stage,[31] although, with current technology, the power costs are too high to make such a process economically attractive.

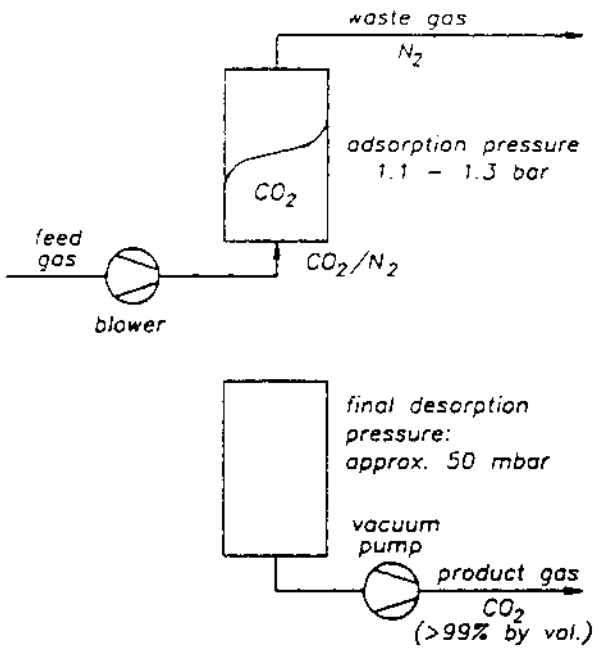

Figure 6.17 Schematic of vacuum swing process for CO_2 recovery from the effluent gas from a steel works. (From Schrdter and Jiintgen,[12] with permission.)

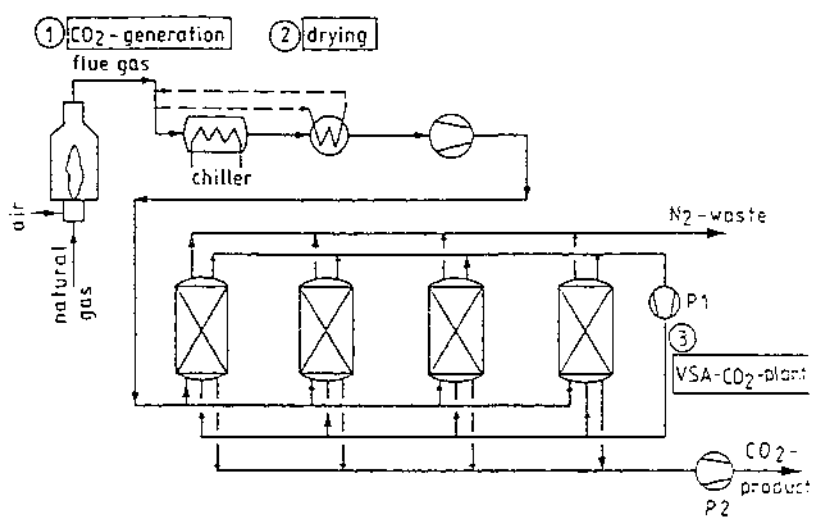

Figure 6.18 Schematic diagram of a four-bed vacuum swing system for recovery of CO_2 from flue gas. (From Pilarczyk and Schrdter,[13] with permission.)

Table 6.4. Performance of Bergbau VSA Process for Recovery of CO_2 from Flue Gas

	Run 1	Run 2	Run 3
Compressor P1 (m^3/h)	65	65	65
Compressor P2 (m^3/h)	350	160	100
CO_2 purity (%)	98.8	98.6	98.7
Product rate (kg/h)	5.9	4.8	4.1

Recovery (%)	72	62	53
Total energy of P1 + P2 kW/hkg CO_2	3.0	1.0	0.8

[a] Feed: flue gas containing ~11 vol% CO_2 at 36 m^3/h (STP); adsorber: four beds, each 96 liters packed with wide-pore CMS.
Source: Ref. 30.

6.7 Recovery of Methane from Landfill Gases

A somewhat similar process has been developed for recovery of methane from landfill gases.[12,13] These gases contain mainly methane (50–65%) and carbon dioxide (35–50%) as well as small amounts of nitrogen, with many different hydrocarbons and sulfur compounds in trace concentrations. A two-stage initial purification process is employed. In the first stage hydrogen sulfide is removed at a temperature of 40–50° C using a bed of iodine-impregnated activated carbon. This acts as an efficient catalyst for conversion to elemental sulfur, and residual H_2S levels as low as 1 ppm can be achieved. In the second stage halocarbons and heavier hydrocarbons are removed in a conventional activated carbon adsorber. The final stage of the process utilizes a four-bed vacuum swing system to recover methane from the purified landfill gas using a narrow-pore carbon molecular sieve. The remaining impurities (CO_2, N_2, O_2) diffuse into the adsorbent much faster than methane, which is therefore produced as the raffinate product. A high recovery (over 90%) is reported, with the product containing 87–89% methane with the balance CO_2 + N_2.

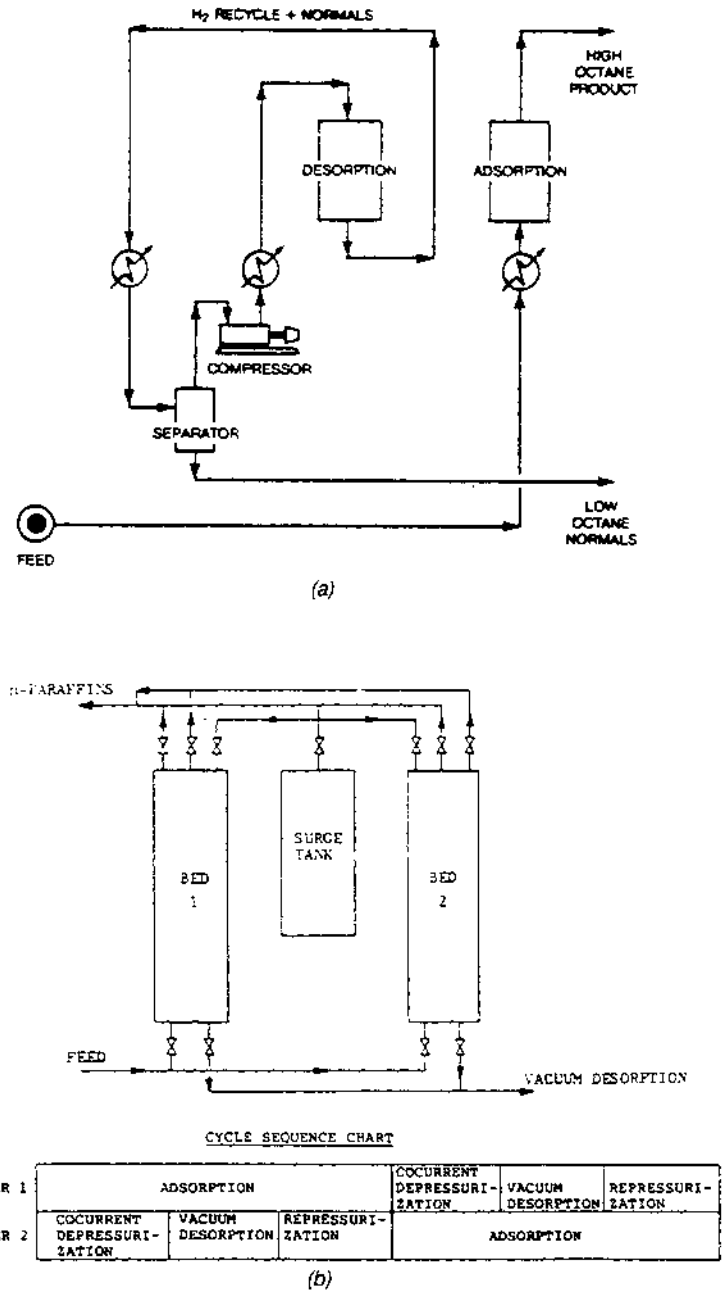

Figure 6.19 (a) Simplified flow diagram and (b) cycle sequence for the Isosiv paraffin separation process. (From Cassidy and Holmes,[27] with permission.)

6.8 Hydrocarbon Separations

The separation of linear from branched and cyclic hydrocarbons using 5A zeolite as the adsorbent is one of the earliest examples of a molecular sieve separation process. In the low-molecular-weight range (up to C_{10}) a pressure swing version of the "Isosiv" process is commonly used. The system, which is in essence a standard pressure/vacuum swing system, is shown schematically in Figure 6.19. High-purity linear paraffins are produced as the desorbate during the evacuation step, while during the adsorption step a raffinate

stream depleted of normals is produced. The operating temperature and pressures depend on the molecular weight range, but for the C_6 feedstock, 350° C with a pressure swing from 20 to 0.2 atm is typical.[27] A somewhat similar process has been developed by B.P.[32]

6.9 Process for Simultaneous Production of H_2 and CO_2 from Reformer Off-Gas

The crude hydrogen stream from a steam reformer contains significant quantities of carbon dioxide, which, by appropriate design of the separation process, can be recovered as a valuable byproduct. A PSA process for simultaneous production of pure hydrogen and carbon dioxide from such a feed gas has recently been developed by Air Products and is described here as an example of the third generation of PSA processes designed to achieve both energy efficiency and dual product recovery. Two variants of this process have been developed. The original version (Gemini-9)[17,33] used nine adsorbent beds in a series-parallel arrangement but in the later version improved performance was obtained, at a somewhat lower capital cost, by using a modified cycle with only eight beds (Gemini-8).[34]

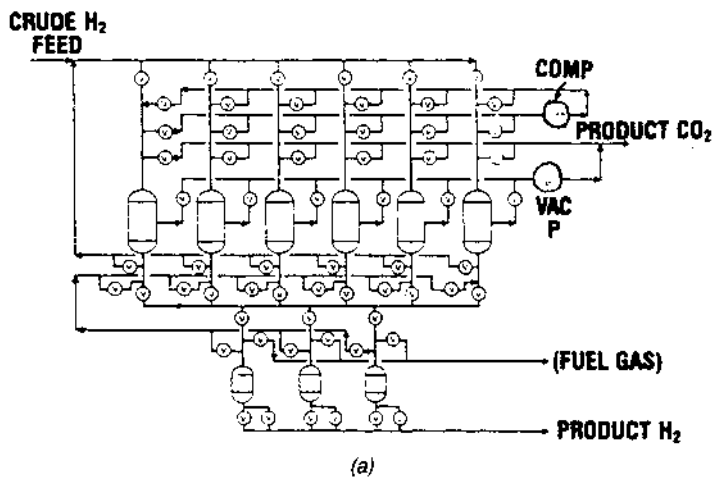

Figure 6.20 (a) Simplified process flow sheet, (b) flow schedule for the Gemini-9 process for simultaneous production of H_2 and CO_2 from reformer gases. (From Sircar[17] and Kumar et al.,[34] with permission.)

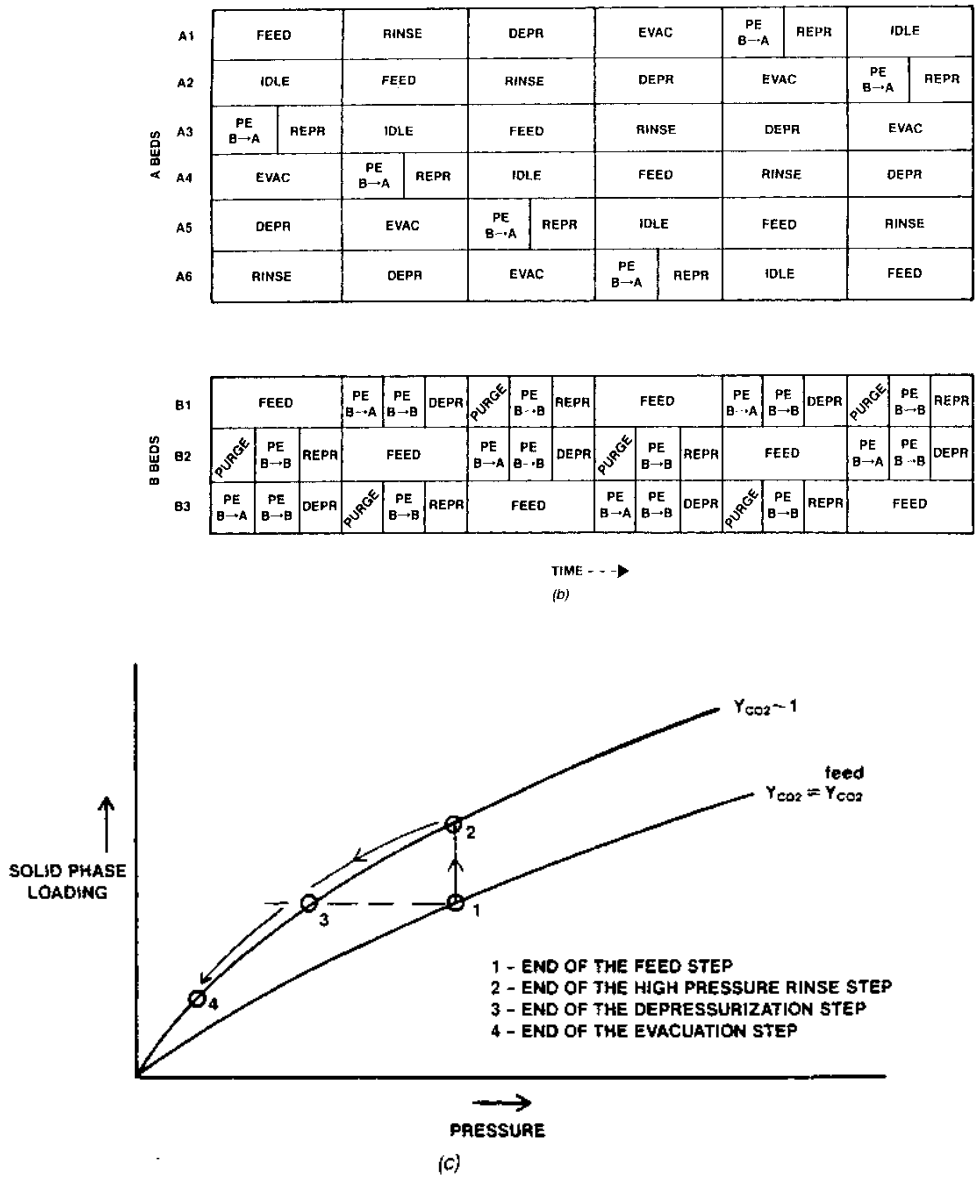

Figure 6.20(c) Variation in CO_2 loading during the cycle for the Gemini-9 Process. (From Kumar et al.,[34] with permission.)

The flowsheet for Gemini-9 is shown schematically in Figure 6.20. There are six parallel beds containing a zeolite adsorbent (NaX) that selectively removes H_2O and CO_2 from the feed gas (the A beds) and three parallel beds packed with a second zeolite adsorbent (a mixture of Na *X* and 5 A) that selectively removes CO_2, CO, CH_4, and N_2 impurities from the hydrogen product (the B beds). During the adsorption steps one A and one B bed are connected in series, but the desorption steps for the A and B beds are different, as will be described.

6.9.1 Cycle for the A Beds

A1. Adsorption. Following pressurization with the hydrogen-rich product gas the feed gas is passed through the bed at the highest pressure of the cycle (P_H). CO_2 and water vapor

are removed, and the effluent passes to a B bed for removal of the trace impurities (CO, CH_4, and N_2) together with any CO_2 that has passed through A bed. This step is terminated just prior to breakthrough of the C_2 mass transfer front.

A2. CO_2 Rinse. At the termination of the adsorption step high-purity CO_2 at the feed gas pressure is passed through the bed in the cocurrent direction. The effluent has a composition similar to that of the feed, and it is recycled as feed to another of the A beds. This step is continued until the bed is essentially saturated with high-purity CO_2.

A3. Countercurrent Depressurization. The A bed is blown down countercurrently to atmospheric pressure, and the effluent from this step, which consists of high-purity CO_2, is collected as byproduct. Part of this gas is recompressed to P_H for use in the CO_2 rinse step A2.

A4. Countercurrent Evacuation. The bed is evacuated from the feed end to the lowest pressure of the cycle (P_L). The residual CO_2 from this step is added to the byproduct stream.

A5. Countercurrent Pressurization I. The evacuated A bed is connected with a B bed undergoing B2 (see Section 6.9.2) in order to transfer a part of the residual gases from the B bed to the A bed (product end), thus raising the pressure in the A bed to an intermediate level $P_1 \cdot (P_L < P_1 < P_H)$.

A6. Countercurrent Pressurization II. To complete the cycle is pressurized to P_H using the hydrogen product gas introduced at the product end. The pressurizing gas is in fact the recycled effluent from a B bed undergoing step B7.

The variation in CO_2 loading during the cycle (for the A beds) is shown schematically in Figure 20(c). At the end of the feedstep (Al) the beds are at point (1) on the feed isotherm. At the end of the rinse step (A2) the loading corresponds to point (2) on the pure CO_2 isotherm. At the end of the blowdown step (A3) the CO_2 loading has fallen to point (3) and the gas released is recompressed for use as the high-pressure rinse gas. During the evacuation (step A4) the loading falls to point 4 and the CO_2 desorbed in this step constitutes the product stream.

6.9.2 Cycle for the B Beds

B1. Adsorption. Prior to this step the B bed is pressurized to P_H with hydrogen product gas. The B bed in series with an A bed during step Al receives the CO_2 depleted gas from the A bed and removes the remaining CO_2 and other impurities to yield highly pure hydrogen as effluent. Part of the hydrogen product is used to purge another B bed (step B5) and to pressurize both B and A beds (steps B7 and A6). The adsorption/product withdrawal step is terminated just before the leading impurity breaks through.

B2. Countercurrent Depressurization I. The B bed is connected with an A bed, which is undergoing step A5 and a portion of the desorbed and interstitial gas is transferred through the feed end to the A bed (countercurrent), thus reducing the pressure from P_H to P_1.

B3. Countercurrent Depressurization II. The bed is connected to another B bed, which is undergoing step B6 and more of the desorbate and interstitial gas is removed (countercurrently) through the feed end, reducing the pressure to P_2.

B4. Countercurrent Depressurization III. The bed is blown down from P_2 to atmospheric pressure, and the effluent gas, which contains a proportion of the feed impurities together with some hydrogen, is rejected.

B5. Countercurrent Purge. The bed is purged at atmospheric pressure with high-purity hydrogen product to desorb any impurities further. The effluent is rejected.

B6. Cocurrent Pressurization. The pressure in the bed is raised to P_2 by connecting with another B bed undergoing step B5.

B7. Countercurrent Pressurization. Final pressurization of the B bed to P_H is accomplished with hydrogen product, introduced from the product end. During the later part of this step the B bed is connected with another A bed undergoing step A6 and both beds are then pressurized to P_H.

Table 6.5. Performance of Gemini-9 Process for Simultaneous Production of H_2 and CO_2

Run	Feed" (psig)	P Relative amounts of gases				H_2 Product			CO_2 Product			Fuel gas[0]
		CO_2 rinse	A desorption	bedA bed evacuation	H_2 purge to B bed	Amount	%H_2	Recovery	Amount	%CO_2	Recovery	Amount
A	200	0.252	0.275	0.160	0.078	0.645	99.999 +	85.9%	0.183	99.4	90.1%	0.180
B	250	0.259	0.295	0.152	0.061	0.657	99.999 +	87.1%	0.188	99.4	94.0%	0.172
C	300	0.283	0.310	0.144	0.050	0.656	99.999 +	86.7%	0.171	99.4	86.9%	0.165

Performance Comparison

	Gemini-8	Gemini-9
H_2 purity (mol %)	99.999	99.999
H_2 recovery (%)	86	87
CO_2 purity (mol %)	97.0 +	99.0 +
CO_2 recovery (%)	86	91
Relative compressor size	0.43	1.00
Relative compressor power	0.57	1.00
Relative vacuum blower power	0.86	1.00
Number of adsorbent beds	8	9
Number of switch valves	508w.	68

[a] Feed gas contains 75.4% H_2, 19.9% CO_2, 0.96% CO, and 3.73% CH_4.
[b] Fuel gas composition: 9.5% CO_2, 6.1% CO, 22.5% CH_4, and 61.9% H_2.

The B beds pass through two complete cycles (steps B1 to B7) while the A beds go through one cycle so that each B bed handles the gas from two A beds during the complete cycle. This approach reduces significantly the size of the B beds. A key feature of this cycle is that the A and B beds are connected in series during the adsorption step but they are regenerated by two entirely different sequences. The overall performance is summarized in Table 6.5. It is evident that the hydrogen product has a purity greater than 99.999% and the fractional recovery is about 86–87%, while the CO_2 product is produced at a purity of about 99.4% with about 90% recovery. The Gemini-8 process gives slightly lower purity and recovery of CO_2, but there is a significant reduction in the size of the compressors and the power consumption.

6.10 PSA Process for Concentrating a Trace Component

In the processes described so far in this chapter the objective has generally been to produce a pure raffinate product, although in some cases the more strongly adsorbed species (the extract product) is also recovered in concentrated form. However, particularly in environmental applications, it is often necessary to concentrate a trace component for disposal or further processing. Provided that a sufficiently selective adsorbent is available, PSA appears to be well suited to such applications, although to date few, if any, processes of this kind have been commercialized. Examples of two such processes that have been developed to the pilot plant scale are described in this section.

The basic principle of a PSA "concentration process" may be understood from equilibrium theory (see Section 4.2 and Figure 4.25). Consider an adsorbent bed equilibrated at pressure P_0 and mole fraction (of the more strongly adsorbed species) y_0. If the equilibria are linear:

$$q_A^* = K_A c_A = K_A y \frac{P}{RT}; \quad q_B^* = K_B c_B = K_B (1-y) \frac{P}{RT} \tag{6.3}$$

By combining the differential mass balance expressions for both components (Eq. 4.4), we obtain:

$$\frac{1}{\beta_B}\frac{\partial P}{\partial t} + \left(\frac{1}{\beta_A} - \frac{1}{\beta_B}\right)\frac{\partial (Py)}{\partial t} + \frac{\partial (Pv)}{\partial z} = 0 \tag{6.4}$$

and by eliminating the term $\partial v/\partial z$ between Eqs. 4.4 and 6.3:

$$\left(\frac{\partial y}{\partial t}\right)_z + \frac{\beta_A v}{1+(\beta-1)y}\left(\frac{\partial y}{\partial z}\right)_t = \frac{(\beta-1)(1-y)y}{1+(\beta-1)y}\frac{d \ln P}{dt} \tag{6.5}$$

in which $\beta = \beta_A/\beta_B$ and the total pressure differential arises from the assumption of negligible pressure drop across the column [$P = P(t)$]. Since $y = y(z, t)$, the left-hand side of Eq. 6.5 is simply the total time derivative of y, and the variation of composition during pressurization or blowdown steps is given by Eq. 4.8. It follows by direct integration that the variation in composition during pressurization or blowdown will be given by:

$$\frac{y}{y_0} = \left(\frac{1-y}{1-y_0}\right)^{\beta}\left(\frac{P}{P_0}\right)^{\beta-1} \tag{6.6}$$

Equations 4.4 and 6.4 yield:

$$\frac{1}{\beta_B}\frac{\partial P}{\partial t} + (\beta-1)\frac{\partial (vPy)}{\partial z} + \frac{\partial (vP)}{\partial z} = 0 \tag{6.7}$$

Neglecting the axial variation of pressure leaves only the time dependence; so the velocity during a pressurization or blowdown step can be found simply integrating from the closed end:

$$v = \frac{-z}{\beta_B\left[1+(\beta-1)y\right]}\frac{d\ln P}{dt} \tag{6.8}$$

The fraction of A desorbed during blowdown from pressure P_0 to P is given by:

$$F_A = \int_{P_0}^{P} \beta_A \frac{vyP\,dt}{zy_0P_0} \tag{6.9}$$

and substituting for v and y from Eqs. 6.8 and 6.6:

$$F_A = \frac{\beta}{1-\beta}\left(\frac{1-y_0}{y_0}\right)^{\beta/(\beta-1)} \int_{P_0}^{P} \frac{y^{1/(\beta-1)}}{(1-y)^{(2\beta-1)/(\beta-1)}}\,dy \tag{6.10}$$

Similarly, for the fraction of B desorbed:

$$F_B = \frac{1}{1-\beta}\left(\frac{y_0}{1-y_0}\right)^{1/(1-\beta)} \int_{P}^{P_0} \frac{y^{(2-\beta)/(\beta-1)}}{(1-y)^{\beta/(\beta-1)}}\,dy \tag{6.11}$$

In the limit of $y_0 \to 0$ and $\beta \to 0$ (high selectivity) these expressions reduce to:

$$\begin{aligned} \frac{y}{y_0} &= \frac{P_0}{P} \\ F_A &= \beta \ln\left(\frac{y/y_0}{1-y}\right) \\ F_B &= 1 - P/P_0 \end{aligned} \tag{6.12}$$

Figure 6.21 shows F_A and F_B plotted against the pressure ratio for different values of y_0. The curves are nonlinear, but, when the selectivity is modest (β = 0.5) and the initial mole fraction is large (y_0 = 0.5), the deviations from linearity, for both F_A and F_B, are small. However, when the selectivity is high and the initial mole fraction of A is small, the curve for F_B becomes essentially linear, but the curve for F_A assumes a highly nonlinear form. It is clear that, in this situation, by a sufficiently large reduction in total pressure almost all of component B can be desorbed with very little desorption of A. A further deep blowdown or evacuation step then allows A to be removed in concentrated form.

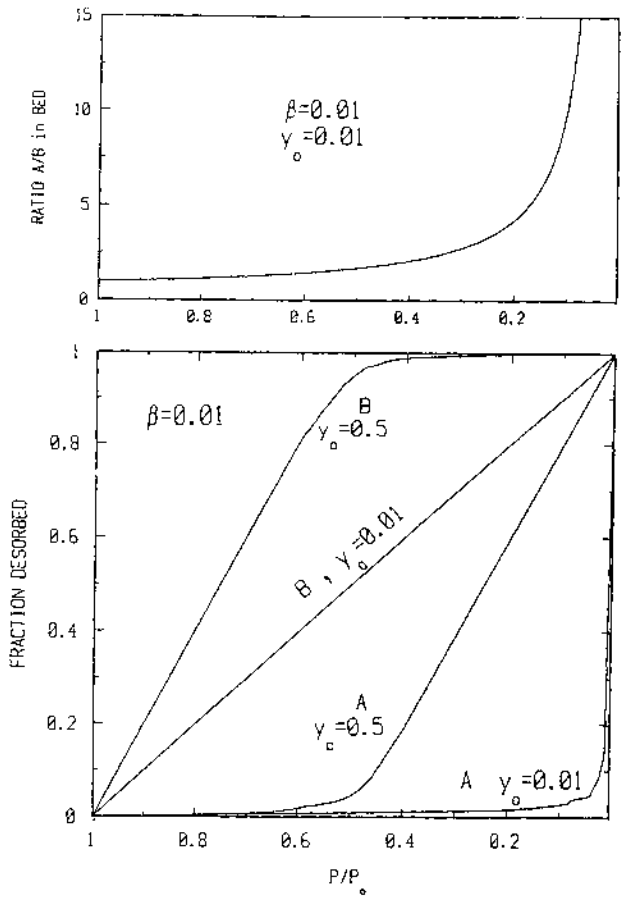

Figure 6.21 Fractional desorption during blowdown for different combinations of y_0 and ft, calculated according to Eqs. 6.10 and 6.11.

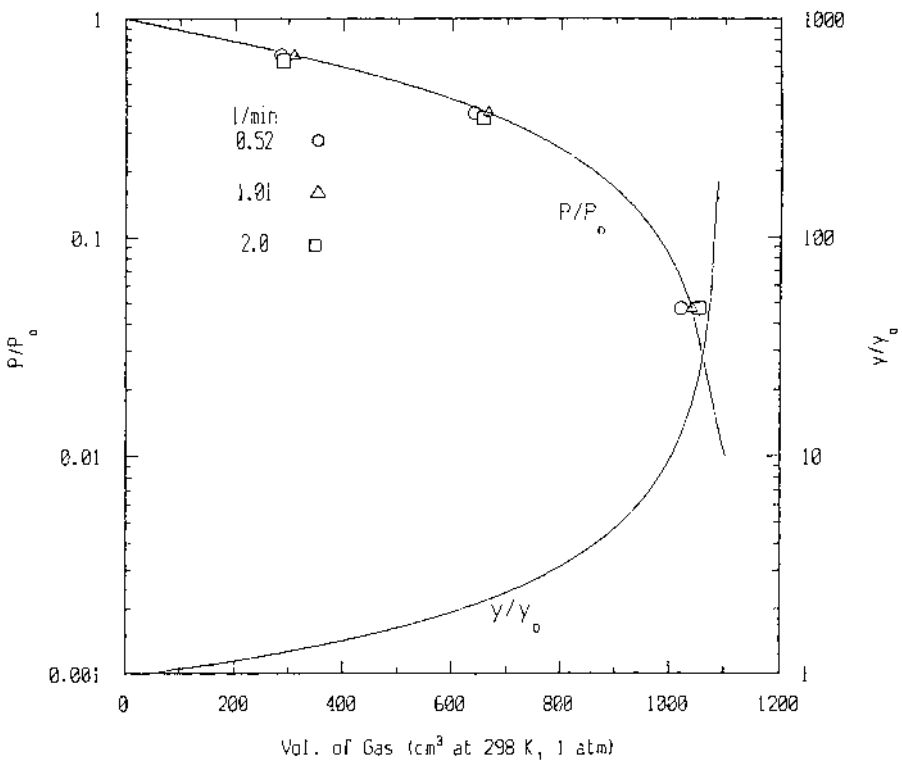

Figure 6.22 Experimental data showing concentration of hydrogen from a H_2–He mixture during blowdown of a small experimental column of 5A zeolite, equilibrated initially at 77 K with a stream containing 0.16% H_2 in He at 21.4 atm. Column 15.6 cm × 0.77 cm i.d. packed with 20–40 mesh 5A mol sieve particles. (From Ruthven and Farooq.[36])

Table 6.6. Recovery of H_2 from the He by Cryogenic PSA[36a]

Adsorbent	5.6 g 5A zeolite (pelleted)
Feed	0.18% H_2 in He at 21.4 atm
Hydrogen uptake	240 cm^3 STP
Exhaust gas	220 cm^3 STP
Purity	93% H_2
Recovery	85%

[a] Bed was equilibrated with feed, blown down to atmospheric pressure, and evacuated to 0.01 atm. Exhaust gas was collected from vacuum pump.

This analysis is for a linear equilibrium system, but the effect of isotherm nonlinearity is actually to enhance the degree of separation and concentration that can be achieved in this type of process. Since the isotherm for the more strongly adsorbed species will generally have the higher curvature, even less of this component is desorbed during the initial blowdown compared with the equivalent linear equilibrium system.

A process of this kind has recently been developed as a means of concentrating and removing the traces of tritium from the helium purge stream of a lithium breeder reactor.[35] To achieve a high concentration ratio (~ 10^3) requires a high selectivity ratio (as well as a high pressure ratio), and for H_2 (or tritium) this can be achieved only by operating at cryogenic temperatures with vacuum desorption at a very low pressure. Laboratory data showing the feasibility of recovering hydrogen at greater than 90% purity and with a similarily high fractional recovery from a stream containing traces of H_2 in He are summarized in Figure 6.22 and Table 6.6. The process schematic is shown in Figure 6.23.

The same principle was used by Yang and co-workers[37,38] in recent studies of the possibility of removing and concentrating trace organics from air and SO_2 from flue gas. It is also utilized in the Air Products fractional vacuum swing adsorption process (FVSA), which produces 90% oxygen together with 98–99% nitrogen.[39] The cycle, which is essentially similar to that used in the hydrogen recovery process, involves four steps:

- Adsorption with feed air at 1.1 atm abs. with simultaneous withdrawal of oxygen product.
- Reverse flow blowdown with discharge of the blowdown gas (impure nitrogen) to waste.
- Evacuation to 0.1 atm with collection and recompression of the nitrogen product.
- Pressurization with product oxygen.

With CaX zeolite as the adsorbent the selectivity (a ~ 10) is high enough that most of the oxygen is eliminated in the blowdown step. About half the adsorbed nitrogen can be recovered at 98–99% purity during the evacuation step which run at about 0.1 atm abs. The schematic diagram together with performance data are shown in Figure 6.24.

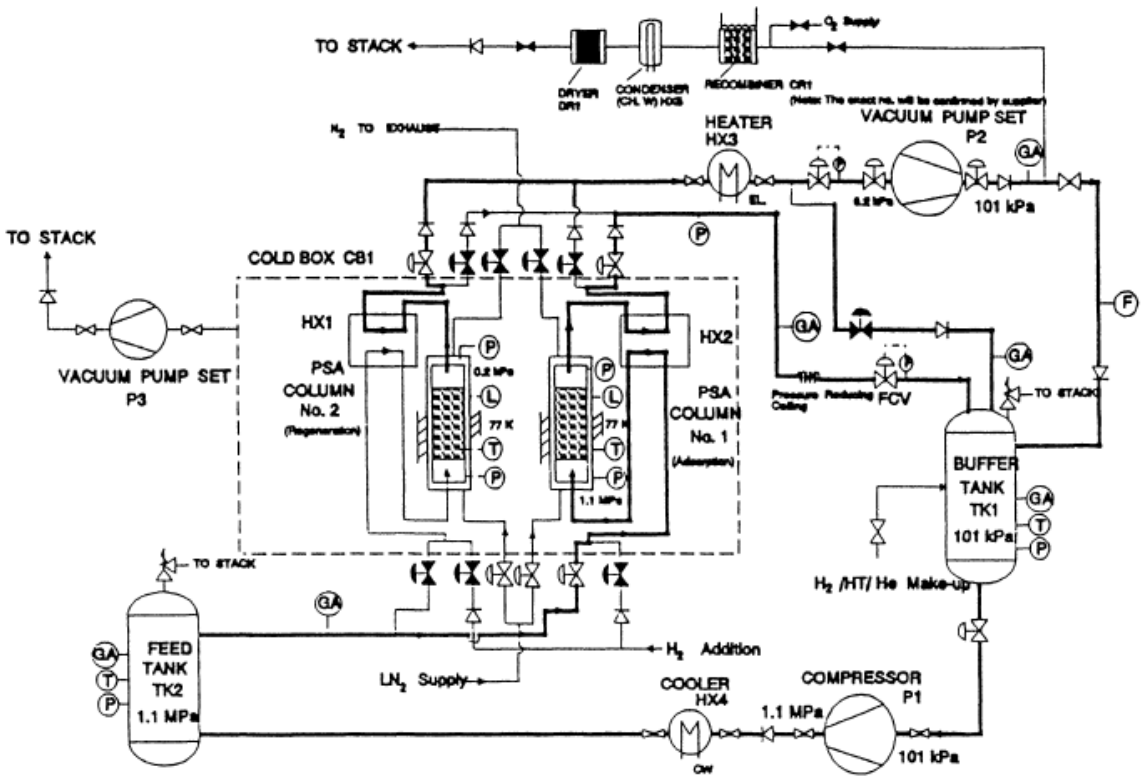

Figure 6.23 Schematic diagram of pilot plant for tritium concentration by cryogenic PSA. (From Sood et al.[35]) Feed: 2.2 mole/sec, 99.9% He, 0.1% hydrogen isotopes at 12 ats. abs. Blowdown to atmosphere; evacuation to 0.01 atm.

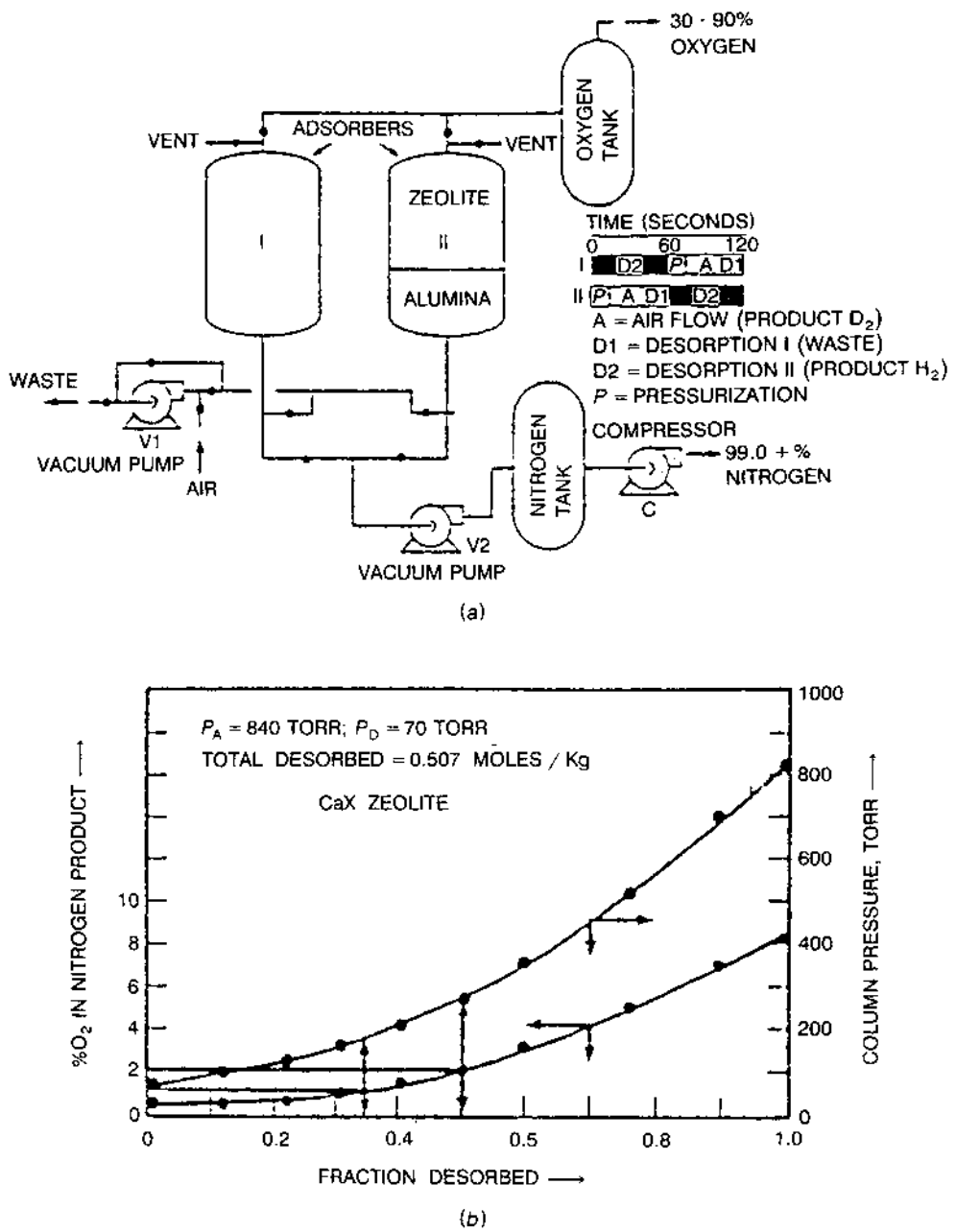

Figure 6.24 The Air Products FVSA air separation process, (a) Process schematic; (b) performance data. (From Sircar,[39] with permission.)

6.11 Efficiency of PSA Processes

The thermodynamic efficiency of any separation process (the First Law efficiency) can be defined simply as the ratio of the minimum work of separation (the negative free energy of mixing) to the actual work required to drive the separation process. Such efficiencies are generally less than 15% and even lower than this for most PSA systems. The values for two representative air separation processes are given in Table 6.7. The nitrogen production process is markedly less efficient than oxygen production, reflecting the irreversibility inherent in a kinetically based separation. Although thermodynamic efficiency provides a rational basis for comparing the efficiency of different PSA processes based on the same type of cycle, it is much less useful for comparing different types of separation process or even radically different PSA cycles. Furthermore, the thermodynamic efficiency gives only an overall measure of performance and provides no information as to the sources of efficiency. An exergy analysis

provides far greater insight.

The exergy of a substance is the maximum useful work that can be obtained by interaction with the environment. It is in essence the free energy relative to the normal environment as standard state. For a nonreacting system in which potential and kinetic energies are insignificant:

$$\mathrm{Ex} = \left(h - h_0\right) - T_0\left(s - s_0\right) \tag{6.13}$$

The exergetic efficiency is then defined as:

$$\frac{\text{moles product}}{\text{moles feed}} \times \frac{\mathrm{Ex}_{\text{product}}}{\mathrm{Ex}_{\text{feed}}} \tag{6.14}$$

The feed exergy ($\mathrm{Ex}_{\text{feed}}$) includes the work of compression while the product exergy ($\mathrm{Ex}_{\text{product}}$) includes the energy of compression (or expansion) to reduce the product to atmospheric pressure. For comparing different PSA processes, operated over different pressure ranges, a more useful definition is the overall efficiency (η) defined by:

$$\eta = \frac{\text{molar energy of product, corrected to 1 atm}}{\text{net energy input}} \tag{6.15}$$

where the net energy input is the energy of feed compression less the energy of expansion of the product to atmospheric pressure. For a vacuum swing process in which the product is produced at subatmospheric pressure, the latter quantity will be negative. Equation 6.15 differs from the normal definition of the First Law efficiency in that the separative work associated with the waste product is excluded and the energy of compression (or expansion) of the product to atmospheric pressure is allowed for.

Table 6.7. Thermodynamic (First Law) Efficiencies for PSA Air Separation Processes

Process	Principal product	Process Energy (J/g mole product)	Separative work (J/g mole product)	Efficiency (%)
"Lindox" (Figure 6.8)	90% O_2	4.8×10^4	3055	6.3
"Nitrotec" (Figure 6.11 and Table 6.1)	99% N_2	3.2×10^4	660	2.1

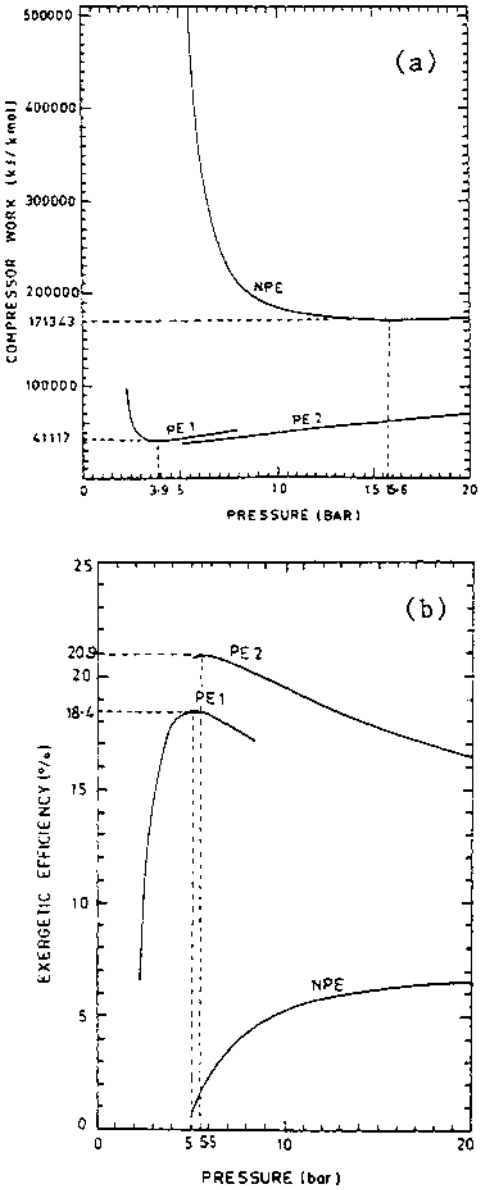

Figure 6.25 Variation of (a) compressor work and (b) exergetic efficiency with operating pressure for a two-bed Skarstrom cycle for oxygen production with and without pressure equalization. (From Banerjee et al.,[40] with permission.)

A detailed exergy analysis of PSA air separation processes has been reported by Banerjee et al.[40,41] For oxygen production two process configurations were considered: the two-bed Skarstrom cycle with and without a pressure equalization step. The variation of compressor work and exergetic efficiency with operating pressure is shown in Figure 6.25. For the cycle without pressure equalization there is a shallow minimum in the compressor work curve at about 15 atm, while for the process with pressure equalization the compressor work is greatly reduced and there is a sharper minimum at about 4 atm. The exergetic efficiency reaches a maximum at about 5 atm for the process with pressure equalization but increases monotonically for the process without pressure equalization. The corresponding Grassman diagrams for operation at their optimal pressures (in terms of compressor work) are shown in Figure 6.26. The exergetic efficiency is about 17% for the process with pressure equalization when operated under optimal conditions in terms of the power requirement.

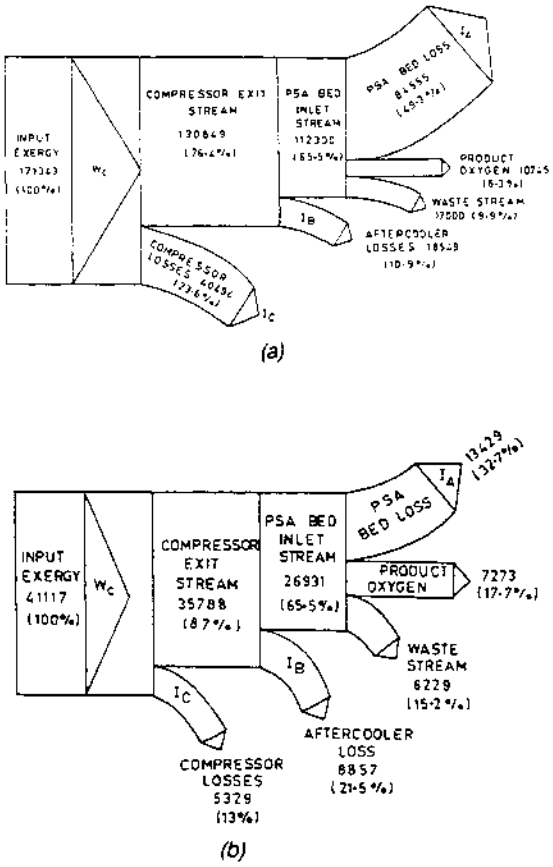

Figure 6.26 Grassman diagrams showing losses of exergy for Skarstrom cycle (blowdown to atmospheric pressure) for oxygen production (a) without and (b) with pressure equalization. Operating pressures are, respectively, 15.6 and 3.9 bar, the values for which the compressor work is minimized. (From Banerjee et al.,[39] with permission.)

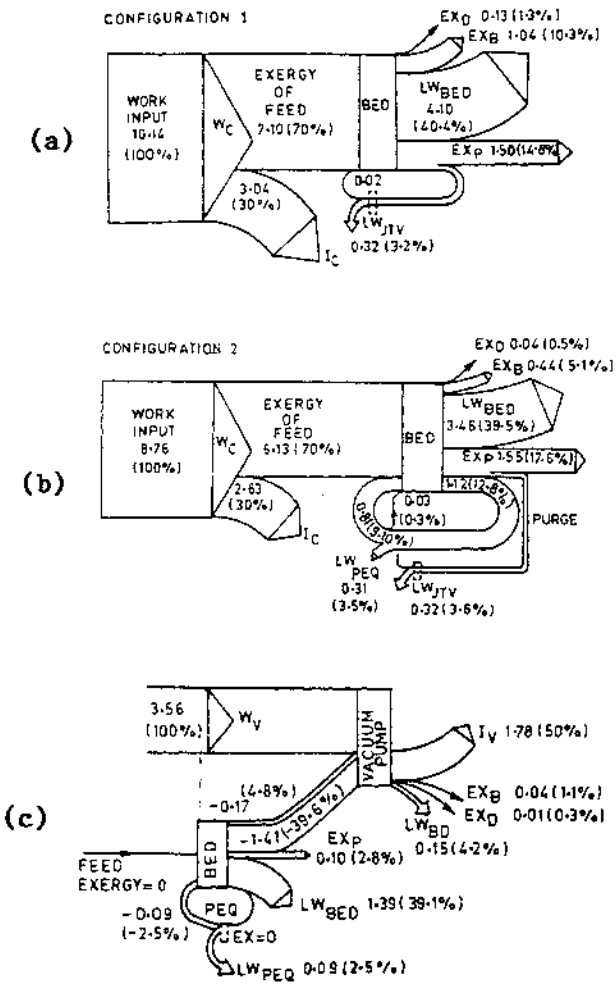

Figure 6.27 Grassman diagrams showing exergy losses for nitrogen production with three different cycles, (a) Skarstrom cycle and (b) Skarstrom cycle with pressure equalization (P_H) = 8 atm, P_L = 1 atm); (c) vacuum swing cycle (P_H = 1 atm. P_1 = 0.2 atm). (From Banerjee et al.,[41] with permission.)

Table 6.8. Exergy Analysis of Three PSA Air Separation Processes[a]

	(1) PSA O_2 process		(2) PSA N_2 process		(3) VSA N_2 process	
Adsorbent	5A zeolite		CMS		CMS	
Cycle	Skarstrom + P.E.		Self-purging + P.E.		Vac. swing	
P_H/P_1 (atm)	3.9/1.0		8.0/1.0		1.0/0.2	
Recovery (%)	60		33		63	
Energy input						
(a) Compressor/vac.	41,120		31.500		12,800	
(b) Product compression /expression	– 2,800	(%)	– 4,800	(%)	+ 5,700	(%)
Total input	38,320	100	26,700	100	18,500	100
Product exergy	7,270		5,600		360	
Product exergy at 1 atm	4,470	11.7	800	3.0	4,360	23.5
Waste product	6,230	16.3	1,730	6.5	720	3.9
Bed loss	13,430	35.0	12,450	46.5	5,100	27.6
Compressor/cooler losses	14,200	37	9,470	35.5	8,050	43.43
Other losses (e.g., valves, etc.)			2,270	8.5	320	1.7

Process efficiency (%)	11.7	3.0	23.5

[a] Energy and exergy expressed as J/mole product. Product exergy is corrected to 1 atm, in all cases, by allowing for work of expansion or compression. Process efficiency is defined by Eq. 6.15.

A similar analysis has also been made for the two-bed nitrogen production process including both the self-purging cycle and the vacuum swing cycle (Figures 3.12 and 3.17). The corresponding Grassman diagrams are shown in Figure 6.27. The exergetic efficiency of the self-purging process is about 17.6% at an operating pressure of 8 atm, and the corresponding energy requirement is about 8.7 kWh per kmole of product. For the vacuum swing cycle the exergetic efficiency is much lower (~ 2.8%) since the product is delivered at subatmospheric pressure. However, the energy requirement is also lower (about 3.6 kWh per kmole of product). If the product nitrogen were compressed to 8 atm, the total work requirement would be increased to 5.6 kWh/kmole product, but this is still substantially lower than for the pressure swing process.

A detailed thermodynamic comparison of the three air separation processes, based on Banerjee's figures, is given in Table 6.8. For all three processes the major sources of inefficiency are the losses in the feed compressor or the vacuum pump and in the adsorbent bed. Comparing the two supra-atmospheric pressure processes (1 and 2), the efficiency of the kinetically controlled nitrogen process is substantially lower than that of the equilibrium-based oxygen process, reflecting the inherent irreversibility of the kinetic process. More significantly, however, the comparison between the vacuum swing process (3) and the supra-atmospheric processes (1 and 2) shows clearly the thermodynamic advantage of vacuum swing. This advantage stems from the large reduction in the energy input so that, even when the energy required to compress the product is allowed for, the net energy requirement is substantially reduced. However, this advantage, which translates directly into a reduction of the process operating cost, must be offset against the increased capital costs associated with vacuum swing operation, which requires both a compressor and a vacuum pump as well as much larger ducts and valves.

References

1. C.W. Skarstrom, "Heatless Fractionation of Gases over Solid Adsorbents," in *Recent Developments in Separation Science,* pp. 95–106, Vol. 2, N. N. Li, ed., CRC Press, Cleveland (1972).
2. D.H. White, *The Pressure Swing Adsorption Process,* AIChE National Meeting, paper 87b, New Orleans, LA, March 8 (1988). See also D. H. White and G. Barclay, *Chem. Eng. Prog.* **85**(1), 25 (1989).
3. D.M. Ruthven, *Principles of Adsorption and Adsorption Processes,* Chap. 7, Wiley, New York (1984).
4. A. Anzelius, *Zeit. Angew. Math. Meeh.* **6**, 291–94 (1926).
5. C.W. Skarstrom, U.S. Patents 2,944,627 (1958) and 3,237,377 (1966) to Esso Research and Engineering.
6. G.A. Serial, W. H. Granville, and W. O. Daley, *Chem. Eng. Sci.* **38**, 1517 (1983).
7. C.G. Coe, G. E. Parris, R. Srinivasan, and S. R. Auvil, in *Proceedings of Seventh International Zeolite Conference,* Tokyo, p. 1033, Y. Murakami, A. Lijima, and J. W. Ward, eds., Kodansha–Elsevier, Tokyo (1986).
8. C.G. Coe, in *Gas Separation Technology,* pp. 149-59, E. F. Vansant and R. Dewolfs, eds., Elsevier, Amsterdam (1990).
9. J. Smolarek and M. J. Campbell, in *Gas Separation Technology,* p. 281, E. F. Vansant and R. Dewolfs, eds., Elsevier, Amsterdam (1990).
10. L.B. Batta, U.S. Patent 3,636,679 to Union Carbide (1972).
11. K. Knoblauch, H. Heinback, and B. Harder, U.S. Patent 4,548,799 (1985), to Bergbau Forschung.
12. H.J. Schrdter and H. Jiintgen, in *Adsorption: Science and Technology,* p. 269, NATO ASI 158, A. E.

Rodrigues, M. D. LeVan, and D. Tondeur, eds., Kluwer, Dordrecht (1989).

13. E. Pilarczyk and K. Knoblauch, *Separation Technology,* p. 522, N. Li and H. Strathmann, eds., Eng. Foundation, NY (1988).
14. Nitrotec brochure, Nitrotec Engineering Co., Glen Burnie, MD (1988).
15. Anon., "Pressure Swing Adsorption Picks Up Steam," *Chem. Eng., 95,* Sept. 26, 1988, p. 26.
16. S. Sircar and J. W. Zondlo, U.S. Patent 4,013,429 (1977) to Air Products.
17. S. Sircar, in *Adsorption: Science and Technology,* p. 285, NATO ASI E158 A. E. Rodrigues, M. D. LeVan, and D. Tondeur, eds., Kluwer, Dordrecht (1989).
18. J.L. Wagner, U.S. Patent 3,430,418 to Union Carbide (1969).
19. L.B. Batta, U.S. Patent 3,564,816 to Union Carbide (1971).
20. R.W. Alexis, *Chem. Eng. Prog. Symp. Ser.* **63**(74), 50 (1968).
21. H.A. Stewart and J. L. Heck, *Chem. Eng. Prog.* **65**(9), 78 (1969).
22. K.J. Doshi, C. H. Katiro, and H. A. Stewart, *AIChE Symp. Ser.* **67**(117) (1971).
23. T. Tomita, T. Sakamoto, U. Ohkamo, and M. Suzuki, in *Fundamentals of Adsorption II,* p. 89, A. I. Liapis, ed., Eng. Foundation, NY (1987).
24. J.L. Heck and T. Johansen, *Hydrocarbon Processing,* p. 175 (Jan. 1978).
25. A. Fuderer and E. Rudelstorfer, U.S. Patent 3,846,849 to Union Carbide (1976).
26. R.T. Cassidy, "Polybed Pressure Swing Hydrogen Processes," in *Adsorption and Ion Exchange with Synthetic Zeolites,* W. H. Flanck, ed., *ACS Symp. Ser.* **135**, p. 247, Am. Chem. Soc., Washington D.C. (1980).
27. R.T. Cassidy and E. S. Holmes, *AIChE Symp. Ser.* **80**(233), 68 (1984).
28. G. Keller, "Gas Adsorption Processes: State of the Art in Industrial Gas Separations," *Am. Chem. Soc. Symp. Ser.* (223) (1983).
29. M. Suzuki, *Adsorption Engineering,* p. 247, Kodansha Elsevier, Tokyo (1990).
30. O.J. Smith and A. W. Westerberg, *Chem. Eng. Sci.* **46**, 2967 (1991).
31. J. Izumi, Mitsubishi Heavy Industries Ltd., personal communication (1992).
32. J. Grebbell, *Oil and Gas Journal,* p. 85, April 14 (1985).
33. W.C. Kratz, D. L. Rarig, and J. M. Pietrantonio, *AIChE Symp. Ser.* **84**(264) (1988).
34. R. Kumar, W. C. Kratz, D. E. Guro, D. L. Rarig, and W. P. Schmidt, "Gas Mixture Fractionation to Produce Two High Purity Products by PSA," Sep. Sci. and Technol. **27**, 509 (1992).
35. S.K. Sood, C. Fong, K. M. Kalyanam, A. Busigin, O. V. Kveton, and D. M. Ruthven, *Fusion Technology* **24**, 299 (1992).
36. D.M. Ruthven and S. Farooq, *Chem. Eng. Sci.* (in press).
37. J.A. Ritter and R. T. Yang, *I and E.C. Research* **30**, 1023 (1991).
38. E.S. Rikkinides and R. T. Yang, *I and E.C. Research* **30,** 1981 (1991).
39. S. Sircar, Fourth International Conferences on Adsorption, Kyoto, Japan, May, 1992, plenary lecture, "Novel Applications of Adsorption Technology."
40. R. Banerjee, K. G. Narayankhedkar. and S. P. Sukhatine, *Chem. Eng. Sci.* **45**, 467 (1990).
41. R. Banerjee, K. G. Narayankhedkar. and S. P. Sukhatine, *Chem. Eng. Sci.* **47**, 1307 (1992).

APPENDIX
C
Synopsis of PSA Patent Literature

C.1 Introduction

This appendix reviews some PSA developments that appeared as patents, a few of which were cited in Chapter 1. In addition, it covers the origins of many cycles that are mentioned throughout the book, especially in Chapters 4 and 6. The subject has been set aside here because there was no ideal place for it in the body, yet it seemed too important to omit.

Although individual patents are commonly filled with new technology, their focus is generally very narrow. Sometimes, if there are profound new ideas in a patent, instead of subtle modifications of existing know-how, the ideas are muddled because of the verbose legalistic jargon and baffling drawings. Sometimes they are merely austere announcements that technical milestones have been passed, and not necessarily that commercialization elforts are underway. In fact, the earliest known patents, awarded to Hasche and Dargan in 1931[1] and Finlayson and Sharp in 1932,[2] seem to have been largely ignored. Perhaps their ideas were made to work on a small scale but not on a large scale, and consequently, they were viewed by those few who became aware of them as laboratory curiosities and were quickly forgotten. Nevertheless, they explained the basic ideas of PSA.

Patents awarded since the 1930s have also frequently escaped notice, and early accomplishments and ideas have been overlooked or forgotten. Perhaps this has occurred because keeping track of patented technology is extremely time consuming, and reading patents is tedious and confusing. An unfortunate outcome has been that some of the basic ideas of PSA have been claimed an innovations over and over again. For example, several patents that were issued in the 1930s, 1940s, and 1950s described the principles of PSA, yet Skarstrom frequently receives credit for inventing PSA, apparently because of the thoroughness of his first patent, which was issued in I960.[3]

This appendix covers a variety of PSA patents, emphasizing cycles and key concepts and the rieh diversity of ideas that led to success. There are hundreds from which to choose, so the coverage presented here is by no means comprehensive; it is regrettable but unavoidable that some seminal contributions have been overlooked. That the material discussed here is predominately drawn from U.S. patents is not meant to slight the development of PSA technology by inventors in other nations. For those who seek additional information, Tondeur and Wankat[4] reviewed the field of PSA technology by categorizing patents and publications according to cycle attributes (such as the number of Steps and number of columns), Separation applications, and corporations to which patent rights had been assigned. They cited well over 100 sources, many of which were patents. Similarly, Ball[5] reviewed many U.S. patents and compiled an annotated bibliography. In addition, rather than restricting this review to very recent patents, the emphasis is on earlier patents because they contain most of the fundamental ideas that have proved to be widely

applicable to various adsorbents and gas mixtures. In fact, one might observe that most recent patents tend to be permutations of the fundamental ideas introduced in the early patents. Considering that, one cynical reaction might be that, by now, all the patentable ideas in the field of PSA have already been claimed. There is a strong case for that opinion, but it is a complex issue that should be left to patent attorneys to argue.

Timing is critical for patents, not only for legal reasons, but also because one of the few rewards an inventor receives is recognition. An unfortunate experience for some patents is that they have languished, some for more than five years, while being reviewed in the Patent Office. So, from that point of view, the filing date often reveals more about the context of an invention (i.e., what other ideas were accessible in the public domain) than the date of issue. Thus, both dates are often mentioned here. In fact, patents are introduced roughly in chronological Order, with cross references to more recent patents that have used some of the same approaches.

C.2 Inventors and Patents

C.2.1 Hasche and Dargan

In their patent application, filed in 1927 and approved in 1931, Hasche and Dargan[1] described a pressure swing process for recovering sulfur dioxide from smelter gases using silica gel. In that process, the feed was compressed so that the partial pressure of sulfur dioxide was above atmospheric but below its critical pressure. The compressed gas was then cooled and admitted to the adsorbent bed, while purified gas was withdrawn. Upon imminent breakthrough, the column was blown down, and the energy of compression was recovered. They stated that "The process may, therefore, be described as substantially isothermal and utilizes the property of the adsorptive material whereby the amount of gases held therein is substantially proportional to the gaseous pressure." They did not, however, include a process flowsheet, and no specific performance was claimed, for example, in terms of purity, recovery, or energy consumption.

C.2.2 Finlayson and Sharp

The patent by Finlayson and Sharp was filed in 1931 and approved in 1932,[2] and it covered more of the basic concepts of PSA. For example, they explained several specific principles that are fundamental to the Operation of PSA cycles and gave a detailed example of a single PSA System being used to alter the ratio of hydrogen to carbon monoxide in water gas. Most notably, they described a pressurization Step followed by a production Step in which "the first fraction or fractions being richer in the less easily adsorbed component or components… and the final fraction or fractions being richer in the more easily adsorbed component or components." Furthermore, they noted that the "pressure of the adsorbed gas may be released for instance to a limited extent or substantially to atmospheric pressure or even a vacuum may be applied." This idea was embellished later by Skarstrom and Heilman.[6] Even their simple idea of using subatmospheric pressure for desorption has been listed among the Claims of several other patents,[7–9] and recently it has been popular to tout this version of PSA as VSA, as discussed in Sections 3.2 and 6.2. They did not include a schematic diagram of their process or any information describing performance or timing.

C.2.3 Perley

A patent by Perley[10] happened to overlap, not only with the intended application, but also with the dates of the patent by Finlayson and Sharp[2] (it was submitted in 1928, and awarded in 1933). It described a process for adsorbing carbon monoxide and carbon dioxide from a water gas mixture, to yield technically pure hydrogen. A schematic diagram is shown in Figure C.1. The adsorbent was regenerated by reducing the pressure and, optionally, heating the adsorbent via purge gas. Interestingly, the idea of combining pressure Swings with temperature Swings is still considered novel, and has been covered in recent patents.[11–13]

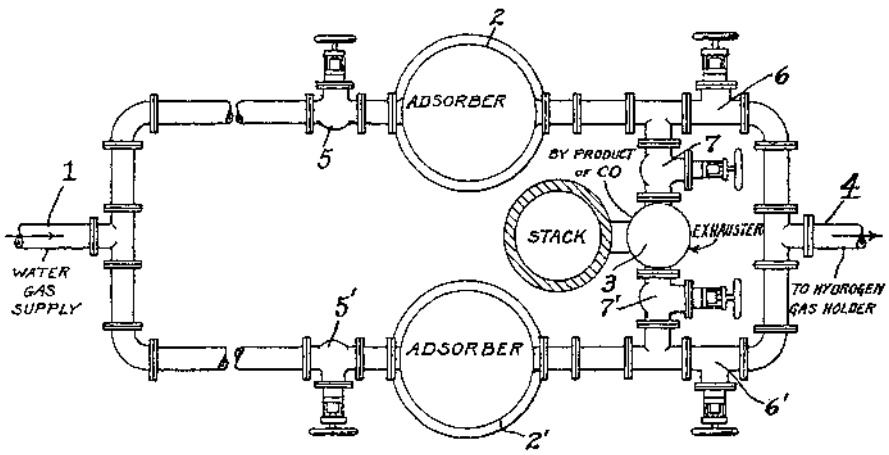

Figure C.1 Flowsheet of the PSA apparatus suggested by Perley in 1928, which appeared in U.S. Patent No. 1,896,916 in 1933. This equipment was apparently operated manually, and was designed for splitting hydrogen from water gas.

C.2.4 Erdmann

Another early patent that was essentially ignored was awarded to Erdmann in 1941.[14] His process seemed to be a reduction to practice of some of the ideas suggested by Finlayson and Sharp[2] and Perley.[10] Specifically, he used activated carbon and a feed of 93% hydrogen and the balance carbon monoxide to produce a pure product of 98 to 99% hydrogen, and an equimolar byproduct. The operating temperature was –50°C (to exploit higher adsorption capacities at such a low temperature), and the pressure range was apparently 1 to 0.13 atm.

C.2.5 Guerin de Montgareuil and Domine

A patent that has received some recognition was awarded in 1957 to Guerin de Montgareuil and Domine.[15] It employed pressurization by feed, followed by cocurrent blowdown, exploiting a type of kinetic effect, to yield the light product, and finally complete blowdown, yielding an enriched heavy component. One advantage it oifered was simplicity, due to the absence of flow reversal, but that was met by the disadvantage of obtaining both products at relatively low pressures. Despite that, it exploited, to a greater degree than previous patents, the coupling of pressure and flow to achieve PSA separations.

C.2.6 Skarstrom

Skarstrom's first PSA patent[3] was filed in 1958 and approved in 1960. He described PSA Systems for gas drying and carbon dioxide removal, for oxygen enrichment from air (up to about 85% at nearly nil recovery), and for nitrogen enrichment from air (up to 99% at nearly nil recovery). The latter was the first kinetics-based PSA separation (in fact, the equilibrium selectivity is in opposition to the kinetic selectivity), while the other applications he cited exploited equilibrium selectivity. The adsorbents he cited were silica gel and activated alumina, zeolite 5A, and zeolite 4A, respectively. He showed how hydrocarbons, including paraffins, isoparaffins, olefins, diolefins, and aromatics could be split via three zeolites. He also explained high-pressure feed, blowdown, purge, and pressurization steps. A flowsheet of his basic cycle is shown in Figure C.2. Finally, Skarstrom suggested linking oxygen- and nitrogen-producing systems by recycling the secondary products "to provide at least a portion of the feed for the other adsorber concentration system." This combined cycle is shown in Figure C.3. That idea, (i.e., using two or more adsorbents and coupling PSA systems) has been reinvented (with subtle twists) or borrowed several times.[16–24]

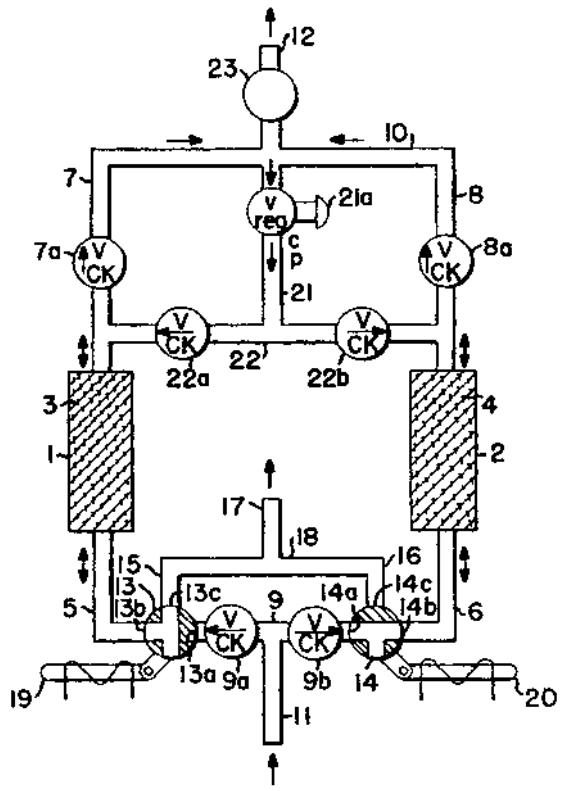

Figure C.2 Flowsheet of the basic PSA apparatus suggested by Skarstrom in 1958, which appeared in U.S. Patent No. 2,944,627 in 1960. This equipment was apparently designed for general purposes, from air drying to Splitting nitrogen or oxygen from air.

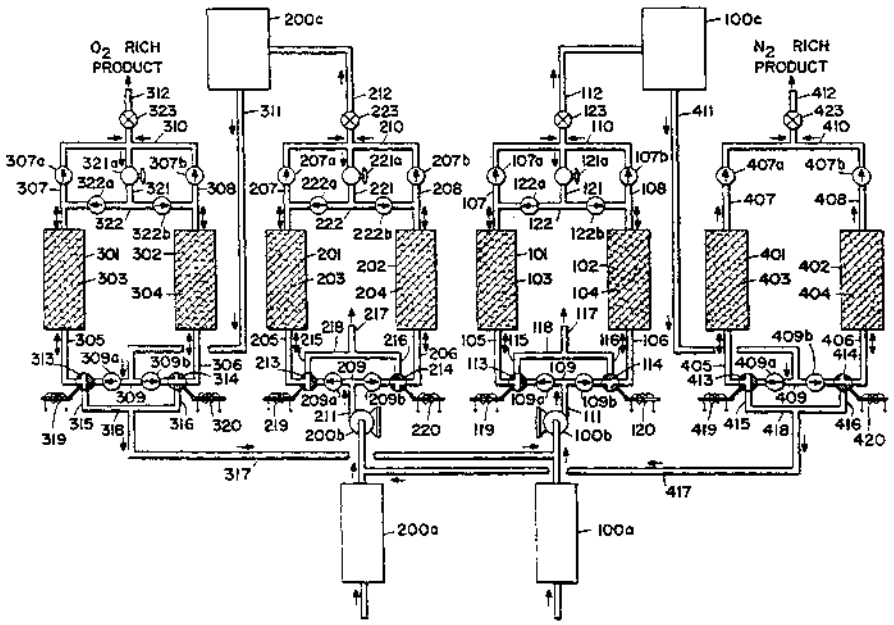

Figure C.3 Flowsheet of a second PSA apparatus suggested by Skarstrom in 1958, which appeared in U.S. Patent No. 2,944,627 in 1960. This equipment was apparently designed for extracting two nearly pure products from a single feed, such as Splitting nitrogen and oxygen from air.

C.2.7 Skarstrom

Some early PSA patents concerned with hydrogen purification, which followed up on much earlier suggestions by Perley[10] and Erdmann,[14] were filed by Skarstrom in 1960 and awarded in 1963–64.[25–27] The first patent[25] described upgrading reformer recycle gases from various types of processes, in the range of 50 to 80% hydrogen, with an ultimate purity of greater than 95% hydrogen, using activated carbon as the adsorbent. The second described specific operating conditions, but did not specify the resulting performance. The third revealed more process details, and mentioned a potential recovery of 70%, but did not state the corresponding purity.

C.2.8 Hoke, Marsh, et al.

Within a year of filing of Skarstrom's PSA patents related to hydrogen purification, his colleagues, Hoke, Marsh, Bernstein, Pramuk, and he filed related disclosures that were approved in 1964.[28,29] Their first process was also used for upgrading reformer recycle gas, in the range of 50% hydrogen, with an ultimate purity of greater than 99% hydrogen, using activated carbon and activated alumina as the adsorbents. The operating conditions included a pressure range of from 200 to 650 psig for adsorption, and 8 to 12 psia for desorption and purging. The cycle included a monthly thermal regeneration at about 600°F, via an inert gas. The second patented process was apparently the first that explicitly mentioned a cocurrent blowdown step that was used directly partially to pressurize a parallel column. That idea, which is often referred to as *pressure equalization*, has been claimed as a vital part of *many* other patents, of which only a few are cited here as examples.[30–34]

C.2.9 Wilson

Another early patent application concerning the actual (versus hypothetical) Separation of oxygen and nitrogen from air in a single System was filed by Wilson in 1959, although it was not approved until 1965.[7] It contained several novel ideas that recurred in later patents. For example, a three-step cycle was used: pressurization (with predried air), cocurrent blowdown (producing enriched oxygen, at 70 to 90%), and countercurrent blowdown (producing enriched nitrogen, at subatmospheric pressure). He suggested an Option of using heat to achieve a higher degree of desorption than by pressure alone. He also suggested using an oscillating piston to drive the pressure swing, and that idea has been borrowed, slightly modified, or reinvented several times.[35–39] He suggested that the same ideas could be used to remove carbon dioxide from air (e.g., in submarines) and to separate helium from natural gas.

C.2.10 Stark

About 2 years after the flurry of patent applications for PSA hydrogen purification were filed by Skarstrom and his colleagues (see C.2.7), another patent that extended the Separation capability was filed by the same Company (Stark, filed in 1963 and awarded in 1966[16]). The application was also the upgrading of reformer recycle gas, in the range of 80% hydrogen, to attain an ultimate purity of 99.9% hydrogen at a recovery of 75%, using silica gel as the adsorbent. The operating conditions included a pressure range of from 500 psig for adsorption and 0 psig for desorption and purging.

C.2.11 Basmadjian and Pogorski

An early PSA cycle that was apparently the first to use a rinse Step (see Section 4.4.5) was invented by Basmadjian and Pogorski. Their application was filed in 1963 and the patent issued in 1966.[40] This cycle was intended to recover helium and possibly other light components from nitrogen or natural gas. The basic cycle consisted of pressurization with feed, rinse and production of enriched light product, blowdown and recovery of the heavy component. They improved the purity of the light component by conducting the pressurization and rinse in discrete steps in sequential columns. More recent patents usually employ a different set of steps. That might make the resemblance difficult to recognize. Nevertheless, a wide variety of other patents have borrowed, subtly modified, or reinvented the idea of rinse.[9,41–48]

C.2.12 Berlin

The first high-performance PSA oxygen generator was disclosed by Berlin in two applications filed in 1963 and approved in 1966–1967.[8,49] He claimed oxygen purities up to 93% (for which the balance was claimed to be 7% argon), at 53% recovery, but at a pressure ratio of 50 to 1000, and he suggested a strontium-exchanged X zeolite as the adsorbent.

C.2.13 Feldbauer

Shortly after the patent application for PSA hydrogen purification was filed by Stark (see C.2.10), another was filed from the same Company that further extended the Separation capability. In particular, Feldbauer filed in 1964 and the patent was awarded in 1967.[50] The

concepts also applied to upgrading of reformer recycle gas, in the range of 40% hydrogen, to attain an ultimate purity of 96% hydrogen and a recovery of 94%, using 5A zeolite, activated carbon, and/or activated alumina as the adsorbent. The operating conditions included a pressure range of from 35 bar (500 psig) for adsorption and 1.4 bar (5 psig) for desorption and purging.

C.2.14 Wagner

Shortly before the patent for PSA hydrogen purification was awarded to Stark in 1967, another patent was filed by Wagner (awarded in 1969[31]) that significantly extended the Separation capability. The concepts also applied to upgrading of reformer recycle gas, using a four-bed process, with a feed of about 77.1% hydrogen and 22.5% CO_2 with traces of other components. The process attained an ultimate purity of 99.9999 + % hydrogen and a recovery of 76.5%, using activated carbon and 5A zeolite as the adsorbents in a compound bed. The operating conditions included a pressure range of from 13.4 bar (200 psia) for adsorption and 15 psia for desorption and purging.

C.2.15 Batta

After the patent application was filed by Wagner in 1967 for PSA hydrogen purification, another was filed by Batta (awarded in 1971[51]) that slightly improved the inherent recovery. Among the patented concepts were: upgrading of reformer recycle gas containing about 75% hydrogen, attaining an ultimate purity of 99.999% hydrogen and a recovery of 80%, and using a four-bed process with 5A zeolite or activated carbon as the adsorbent. The operating conditions included a pressure range of from 9.7 bar (145 psia) for adsorption and 1 bar (15 psia) for desorption and purging. A patent having similar chains was awarded to Shell et al. in 1974.[52]

C.2.16 Batta

Following up on Berlin's patent[8] for oxygen Separation from air, another application was filed by Batta that slightly improved the oxygen purity. It did not quite match the former patent's recovery, but it employed a pressure ratio of only about 3 rather than 50 (or greater). It was awarded in 1973.[53] The general concepts claimed had been discovered earlier for other applications. For example, he suggested a four-bed process, cocurrent blowdown, and pressure equalization. These ideas allowed an ultimate purity of 95 to 96% oxygen and a recovery of 40 to 45% to be achieved, using 5A or 13X zeolite as the adsorbent. The operating conditions included pressures of 3.2 bar (47 psia) for adsorption to 1 bar (15 psia) for desorption and purging.

C.2.17 Fuderer and Rudelstorfer

Until the mid-1970s, PSA Systems had generally consisted of four parallel beds or fewer. Fuderer and Rudelstorfer, in a patent awarded in 1976,[54] changed all that with a System of as many as ten parallel beds. For that embodiment, the cycle comprised twenty Steps, employing 54 timed valves, although any individual column only underwent 11 separate Steps. Their application was Splitting hydrogen from impurities such as carbon dioxide and nitrogen. They gave specific pressures, Step times, pressure ratios, and other process details.

C.2.18 Munzner, Jüntgen, et al.

One of the most significant patents in the past 2 decades disclosed a process for separating nearly pure nitrogen from air by exploiting a carbon molecular sieve (CMS) adsorbent in which the diffusion rate differences of oxygen and nitrogen were dramatic. The original patent was granted in Germany in 1976.[55] Patents were awarded to Munzner et al. in 1977[56,57] and to Jüntgen et al. 1981,[58] which were assigned to Bergwerksverband GmbH. The idea and technology were not radically new, since CMS had been introduced separately in 1971,[59] and Skarstrom[3] had already shown that kinetic separations were possible. The patent by Jüntgen et al., however, showed significantly better performance than the System of Skarstrom: 99.9% nitrogen at a recovery of about 40% versus 99% nitrogen at essentially nil recovery. A schematic diagram of the process is shown in Figure C.4. It is instructive to notice the minor differences between this process and the one suggested by Perley.

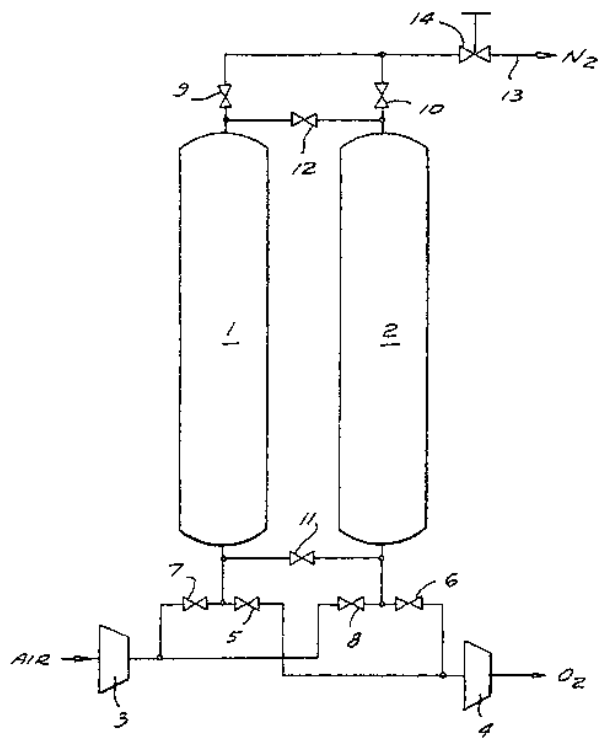

Figure C.4 Flowsheet of the kinetics-based PSA apparatus suggested by Juntgen et al. in 1979, which appeared in U.S. Patent No. 4,264,339 in 1981. This equipment was designed for splitting nitrogen from air, using a carbon molecular sieve.

C.2.19 Collins

One of the less conventional patent applications was filed by Collins in 1975 for PSA oxygen Separation from air. The patent, awarded in 1977,[34] sheds light on the deviations from isothermal behavior of relatively large diameter beds of zeolite (e.g., 30 cm diameter or larger). It shows that expected recoveries often exceed those achieved in such large columns due to depressed temperatures within the bed. Accordingly, it shows actual temperature profiles along the bed axis during the PSA cycle. The primary contribution

was a means for suppressing the temperature deviations by inserting aluminum plates or rods in the bed to conduct heat axially, thus reducing or eliminating temperature gradients.

C.2.20 Sircar and Co-Workers

Several patents were awarded to Sircar and his colleagues in the span of 1977–1988 that applied to hydrogen purification,[60] air separation,[9,23] air purification,[61] splitting reformer off-gas to get hydrogen and carbon dioxide, and recovering hydrogen and methane from hydrodesulfurization plant effluent.[62,63] The key unifying feature of these patents was: two or more sets of parallel beds were connected sequentially, and the sets usually contained different adsorbents in order to isolate different components of the feed mixture. They were also orchestrated to ensure that each product was obtained with as little power input as practical, and that each byproduct was fully exploited before it was released.

C.2.21 Jones, Keller, and Wells

The patent by Jones, Keller, and Wells, which issued in 1980,[64] pushed the limits of fast cycling close to the limits allowed by fluid mechanics and valve dynamics (see Figure C.5). That is, it employed feed Step times of about 0.5 to 2.0 s, and exhaust times of 0.5 to 20 s. It also systematically explored the relations between bed length, particle size, feed pressure, and adsorbent type on product purity and recovery. It covered several applications, including air Separation, Splitting nitrogen and ethylene, and Splitting hydrogen from methane, carbon monoxide, and carbon dioxide.

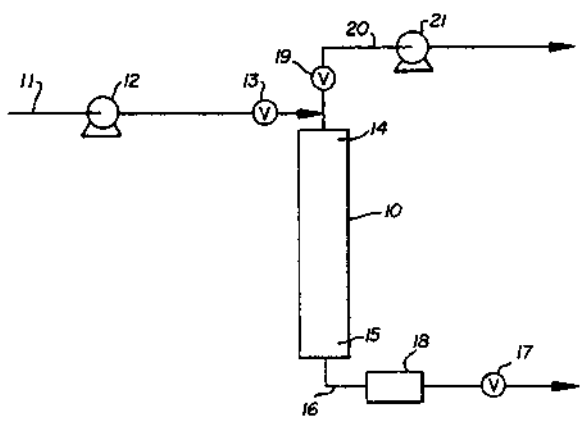

Figure C.5 Flowsheet of the rapid PSA process suggested by Jones et al. in 1979, which appeared in U.S. Patent No. 4,264,339 in 1981. This equipment was designed for Splitting oxygen from air, using a zeolite molecular sieve. It employed smaller particles and exploited pressure waves that propagate along the axis by coupling flow and pressure shifts in a synchronous way. Two relatively pure products are produced, and the adsorbent productivity is high.

C.2.22 Kumar et al.

One of the more difficult separations among atmospheric gases is to split argon from oxygen. this is due to nearly identical adsorption isotherms that these components exhibit with most zeolites. Kumar et al., who filed in 1982 and received a patent in 1984,[19] approached the problem of purifying argon containing minor amounts (e.g., less than 10% each) of nitrogen and oxygen by first removing the nitrogen via zeolite, then removing

oxygen using carbon molecular sieve. Essentially, they used loosely coupled PSA Systems in which the product of the first was the feed to the second. Following similar reasoning, Hayashi et al., who filed in 1983 and were awarded a patent in 1985,[20] were able to split air to obtain both high-purity oxygen and argon.

C.2.23 Wiessner and Boikart

A subtle Variation on the technique for recovering the most strongly adsorbed components from a mixture was suggested by Wiessner and Boikart in 1988.[65] They allowed blowdown to an intermediate pressure, then purged the residual heavy component. Subsequently, they completed blowdown, and as an Option purged again. This allows a valuable component to be recovered at a moderate pressure, above the minimum pressure in the PSA cycle, allowing higher Overall recovery with minimal recompression cost. It could also permit a moderately adsorbed component to be removed prior to dropping the pressure sufficiently to desorb a more strongly adsorbed component.

C.2.24 Tagawa et al.

An example of the refinement that is prevalent in recent PSA patents was given by Tagawa et al. in 1988.[66] They compared three different methods for pressure equalization, in a process to split oxygen from air using 5A zeolite. Their options included: (1) from the product end of one column to the feed end of a parallel column, (2) from the product end of one column to the product end of a parallel column, and (3) from the feed end of one column to the feed end of a parallel column. They state that the first is in the prior art. They also Claim that (2) and (3) can be conducted simultaneously.

C.3 Concluding Remarks

To close this appendix, some comments are appropriate. First, a few overall impressions are given about specific patents and phases that they seem to fall into. Then a few comments are made about the relation of this appendix to other parts of this book.

First, it is remarkable that the basic flowsheet for PSA has been in the public domain for over sixty vears (cf. Figure C.1), yet some aspects are still not perfectly understood. In addition, it has been possible to secure patents with equivalent flowsheets even in the 1980s (cf. Figure C.3). Those facts speak volumes about the subtleties involved in PSA.

In one of the very first disclosures of PSA concepts, Finlayson and Sharp[2] made some suggestions that *now* might be thought of as mundane, but were truly farsighted at the time. For example, they gave a detailed example of a single PSA System being used to alter the ratio of hydrogen and carbon monoxide in water gas from about 1:1 to 9:1, 2:1 and 1: 8, respectively, for subsequent synthesis of ammonia, methanol, and aliphatic acids. They also recognized activated carbon and silica gel as promising adsorbents. Finally, they suggested that, "nitrogen, hydrogen, oxygen, carbon monoxide, and methane" were candidates for purification by PSA. Even though these applications were suggested over *60 years ago*, the PSA hydrogen purification (the easiest of the group) did not become practical on a commercial scale until the late 1960s. Similarly, Separation of either relatively pure oxygen or nitrogen from air did not become commercially viable until the late 1970s, and Splitting carbon monoxide and methane from contaminants only became moderately successful in the late 1980s. Despite the achievements of modern technology, improvements in all of the applications are still being sought. One wonders what, if

Finlayson and Sharp were with us today, they would expect to be possible via PSA 60 years from now.

In view of the incremental nature of Batta's patent in 1971,[51] it could be though of as a sort of turning point, at least for hydrogen production. It seemed to mark the passage from dramatic innovations in which substantial improvements over prior art were claimed, to an onslaught of minor refinements of existing cycles. A similar turning point occurred for PSA oxygen production in the early 1980s. That is not to say that innovations ceased. It was just that most of the "obvious" modes of PSA Operation had already been discovered, if not perfected.

Most of the topics covered in this book are based on mathematical models, although in some instances experimental verification is mentioned. Conversely, this appendix covers the main repository of original ideas related to pressure swing adsorption cycles, and apparently none of them depended on mathematical models to reach fruition. this is not to say that some may not have achieved more resounding success if an adequate mathematical model had been available. It may be worthwhile to consider, for a moment, the reinforcing aspects of the patent literature and the conclusions obtained independently, though much later, via mathematical models.

For example, there are significant distinctions in the ways in which even the simplest Steps can be accomplished. From a theoretical point of view, Section 4.6 shows that pressurization with product is virtually always superior to pressurization with feed. That point is made as strongly, if not as succinctly, in patents by different methods of pressure equalization, as illustrated by the references listed in Sections C.2.8 and C.2.24. Specifically, when the purified product from one column is used partially to pressurize a parallel column by interconnecting the product ends, it is possible to obtain more high-quality product than when the feed ends are interconnected. Another point that was made in Section 4.4.4 was that simultaneous depressurization and production always improves recovery over isobaric production or simultaneous pressurization and production. Accordingly, in patents the concepts of cocurrent blowdown either into a parallel bed (in tandem with the concept of pressurization with product and pressure equalization topic mentioned previously) or to obtain the light product has also appeared in several forms, as discussed in Sections C.2.5, C.2.9, and C.2.16, to name a few. Finally, the idea of a rinse Step was discussed in Section 4.4.5 from a theoretical perspective. That section showed the advantages in terms of recovery that could be realized by adding that step. Long before that theory was conceived, however, the idea of the rinse step had been invented and reduced to practice by Basmadjian and Pogorski[40] (cf. Section C.2.11). They and several others have used it as a means for recovering the heavy component(s) or recycling unadsorbed feed. In view of all that, it is clear that the results of mathematical models reinforce what has already been learned in practice. With that in mind, it is promising that such models could provide guidance for improving performance of existing PSA cycles, and for moving efficiently towards nearly optimum conditions for new cycles.

References

1. R. L. Hasche and W. N. Dargan, "Separation of Gases," U.S. Patent No. 1,794,377 (1931).
2. D. Finlayson and A. J. Sharp, "Improvements in or Relating to the Treatment of Gaseous Mixtures for the Purpose of Separating Them into Their Components or Enriching Them with Respect to One or More of Their Components," British Patent No. 365,092 (1932).

3. C. W. Skarstrom, “Method and Apparatus for Fractionating Gaseous Mixtures by Adsorption,” U.S. Patent No. 2,944,627 (1960).

4. D. Tondeur and P. C. Wankat, “Gas Purification by Pressure Swing Adsorption,” *Separ. and Purif. Methods* **14,** 157–212 (1985).

5. D. J. Ball, “Patent Search of Pressure Swing Adsorption Related Processes,” unpublished (1985).

6. C. W. Skarstrom and W. O. Heilman, “Technique with the Fractionation of Separation of Components in a Gaseous Feed Stream,” U.S. Patent No. 3,086,339 (1963).

7. E. M. Wilson, “Method of Separating Oxygen from Air,” U.S. Patent 3,164,454 (1965).

8. N. H. Berlin, “Vacuum Cycle Adsorption,” U.S. Patent No. 3,313,091 (1967).

9. S. Sircar and T. R. White, “Vacuum Swing Adsorption for Air Separation,” U.S. Patent 4,264,340 (1981).

10. G. A. Perley, “Method of Making Commercial Hydrogen,” U.S. Patent No. 1,896,916 (1933).

11. R. Kumar, S. Sircar, and W. C. Kratz, “Adsorptive Process for the Removal of Carbon Dioxide from a Gas,” U.S. Patent No. 4,472,178 (1984).

12. S. Sircar, “Regeneration of Adsorbents,” U.S. Patent No. 4,784,672 (1988).

13. S. Sircar, “Closed-Loop Regeneration of Adsorbents Containing Reactive Adsorbates,” U.S. Patent No. 4,971,606 (1990).

14. K. Erdmann, “Process of the Removal of Carbon Monoxide from Mixtures thereof with Hydrogen,” U.S. Patent No. 2,254,799 (1941).

15. P. Guerin de Montgareuil and D. Domine, French Patent No. 1,233,261 (1957).

16. T. M. Stark, “Gas Separation by Adsorption Process,” U.S. Patent No. 3,252,268 (1966).

17. D. Domine and L. Hay, “Gas Separation by Adsorption,” U.S. Patent No. 3,619,984 (1971).

18. P. J. Gardner, “Process and Compound Bed Means for Evolving a First Component Enriched Gas,” U.S. Patent No. 4,386,945 (1983).

19. R. Kumar, S. Sircar, T. R. White, and E. J. Greskovitch, “Argon Purification, U.S. Patent No. 4,477,265 (1984).

20. S. Hayashi, H. Tsuchiya, and K. Haruna, “Process for Obtaining High Concentration Argon by Pressure Swing Adsorption,” U.S. Patent No. 4,529,412 (1985).

21. G. S. Glenn, V. K. Rajpaul, and R. F. Yurczyk, “Integrated System for Generating Inert Gas and Breathing Gas on Aircraft,” U.S. Patent No. 4,681,602 (1987).

22. K. S. Knaebel, “Complementary Pressure Swing Adsorption,” U.S. Patent No. 4,744,803 (1988).

23. S. Sircar, “Preparation of High Purity Oxygen,” U.S. Patent No. 4,756,723 (1988).

24. K. Haruna, K. Ueda, M. Inoue, and H. Someda, “Process for Producing High Purity Oxygen Gas from Air,” U.S. Patent No. 4,985,052 (1991).

25. C. W. Skarstrom, “Process for the Recovery of Hydrogen from Hydrocarbon Gas Streams,” U.S. Patent No. 3,101,261 (1963).

26. C. W. Skarstrom, “Timing Cycle for Improved Heatless Fractionation of Gaseous Materials,” U.S. Patent No. 3,104,162 (1963).

27. C. W. Skarstrom, “Apparatus and Process for Heatless Fractionation of Gaseous Constituents,” U.S. Patent No. 3,138,439 (1964).

28. R. C. Hoke, W. D. Marsh, J. Bernstein, and F. S. Pramuk, “Hydrogen Purification Process,” U.S. Patent No. 3,141,748 (1964).

29. W. D. Marsh, F. S. Pramuk, R. C. Hoke, and C. W. Skarstrom, "Pressure Equalization Depressuring in Heatless Adsorption," U.S. Patent No. 3,142,547 (1964)

30. C. W. Skarstrom, "Oxygen Concentration Process," U.S. Patent No. 3,237,377 (1966).

31. J. L. Wagner, "Selective Adsorption Process," U.S. Patent No. 3,430,418 (1969).

32. N. R. McCombs, "Selective Adsorption Gas Separation Process," U.S. Patent No. 3,738,087 (1973).

33. H. Lee and D. E. Stahl, "Pressure Equalization and Purging System for Heatless Adsorption," U.S. Patent No. 3,788,036 (1974).

34. J. J. Collins, "Air Separation by Adsorption," U.S. Patent No. 4,026,680 (1977).

35. D. B. Broughton, "Adsorptive Separation of Gas Mixtures," U.S. Patent No. 3,121,625 (1964).

36. G. A. Rutan, "Apparatus and Method for Drying a Gaseous Medium," U.S. Patent No. 3,236,028 (1966).

37. W. Betteridge and J. Hope, "Separation of Hydrogen from other Gases," U.S. Patent No. 3,438,178 (1969).

38. R. Eriksson, "Fractionating Apparatus," U.S. Patent No. 4,169,715 (1979).

39. G. E. Keller II and C.-H. A. Kuo, "Enhanced Gas Separation by Selective Adsorption," U.S. Patent No. 4,354,859 (1982).

40. D. Basmadjian and L. A. Pogorski, "Process for the Separation of Gases by Adsorption," U.S. Patent No. 3,279,153 (1966).

41. T. Tamura, "Absorption Process for Gas Separation," U.S. Patent No. 3,797,201 (1974).

42. P. Wilson, "Inverted Pressure Swing Adsorption Process," U.S. Patent No. 4,359,328 (1982).

43. S. Matsui, Y. Tukahara, S. Hayashi, and M. Kumagai, "Process for Removing a Nitrogen Gas from Mixture Comprising N_2 and CO or N_2, CO_2, and CO," U.S. Patent No. 4,468,238 (1984).

44. M. Whysall, "Pressure Swing Adsorption Process," U.S. Patent No. 4,482,361 (1984).

45. T. Inoue and K. Miwa, "Separation Process for a Gas Mixture," U.S. Patent No. 4,515,605 (1985).

46. E. Richter, W. Korbacher, K. Knoblauch, K. Giessler, and K. Harder, "Method of Separating Highly Adsorbable Components in a Gas Stream in a Pressure-Sensing Adsorber System," U.S. Patent No. 4,578,089 (1988).

47. M. Yamano, T. Aono, and M. Uno, "Process for Separation of High Purity Gas from Mixed Gas," U.S. Patent No. 4,775,394 (1988).

48. K. S. Knaebel, "Pressure Swing Adsorption," U.S. Patent No. 5,032,150 (1991).

49. N. H. Berlin, "Method for Proving an Oxygen-Enriched Environment," U.S. Patent No. 3,280,536 (1966).

50. G. F. Feldbauer, "Depressuring Technique for ΔP Adsorption Process," U.S. Patent No. 3,338,030 (1967).

51. L. B. Batta, "Selective Adsorption Process," U.S. Patent No. 3,564,816 (1971).

52. D. C. Shell, D. A. Tanner, and R. D. Brazzel, "Separation Process," U.S. Patent No. 3,788,037 (1974).

53. L. B. Batta, "Selective Adsorption Process for Air Separation," U.S. Patent No. 3,717,974 (1973).

54. A. Fuderer and E. Rudelstorfer, "Selective Adsorption Process," U.S. Patent No. 3,986,849 (1976).

55. H. Jüntgen et al., F.R.G. Patent No. 2,652,486 (1976).

56. H. Munzner, U.S. Patent No. 4,011,065 (1977).

57. H. Munzner, U.S. Patent No. 4,015,956 (1977).

58. H. Jüntgen, K. Knoblauch, J. Reichenberger, H. Heimbach, and F. Tarnow, "Process for the Recovery of

Nitrogen-Rich Gases from Gases Containing at Least Oxygen as Other Component," U.S. Patent No. 4,264,339 (1981).

59. H. Munzner et al., F.R.G. Patent No. 2,119,829 (1971).
60. S. Sircar and J. W. Zondlo, "Hydrogen Purification by Selective Adsorption," U.S. Patent No. 4,077,779 (1978).
61. S. Sircar and W. C. Kratz, "Removal of Water and Carbon Dioxide from Air," U.S. Patent No. 4,249,915 (1981).
62. S. Sircar, "Separation of Multicomponent Gas Mixtures," U.S. Patent No. 4,171,206 (1979).
63. S. Sircar, "Separation of Multicomponent Gas Mixtures by Pressure Swing Adsorption," U.S. Patent No. 4,171,207 (1979).
64. R. L. Jones, G. E. Keller II, and R. C. Wells, "Rapid Pressure Swing Adsorption Process with High Enrichment Factor," U.S. Patent No. 4,194,892 (1980).
65. F. Wiessner and A. Boikart, "Adsorbate Recovery in PSA Process," U.S. Patent No. 4,717,397 (1988).
66. T. Tagawa, Y. Suzu, S. Hayashi, and Y. Mizuguchi, "Enrichment in Oxygen Gas," U.S. Patent No. 4,781,735 (1988).

Subject Index

Activated alumina, 21
Activated carbon, 17–20
Adsorbents, 11–23
    physical properties, 19
    pore size distribution, 13
    structure, 35
Adsorption equilibrium, 23
Adsorption step, 68
Air drier, 73, 75, 148, 211–26, 331
Air Liquide cycle, 82
Air separation, 70, 71, 74, 78, 80, 87, 90, 93, 187, 196, 226–35, 281, 330–34, 337
    Bergbau-Forschung process, 87, 230
    equilibrium theory, 133–42
    Lindox process, 228
    nitrogen production, 195–201, 230, 331, 335
    oxygen and nitrogen, 232, 256, 275
    oxygen production, 187,190, 226, 331–38
    RPSA, 283–86
    TCPSA, 276
    vacuum swing process, 230
Applications of PSA, 7
Argon recovery, 338
Atmospheric gases
    adsorption data, 32–34

Blowdown step, 68, 88, 151–62
    concentration of heavy component, 253
    losses, 76
Burnauer's classification, 25
Bulk separation, 173

Carbon dioxide
    recovery, 242–44
    separation (from methane), 91, 192
Carbon molecular sieve, 17–20, 86–88, 196–201
Characteristics, method of, 100, 184, 307–11
Co-current depressurization, 88
Coke oven gas, 242
Collocation, 184, 313–25
Column pressure,
    constant, 173
    variable, 174

Compensation, diffusivity/solubility, 291
Concentration (of trace component), 157, 251
Concentration profiles (during pressurization), 71
Constant pattern, 55, 101
Continuous counter-current model, 201
Corrected diffusivity, 40
Cryogenic PSA, 255
Cycles (for PSA), 67–94
    analysis of, 105–33
    five-step, 122
    four-step, 98, 107
    self-purging, 88
    Skarstrom, 106

Dead volume, 125
Depressurization, 83
Desiccants, 20
Design example, 143–46
Desorption, 68
Diffusion,
    Fickian, 40
    Knudsen, 37
    macropore, 36
    micropore, 43
    model, 191–201, 318–24
    molecular, 37
    Poiseuille flow, 37
Diffusivity, 40
    corrected, 40
    effective, 46
Dispersed plug flow, 174
Dispersive front, 101
Dynamic modelling, 57, 165–219
Dynamic models, summary of, 167
Dynamics (adsorption column), 52

Economics of PSA (N_2), 231
Efficiency (of PSA process), 258–63
Elementary steps (of PSA process), 67
Enrichment, 108
Equilibrium controlled separations, 71, 95–162
Equilibrium/kinetic effects reinforce, 90
Equilibrium selectivity, 50
Equilibrium theory, 53, 95–163
    data for atmospheric gases, 32–34
    experimental validation, 133–37
Energy analysis, 258–62

Experimental PSA system, 89
    verification of equilibrium theory, 133–37
Extensions of PSA concept, 265–87
Extract, 1

Favorable and unfavorable isotherms, 25
Five-step cycle, 84
Flow models, 172
Fluid film resistance, 42
Forces of adsorption, 11
Four-step cycle, 107, 137–42

Gemini-8 process, 248
Gemini-9 process, 246

Heat effects in PSA processes, 146–51, 207–17
Heat transfer, 47
Heats of sorption, 13
Helium recovery, 333
Henry constants, 23
    for atmospheric gases, 32
Henry's law, 23
History of PSA, 4, 95, 327–40
Hydrocarbon separations, 246
Hydrogen and carbon dioxide, PSA process, 246
Hydrogen recovery, 235–42,274, 330, 332, 334, 335, 337
    Bergbau-Forschung process, 242
    four-bed process, 236
    polybed process, 239
Hydrogen-helium separation, 254
Hydrophilic/hydrophobic properties, 12

Ideal adsorbed solution theory, 31
Isosiv process, 245
Isotherm, 25–32, 177–80
    BET, 28
    binary and multicomponent, 29
    carbon sieve, 91
    favorable/unfavorable, 25
    Freundlich, 27
    Gibbs, 28, 31
    Langmuir, 25
    Sipps, 30

Kinetic selectivity, 48, 52, 87
Kinetics (of sorption), 34–61
Knudsen diffusion, 290

Langmuir isotherm, 25, 179
LDF model, 180–83,185–93, 209, 313–18
    rate expression, 57
Lindox process, 228
Losses, blowdown, 76
Macropore diffusion, 36, 45
Mass transfer models, 180
Mass transfer resistance, 55
    effect on productivity, 190
Membrane, 289
    cascades, 301
    modules, 295
    process, cascades for, 301, 302
    process, comparison with PSA, 289–305
    process, effect of back pressure, 292
    process, effect of flow pattern, 298
    process for N_2, 303
    process for O_2, 304
    zeolite, 295
Mesopores, diffusion in, 36
Methane recovery, 244
Methane-carbon dioxide separation, 192
Micropore diffusion, 37, 43
Model,
    continuous countercurrent, 201–7
    diffusion, 191–201, 318–24
    LDF, 184–91, 313–18
Molecular diameter, effect on diffusion, 19, 23, 41
Molecular gate, 267, 287
Molecular sieve carbon, 17, 49
Moments (chromatographic), 60
Multicomponent systems, 61
Multiple bed systems, 79, 239, 335
Multiple cyclic states, 213–17, 230–32

Nitrogen PSA, 196–200, 205, 230–32, 331
Non-isothermal systems, 61, 146–51, 207–13
Numerical methods, 183, 313–25

Oxygen production, 74, 187, 226–30, 304, 331
    and nitrogen production, 232–35

Parametric pump, 265
Patents (PSA), 3, 327–43
Permeability, 289, 294
Physical strength (of adsorbents), 17
Polybed process, 239, 335

Pore diffusion, 36
    model, 318
Pore size distribution, 13
Pressure,
    equalization, 69, 76, 193, 333, 338
    profile, 151–61
    ratio, effect of, 90, 108–32
    variation, effect of, 118, 158
Pressurization, 68
    feed, 110, 112, 141
    product, 107, 137, 139
    step, 151–62
Proportionate pattern, 55, 101
Publications (PSA), 3
Purge, 68, 88, 224
    incomplete, 73, 114, 118
    pressure, effect of, 90
    with strong adsorptive, 84

Raffinate, 1
    product, 71
Rapid PSA. *See* RPSA
Recovery. *See also* Individual gases
    effect of dead composition, 109, 112
    effect of dead volume, 131
    effect of pressure, 109–32, 142
    light product, 85, 118
    purity profile, 301
    rapidly diffusing species, 93
    strong adsorptive, 83, 251–57
Reformer gases (H_2 recovery), 246, 330, 332, 335
Resistances to mass transfer,
    combination of, 60
    diffusional, 36–45
    effect of, 55
    fluid film, 42
    surface, 42, 49
Rinse, 69, 122
RPSA, 278–86, 337
    air separation, 283
    future prospects, 286
    modelling, 279
    performance, 281

Selectivity
    effect of, 104
    equilibrium, 12, 50, 90–93

kinetic, 12, 52, 90–93
membrane, 290
permeability, 294
temperature dependence, 293
Self-purging cycles, 85, 87, 88, 230–32
Self-sharpening profile, 101
Separation factor, 30, 51, 289, 290
effect of back pressure, 292
effect of temperature, 293
Shock wave, 55, 101
Silica gel, 20
Simple wave, 101
Simulation of PSA processes, 165–219
continuous countercurrent model, 201–7
LDF model, 184–91
pore diffusion model, 191–201
Size selectivity, 23
Skarstrom cycle, 72, 106, 221–26
Smelter gases (purification), 328
Spreading pressure, 28
Stirling engine, 271
Sulfur dioxide (recovery), 328
Surface resistance, 42

TCPSA, 270–77
air separation, 275
comparison with PSA, 277
scale-up, 278
synthesis gas separation, 274
Temperature variation, 146–51, 207–17
Thermal wave, 63
Thermally coupled PSA. *See* TCPSA
Trace component concentration, 251–57
Trace systems, 172

Uptake rates, 41–50

Vacuum swing, See VSA
Voidage, 99
VSA, 7, 329
cycle, 81
economics, 230
process, 229

Water gas, 330
Wave velocity, 266

Zeolites, 21–23